

©[2009]

Aurora Cassandra Elmore

ALL RIGHTS RESERVED

LATE PLEISTOCENE CHANGES IN NORTHERN COMPONENT WATER:
INFERENCES FROM GEOCHEMICAL AND SEDIMENTOLOGICAL RECORDS
FROM GARDAR DRIFT

by

AURORA CASSANDRA ELMORE

A Dissertation submitted to the
Graduate School-New Brunswick
Rutgers, The State University of New Jersey

In partial fulfillment of the requirements

for the degree of

Doctor of Philosophy

Graduate Program in Geological Sciences

written under the direction of

James D. Wright

and approved by

Jerry F. McManus _____

Kenneth G. Miller _____

Gregory S. Mountain _____

Yair Rosenthal _____

James D. Wright _____

New Brunswick, New Jersey

[May, 2009]

ABSTRACT OF THE DISSERTATION

LATE PLEISTOCENE CHANGES IN NORTHERN COMPONENT WATER:
INFERENCES FROM GEOCHEMICAL AND SEDIMENTOLOGICAL RECORDS
FROM GARDAR DRIFT

by AURORA CASSANDRA ELMORE

Dissertation Director:

James D. Wright

This dissertation reconstructs late Pleistocene oceanic circulation variability within the North Atlantic, a critical region of deep-water formation, using proxies that reconstruct surface and deepwater changes. Unlike other studies that examine North Atlantic circulation as a whole, my study focuses on changes in Iceland Scotland Overflow Water (ISOW), one of the largest contributors to Northern Component Water (NCW). Each NCW component reflects the regional climate within its formation region; thus, different climates may produce different deepwater states by changing the relative contribution from each component. Southern Gardar Drift is bathed by ISOW, thus the accumulating sediments are ideal for examining ISOW.

A high-resolution record of the Younger Dryas cold event provides an analog for abrupt climate events. The benthic foraminiferal $\delta^{13}\text{C}$ record from core 11JPC (2707m) on Gardar Drift reveals NCW shoaled during the early and late Younger Dryas. These reductions are coincident with increased meltwater from Northern Hemisphere ice sheets, linking surface freshening to NCW production changes on short-timescales.

On longer time-scales, benthic foraminiferal $\delta^{13}\text{C}$ records from Gardar Drift show ISOW density was paced by northern high-latitude summer insolation, particularly within the precessional band. Uniform benthic foraminiferal $\delta^{13}\text{C}$ values on Gardar Drift indicate that the mixing zone between NCW and Southern Component Water (SCW) was positioned to the south of Gardar Drift during interglacial periods. Conversely a large north-south gradient in benthic foraminiferal $\delta^{13}\text{C}$ values during glacial periods indicates that ISOW shoaled, allowing SCW to bathe southern Gardar Drift. High-frequency ISOW variability caused by surface freshening during intermediate climate states is superimposed on the orbitally paced variations.

A study of the trace metal compositions in *Krithe* carapaces found in core top samples demonstrates that calcification temperature is the dominant control on magnesium incorporation. Carbonate ion concentration is a secondary control on magnesium to calcium (Mg/Ca) ratios at low temperatures ($<3^\circ\text{C}$). Correcting for carbonate ion effects results in a linear paleotemperature equation with higher temperature sensitivity in the lower temperature range than previously published equations. This study indicates that *Krithe* magnesium to calcium ratios are reliable in reconstructing paleotemperatures.

ACKNOWLEDGEMENTS

I would like to thank my committee, Jerry McManus, Ken Miller, Greg Mountain, and Yair Rosenthal, for their helpful discussions and support, both of which were invaluable to this research. My advisor, Jim Wright, was particularly important for the evolution of this project and my growth as a researcher. I am especially grateful to Jim for his willingness to allow me to steer my project in new directions. I will always remember our chats in his office, where many of the ideas in this dissertation were born.

I would also like to acknowledge John Southon, who provided AMS ^{14}C dates, Tom Cronin, who taught me ostracod taxonomy, Mimi Katz, who taught me benthic foraminiferal taxonomy, and Gary Dwyer, who provided supplementary data. This research benefited from discussions with Michelle Hardee, Alex Piotrowski, Sindia Sosidan, David Thornalley, and many others.

The members of the Stable Isotope Laboratory at Rutgers University, Alex Cotet, Linda Godfrey, Sam Henderson, Rick Mortlock, and Lauren Neitzke, were extremely helpful for discussions. Members of the Marine Biogeochemistry and Paleoceanography Lab Group at Rutgers University, Eleni Anagnostou, Tali Babila, Marina Chong, Paul Field, Michele Lavigne, Kate Jordan, and Rob Sherrell, were helpful in measuring trace element geochemistry and discussions. I would also like to thank the other faculty, staff, and graduate students of the Earth and Planetary Sciences Department and the Institute of Marine and Coastal Sciences for their help through this process.

Portions of this research were funded by grants to A.C. Elmore from the Department of Earth and Planetary Sciences at Rutgers University, Steven K. Fox Fund,

Rutgers University Graduate School- New Brunswick, Geologic Society of America, and Geochemical Society of America. Funding for the cruise that collected sediment cores 11JPC and 3GGC was from grant NSF OCE-0309064 to J.D. Wright, G.S. Mountain, P. Manley, and K. Miller. Y. Rosenthal generously provided sediment cores for the calibration study.

Finally, I would like to thank my friends (CA, SA, EB, IB, JB, MB, SB, TB, STB, JC, ZC, NE, MF, BG, SG, BH, JGH, JH, MH, EK, SN, JO, CP, SP, NR, BS, RS, JS, PS, DT, PT, KW), especially Kat, Sarah, Nina, and Erica, for their unwavering support through the years! Your emails, phone calls, post cards, letters, and other signs of support are what got me through. I love you all!

This dissertation is dedicated to my family, and to my grandparents: To Anne and James Elmore, who both passed away during the writing of this dissertation, I know you would be proud to see this work completed. I hope that I can make even a fraction of the difference that you did, Papa Jim. To Judy Kaliner, thank you for always being there for me when I need to talk, or to get away, and for understanding when I couldn't do either. Your support means the world, and I know Da would feel the same. To my mom, dad, and brother, who can always make me smile, a million times, THANK YOU.

TABLE OF CONTENTS

Abstract of the Dissertation	ii
Acknowledgements	iv
Table of Contents	vi
List of Tables	ix
List of Illustrations	xi
1.0 Chapter 1: Dissertation Introduction	1
1.1 Background	1
1.2 Importance of Studying Iceland-Scotland Overflow Water.....	5
1.3 Region of Study	7
1.4 Paleooceanographic Proxies	8
1.5 Chapter Overviews	10
1.5.1 Chapter 2	10
1.5.2 Chapter 3	11
1.5.3 Chapter 4	12
1.6 References	12
2.0 Chapter 2: Meltwater Influence on Northern Component Water During the Younger Dryas	22
2.1 Abstract	22
2.2 Introduction	23
2.3 Methods	25
2.3.1 Sample Processing	25
2.3.2 Age Model	27

2.4 Results	30
2.4.1 Surface Water Results	30
2.4.2 Deepwater Results	32
2.5 Discussion	33
2.5.1 Implications for the Holocene	33
2.5.2 Implications for the Younger Dryas	39
2.6 Conclusions	41
2.7 References	42
3.0 Chapter 3. Precession-driven Changes in Iceland-Scotland Overflow Water Density and Bottomwater Circulation on Gardar Drift Since ~ 200 ka	59
3.1 Abstract	59
3.2 Introduction	59
3.3 Methods	64
3.3.1 Site Locations	64
3.3.2 Data Collection	65
3.3.3 Age Models	67
3.3.4 Transect Construction	68
3.4 Results	70
3.4.1 Core KN166-14 11JPC	70
3.4.2 Core KN166-14 3GGC	71
3.4.3 Transect Results	72
3.5 Discussion	76
3.5.1 Orbital Scale ISOW Variability	76

3.5.2 Millennial Scale ISOW Variability	79
3.6 Conclusions	80
3.7 References	81
4.0 Chapter 4. Examination of Temperature and Carbonate Ion Effects on Mg/Ca Ratios of Ostracod Genus <i>Krithe</i>	104
4.1 Abstract	104
4.2 Introduction	104
4.3 Methods	110
4.3.1 Core Top Locations	110
4.3.2 Core Top Hydrography	113
4.3.3 Core Top Sample Processing	114
4.3.4 Core KN166-14 11JPC	115
4.3.5 Analytical Methods	115
4.4 Results	117
4.4.1 Post Depositional Dissolution	117
4.4.2 Adult and A-1 Juvenile Carapaces	118
4.4.3 The Mg/Ca – Depth Relationship	118
4.4.4 The Mg/Ca – Temperature Relationship	119
4.4.5 Secondary Effects on Mg/Ca Ratios	120
4.4.6 Temperature Calibration	120
4.4.7 Carbonate Ion Effects	123
4.4.8 Global Paleotemperature Equation	125
4.4.9 Comparison to Published Calibration Studies	126

4.5 Paleooceanographic Applications	130
4.6 Conclusions	134
4.7 References	135
5.0 Chapter 5. Dissertation Conclusions and Future Work	162
5.1 Summary of Results	162
5.2 Future Work	164
5.3 References	167
6.0 Appendices	169
7.0 Curriculum Vitae	225

LIST OF TABLES

Table 2.1: Locations of cores used in this study	52
Table 2.2: Age model for the top of core 11JPC including AMS ^{14}C dates and 1 chronostratigraphic tie point (blue). AMS ^{14}C dates in red were not included in the age model as they caused slight age reversals. AMS ^{14}C dates were corrected by 400 years to account for the reservoir correction and calibrated to calendar years using the Fairbanks 0805 calibration (Fairbanks et al., 2005). Activity of ^{14}C , bioturbated activity, corrected activity, and final calendar ages were determined according to the methods outlined above in section 2.2.2. All ages are given in years.	53
Table 2.3: Summary of results	54
Table 3.1: Locations and water depths of cores used in this study	90
Table 3.2: Age model for core KN166-14 11JPC. Tie points were determined by AMS ^{14}C (white boxes), magneto-stratigraphy (orange box) or chrono-stratigraphic comparison to a stacked benthic foraminiferal $\delta^{18}\text{O}$ record by Liseicki and Raymo (2005; blue boxes). AMS ^{14}C ages in red were not included in the age model. AMS ^{14}C dates designated by asterisks were corrected due to account for the bioturbation of sub-hiatus material (see section 2.3.2).....	91
Table 3.3: Age model for core KN166-14 3GGC was determined based on chrono- stratigraphic comparison to a stacked benthic foraminiferal $\delta^{18}\text{O}$ record by Liseicki and Raymo (2005).....	92
Table 4.1: Previously published paleotemperature equations for <i>Krithe</i> Mg/Ca. Location abbreviations are; South Coral Sea (SCS), Little Bahama Bank (LBB), Shallow Arctic less than 900 m (SA), Ontong Java Plateau (OJP), and Chilean Fjords (CF). Units for the	

equations are mmol/mol for Mg/Ca, °C for BWT, and $\mu\text{mol/kg}$ for $\Delta[\text{CO}_3^{2-}]$. Intercepts from previously published equations were corrected for inter-laboratory differences by 3.40 mmol/mol (*) according to section 4.4.6..... 146

Table 4.2: Hydrographic information for sites used in this core top calibration including; region, core, water depth, bottom water temperature (BWT), bottom water salinity (BWS), $\Delta[\text{CO}_3^{2-}]$, and Mg/Ca. Asterisks indicate $\Delta[\text{CO}_3^{2-}]$ values that were corrected for anthropogenic CO_2 input according to Section 4.3.2. Extended hydrographical information is given in Appendix 6 147

Table 4.3: *Krithe* Mg/Ca and *P. wuellerstorfi* $\delta^{18}\text{O}$ data from Holocene and late MIC 3 sections of core 11JPC used for independent paleotemperature estimates. Average Mg/Ca and estimated $\Delta[\text{CO}_3^{2-}]$ values for modern (Table 4.2) and glacial (Yu et al., 2008) were used to determine bottom water temperatures from Mg/Ca with and without carbonate ion effects using Equations 5 and 6, respectively. *Planulina wuellerstorfi* $\delta^{18}\text{O}$ data has been corrected by 0.64 ‰ to account for disequilibrium from sea water during calcification (Adj. $\delta^{18}\text{O}$ *P. wuell.*; Shackleton, 1974). Temperatures based on *P. wuellerstorfi* $\delta^{18}\text{O}$ (BWT $\delta^{18}\text{O}$) and $\delta^{18}\text{O}_{\text{sw}}$ (Waelbroeck et al., 2002) were estimated using equation 7. 149

LIST OF FIGURES

Figure 1.1: Shaded bathymetry (Smith and Sandwell, 1994) of the North Atlantic Ocean showing major drifts (uppercase lettering), generalized bottom currents (blue arrows), Iceland Scotland Overflow (ISOW), Denmark Straits Overflow (DSOW), and Labrador Sea Water (LSW; gray arrows)	20
Figure 1.2: (A) Insolation (Berger, 1992) and (B) benthic foraminiferal $\delta^{18}\text{O}$ (Liseicki and Raymo, 2005) since 300 ka. Shown are the Holocene, Younger Dryas, Last Glacial Maximum (LGM), and MIC 3-9.....	21
Figure 2.1: Bathymetric map of the North Atlantic showing generalized bottom water currents. The location of KN166 11JPC on Gardar Drift from this study, and ODP 984 (Praetorius et al., 2008) and VM29-191 (Bond et al., 1997), are also shown	55
Figure 2.2: Proxy records from core 11JPC plotted versus sediment depth. (A) planktonic foraminiferal abundances, (B) $\delta^{18}\text{O}$ <i>G. bulloides</i> , $\delta^{18}\text{O}$ <i>N. pachyderma</i> , (C) $\delta^{18}\text{O}$ <i>P. wuellerstorfi</i> , (D) $\delta^{13}\text{C}$ <i>P. wuellerstorfi</i> , (E) the age model, and (F) sedimentation rates are shown.....	56
Figure 2.3: Proxy records from core 11JPC shown versus age from 6 to 13.5 ka plotted with (A) the $\delta^{18}\text{O}$ record of ice from a Greenland ice core (GISP2; Stuiver et al., 1995). (B) Lithics/gram (brown), (C) $\Delta\delta^{18}\text{O}_{G.bulloides - N.pachyderma}$ (pink), (D) a histogram of published meltwater occurrence (see Appendix 2), and (E) $\delta^{13}\text{C}$ <i>P. wuellerstorfi</i>	57
Figure 2.4: δ Comparison of (A) the $\delta^{13}\text{C}$ <i>P. wuellerstorfi</i> from 11JPC plotted with other North Atlantic deepwater proxy records. (B) $\delta^{13}\text{C}$ <i>P. wuellerstorfi</i> from core JPC37 (Hagen and Keigwin, 2002), (C) <i>P. wuellerstorfi</i> from ODP site 984 (Pretorius et al.,	

2008), **(D)** sortable silt from ODP site 984 (Pretorius et al., 2008), and **(E)** Pa/Th from core OCE326-GGC5 (McManus et al., 2004) 58

Figure 3.1: Bathymetric map of the North Atlantic, including bottom water currents (blue), contourite drifts (uppercase lettering), and the northern components of NADW (grey arrows). Core locations from this study and previously published studies are shown (yellow). The location of the cross section is shown by a white line. The location of map inset for Figure 3.5a is designated by the black box 93

Figure 3.2: Bathymetric cross section of the southern Norwegian Sea (NS) and the region south of the Iceland-Faeroe's Ridge (IFR), as shown by the white line on Figure 3.1. The location of Bjorn and Gardar Drifts are shown, as are the projected locations of all cores used in this study (yellow circles). Bold lines show idealized directions of the major water masses, North Atlantic Current (NAC) and Iceland-Scotland Overflow Water (ISOW). Late Holocene *P. wuellerstorfi* and *N. Pachyderma* $\delta^{13}\text{C}$ values are shown 94

Figure 3.3: Proxy records from core 11JPC plotted versus sediment depth. **(A)** $\delta^{18}\text{O}$ *G. bulloides* (pink) and $\delta^{18}\text{O}$ *P. wuellerstorfi* (red), **(B)** $\delta^{13}\text{C}$ *G. bulloides* (blue) and $\delta^{13}\text{C}$ *P. wuellerstorfi* (navy), **(C)** % coarse fraction (orange), **(D)** % carbonate, and **(E)** the age model are shown. Marine Isotope Chrons 1 through 8 are also shown 95

Figure 3.4: Proxy records for core 3GGC plotted versus sediment depth. **(A)** $\delta^{18}\text{O}$ *G. bulloides* (pink), $\delta^{18}\text{O}$ *N. pachyderma* (s; light green), and $\delta^{18}\text{O}$ *P. wuellerstorfi* (red), **(B)** $\delta^{13}\text{C}$ *G. bulloides* (blue), $\delta^{13}\text{C}$ *N. pachyderma* (s; green), and $\delta^{13}\text{C}$ *P. wuellerstorfi* (navy), **(C)** % coarse fraction (orange), **(D)** the age model are shown. The Holocene, Younger

Dryas (YD), Bolling/Allerod (BA), Last Glacial Maximum (LGM) and MIC 3 are also shown 96

Figure 3.5a: 3.5 kHz seismic image of the cruise track over the mudwave field on southern Gardar Drift showing the location of core KN166-14 11JPC. The location of the cruise track is given by the black line in the map inset. Two-way travel time and approximate water depth assuming 1500 m/s velocity through water are shown 97

Figure 3.5b: 3.5 kHz seismic image hove to the site of core KN166-14 11JPC (See Figure 3.5a), depth below sea floor was determined by assuming a sediment velocity of 1505 m/s (G. Mountain, personal communication). Percent coarse fraction and % carbonate for the core are also shown plotted with depth 98

Figure 3.6: Records of $\delta^{13}\text{C}$ *P. wuellerstorfi* from the northern portion of the depth transect (red), the southern portion of the transect (blue), the mid-latitude North Atlantic (DSDP site 607; green line) and South Atlantic (ODP site 1090; black line). The grey shading is a non-statistical representation of the maximum and minimum benthic foraminiferal $\delta^{13}\text{C}$ values of the transect 99

Figure 3.7: Interpolated $\delta^{13}\text{C}$ *P. wuellerstorfi* records from the northern transect sites (red; ODP site 984, EW9302 JPC8, ODP site 983, and V29-202), the southern transect sites (blue; 11JPC, 3GGC, and Neap18k), the mid-latitude North Atlantic (DSDP site 607; green line) and South Atlantic (ODP site 1090; black line) 100

Figure 3.8: (A) Average of transect *P. wuellerstorfi* $\delta^{13}\text{C}$ values interpolated in 2-kyr intervals (black line) plotted with +/- 1 standard deviation is shown versus age from 0 to 200 ka. (B) Standard deviation of transect *P. wuellerstorfi* $\delta^{13}\text{C}$ values interpolated in 2-kyr intervals (green), (C) difference between *P. wuellerstorfi* $\delta^{13}\text{C}$ values of the smoothed

northern and southern transects (orange), and **(D)** northern hemisphere summer insolation at 65°N (Laskar et al., 2004) are also shown 101

Figure 3.9: Spectral analysis of the standard deviation benthic foraminiferal $\delta^{13}\text{C}$ values for the Gardar Drift transect from 0 to 200 ka determined using AnalySeries. 95 % confidence intervals are shown 102

Figure 3.10: Proxy records for core 11JPC plotted versus age from ~ 30 to 70 ka. **(A)** *G. bulloides* $\delta^{18}\text{O}$ (blue), **(B)** *P. wuellerstorfi* $\delta^{13}\text{C}$ (red), **(C)** % Carbonate (green), **(D)** insolation at 65°N (Laskar et al., 2004), **(E)** and IRD/gram (black), **(F)** % Coarse Fraction (orange), **(G)** Standard deviation of the average of *P. wuellerstorfi* $\delta^{13}\text{C}$ values in 1-kyr intervals (pink) are also shown. Shaded areas mark periods of increased ice rafting, likely caused by Heinrich Events. 103

Figure 4.1: Map showing the global distribution of core tops used in this study. Location abbreviations from this study (black) are; Norwegian Sea (NS), Cape Hatteras (CH), Gulf of Mexico (GoM), Ceara Rise (CR), Sulawesi Margin Indonesia (Indo), and New Zealand shelf (NZ). Location abbreviations for locations used in previous studies (red) are; Little Bahama Bank (LBB), Coral Sea (Coral), Chilean Fjords (Chile), and Southern Indian Ocean (SI)..... 150

Figure 4.2: A comparison of the Mg/Ca of adult *Krithe* carapaces and the Mg/Ca of A-1 juvenile *Krithe* carapaces from the same locations falls close to the 1:1 relationship suggesting similar Mg-incorporation mechanisms. The Mg/Ca of Rose Bengal stained carapaces versus unstained carapaces of *Krithe* also shows a 1:1 relationship, indicating no post-mortem dissolution effects. Adult and stained carapaces are plotted on the x-axis as Mg/Ca*. Samples are from the North Atlantic Ocean (blue), Cape Hatteras (dark

green), Gulf of Mexico (green), Ceara Rise (orange), or New Zealand shelf (red)..... 151

Figure 4.3: *Krithe* Mg/Ca and bottom water temperature versus water depth for sites from the Norwegian Sea (purple), North Atlantic Ocean (blue), Cape Hatteras (dark green), Gulf of Mexico (light green), Ceara Rise (orange), New Zealand shelf (red), and Sulawesi Margin, Indonesia (pink)..... 152

Figure 4.4: Comparison of *Krithe* Mg/Ca ratios and bottom water temperature for core tops from the Norwegian Sea (purple), North Atlantic Ocean (blue), Cape Hatteras shelf (dark green), Gulf of Mexico (light green), Ceara Rise (orange), New Zealand shelf (red), and Sulawesi Margin, Indonesia (pink). A linear regression is shown. Shaded regions represent a non-statistical grouping of data of data from Norwegian Sea (purple), Norwegian Sea (red), and Indonesia (pink)..... 153

Figure 4.5a: Core top Mg/Ca data versus $\Delta[\text{CO}_3^{2-}]$ from this study; Norwegian Sea (purple), North Atlantic Ocean (blue), Cape Hatteras (dark green), Gulf of Mexico (light green), Ceara Rise (orange), New Zealand shelf (red), and Sulawesi Margin, Indonesia (pink). A linear regression for all the data is shown in black..... 154

Figure 4.5b: Core top Mg/Ca data versus $\Delta[\text{CO}_3^{2-}]$ from this study; Norwegian Sea (purple), North Atlantic Ocean, Cape Hatteras, Gulf of Mexico, Ceara Rise, New Zealand shelf, and Sulawesi Margin, Indonesia (grey) sites plotted. A linear regression for all the data is shown in grey; a linear regression for the homo-thermal, homo-haline transect of the Norwegian Sea (purple) is also shown..... 155

Figure 4.5c: Core top Mg/Ca data versus $\Delta[\text{CO}_3^{2-}]$ from this study; Norwegian Sea, North Atlantic Ocean, Cape Hatteras, Gulf of Mexico (light green), Ceara Rise, New

Zealand shelf, and Sulawesi Margin, Indonesia (grey). A linear regression for all the data is shown in grey; a linear regression for the homo-thermal, homo-haline transect of the Gulf of Mexico (light green) is also shown..... 156

Figure 4.6: Mg/Ca data from core top sites from this study (red squares) plotted against temperature for bottom water temperatures above 3 °C. Data from previously published studies (black diamonds) are also plotted against temperatures. The correction factor due to differences in cleaning protocols calculated by the difference between the linear regression intercepts, 3.40 mmol/mol is shown 157

Figure 4.7: Mg/Ca data from core top sites from this study (red squares) plotted against temperature. Data from Little Bahama Bank (Dwyer et al., 1995; black squares), Ontong-Java Plateau (Dwyer et al., 2002; black diamonds), Arctic Ocean < 900 m (Cronin et al., 1996; black x-s), the Arctic Ocean > 900 m (Cronin et al., 1996; black crosses), and all other sources (Cadot et al., 1972; Cadot and Kaesler, 1977; Corregge et al., 1993; Corregge and DeDecker, 1997; small black circles) have all been corrected to account for differences in cleaning. The black line represents a linear regression of all of the data, and the blue line represents a linear regression of data from sites where temperature > 3 °C. Data tables are given in Appendices 6 and 7..... 158

Figure 4.8: The deviation between measured Mg/Ca and temperature based expected Mg/Ca ($\Delta\text{Mg/Ca}$) from Equation 4 plotted versus $\Delta[\text{CO}_3^{2-}]$ for core top sites from the Norwegian Sea (purple), North Atlantic Ocean (blue), Cape Hatteras (dark green), Gulf of Mexico (light green), Ceara Rise (orange), New Zealand shelf (red), and Sulawesi Margin, Indonesia (pink). The black line represents a linear regression of all of the data.

Core top sites with BWT < 3 °C are identified by outer squares, and defined by the blue linear regression..... 159

Figure 4.9: Mg/Ca data corrected for carbonate ion effects from this core top study (red squares) plotted against temperature. Data from Little Bahama Bank (Dwyer et al., 1995; black squares), Ontong-Java Plateau (Dwyer et al., 2002; black diamonds), Arctic Ocean < 900 m (Cronin et al., 1996; black x-s), and the Arctic Ocean > 900 m (Cronin et al., 1996; black crosses) have been corrected to account for differences in cleaning. The black line represents a linear regression of all data, and the green lines represent the 95% confidence intervals..... 160

Figure 4.10: Comparison of published Mg/Ca-temperature calibrations (Table 4.1) with the calibration proposed by this study..... 161

1.0 Dissertation Introduction

1.1 Background

Understanding past variability in oceanic circulation and temperatures is integral to understanding the mechanisms of past climate changes, and gives more confidence in modeled simulations of future climates under changing atmospheric conditions.

Paleoceanography is the study of the history of Earth's oceans, including their chemistry, biology, geology, and oceanography; many of these characteristics are inter-dependent.

Proposed mechanisms for oceanic variability include the amount of incoming solar radiation (insolation; Laskar et al., 1993), location and fluxes of glacial melt water (Broecker and Denton, 1989; Fairbanks, 1989), variability in large-scale wind patterns (Wunsch, 2002; Tedesco and Thunell, 2003; Brauer et al., 2008), and extent of sea ice (Crosta et al., 1998). Geochemical, faunal, and sedimentological proxies are used to reconstruct the various aspects of the past oceans.

Large-scale, deep-ocean circulation is driven by density (temperature and salinity) variations between water masses (Stommel, 1961; Gordon, 1986; Broecker and Denton, 1989); the energy required to mix the deep oceans is supplied by winds and tides (Legrand and Wunsch, 1995; Munk and Wunsch, 1998; Wunsch, 2002; Wunsch, 2003; Toggweiler and Russell, 2008). In the classic view of thermohaline circulation, the trade winds bring tropical waters into the Caribbean Sea, where they further warm and increase in salinity due to increased evaporation (Stommel, 1961; Broecker and Denton, 1989). This warm, salty water flows toward the mid- to high latitudes of the North Atlantic via the Gulf Stream (Broecker and Denton, 1989). Around 35 – 40 °N, the Gulf Stream

bifurcates with some water flowing east into the subtropical gyre, and another portion continuing to the northeast as the North Atlantic Current (NAC; Rossby, 1996). In the mid to high latitude North Atlantic, the NAC loses heat to the atmosphere and mixes with local inputs until it becomes dense enough to sink (Worthington, 1976). This sinking water, termed North Atlantic Deep Water (NADW) flows south and mixes with dense Antarctic Bottom Water, which flows north through the western Atlantic Trough and into the northeastern basin via fracture zones (McCartney and Curry, 1993; Schmitz and McCartney, 1993). NADW flows into the Southern Ocean, where it becomes entrained within the Antarctic Circumpolar Current (Gordon, 1986). This deep water mass slowly upwells in the Indian and Pacific Oceans (Broecker, 1991). Surface and thermocline waters return back to the North Atlantic via the Indo-Pacific Seaway and the Drake Passage, forming an upper limb of the “Conveyor” circulation (Gordon, 1986; Schmitz and McCartney, 1993; Broecker, 1991).

A differing view of what drives global oceanic circulation focuses on the energy inputs into the deep ocean that promotes isopycnal mixing (Wunsch, 2002; Wunsch, 2003). According to this view, large-scale water mass movement is driven by wind and tidal forcings via surface sheer stress (Legrand and Wunsch, 1995; Munk and Wunsch, 1998; Wunsch, 2002; Wunsch, 2003; Toggweiler and Russell, 2008). However, according to this view, climate is still a controlling factor for oceanic circulation because changes in the equatorial-polar temperature gradient cause wind strength variability, which then drives the oceanic circulation system (Wunsch, 2002; Wunsch, 2003; Toggweiler and Russell, 2008). Lowered sea level as a result of the formation of large

continental ice sheets would also affect tidal dynamics, thus altering circulation patterns (Wunsch, 2003).

The growth and decay of large Northern Hemisphere Ice Sheets are linked to insolation changes in the high northern latitudes (Imbrie and Imbrie, 1980; Imbrie et al., 1993). During the Pleistocene, insolation variability resulted from longer-scale eccentricity (~ 100 kyr) modulation of the shorter precession (~ 20 kyr) and obliquity (~ 40 kyr) variations (Laskar et al., 1993). Since past variations in Northern Component Water (NCW, analogous to modern NADW) production is tied to climatic conditions (including surface water temperature and wind strength), studies have linked particular NCW circulation patterns to different climate states, notably the glacial and interglacial end members (e.g., Broecker et al., 1985; Imbrie et al., 1993; Liseicki et al., 2008). However, since the record of insolation is derived from distinct orbital periodicities, it is not simply sinusoidal (Laskar et al., 1993), and therefore, the climate, sea level, and deep-water circulation state may be unique for each glacial and interglacial period, as well as for intermediate climate states. For example, sea level stood ~ 5 m higher during the last interglacial than during the present interglacial (e.g., Broecker et al., 1968; Matthews, 1973).

A decrease in high northern latitude insolation at the Last Glacial Maximum (LGM; ~ 20 ka; Laskar et al., 1993) produced either a weakening (Broecker and Denton, 1989) or a strengthening (Wunsch, 2003) of deep ocean circulation according to the two competing hypotheses. The Oceanic Conveyor hypothesis of thermohaline circulation suggests that decreased insolation led to the build-up of large continental ice sheets, which released fresh water into the northern North Atlantic, decreasing surface salinity,

and thus weakened deepwater formation (Broecker and Denton, 1989). Conversely, decreased insolation would lead to an increase in the equatorial to polar temperature gradient, increasing wind strength, and thus increasing deepwater formation; the decrease in sea level caused by continental ice sheet build-up would also increase tidal forcings, leading to increased circulation vigor (Wunsch, 2002; Wunsch, 2003; Toggweiler and Russell, 2008). Many records that are interpreted to show slower circulation during the LGM (Broecker et al., 1990; Piotrowski et al., 2005; Lynch-Stieglitz et al., 2007) can also be explained by a shoaling of the current axis during the LGM (Wunsch, 2003).

A detailed examination of circulation patterns within the northern North Atlantic shows a more complicated circulation system whereby NADW is produced by the interplay of five components (Figure 1; Worthington, 1976). Two of these components result from the sinking of cold, salty water in the Norwegian and Greenland Seas, which form the Iceland-Scotland Overflow Water (ISOW) and Denmark Straights Overflow Water, respectively (Figure 1; Mann, 1969; Worthington, 1969; 1976). Labrador Sea Water also contributes to NADW, sinking in the Labrador Sea (Figure 1; Mann, 1969). Northward bound AABW flows through the Vema Channel and also contributes to NADW, as does Mediterranean Overflow Water (Reid, 1979; Bryden and Stommel, 1984). It is hypothesized that past variations in these components produced NCW with differing physio-chemical characteristics, and that such changes followed orbital-scale insolation, affecting climate through feedbacks (Hillaire-Marcel et al., 2001, Raymo, 2004).

1.2 Importance of Studying Iceland-Scotland Overflow Water

General patterns of surface and deep-ocean circulation are fairly well established for the Holocene, which in general, are similar to modern circulation (Worthington, 1976; Broecker et al., 1989), and for the LGM, when NCW shoaled allowing dense SCW to extend into the North Atlantic (CLIMAP, 1981; 1984; Curry et al., 1988; Duplessy et al., 1988a; Broecker et al., 1989). The Holocene and LGM circulation patterns are often used as analogs for other interglacial and glacial periods; however, insolation trends are unique for each period (Laskar, 1993) and thus the Holocene and LGM circulations may differ from previous interglacial and glacial circulation patterns. Additionally, less information is available about circulation patterns during intermediate climate states. This is particularly important since, during the past climate cycle of Marine Isotope Chron (MIC) 5e to 1, which spanned ~ 125 kyr, ~ 80 % of that time was spent in intermediate climate states (MIC 5d to 3).

In addition to orbital-scale variability, higher-frequency (millennial, decadal, inter-annual, and seasonal) variability also exists in the climate system (e.g., Broecker et al., 1989; Bond and Lotti, 1995; Bianchi and McCave, 1999). Proposed causes for this variability include; meltwater events (Heinrich, 1988; Broecker et al., 1989; Bond and Lotti, 1995; Kleiven et al., 2008), increased sea ice (Mercer, 1969; Ruddiman and McIntyre, 1981; Bradley and England, 2008); orbital variability (Clement et al., 2001); an extraterrestrial impact (Firestone et al., 2007); and a change in wind patterns (Brauer et al., 2008). Thus, understanding the cause, duration, and circulation response of high-frequency climate events such as the Younger Dryas and Heinrich Events is an active area for paleoceanographic research.

The history of Iceland-Scotland Overflow Water, which contributes about 25 % of modern NCW (Worthington, 1969; 1976), is also poorly understood. Many factors have been proposed to control ISOW strength on a variety of time-scales, including: surface temperature and salinity in the Nordic Seas (Duplessy et al., 1988a), surface inflow (Worthington, 1976), sill depth (Millo et al., 2006), sea ice cover (Prins et al., 2002; Raymo et al., 2004) and tectonics (Wright and Miller, 1996). Iceland-Scotland Overflow Water formation was vigorous during interglacial MIC 1 and 5e (Duplessy et al., 1988a; 1988b; Kissel et al., 1997); however, the history of ISOW strength is unclear for intermediate climate states. Kissel et al. (1997) presumed ISOW was vigorous during MIC 5d, while Kuijpers et al. (1998) and Rasmussen et al. (1996) suggest that it was minimal. Additionally, several studies suggest ISOW was vigorous throughout MIC 3 (Duplessy et al., 1998b; Sarnthein et al., 1994; Kissel et al., 1997; Kuijpers et al., 1998), while others suggest variable ISOW strength due to higher-frequency Heinrich Events and Dansgaard/Oeschger Cycles (Rasmussen et al., 1996; Kissel et al., 1999; Prins et al., 2001; 2002; Rasmussen and Thomsen, 2009). Because ISOW is such a large contributor to NCW (Schmitz and McCartney, 1993; Kissel et al., 1997), ISOW strength has been proposed to control overall NCW circulation patterns (Kuijpers et al., 1998).

The development and improvement of proxies is another critical area of paleoceanographic research. Useful proxies must be widely applicable in the world's oceans and provide reasonable historical results; thus the chemical analysis of biogenic calcite is an often-used paleoceanographic proxy (Urey, 1947; Epstein, 1953; Emiliani, 1955; Chave, 1954; Kennett and Srinivasan, 1983; Boyle and Keigwin, 1987; Oppo and Fairbanks, 1987). Trace metal composition of marine biogenic calcite has become a

useful tool for the estimation of paleo-temperature and paleo-nutrients (Chave, 1954; Boyle and Keigwin, 1987; Dwyer et al., 1995; Rosenthal et al., 1997); however, secondary effects, such as carbonate ion concentration, are also noted (Rosenthal et al., 2006; Elderfield et al., 2006). The ostracod genus *Krithe* is the preferred genus for deepwater trace metal studies in these crustaceans (e.g., Dwyer et al., 1995); however, trace metal incorporation into this microfossil has not been studied as extensively as for foraminifera.

1.3 Region of Study

This dissertation uses sediment cores collected from the Bjorn and Gardar Drifts in the northern North Atlantic to study variability in ISOW strength and NCW circulation patterns (Figure 1). Contourite drifts, like Bjorn and Gardar, are found throughout the North Atlantic where large quantities of sediment are ‘plastered’ against already existing bathymetric features; these regions provide an excellent location for sediment core research because of their high rates of sedimentation (Figure 1; e.g., Hollister et al., 1978; McCave et al., 1980; McCave and Tucholke, 1986; Channell et al., 1997; Hall et al., 1998; Bianchi and McCave, 1999; Faugers et al., 1999; McCave, 2002). As ISOW flows to the southwest along the Reykjanes Ridge, a drift forms along each side of the current axis, with Bjorn Drift to the northwest, and Gardar Drift to the southeast (Figure 1; Davies and Laughton, 1972). Therefore, Bjorn and Gardar Drifts are in key locations to monitor the production history of ISOW (Figure 1; e.g., Oppo and Lehman, 1995; Bianchi and McCave, 1999).

1.4 Paleoceanographic Proxies

Geochemical paleoceanographic proxies, including the stable isotope and trace metal composition of biogenic calcite, are the primary source of information regarding past oceans. Microfossils such as foraminifera and ostracods are common in marine sediment cores and are, thus, often utilized for paleoceanographic reconstructions (Kennett and Srinivasan, 1983). Foraminifera are a nearly ubiquitous group of unicellular protists with calcium carbonate tests; they are described either as planktonic or benthonic (Kennett and Srinivasan, 1983). Planktonic foraminiferal faunal studies are useful for paleotemperature and paleostratification reconstructions (Imbrie and Kipp, 1971; Bé and Tolderlund, 1971; Bé, 1977). Faunal, stable isotopes, and trace metal studies of benthic have been successful in establishing bottom water conditions (Chave, 1954; Boyle and Keigwin, 1987). Benthic ostracods are miniature bi-valved Crustacea with calcium carbonate carapaces (e.g., Brady et al., 1874). Stable isotope and trace metal analysis of the calcium carbonate microfossils secreted by these fauna can provide important information about past oceans (Urey, 1947; Epstein, 1953; Emiliani, 1955; Chave, 1954; Boyle and Keigwin, 1987).

The oxygen isotopic composition of biogenic calcite is a function of both the calcification temperature and the isotopic composition of ambient seawater (Urey, 1947; Epstein, 1953; Emiliani, 1955). Since ^{16}O is preferentially stored in large continental ice sheets, mean ocean oxygen isotopic changes are mainly derived from ice-volume changes, although there is an additional, local component (Urey, 1947; Epstein, 1953; Emiliani, 1955; Shackleton, 1976; Shackleton, 2000). Owing to minimal local changes in deepwater temperature, smoothed benthic oxygen isotopic records are globally similar,

and thus can be used to construct a common chronology (Figure 2; Liseicki and Raymo, 2005).

The carbon isotopic composition of certain benthic foraminifera is shown to reflect ambient seawater composition (e.g., Oppo and Fairbanks, 1987). Large variations in the $\delta^{13}\text{C}$ of water masses allow the potential to reconstruct past water mass changes (e.g., Kroopnick, 1980; Oppo and Fairbanks, 1987; Curry et al, 1988; Venz and Hodell, 2001; Piotrowski et al., 2005). North Atlantic Deep Water is relatively nutrient depleted, yielding high $\delta^{13}\text{C}$ values (Kroopnick, 1980). In contrast, the residence time of deep water in the Pacific Ocean is long, allowing regenerated organic matter to accumulate and decrease $\delta^{13}\text{C}$ values. The Southern Ocean is well mixed vertically owing to the strong West Wind Drift. Southern Ocean $\delta^{13}\text{C}$ values reflect the relative inputs from the North Atlantic, South Atlantic, Indian, and Pacific Oceans. North Atlantic Deep Water has high values ($\sim 1.0\text{‰}$) while the modern Pacific is close to 0.0‰ ; Southern Ocean values are intermediate, around 0.4‰ (Kroopnick, 1980).

The shell chemistry of marine biogenic calcite also records the elemental composition of the ambient seawater during calcification (Chave, 1954; Boyle and Keigwin, 1987; Dwyer et al., 1995). The incorporation of magnesium into foraminiferal and ostracodal calcite varies with calcification temperature (e.g., Chave, 1954; Dwyer et al., 1995; Rosenthal et al., 1997); however, secondary effects due to other parameters, such as carbonate ion concentration, are also noted for benthic foraminifera (Rosenthal et al., 2006; Elderfield et al., 2006). The ostracod genus *Krithe* is the preferred genus for deepwater trace metal studies because *Krithe* carapaces are dissolution-resistant, smooth, and have few pores, minimizing the potential for contamination (Bodergat, 1983;

Swanson and van der Lingen, 1994; Dwyer et al., 1995). The relationship between *Krithe* Mg/Ca ratios and temperature is typically described as linear (Cadot and Kaesler, 1997; Dwyer et al., 1995), suggesting a possible advantage of *Krithe* over benthic foraminiferal studies, which show decreased temperature sensitivity at low temperatures resulting from an exponential Mg/Ca – temperature relationship (Rosenthal et al., 1997; Lear et al., 2002).

The research presented herein uses sedimentological and geochemical proxies outlined above to reconstruct surface and deepwater circulation patterns. Magnetic susceptibility, a measurement for the quantity of magnetic grains within sediment, determined shipboard, is helpful in making core-to-core comparisons (Manley, unpublished). The number of lithic grains ($> 150 \mu\text{m}$) per gram of sediment represents ice-rafted debris (Bond and Lotti, 1995). Percent coarse fraction (sediment $> 63 \mu\text{m}$) and percent carbonate were also determined to characterize the biogenic versus terrigenous sources of sedimentation.

1.5 Chapter Overviews

1.5.1 Chapter 2

The second chapter of this dissertation uses proxies for surface and deepwater conditions from a high sedimentation rate core from southern Gardar Drift to track circulation changes during the Younger Dryas and Holocene (Figure 2). The Younger Dryas period ($\sim 12.9 - 11.5 \text{ ka}$) is characterized by an abrupt, large-scale cooling that interrupted the warming associated with the last deglaciation, and is recorded in terrestrial and oceanic records in the circum-North Atlantic region (Figure 2; Jensen, 1938; Broecker et al., 1989). In contrast with earlier views of decreased deepwater

formation throughout the Younger Dryas (Broecker et al., 1989), the benthic foraminiferal $\delta^{13}\text{C}$ record from Gardar Drift indicates an increase in southern sourced deep waters in the North Atlantic during the early and late Younger Dryas, but not during the mid Younger Dryas. The intervals of lower $\delta^{13}\text{C}$ values are coincident with proxy evidence for a stratified water-column and increased lithic grains per gram of sediment, indicating that increased meltwater delivery and ice rafting during the early and late Younger Dryas lowered the density of surface waters and led to a shoaling of NCW. Our records support recent studies that have identified deepwater variability within the Younger Dryas chron, and provide a mechanistic link between the oceans, cryosphere, and atmosphere during this period of abrupt climate change.

1.5.2. Chapter 3

The third chapter uses benthic foraminiferal $\delta^{13}\text{C}$ records from a transect of cores from Bjorn and Gardar Drifts to investigate variations in ISOW strength (Figure 1; Figure 2). Similar benthic foraminiferal $\delta^{13}\text{C}$ values are recorded at all transect sites during interglacials, indicating a deep, vigorous ISOW. Increased north-south gradient in benthic foraminiferal $\delta^{13}\text{C}$ values indicates that ISOW shoaled during glacial periods, allowing for the intrusion of southern sourced deep waters. During intermediate and glacial climate states, ISOW variability is driven by changes in high northern latitude insolation paced by precessional cycles. Higher-frequency variability in the north-south gradient of benthic foraminiferal $\delta^{13}\text{C}$ during MIC 3 links changes in ISOW to variations in surface water hydrography as recorded by ice rafted debris and cold sea surface temperatures.

1.5.3 Chapter 4

The fourth chapter of this dissertation examines the roles of temperature and carbonate ion concentration on the incorporation of Mg into the carapaces of *Krithe*. Magnesium to calcium (Mg/Ca) ratios were determined for new core tops from the Norwegian Sea, Cape Hatteras shelf, Gulf of Mexico, Sulawesi Margin (Indonesia), New Zealand Shelf, and North Atlantic Ocean; these data were combined with that of previous studies (e.g., Dwyer et al., 2002) to generate a revised coretop calibration. Results from this research show that temperature is the primary control on Mg/Ca ratios and that the Mg/Ca – temperature relationship is best described as linear. Carbonate ion concentration is a secondary control, affecting the Mg/Ca ratios only at low temperatures ($< 3\text{ }^{\circ}\text{C}$). The identification of a ‘Carbonate Ion Effect’ on the magnesium incorporation in ostracodal calcite below $3\text{ }^{\circ}\text{C}$ is identical to the threshold identified for benthic foraminifera (Elderfield et al., 2006), suggesting that the Carbonate Ion Effect is not restricted to benthic foraminifera.

1.6 References

- Bé, A.W.H.. 1977. An ecological, zoogeographic and taxonomic review of recent planktonic foraminifera, in Ramsay, A.T.S. (ed.). Oceanic Micropaleontology. Academic Press, London. 1; 1-100.
- Bé, A.W.H. and D.S. Tolderlund. 1971. Distribution and ecology of living planktonic foraminifera in surface waters of the Atlantic and Indian Oceans, in Funnel, B.M. and Riedel, W.R. (eds.), in: *The Micropaleontology of Oceans*; 105-149.
- Berger, A.. 1992. Orbital Variations and Insolation Database. IGBP PAGES/World Data Center for Paleoclimatology Data Contribution Series # 92-007. NOAA/NGDC Paleoclimatology Program, Boulder CO, USA.
- Bloom, A.L., Broecker, W.A., Chappell, J.M.A., Matthews, R.K., and Mesolella, K.J.. 1974. Quaternary sea level fluctuations on a tectonic coast: New $^{230}\text{Th}/^{234}\text{U}$ dates from the Huon Peninsula, New Guinea. *Quaternary Research*. 4; 185-205.

- Bianchi, G.G. and N. McCave. 1999. Holocene periodicity in North Atlantic climate and deep-ocean flow south of Iceland. *Nature*. 397; 515-517.
- Bond, G.C. and R. Lotti. 1995. Iceberg Discharges into the North Atlantic on Millennial Time Scales During the Last Glaciation. *Science*. 267; 1005-1010
- Boyle, E.A. and L.D. Keigwin. 1987. North Atlantic thermohaline circulation during the past 20,000 years linked to high-latitude surface temperature. *Nature*. 330; 35-40.
- Bradley, R.S. and J.H. England. 2008. The Younger Dryas and the Sea of Ancient Ice. *Quaternary Research*. 70; 1-10.
- Brady, G.S., Crossey, H.W., and D. Robertson. 1874. A monograph of the Post-Tertiary Entomostraca of Scotland Including Species from England and Ireland. Palaeontographical Society of London. 274 pp.
- Brauer, A., Haug, G.H., Dulski, P., Sigman, D.M., and J.W. Negendank. 2008. An abrupt wind shift in Western Europe at the onset of the Younger Dryas cold period. *Nature Geoscience*. 1; 520-524.
- Broecker, W.S., Thurber, D.L., Goddard, J., Ku, T.L., Matthews, R.K., and Mesollela, K.J.. 1968, Milankovitch hypothesis supported by precise dating of coral reefs and deep sea sediments. *Science*. 159; 297-300.
- Broecker, W.S., Peteet, D.M., and D. Rind. 1985. Does the ocean-atmosphere system have more than one stable mode of operation? *Nature*. 315; 21-26.
- Broecker, W.S. and G.H. Denton. 1989. The role of ocean-atmosphere reorganizations in glacial cycles. *Geochimica et Cosmochimica Acta*. 53; 2465-2501.
- Broecker, W.S., Kennett, J.P., Flower, B.P., Teller, J.T., Trumbore, S., Bonani, G., and W. Wolfi. 1989. Routing of meltwater from the Laurentide Ice Sheet during the Younger Dryas cold episode. *Nature*. 341; 318-321.
- Broecker, W.S.. 1991. The great conveyor belt. *Oceanography*. 4 (2); 79-89.
- Bryden, H.L. and H.M. Stommel. 1984. Limiting processes that determine basic features of circulation of the Mediterranean Sea. *Oceanography Acta*. 7; 289-296.
- Channell, J.E.T., Hodell, D.A., and B. Lehman. 1997. Relative geomagnetic paleointensity and $\delta^{18}\text{O}$ at ODP Site 983 (Gardar Drift, North Atlantic) since 350 ka. *Earth and Planetary Science Letters*. 153; 103-118.
- Chave, K.E.. 1954. Aspects of the Biogeochemistry of Magnesium 1: Calcareous Marine Organisms. *Journal of Geology*. 62; 266-283.

- Clement, A.C., Cane, M.A., and R. Seager. 2001. An orbitally driven source for abrupt climate change. *Journal of Climate*. 14 (11); 2369-2372.
- CLIMAP Project Members. 1981. Seasonal reconstructions of the Earth's surface at the last glacial maximum in Map Series, Technical Report MC-36. Boulder, Colorado: Geological Society of America.
- CLIMAP Project Members. 1984. The last Interglacial Ocean. *Quaternary Research*. 21; 123-224.
- Curry, W.B., Duplessy, J.C., Labeyrie, L.D., and N.J. Shackleton. 1988. Changes in the distribution of $\delta^{13}\text{C}$ of deep water sigma CO_2 between the last glaciation and the Holocene. *Paleoceanography*. 3(3); 317-341.
- Crosta, X., Pichon, J.-J., and L.H. Burckle. 1998. Application of modern analog technique to marine Antarctic diatoms: Reconstruction of maximum sea-ice extent at the Last Glacial Maximum. *Paleoceanography*. 13 (3); 284-297.
- Davies, T.A. and A.S. Laughton. 1972. Sedimentary processes in the North Atlantic. *in: Initial Reports of the D.S.D.P.* (Ed. A.S. Laughton, W.A. Berggren). 12; 905-934.
- Duplessy, J.C., Shackleton, N.J., Fairbanks, R.G., Labeyrie, L., Oppo, D.W., and N. Kallel. 1988a. Deepwater source variations during the last climatic cycle and their impact on the global deep-water circulation. *Paleoceanography*. 3(3); 342-360.
- Duplessy, J.C., Labeyrie, L., and P.L. Blanc. 1988b. Norwegian Sea Deep Water Variations Over the Last Climatic Cycle: Paleo-oceanographical Implications. *Long and Short Term Variability of Climate*. 16; 86-116.
- Dwyer, G.S., Cronin, T.M., and P.A. Baker. 2002. Trace elements in marine ostracods. *Geophysical monograph*. 131; 205-225.
- Elderfield, H., Yu, J., Anand, P., Kiefer, T., and B. Nyland. 2006. Calibrations for benthic foraminiferal Mg/Ca paleothermometry and the carbonate ion hypothesis. *Earth and Planetary Science Letters*. 250; 633-649.
- Emiliani, C.. 1955. Tropical Paleotemperatures. *Science*. 268; 1264.
- Epstein, S., Buchsbaum, R., Lowenstam, H.A., and H.C. Urey. 1953. Revised carbonate-water isotopic temperature scale. *Geological Society of America Bulletin*. 64; 1315-1326.
- Faugers, J.C., Stow, D.A.C., Imbert, P., and A. Viana. 1999. Seismic features diagnostic of contourite drifts. *Marine Geology*. 162; 1-38.

- Firestone, R.B., et al.. 2007. Evidence for an extraterrestrial impact 12,900 years ago that contributed to the megafaunal extinctions and the Younger Dryas cooling. *PNAS*. 104 (41); 16016-16021.
- Gordon, A.J.. 1986. Interocean exchange of thermocline water. *Journal of Geophysical Research*. 91; 5037-5046.
- Hall, I.R., McCave, I.N., Chapman, M.R., and N.J. Shackleton. 1998. Coherent deep flow variation in the Iceland and American basins during the last interglacial. *Earth and Planetary Science Letters*. 164; 15-21.
- Heinrich, H.. 1988. Origin and Consequences of Cyclic Ice Rafting in the Northeast Atlantic Ocean during the past 130,000 Years. *Quaternary Research*. 29; 142-152.
- Hillaire-Marcel, C., de Vernal, A., Bilodeau, G., and A.J. Weaver. 2001. Absence of deep-water formation in the Labrador Sea During the last interglacial period. *Nature*. 410; 1073-1078.
- Hollister, C.D., Flood, R.D., and I.N. McCave. 1978. Plastering and decorating in the North Atlantic. *Oceanus*. 21 (1); 5-13.
- Imbrie, J. and N.G. Kipp. 1971. A new micropaleontological method for Quantitative Paleoclimatology: Application to a late Pleistocene Caribbean Core, in *The Late Cenozoic Glacial Ages*. ed. K.K. Turekian, Yale Univ. Press, New Haven, CT. pp. 71-181.
- Imbrie, J. and J.Z. Imbrie. 1980. Modeling the Climatic Response to Orbital Variations. *Science*. 207; 943-953.
- Imbrie, J., A., Berger, E.A. Boyle, S.C. Clemens, A. Duffy, W.R. Howard, G. Kulka, J. Kitzbach, D.G. Martinon, A. McIntyre, A.C. Mix, B. Molfino, J.J. Morley, L.C. Peterson, N.G. Pisias, W.L. Prell, M.E. Raymo, N.J. Shackleton, and J. R. Toggweiler. 1993. On the structure and origin of major glaciation cycles 2. The 100,000-year cycle. *Paleoceanography*. 8 (6); 699-736.
- Jensen, K. 1938. Some west Baltic pollen diagrams. *Quartar*. 1; 124-139.
- Kennett, J.P. and M.S. Srinivasan. 1983. Neogene Planktonic Foraminifera: A Phylogenetic Atlas. Hutchinson Ross. pp. 265.
- Kissel, C., Laj, C., Lehman, B., Labyrie, L., and V. Bout-Roumazeilles. 1997. Changes in the strength of the Iceland-Scotland Overflow Water in the last 200,000 years: Evidence from magnetic anisotropy analysis of core SU90-33. *Earth and Planetary Science Letters*. 152; 25-36.

- Kleiven, H., Kissel, C., Laj, C., Ninnemann, U.S., Richter, T.O., and E. Cortijo. 2008. Reduced North Atlantic Deep Water Coeval with Glacial Lake Agassiz Freshwater Outburst. *Science*. 319; 60-64.
- Kroopnick, P.. 1980. The Distribution of ^{13}C in the Atlantic Ocean. *Earth and Planetary Science Letters*. 49; 469-484.
- Kuijpers, A., Troelstra, S.R., Wisse, M., Nielsen, S.H., T.C.E. van Weering. 1998. Norwegian Sea overflow variability and NE Atlantic surface hydrography during the past 150,000 years. *Marine Geology*. 152; 75-99.
- Laskar, J., Joutel, F., and F. Boudin. 1993. Orbital, precessional, and insolation quantities for the Earth from -20 Myr to +10 Myr. *Astronomy and Astrophysics*. 270; 522-533.
- Lisiecki, L.E. and M.E. Raymo. 2005. A Pliocene-Pleistocene stack of 57 globally distributed benthic $\delta^{18}\text{O}$ records. *Paleoceanography*. 20 (1003); 1-17.
- Liseicki, L.E., Raymo, M.E., and W.B. Curry. 2008. Atlantic overturning responses to Late Pleistocene climate forcings. *Nature*. 456; 85-88.
- Lynch-Stiegliz, J., Adkins, J.F., Curry, W.B., Dokken, T., Hall, I.R., Herguera, J.C., Hirschi, J.J.M., Ivanova, E.V., Kissel, C., Marchal, O., Marchitto, T.M., McCave, I.N., McManus, J.F., Mulitza, S., Ninnemann, U., Peeters, F., Yu, E.-F., and R. Zahn. 2007. Atlantic Meridonal Overturning Circulation During the Last Glacial Maximum. 316; 66-69.
- Matthews, R.K.. 1973. Relative elevation of late Pleistocene high sea level stands: Barbados uplift rates and their implication. *Quaternary Research*. 3; 147-153.
- Mann, C.R.. 1969. Temperature and salinity characteristics of the Denmark Strait overflow. *Deep-Sea Research*. 16; 125-137.
- McCartney, M.S. and R.A. Curry. 1993. Transequatorial Flow of Antarctic Bottom Water in the Western Atlantic Ocean: Abyssal Geostrophy at the Equator. *Journal of Physical Oceanography*. 23; 1264-1277.
- McCave, I.N., Lonsdale P.F., Hollister C.D., and W.D. Gardner. 1980. Sediment Transport over the Hatton and Gardar Contourite Drifts. *Journal of Sedimentary Petrology*. 50 (4); 1049-1062.
- McCave, I.N. and B.E. Tucholke. 1986. Deep current-controlled sedimentation in the western North Atlantic. In Vogt, P.R. and B.E. Tucholke (Eds.), *The Geology of North America, Vol. M, The Western North Atlantic Region*. Geological Society of America, Boulder, CO; 451-468.

- McCave, I.N.. 2002. A Poisoned Chalice? *Science*. 298 (5596); 1186-1187.
- Mercer, J.H.. 1969. The Allerod Oscillation: A European Climatic Anomaly? *Arctic and Alpine Research*. 1 (4); 227-234.
- Millo, C., Sarnthein, M., Voelker, A., and H. Erlenkeuser. 2006. Variability of the Denmark Strait Overflow during the Last Glacial Maximum. *Boreas*. 1; 50-60.
- Munk, W. and C. Wunsch. 1998. Abyssal recipes II: energetics of tidal and wind mixing. *Deep Sea Research Part I: Oceanic Research Papers*. 45 (12); 1977-2010.
- Oppo, D.W. and R.G. Fairbanks. 1987. Variability in the deep and intermediate water circulation of the Atlantic Ocean during the past 25,000 years; Northern Hemisphere modulation of the Southern Ocean. *Earth and Planetary Science Letters*. 86 (1); 1-15.
- Oppo, D.W. and S.J. Lehman. 1995. Suborbital timescale variability of North Atlantic Deep Water during the past 200,000 years. *Paleoceanography*. 10(5); 901-910.
- Piotrowski, A.M., Goldstein, S.L., Hemming, S.R., and R.G. Fairbanks. 2005. Temporal relationships of carbon cycling and ocean circulation at glacial boundaries. *Science*. 307; 1933-1938.
- Prins, M.A., Troelstra, S.R., Kruk, R.W., van der Borg, K., de Jong, A.F.M., and G.J. Weltje. 2001. The Late Quaternary Sediment Record of the Reykjanes Ridge, North Atlantic. *Radiocarbon*. 43 (2B); 939-947.
- Rasmussen, T.L Thomson, E., van Weering, T.C.E., and L. Labeyrie. 1996. Rapid changes in surface and deep water conditions at the Faeroe Margin during the last 58,000 years. *Paleoceanography*. 11(6); 757-771.
- Rasmussen, T.L. and E. Thomson. 2009. Ventilation changes in intermediate water on millennial time scales in the SE Nordic seas, 65-11 kyr BP. *Geophysical Research Letters*. 36 1-5.
- Raymo, M.E., Oppo, D.W., Flower, B.P., Flower, Hodell, D.A., McManus, J.F., Venz, K.A., Kleiven, K.F., and K. McIntyre. 2004. Stability of North Atlantic Water Masses in Face of Pronounced Climate Variability During the Pleistocene. *Paleoceanography*. 19; 1-13.
- Reid, J.. 1979. On the contribution of the Mediterranean Sea outflow to the Norwegian-Greenland Sea. *Deep Sea Research Part A. Oceanographic Research Papers*. 26(11); 1199-1223.
- Rosenthal, Y., Boyle, E.A., and N. Slowey. 1997. Temperature control on the incorporation of Mg, Sr, F, and Cd into benthic foraminiferal shells from Little

- Bahama Bank: prospects for thermocline Paleoceanography. *Geochimica et Cosmochimica Acta*. 61; 3363-3643.
- Rosenthal, Y., Lear, C.H., Oppo, D.W., and Linsley, B.K. 2006. Temperature and carbonate ion effects on Mg/Ca and Sr/Ca ratios in benthic foraminifera: aragonitic species *Hoeglundia elegans*. *Paleoceanography*. 21; 1-14.
- Rosby, T.. 1996. The North Atlantic Current and surrounding waters: At the crossroads. *Reviews in Geophysics*. 34; 463-481.
- Ruddiman, W.F. and A. McIntyre. 1981. The North Atlantic Ocean during the last deglaciation. *Paleogeography, Paleoclimatology, Paleoecology*. 35; 145-214.
- Sarnthein, M., Winn, K., Jung, S.J.A., Duplessy, J.-C., Labeyrie, L., Erlenkeuser, H., and G. Ganssen. 1994. Changes in east Atlantic deepwater circulation over the last 30,000 years: Eight time slice reconstructions. *Paleoceanography*. 9(2); 209-267.
- Schmitz, W.J. and M.S. McCartney. 1993. On the North Atlantic Circulation. *Reviews of Geophysics*. 31 (1); 29-49.
- Shackleton, N.J.. 2000. The 100,000-year Ice-Age cycle identified and found to lag temperature, carbon dioxide, and orbital eccentricity. *Science*. 289; 1897-1902.
- Stommel, H.. 1961. Thermohaline convection with two stable regimes of flow. *Tellus*. 13; 224-230.
- Tedesco, K. and R.C. Thunell. 2003. High Resolution Tropical Climate Record for the last 6,000 years. *Geophysical Research Letters*. 30(17); 1-4.
- Urey, H.C.. 1947. The thermodynamic properties of isotopic substances. *Journal of the Chemical Society London*; 562-581.
- Venz, K.A., and D.A. Hodell. 2001. New evidence for changes in Plio-Pleistocene deep circulation from Southern Ocean ODP Leg 177 Site 1090. *Paleogeography, Paleoclimatology, Paleoecology*. 182; 197-220.
- Waelbroeck, C., Labeyrie, L., Michel, E., Duplessy, J.C., McManus, J.F., Lambeck, K., Balbon, E., and M. Labracherie. 2002. Sea-level and deep water temperature changes derived from benthic foraminifera isotopic records. *Quaternary Science Reviews*. 21; 295-305.
- Worthington, L.V.. 1969. An attempt to measure the volume transport of Norwegian Sea overflow water through the Denmark Strait. *Deep-Sea Research*. 16; 421-432.
- Worthington, L.V.. 1976. On the North Atlantic Circulation. Johns Hopkins University Press; Baltimore, MD.

- Wright, J.D. and K.G. Miller. 1996. Control of North Atlantic Deep Water circulation by the Greenland-Scotland Ridge. *Paleoceanography*. 11(2); 157-170.
- Wright, J.D., Sheridan, R.E., Miller, K.G., Uptegrove, J., Cramer, B.S., and J.V. Browning. 2009. Late Pleistocene Sea level on the New Jersey Margin: Implications to eustacy and deep-sea temperature. *Global and Planetary Change*. 66; 93-99.

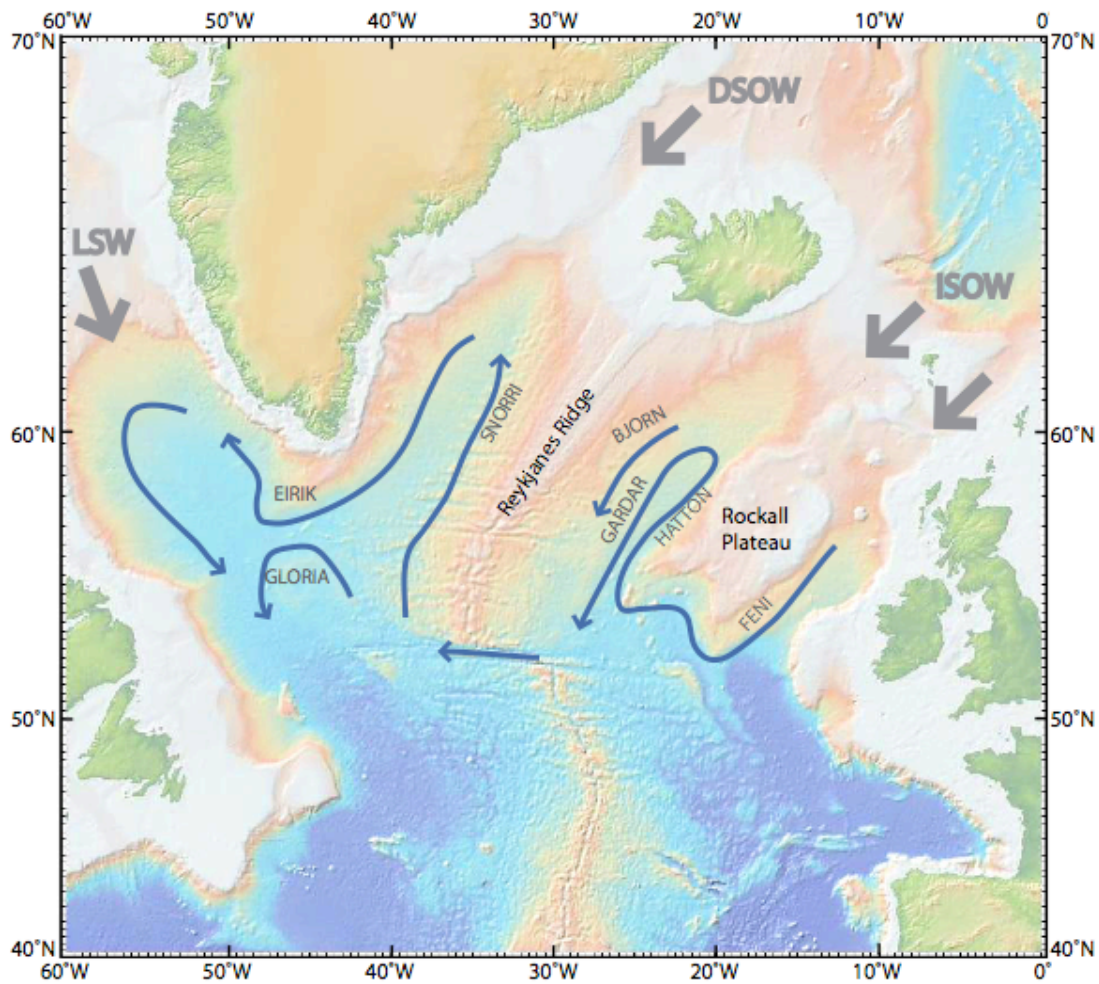


Figure 1.1: Shaded bathymetry (Smith and Sandwell, 1994) of the North Atlantic Ocean showing major drifts (uppercase lettering), generalized bottom currents (blue arrows), Iceland Scotland Overflow (ISOW), Denmark Straits Overflow (DSOW), and Labrador Sea Water (LSW; gray arrows).

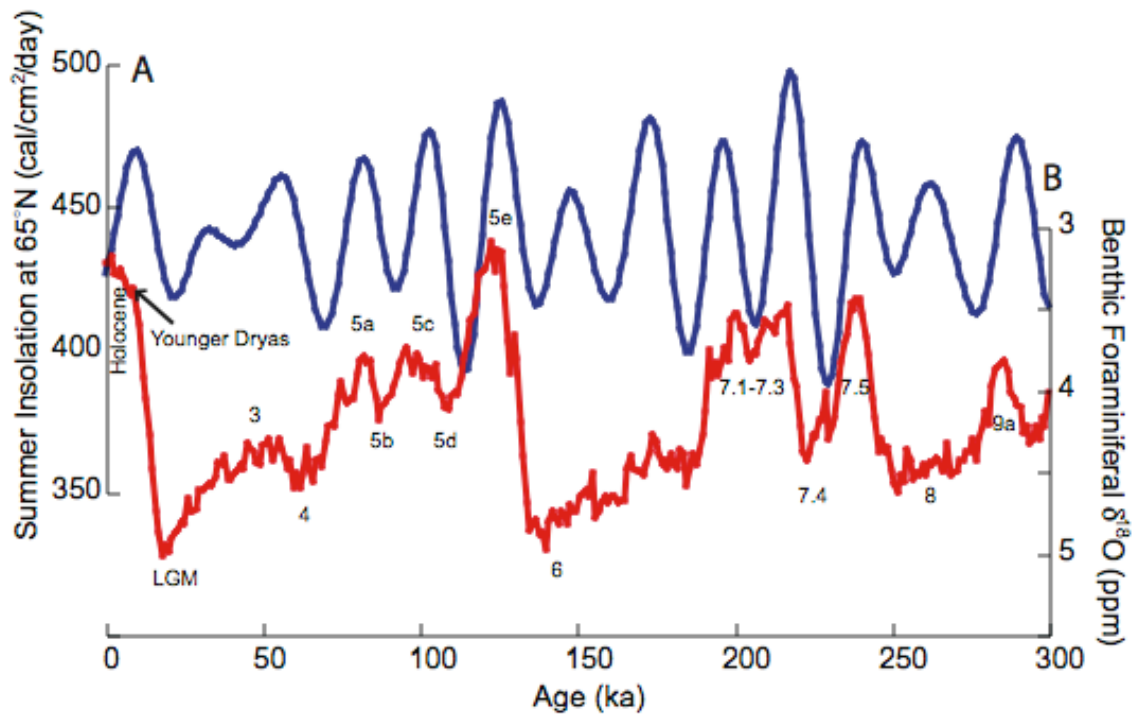


Figure 1.2: (A) Insolation (Berger, 1992) and (B) benthic foraminiferal $\delta^{18}\text{O}$ (Liseicki and Raymo, 2005) since 300 ka. Shown are the Holocene, Younger Dryas, Last Glacial Maximum (LGM), and MIC 3-9.

2.0 Meltwater Influence on Northern Component Water During the Younger Dryas

2.1 Abstract

Abrupt, large-scale climate events within the Younger Dryas chonozone are recorded in terrestrial and oceanic records in the circum North Atlantic region, the triggering mechanism is still debated. Here, I present high-resolution records from southern Gardar Drift, south of Iceland, that show decreases in benthic foraminiferal $\delta^{13}\text{C}$ values ($\sim 0.4\text{‰}$) at the beginning (~ 13.0 to 12.9 ka) and end of the Younger Dryas (~ 11.8 to 11.5 ka), with a return to high values ($\sim 1.0\text{‰}$) during the mid- Younger Dryas (~ 12.8 to 12.0 ka). Intervals of lower $\delta^{13}\text{C}$ values are coincident with high $\Delta\delta^{18}\text{O}_{N.pachyderma(s) - G. bulloides}$ and high abundance of lithic grains/gram. These records indicate that Northern Component Water (NCW) shoaled at the beginning of the Younger Dryas, but deepened during the mid-Younger Dryas, suggesting that NCW weakened at the start of the Younger Dryas but recovered after ~ 300 years. A second shoaling and recovery of NCW occurred during the late Younger Dryas, coinciding with the termination of the Younger Dryas cool period. Surface water $\delta^{18}\text{O}$ records indicate increased stratification reflecting surface freshening. Lithic abundances and reported occurrences of meltwater events indicate increased meltwater delivery during the early and late Younger Dryas. These intervals of higher meltwater led to brief reorganizations of deepwater currents. This southern Gardar deepwater record contrasts with earlier studies that suggested that the persistent cold conditions during the Younger Dryas were associated with depressed NCW formation throughout this interval.

2.2. Introduction

The last deglaciation was interrupted from ~ 12.9 to 11.6 ka by a return to cold, glacial-like temperatures in the circum North Atlantic region, termed the Younger Dryas chronozone because of the dominance of *Dryas octopetala* pollen in the British Isles and in parts of Europe (Mangerud et al., 1974). In the circum North Atlantic region, the Younger Dryas was initially observed as a cold event in terrestrial records (Jensen, 1938). Subsequent studies have identified cool to cold conditions in North Atlantic sediment cores, as well as in ice core records (Dansgaard, 1984; Broecker et al., 1989; Alley et al., 1995). The magnitude of the abrupt climatic changes recorded in the circum-North Atlantic region during the Younger Dryas have led researchers to search for links among the oceans, atmosphere, and cryosphere.

Broecker et al. (1989) proposed that the abrupt Younger Dryas cooling was caused by the addition of meltwater to the northern North Atlantic (Johnson and McClure, 1976) that disrupted thermohaline circulation (Rooth, 1982). Broecker et al. (1989) attributed the meltwater to a rerouting of Laurentide meltwater drainage from the Mississippi River to the St. Lawrence River. It was proposed that this meltwater intrusion diverted the northward flow of the warm, salty Gulf Stream, causing cooling of the North Atlantic region (Broecker et al., 1989). Broecker et al. (1989) suggested that a ‘fresh water cap’ in the northern North Atlantic would have altered deepwater formation for the duration of the Younger Dryas.

Previous studies have linked the Younger Dryas cooling with a weakened NCW flux in sedimentologic records including: benthic foraminiferal $\delta^{13}\text{C}$ (e.g., Boyle and Keigwin, 1987); Pa/Th (McManus et al., 2004); ϵNd (Piotrowski et al., 2005; Pahnke et

al., 2008); ^{14}C (Hughen et al., 1998; Goslar et al., 1995; Robinson et al., 2005; Eltgroth et al., 2006); benthic foraminiferal Cd/Ca (Boyle and Keigwin, 1987; Came et al., 2008); and sortable silt (Evans and Hall, 2008; Praetorius et al., 2008). Records of deepwater circulation with higher resolution indicate some variability in NCW circulation patterns within the Younger Dryas, but have yet to establish a coherent pattern (McManus et al., 2004; Eltgroth et al., 2006; Carlson et al., 2007).

In addition to the “Meltwater Hypothesis,” other mechanisms have been proposed to explain the Younger Dryas chronozone including: increased Arctic sea ice (Mercer, 1969; Ruddiman and McIntyre, 1981; Bradley and England, 2008); a change in the El-Nino Southern Oscillation (Clement et al., 2001); an extraterrestrial impact (Firestone et al., 2007); and a change in wind patterns (Brauer et al., 2008). Understanding the mechanism(s) that caused the surface cooling and altered North Atlantic circulation patterns during the Younger Dryas is critical for understanding how quickly external forcings are propagated to the climate and ocean systems. Additionally, it is important to identify the cause of the termination of the Younger Dryas, which ushered in the warmer Holocene climate.

Here, I present high-resolution proxy records of surface and deepwater environmental conditions from the North Atlantic to test the hypothesis that surface water freshening altered deepwater circulation patterns during the Younger Dryas. Records of proxies for surface water temperature (planktonic foraminiferal assemblage and $\delta^{18}\text{O}$ values), surface water stratification ($\Delta\delta^{18}\text{O}$), ice rafted debris (IRD; % lithics), bottom water temperature ($\delta^{18}\text{O}$ benthic foraminifera), and deep ocean circulation ($\delta^{13}\text{C}$ benthic

foraminifera) are used to constrain the surface and deepwater hydrography during this critical interval.

2.3 Methods

2.3.1. Sample processing

Jumbo piston core 11JPC was collected by the *R/V Knorr* on cruise 166, leg 14, from 2707 m water depth on Gardar Drift (56°14'N, 27°39'W), in the eastern North Atlantic (Figure 2.1). Iceland Scotland Overflow Waters (ISOW), the largest eastern source of modern North Atlantic Deepwater, bathes this site (Worthington, 1979). High sedimentation rates (~ 18 cm/kyr) offer high temporal resolution during the Younger Dryas, and throughout the Holocene.

The top 222 cm of core 11JPC was sampled at 1 cm intervals to study changes in surface water hydrography during the Holocene and Younger Dryas. The > 150 µm fraction of each sample was split using a microsplitter into an aliquot containing at least 300 planktonic foraminifera (Imbrie and Kipp, 1971). Abundances of the planktonic foraminiferal species were determined by counting. The three most common taxa were left-coiling *Neogloboquadrina pachyderma* (sinistral; s), right-coiling *Neogloboquadrina pachyderma* (dextral; d), and *Globogerina bulloides*. These results are reported as percent, with respect to the total planktonic foraminiferal assemblage. The polar biogeographic region is dominated by *N. pachyderma* (s), thus % *N. pachyderma* (s) has been used as an indicator of relative temperature changes for polar to subpolar regions (Bé and Tolderlund, 1971; Bé, 1977).

Up to 15 tests of each of the planktonic foraminifera species *N. pachyderma* (s) and *G. bulloides* were selected using a binocular microscope from the 250 – 350 µm size

fraction of each sample and analyzed for stable isotopic composition on an Optima Mass Spectrometer at Rutgers University (1 σ laboratory precision of an internal lab standard is 0.08 ‰ for $\delta^{18}\text{O}$ and 0.05 ‰ for $\delta^{13}\text{C}$). The difference ($\Delta\delta^{18}\text{O}$) between the $\delta^{18}\text{O}$ values of the surface-dwelling *G. bulloides* and thermocline-dwelling *N. pachyderma* (s) was also calculated by subtracting the *G. bulloides* $\delta^{18}\text{O}$ value from *N. pachyderma* (s) $\delta^{18}\text{O}$ values for each sample to determine the differences in environment of calcification. The $\Delta\delta^{18}\text{O}$ values can reflect temperature due to seasonal biases or vertical stratification due to fresh water inputs (Lagerklint and Wright, 1999). The number of lithic grains (> 150 μm) per gram of sediment was counted as a proxy for ice-rafted detritus (IRD; Bond and Lotti, 1995). The location of 11JPC is too far from terrestrial sources to have a large quantity of lithic grains transported to the site by means other than ice rafting (Bond and Lotti, 1995).

Deepwater variations were reconstructed by measuring downcore benthic foraminiferal $\delta^{13}\text{C}$ values. Up to 5 tests of the benthic foraminifera *Planulina wuellerstorfi* were selected from the 250 – 350 μm size fraction and analyzed for stable oxygen and carbon isotopic composition. Differences between the $\delta^{13}\text{C}$ value of bottom waters in the North Atlantic and the South Atlantic (~ 1 ‰ and ~ 0.4 ‰, respectively in the modern oceans; Kroopnick, 1985), which are recorded in benthic foraminifera, allow for the use of benthic foraminiferal $\delta^{13}\text{C}$ as a water mass tracer (e.g., Belanger et al., 1981; Graham et al., 1981). Only *P. wuellerstorfi* tests were chosen for analysis since my own work shows that some *Cibicidoides* taxa (e.g., *C. robertsoniensis*) do not record equilibrium values and may be up to 1 ‰ lower in $\delta^{13}\text{C}$ values (Elmore and Wright, unpublished data). All data is given in Appendix 1.

2.3.2. Age Model

Fifteen AMS ^{14}C ages constrain the age model for 11JPC (Figure 2.2; Table 2.2). For each AMS ^{14}C analysis, 4 - 6 mg of planktonic foraminifera *Globigerina bulloides* were selected using a binocular microscope and sonified in deionized water. Samples were then analyzed at the Keck Center for Accelerator Mass Spectrometry at the University of California, Irvine. The resulting radiocarbon ages were converted to calendar ages according to the Fairbanks0805 calibration, after a 400-year reservoir correction was applied (Fairbanks et al., 2005; Figure 2.2). The Younger Dryas termination at 183 cm, as recorded in % *N. pachyderma* (s) and in $\delta^{18}\text{O}$ of *N. pachyderma* (s), was used as additional chrono-stratigraphic tie point (11.5 ka; Ellison et al., 2006, Alley et al., 1995). AMS dates at 145 and 149 cm were not included in the age model because they produced slight age reversals (Figure 2.2; Table 2.1).

The resulting age model revealed an ~ 19 kyr hiatus between 220 and 227 cm, from 13.6 to ~ 33 ka; this is consistent with a sediment color change at 222 cm in the core, indicating an unconformity at this depth. Continual sedimentation has been suggested on Gardar Drift since the early- to middle- Miocene on million-year time-scales (Huizhong and McCave, 1990; Wold, 1994). However, at 11JPC, an initial phase of erosion associated with the reinvigoration of NCW during the early Bolling/Allerod (Charles and Fairbanks, 1992), removed sediments that were deposited during Marine Isotope Chrons 2 and 3. Erosion due to bottom water current intensification has been previously suggested for locations in the South Atlantic (e.g., Ciesielski et al., 1982). My age model for the Younger Dryas and Holocene sections of core 11JPC, indicates that continual accumulation immediately followed this erosional event (Figure 2.2).

Given a typical bioturbation depth for the region of 10 cm (Thomson et al., 2000), it is reasonable to expect that the AMS ^{14}C date at 220 cm, immediately above this unconformity, may be contaminated by bioturbation of some older material from below the hiatus; AMS ^{14}C dates at 213 and 198 cm could also be contaminated. To estimate the degree of contamination at 220 cm from older sub-hiatus material, the ^{14}C activity of older material ($A_{\text{pre-hiatus}}$), was calculated by:

$$[1] \quad A_{\text{pre-hiatus}} = A_o * \exp(-\lambda * t)$$

(Rutherford, 1906). Where A_o is the initial activity of ^{14}C (13.56 dpm/g; Karlen et al., 1966), λ is the decay constant for ^{14}C ($1.209 * 10^{-4} \text{ y}^{-1}$; Godwin, 1962 after Libby, 1955), and t is the age of the sub-hiatus material ($\sim 33,000 \text{ y}$). Solving equation 1 yields $A_{\text{pre-hiatus}} = 0.2509$. The excess ^{14}C activity above the hiatus due to bioturbation of the pre-hiatus material ($A_{\text{post-hiatus*}}$) was calculated by the following equation from Berger and Heath (1968):

$$[2] \quad A_{\text{post-hiatus*}} = A_{\text{pre-hiatus}} (1 - \exp(-T/m)) * \exp(-(L_e + m)/m)$$

where T is the thickness of older sediment (1 m; see chapter 3 of this dissertation), m is the thickness of the layer that was mixed due to bioturbation (10 cm; e.g., Thomson et al., 2000), L_e is the depth above the hiatus (2 cm at 220 cm). Solving equation 2 yields an activity at 220 cm of $A_{220\text{cm}*} = 0.07558$.

The effect of bioturbation on the sediment at 220 cm can be deconvolved by:

$$[3] \quad A_{220\text{cm}} = A_{\text{measured}} + A_{\text{post-hiatus*}}$$

where A_{measured} at 220 cm (13.62 ka) = 2.5878, this yields an activity at 220 cm of 2.6634, which is equivalent to an AMS ^{14}C age of 13.46 ka. This indicates that the foraminifera are recording an age 160 years older than the sediment age due to the bioturbation of older material. Doubling the bioturbation distance results in a corrected age of 13.44 ka at 220 cm, which is not significantly different than the original estimate. By following the same method, the bioturbation corrected ages at 213 cm is 13.22 ka, which is 120 years younger than the measured AMS ^{14}C date of 13.34 ka, demonstrating that the bioturbation of older material has a small effect on the age at this depth. Also, by the same method, the bioturbation corrected age at 198 cm is 11.97 ka, which is within the error of the measured AMS ^{14}C date of 11.99 ka, indicating that bioturbation of older material is not affecting the age at this depth.

Following the bioturbation correction, the AMS ^{14}C ages are nearly linear, indicating linear sedimentation rates, suggesting that normal sedimentation has occurred at the site since 13.6 ka (Figure 2.2). Thus, ages between all AMS ^{14}C dated levels, including the bioturbation corrected ages for 220 and 213 cm, and the chrono-stratigraphic tie point at 183 cm were linearly interpreted, yielding a sedimentation rate of ~ 16 cm/kyr throughout the Holocene and Younger Dryas sections.

The age model for core 11JPC is complicated by some uncertainties due to the relatively long hiatus, AMS ^{14}C dating, and the AMS ^{14}C reservoir correction. I addressed these issues by first mathematically modeling the effects of the bioturbation across the

hiatus, which introduces an age uncertainty of ~ 200 years for the sediments immediately above the unconformity. Second, while it is conventional to pick the most common planktonic foraminifera for AMS ^{14}C dating to minimize the effects of bioturbation (Broecker et al., 1988), *G. bulloides* were selected for AMS ^{14}C dates throughout core 11JPC, so as not to introduce species offsets. AMS ^{14}C dates on different species from the same level yielded differences of ~ 500 years in some LGM sediments (Berger et al., 1987; Bard et al., 1988a; 1988b; Broecker et al., 1988; Backstrom et al., 2001).

Globigerina bulloides was chosen for dating because it still makes up nearly 30 % of the planktonic foraminiferal species assemblage in the Younger Dryas section (Figure 2.2). Finally, a large degree of uncertainty surrounds the appropriate reservoir correction for the Younger Dryas, which range from 400 (Stuiver and Polach, 1977; Fairbanks et al., 2005) to 500 (deMenocal et al., 2000) to 800 years (Bard et al., 1994; Hafladason et al., 2005). A reservoir correction of 400 years was applied to all AMS ^{14}C dates for core 11JPC, which probably represents the minimum reservoir correction; applying a larger reservoir correction would yield a younger age for the onset of the Younger Dryas by as much as a few hundred years (Figure 2.3).

2.4. Results

2.4.1. Surface Water Results

The top 222 cm of the core is divided into two chronozones based on the age model. The Younger Dryas section is from 222 to 184 cm and the Holocene section is from 183 cm to the top of the core. The Younger Dryas section of the core is dominated by the polar planktonic foraminiferal species, *N. pachyderma* (s) (Figure 2.2; Table 2.3). In the lower Younger Dryas chronozone, ~ 60 % of the planktonic foraminiferal

assemblage is *N. pachyderma* (s), decreasing to ~ 40 % in the upper Younger Dryas chronozone, indicating a slight increase in the prevalence of subpolar surface waters from the lower to the upper Younger Dryas chronozones (Figure 2.2). A concomitant increase in the subpolar species, *G. bulloides*, from ~ 15 % in the lower Younger Dryas chronozone to ~ 25 % in the upper Younger Dryas chronozone, also indicates an increase in the occurrence of subpolar surface waters through the Younger Dryas section (Figure 2.2).

Planktonic *N. pachyderma* (s) $\delta^{18}\text{O}$ values are variable within the Younger Dryas chronozone (Figure 2.2). In the lower Younger Dryas chronozone, *N. pachyderma* (s) $\delta^{18}\text{O}$ values are between 3.5 and 4.0 ‰, decreasing to 2.0 ‰ in the upper Younger Dryas chronozone (Figure 2.2). The $\delta^{18}\text{O}$ values of *G. bulloides* vary between 2.2 and 2.5 ‰ in the lower Younger Dryas chronozone, decreasing to 1.9 – 2.1 ‰ in the upper Younger Dryas chronozone (Figure 2.2). The decrease in both *N. pachyderma* (s) and *G. bulloides* $\delta^{18}\text{O}$ values indicates a slight warming in surface water from the lower to upper Younger Dryas chronozone (Figure 2.2).

The Younger Dryas chronozone is characterized by high abundances of lithics per gram of sediment (> 150 grains/gram), reflecting increased IRD input (Figure 2.3). Several samples have elevated IRD values (> 400 grains/gram) and are observed between 218 and 190 cm (~ 13.5 – 11.6 ka; Figure 2.3).

The transition from the Younger Dryas section to the Holocene section in core 11JPC is found between ~ 184 and 165 cm (Figure 2.2). A sharp decrease in % *N. pachyderma* (s) and a correspondingly large increase in % *G. bulloides* is observed in this transitional section, indicating a change from polar to subpolar conditions from ~ 184 to

175 cm (~ 11.5 to 11.3 ka; Figure 2.3). *Neogloboquadrina pachyderma* (s) $\delta^{18}\text{O}$ and *G. bulloides* $\delta^{18}\text{O}$ values decrease in this transitional section, recording a transition to lower values from 185 – 175 cm (~ 11.5 – 11.2 ka; Figure 2.3). IRD abundances decrease sharply across the Holocene – Younger Dryas boundary, from 185 to 175 cm (~ 11.5 ka; Figure 2.3).

The Holocene section of core 11JPC is found between 0 and 175 cm (Figure 2.2). In the Holocene chronozone, the abundance of the polar species, *N. pachyderma* (s) is typically less than 3 % (Figure 2.2). The abundance of sub-polar species *G. bulloides* and right coiling *N. pachyderma* (d) is ~ 50 % and ~ 20 %, respectively, indicating that the subpolar waters replaced the polar conditions of the Younger Dryas during the Holocene chronozone (Figure 2.2). *N. pachyderma* (s) $\delta^{18}\text{O}$ values decrease from ~ 2.8 to 1.7 ‰ in the lower Holocene chronozone and are low (~ 1.7 – 1.4 ‰), with limited variability, in the middle and upper Holocene section (Figure 2.2). *G. bulloides* $\delta^{18}\text{O}$ values are also low (~ 1.2 – 1.8 ‰) throughout the Holocene chronozone, indicating relatively warm surface temperatures (Figure 2.2). The abundance of lithic grains per gram is low in the Holocene chronozone, with an average value of 8 grains/gram (Figure 2.3).

2.4.2. Deepwater Results

Deepwater temperature and circulation proxies show variations between Younger Dryas and Holocene conditions at site 11JPC (Figure 2.2; Table 2.3). In the top 222 cm of core 11JPC, *P. wuellerstorfi* $\delta^{13}\text{C}$ values range from 0.4 to 1.5 ‰ (Figure 2.2). The Younger Dryas chronozone is typified by low *P. wuellerstorfi* $\delta^{13}\text{C}$ values at the beginning and end of the chronozone, with distinct minima of ~ 0.4 ‰ at 210 and 191 cm in the lower and upper portions of the Younger Dryas section (Figure 2.2). Between these

minima, the mid-Younger Dryas chronozone is characterized by $\delta^{13}\text{C}$ values of $\sim 1.0\text{‰}$ (Figure 2.2). *Planulina wuellerstorfi* $\delta^{13}\text{C}$ values increase through the lower Holocene chronozone to a mid-Holocene value of $\sim 1.3\text{‰}$ at $\sim 110\text{ cm}$ (Figure 2.2). A long-term decreasing trend in *P. wuellerstorfi* $\delta^{13}\text{C}$ values is observed from 90 to 0 cm, from the middle of the Holocene section ($\sim 100\text{ cm}$) to the core top (Figure 2.2).

Benthic foraminiferal *P. wuellerstorfi* $\delta^{18}\text{O}$ values decrease from $\sim 3.5\text{‰}$ in the lower Younger Dryas chronozone to $\sim 3.0\text{‰}$ in the upper Younger Dryas chronozone. (Figure 2.2). *P. wuellerstorfi* $\delta^{18}\text{O}$ values further decreased to $\sim 2.7\text{‰}$ into the lower Holocene section (Figure 2.2). This represents a total decrease of $\sim 0.8\text{‰}$, of which $\sim 0.6\text{‰}$ is due to the 60 m sea-level rise expected during the Younger Dryas and early Holocene (Figure 2.2; Fairbanks et al., 1989). Throughout the Holocene chronozone, *P. wuellerstorfi* $\delta^{18}\text{O}$ values are low ($\sim 2.6 - 2.8\text{‰}$; Figure 2.2).

2.5 Discussion

2.5.1 Implications for the Younger Dryas

Deepwater circulation patterns in the North Atlantic were paced by orbital cycles during the Pleistocene (e.g., Raymo, et al., 1989; Crowley and Kim, 1992). Subsequently, modes of circulation were described by a shoaling or deepening of the axis of deepwater flow due to buoyancy changes and/or by a weakened or strengthened NCW flux (e.g., Duplessy et al., 1988; Boyle, 1995). It is widely accepted that the core of NCW shoaled during the LGM (Oppo and Fairbanks, 1987; Boyle and Keigwin, 1987; Duplessy et al., 1988; Curry et al., 1988; Curry and Oppo, 2005), though arguments have been made for an LGM deepwater circulation pattern that is less vigorous than modern (McManus et al., 2004; Gherardi et al., 2005; Piotrowski et al., 2005), equal (Legrand and Wunsch, 1995;

Wunsch, 2002; Wunsch, 2003), more vigorous (Yu et al., 1996; Toggweiler and Russell, 2008). An LGM-like circulation pattern has been suggested for the Younger Dryas (Oppo and Fairbanks, 1987; Boyle and Keigwin, 1987; Curry et al., 1988; Duplessy et al., 1988; McManus et al., 2004; Curry and Oppo, 2005; Gherardi et al., 2005; Piotrowski et al., 2005). The benthic foraminiferal $\delta^{13}\text{C}$ record from 11JPC shows an abrupt increase in southern sourced water in the North Atlantic at the onset of the Younger Dryas chronozone (~ 13.0 ka; Figure 2.2), consistent with most published benthic foraminiferal $\delta^{13}\text{C}$ records (e.g., Boyle and Keigwin, 1987), as well as with records of Pa/Th (McManus et al., 2004), ϵNd (Piotrowski et al., 2005), ^{14}C (Goslar et al., 1995; Eltgroth et al., 2006), benthic foraminiferal Cd/Ca (Boyle and Keigwin, 1987; Came et al., 2008), and sortable silt (Evans and Hall, 2008; Praetorius et al., 2008). However, in my record, *P. wuellerstorfi* $\delta^{13}\text{C}$ values increase quickly following this initial excursion, though not to interglacial values, indicating a partial recovery of NCW circulation patterns during the mid-Younger Dryas (Figure 2.2); this result is in apparent contrast to the idea that North Atlantic deepwater formation was suppressed throughout the entire Younger Dryas (e.g., Boyle and Keigwin, 1987). A second decrease in *P. wuellerstorfi* $\delta^{13}\text{C}$ values at ~ 11.8 ka indicates that southern sourced waters were also prevalent in the North Atlantic during the late Younger Dryas; benthic foraminiferal $\delta^{13}\text{C}$ values subsequently rebounded for the second time and remained high during the early and mid Holocene (Figure 2.2).

In support of the benthic foraminiferal $\delta^{13}\text{C}$ record from 11JPC, evidence for large-scale deep-ocean circulation reorganizations during both the early and late Younger Dryas can be seen in several published records of benthic foraminiferal $\delta^{13}\text{C}$, though at a lower resolution (Figure 2.4; Boyle and Keigwin, 1987; Bond et al., 1997; Hagen and

Keigwin, 2002; Millo et al., 2006; Praetorius et al., 2008). Other proxy records also show deep-ocean circulation reorganizations during the early and late Younger Dryas, including records of mean sortable silt, a proxy for bottomwater flow velocity (Figure 2.4; Praetorius, et al., 2008) and Pa/Th, a proxy for North Atlantic deepwater export strength (Figure 2.4; McManus et al., 2004). The similarity in structure of these geographically dispersed records of benthic foraminiferal $\delta^{13}\text{C}$ demonstrates that this two-pronged pattern is not a local phenomenon. Additionally, the strong visual correlation between the carbon independent proxies of sortable silt and Pa/Th and my *P. wuellerstorfi* $\delta^{13}\text{C}$ record indicates that both physical and geochemical proxies were affected by fluctuations in NCW buoyancy.

While I have demonstrated strong evidence for a two-pronged circulation change during the Younger Dryas, this pattern has been unidentified previously because many records of deepwater circulation suffer from low temporal resolution (e.g., Charles and Fairbanks, 1992; Vidal et al, 1997; Elliot et al., 2002; Keigwin, 2004; Piotrowski et al, 2005; Robinson et al., 2005; Evans and Hall, 2008). In fact, high-resolution records of the Younger Dryas are so critical that two records of bottom water circulation from core EN120 GGC1, in the deep western North Atlantic (4500m; 33°40'N, 57°37'W), show distinctly different patterns during the Younger Dryas (Boyle and Keigwin, 1987). In that core, the benthic foraminiferal record of $\delta^{13}\text{C}$ shows large minima during the early and late Younger Dryas with a mid-Younger Dryas peak, while the Cd/Ca record shows lower values, though not to glacial values, throughout the entire Younger Dryas (Boyle and Keigwin, 1987). The disparity between $\delta^{13}\text{C}$ and Cd/Ca records may be due to the fact that large samples (450 μg) that are required for Cd/Ca analysis may have effectively smoothed the higher-frequency variability from the record, and the north-south gradient in deepwater Cd is

smaller than the $\delta^{13}\text{C}$ gradient (Boyle and Keigwin, 1987). It is also possible that, during the early and late Younger Dryas, the intrusion of Southern Component Water to this deep site lowered the carbonate ion saturation to a level where Cd/Ca in benthic foraminifera does not record seawater Cd/Ca concentration (Marchitto et al., 2000).

Evidence for increased meltwater during the Younger Dryas chronozone in the northern North Atlantic can also be found in my records (Figure 2.2; Figure 2.3). The $\delta^{18}\text{O}$ records of *N. pachyderma* (s) and *G. bulloides* are similar throughout the Holocene, indicating that both of these species calcified under similar conditions, but differ by as much as 2 ‰ during the early and late Younger Dryas (Figure 2.2; Figure 2.3). Lagerklint and Wright (1999) noted that the $\Delta\delta^{18}\text{O}$ could be ascribed to differences in the calcification temperature during different seasons or at different depths, owing to the fact that *N. pachyderma* (s) adds ~ 80 % of its shell mass at depth (Kohfeld et al., 2000). A second explanation may be that large $\Delta\delta^{18}\text{O}$ (> 1 ‰) reflects the depth stratification caused by freshening of surface water (Figure 2.3). I interpret that the large increase in IRD indicates significant meltwater over Gardar Drift during the Younger Dryas (Figure 2.3). Studies reporting meltwater pulses released to the North Atlantic from the retreat of the Laurentide and Fenno-Scandinavian ice sheets have ages that cluster around the early (~ 13.2 – 12.4 ka) and late Younger Dryas (~ 11.6 – 11.2 ka; Figure 2.3; Appendix 2). There is a strong correspondence between these published records of meltwater and my proxy evidence for the occurrence of meltwater, indicating that meltwater input to the North Atlantic was highest during the early and late Younger Dryas (Figure 2.3). Geochemical evidence has demonstrated that the formation region of NCW was south of the Iceland-Scotland Ridge, and therefore core 11JPC may have been more proximal to the deep convection, from the Last Glacial Maximum until ~ 9 ka (Fagel, et al., 2002).

Thus, the $\Delta\delta^{18}\text{O}$ and Lithics/gram records from 11JPC, which indicate meltwater pulses during the early and late Younger Dryas, provided substantial fresh water to the NCW formation region.

A paradox remains since, despite my $\Delta\delta^{18}\text{O}$ and IRD records, and published evidence for early and late Younger Dryas meltwater (Figure 2.3), sea-level reconstructions show no evidence for a large volume of meltwater released during the Younger Dryas (e.g., Fairbanks, 1989). Evidence has been shown for the advance of continental ice sheets in North America (Gosse et al., 1995; Ivy-Ochs et al., 1999) and Europe (Andersen et al., 1995), which may suggest that the meltwater observed in these records is related to the melting of icebergs. While Younger Dryas meltwater may have been volumetrically insignificant, it has been linked to decreased NCW formation (Broecker, 1989); conversely, large meltwater pulses that precede and post-date the Younger Dryas are visible in sea-level reconstructions but did not affect NCW formation strength (e.g., Boyle and Keigwin, 1987). In response to this issue, model simulations of the Younger Dryas have shown that relatively small meltwater injections directly to the northern North Atlantic (Fanning and Weaver, 1997) or through the Arctic Ocean (Tarasov and Peltier, 2005) may alter deepwater circulation patterns without significantly affecting sea-level. This indicates that the location of meltwater delivery, and not necessarily the volume of meltwater, is the most important factor in determining whether a meltwater injection will effect deepwater circulation.

It is widely accepted from atmospheric, terrestrial, and oceanic records that the Younger Dryas was a cold interval (Jensen, 1938; Mangerund et al., 1974; Bond et al., 1992; Peteet, 1995; Ivy-Ochs et al., 1999). Decreased deepwater formation is also

postulated throughout the Younger Dryas (Boyle and Keigwin, 1987; Goslar et al., 1995; Piotrowski et al., 2005; Eltgroth et al., 2006; Came et al., 2008; Evans and Hall, 2008; Pahnke et al., 2008; Praetorius et al., 2008) according to the typical view of North Atlantic circulation (Broecker and Denton, 1989). However, high-resolution benthic foraminiferal $\delta^{13}\text{C}$ records from 11JPC show a reinvigoration of deepwater circulation during the mid- Younger Dryas (Figure 2.4), which suggests a disconnect between climate and oceanic circulation if North Atlantic temperatures remained cool during the mid- Younger Dryas. One explanation for this could be that a brief mid-Younger Dryas warming was not recorded in paleoceanographic proxies due to poor temporal resolution or seasonal biases. The Younger Dryas has been proposed to have large seasonal variability with much colder winter conditions (Denton et al., 2005). Records of *N. pachyderma* (s) $\delta^{18}\text{O}$ from 11JPC indicate that sea surface temperatures were variable during the Younger Dryas (Figure 2.2). A record of $\delta^{18}\text{O}$ from a Greenland ice core is highly variable during the Younger Dryas, owing to higher-frequency atmospheric temperature fluctuations and/or variable sea-ice extent (Figure 2.3; Alley et al., 1992; Charles et al., 1994). Corroborating records of planktonic foraminiferal $\delta^{18}\text{O}$ from the Nordic Seas (Bakke et al., 2009) and beetle remains from the British Isles (Atkinson et al., 1987) also show highly variable sea surface and/or atmospheric temperatures during the Younger Dryas. Another explanation for the apparent decoupling between climate and circulation could be the result of an altered atmospheric circulation pattern which altered the strength or direction of the Gulf Stream during the Younger Dryas, resulting in a change in the dynamics of the sub-tropical gyre (Mayewski et al., 1993; Alley, 2000; Ebbsen and Hald, 2004; Brauer et al., 2008).

2.5.2 Implications for the Holocene

The early Holocene chronozone of core 11JPC is typified by decreasing values of $\delta^{18}\text{O}$ *G. bulloides*, *N. pachyderma* (s), and *P. wuellerstorfi*, and decreasing values of % *N. pachyderma*, indicating a continued warming trend from 11.5 to 9.5 ka, which is also observed in ice core records (Figure 2.2; Figure 2.3; Alley et al., 1995). The lithics per gram and $\Delta\delta^{18}\text{O}$ values decrease to < 10 lithics/g and < 0.5 ‰, respectively, through the early Holocene, indicating that meltwater production diminished during this warming period (Figure 2.3). Values of *P. wuellerstorfi* $\delta^{13}\text{C}$ increase through this period, suggesting an increase in northern sourced water (Figure 2.2). These trends can be explained by the residual melting of northern hemisphere ice sheets, which provide episodic pulses of fresh meltwater to the surface of the North Atlantic that hinders deepwater formation. This is consistent with the idea that early Holocene was an unstable period and that the full interglacial period did not begin until 9 ka, coincident with the maximum flux of NCW (Henderson et al., 2009)

Climate events at 8.2 (Alley et al., 1997; Rohling and Palike, 2005), 8.4 (Kleiven et al., 2008), and 8.6 ka (Henderson et al., 2009) have been attributed to a freshwater pulse from Glacial Lake Agassiz and proposed to have altered deepwater circulation patterns (Kleiven et al., 2008; Henderson et al., 2009); these could be the same meltwater event reported using different chronologies or a series of meltwater events. The record of % *N. pachyderma* from 11JPC indicates a slight cooling ~ 8.4 ka; however, the cooling is not seen in records of $\delta^{18}\text{O}$ of *G. bulloides* or *N. pachyderma* (s) (Figure 2.3). The $\Delta\delta^{18}\text{O}$ values are slightly higher during the period from 9 to 8 ka, indicating an increase in meltwater occurrence during that interval (Figure 2.3). During the period from 9 to 8 ka,

the record of *P. wuellerstorfi* $\delta^{13}\text{C}$ has several minima that could be perceived to represent abrupt changes in circulation; however, *P. wuellerstorfi* $\delta^{13}\text{C}$ values are low during the period from 9 to 8 ka, and thus it is difficult to decipher individual events from variability within the record (Figure 2.3).

The mid Holocene, from 8 to 5 ka, is characterized by the warmest surface temperatures according to records of $\delta^{18}\text{O}$ of *G. bulloides* and *N. pachyderma* (s) (Figure 2.2). The lithics per gram and $\Delta\delta^{18}\text{O}$ values approach 0 during this time, indicating minimal seasonal and stratification differences (Figure 2.3). Values of *P. wuellerstorfi* $\delta^{13}\text{C}$ are high, suggesting a maximum NCW component to deepwater flow (Figure 2.3). This indicates that the warmest period of the Holocene, referred to as the Holocene Thermal Maximum, was a period of vigorous deepwater flow (Davis, 1984; Davis et al., 2003; Kaufman et al., 2004; Henderson et al., 2009).

During the late Holocene, temperatures are warm, as indicated by low $\delta^{18}\text{O}$ of *G. bulloides* and *N. pachyderma* (s), and a high % *G. bulloides*, and lithics per gram and $\Delta\delta^{18}\text{O}$ indicate that there was very little meltwater present (Figure 2.2; Figure 2.3). Interestingly, the *P. wuellerstorfi* $\delta^{13}\text{C}$ values decrease from ~1.2 to 0.6 ka, suggesting a change in deepwater circulation (Figure 2.2). This record seems highly anomalous when compared with other proximal records, which show vigorous deepwater formation throughout the late Holocene (Bianchi and McCave, 1999; Praetorius et al., 2008). Thus I propose that the low late Holocene benthic $\delta^{13}\text{C}$ values may have been measured on *C. robertsonianus*, a benthic species which has been shown to record $\delta^{13}\text{C}$ values that are as much as 1 ‰ lower than the *P. wuellerstorfi* $\delta^{13}\text{C}$ values from the same samples (Elmore and Wright, unpublished data).

2.6. Conclusions

High-resolution records from southern Gardar Drift show that the Younger Dryas was not a singular cool event that caused a singular change in NCW circulation patterns, but rather consisted of a two-pronged shoaling and deepening of NCW. I propose that two meltwater events are the most likely cause for deepwater reorganizations during the Younger Dryas period. The $\Delta\delta^{18}\text{O}$ and lithic/gram evidence for meltwater delivery to the North Atlantic during the early and late Younger Dryas, supplemented by referenced evidence for distinct meltwater events originating from the Laurentide and Fenno-Scandinavian Ice Sheets, coincides with benthic foraminiferal $\delta^{13}\text{C}$ evidence for two changes in deepwater circulation. This linkage indicates that abrupt releases of meltwater from the Laurentide and/or Fenno-Scandinavian Ice Sheets directly forced deepwater circulation changes in the North Atlantic. Lower surface salinities throughout the North Atlantic region inhibited deep convection in the northern North Atlantic, which led to the initial early Younger Dryas decrease in benthic foraminiferal $\delta^{13}\text{C}$ values. Following the early Younger Dryas meltwater pulse, circulation recovered in the mid-Younger Dryas. A second meltwater pulse toward the end of the Younger Dryas caused another fresh water barrier to deepwater formation, also leading to a decrease in benthic foraminiferal $\delta^{13}\text{C}$. Circulation fully recovered following the second meltwater event, which allowed the final change in deepwater formation to the present day circulation pattern.

This study provides a direct link between surface water freshening and alterations in deepwater circulation patterns during the Younger Dryas. While my data does not constrain the origin of meltwater, I propose that meltwater events from the Laurentide and/or Fennoscandian Ice Sheets caused the variability in NCW during the Younger

Dryas. This observation supplies a plausible mechanism for both the onset and termination of the Younger Dryas chronozone of two meltwater pulses, which altered deepwater circulation patterns for a short duration.

2.7 References

- Alley, R.B., Gow, A.J., Johnsen, S.J., Kipfstuhl, J., Messe, D.A., T. Thorsteinsson. 1995. Comparison of Deep Ice Cores. *Nature*. 373; 393-394.
- Alley, R.B., Mayewski, P.A., Sowers, T., Stuiver, M., Taylor, K.C., and P.U. Clark. 1997. Holocene climatic instability: A prominent, widespread event 8200 yr ago. *Geology*. 25 (6); 483-486.
- Alley, R.B.. 2000. The Younger Dryas Cold Interval as Viewed from Central Greenland. *Quaternary Science Reviews*. 19; 213-226.
- Andersen, B.G., Lundqvist, J., and M.Saarnisto. 1995. Younger Dryas margin of the Scandanavian Ice Sheet- an introduction. *Quaternary International*. 28; 145-146.
- Andrews, J.T., and G. Dunhill. 2004. Early to mid-Holocene Atlantic water influx and deglacial events, Beaufort Sea slope, Arctic Ocean. *Quaternary Research*. 61; 14-21.
- Atkinson, T.C., Briffa, K.R., and G.R. Coope. 1987. Seasonal temperatures in Britain during the past 22,000 years, reconstructed using beetle remains. *Nature*. 325; 587-592.
- Backstrom, D.L., Kuijpers, A., and J. Heinemeier. 2001. Late Quaternary North Atlantic Paleoceanographic records and stable isotopic variability in four planktonic foraminiferal species. *The Journal of Foraminiferal Research*. 31 (1); 25-32.
- Bakke, J., Lie, O., Heegaard, E., Dokken, T., Haug, G.H., Birks, H.H., Dulski, P., and T. Nilsen. 2009. Rapid oceanic and atmospheric changes during the Younger Dryas cold period. *Nature Geoscience*. 2; 202-205.
- Bard, E.. 1988. Correction of accelerator mass spectrometry ^{14}C ages measured in planktonic foraminifera: paleoceanographic implications. *Paleoceanography*. 3 (6); 635-645.
- Bard, E., et al.. 1988. Sea-level estimates during the last deglaciation based on $\delta^{18}\text{O}$ and accelerator mass spectrometry ^{14}C -ages measured in *Globigerina bulloides*. *Quaternary Research*.
- Bard, E., Arnold, M., Mangerud, J., Paterne, M., Labeyrie, L., Duprat, J., Meliers, M.-A.,

- Sonstegaard, E., and J.-C. Duplessy. 1994. The North Atlantic atmosphere-sea surface ^{14}C gradient during the Younger Dryas climatic event. *Earth and Planetary Science Letters*. 126; 275-287.
- Bé, A.W.H.. 1977. An ecological, zoogeographic and taxonomic review of recent planktonic foraminifera, in Ramsay, A.T.S. (ed.), *Oceanic Micropaleontology*, Academic Press, London. 1; 1-100.
- Bé, A.W.H. and D.S. Tolderlund. 1971. Distribution and ecology of living planktonic foraminifera in surface waters of the Atlantic and Indian Oceans, in Funnell, B.M. and Riedel, W.R. (eds.), *The Micropaleontology of Oceans*, 105-149.
- Belanger, P.E., Curry, W.B., and R.K. Matthews. 1981. Core top evaluation of benthic foraminiferal isotopic ratios for paleoceanographic interpretations, *Palaeoceanography, Palaeoclimatology, Palaeoecology*. 33; 205–220.
- Berger, W.H.. 1987. Ocean ventilation during the last 12,000 years: hypothesis of outcrop deepwater production. *Marine Geology*. 78; 1-10.
- Berger, W.H.. 1990. The Younger Dryas cold spell - a quest for causes. *Global and Planetary Change*. 3 (3); 219–237.
- Berger, W.H. and G.R. Heath. 1986. Vertical Mixing in Pelagic Sediments. *Journal of Marine Research*. 26; 134-143.
- Bodén, P., Fairbanks, R.G., Wright, J.D., and L.H. Burckle. 1997. High-resolution stable isotope records from southwest Sweden: The drainage of the Baltic Ice Lake and Younger Dryas ice margin oscillations. *Paleoceanography*. 12 (1); 39-49.
- Bond, G.C. and R. Lotti. 1995. Iceberg Discharges into the North Atlantic on Millennial Time Scales During the Last Glaciation. *Science*. 267; 1005-1010
- Bond, G.C., Showers, W., Cheseby, M., Lotti, R., Almasi, P., deMenocal, P., Priore, P., Cullen, H., Hajdas, I., and G. Bonani. 1997. A Pervasive Millennial-Scale Cycle in North Atlantic Holocene and Glacial Climates. *Science*. 278; 1257-1267.
- Boyle, E.A. and L.D. Keigwin. 1987. North Atlantic thermohaline circulation during the past 20,000 years linked to high-latitude surface temperature. *Nature*. 330; 35-40.
- Boyle, E.A.. 1995. Last Glacial Maximum North Atlantic Deepwater: On, off or Somewhere In-Between? in *The Role of the North Atlantic in the Global Carbon Cycle*. Philosophical Transactions: Biological Sciences. 348 (1324), 243-253.
- Bradley, R.S. and J.H. England. 2008. The Younger Dryas and the Sea of Ancient Ice. *Quaternary Research*. 70; 1-10.

- Brauer, A., Endres, C., Gunter, C., Litt, T., Stebich, M., and J.F.W. Negendank. 1999. High resolution sediment and vegetation responses to Younger Dryas climate change in varved lake sediments from Meerfelder Maar, Germany. *Quaternary Science Reviews*. 18; 321-329.
- Brauer, A., Haug, G.H., Dulski, P., Sigman, D.M., and J.W. Negendank. 2008. An abrupt wind shift in western Europe at the onset of the Younger Dryas cold period. *Nature Geoscience*. 1; 520-524.
- Broecker, W.S., Andree, M., Bonani, G., Wolfli, W., Klas, M., Mix, A., and H. Oeschger. 1988. The chronology of the last deglaciation: implications to the cause of the Younger Dryas event. *Paleoceanography*. 3; 1-19.
- Broecker, W.S. and G.H. Denton. 1989. The role of ocean-atmosphere reorganizations in glacial cycles. *Geochimica et Cosmochimica Acta*. 53; 2465-2501.
- Broecker, W.S., Kennett, J.P., Flower, B.P., Teller, J.T., Trumbore, S., Bonani, G., and W. Wolfli. 1989. Routing of meltwater from the Laurentide Ice Sheet during the Younger Dryas cold episode. *Nature*. 341; 318-321.
- Broecker, W.S.. 2006. Was the Younger Dryas Triggered by a Flood? *Science*, 312; 1146-1148.
- Came, R.E, Oppo, D.W., Curry, W.B., and J. Lynch-Stieglitz. 2008. Deglacial variability in the surface return flow of the Atlantic meridional overturning circulation. *Paleoceanography*. 23; 1217-1227.
- Carlson, A.E., Clark, P.U., Haley, B.A., Klinkhammer, G.P., Simmons, K., Brook, E.J., and K.J. Meissner. 2007. Geochemical proxies of North American freshwater routing during the Younger Dryas cold event. *PNAS*. 106 (14); 6556-6561.
- Charles, C.D., Rind, D., Jouzel, J., Koster, R.D., and R.G. Fairbanks. 1994. Glacial-Interglacial Changes in Moisture Sources for Greenland: Influences on the Ice Core Record of Climate. *Science*. 263; 508-511.
- Ciesielski, P.F., Ledbetter, M.T., and B.B. Ellwood. 1982. The development of Antarctic glaciation and the Neogene paleoenvironment of the Maurice Ewing Bank. *Marine Geology*. 46; 1-51.
- Clark, P.U., Marshall, S.J., Clarke, G.K.C., Hostetler, S.W., Licciardi, J.M., and J.T. Teller. 2001. Freshwater Forcing of Abrupt Climate Change During the Last Glaciation. *Science*. 293; 283-287.
- Clement, A.C., Cane, M.A., and R. Seager. 2001. An orbitally driven source for abrupt climate change. *Journal of Climate*. 14 (11); 2369-2372.

- Cronin, T.M., Manley, P.L., Brachfeld, S., Manley, T.O., Willard, D.A., Guilbault, J.-P., Thunell, R., and M. Berke. 2008. Impacts of post-glacial lake drainage events and raised chronology of the Champlain Sea episode 13-9 ka. *Palaeogeography, Palaeoclimatology, Palaeoecology*. 262; 46-60.
- Crowley, T. J. and K.-Y. Kim. 1992. Complementary Roles of Orbital Insolation and North Atlantic Deepwater during Late Pleistocene Interglacials. *Paleoceanography*. 7(5); 521-528.
- Curry, W.B. and D.W. Oppo. 2005. Glacial water mass geometry and the distribution of $\delta^{13}\text{C}$ and ΣCO_2 in the western Atlantic Ocean. *Paleoceanography*. 20; 1-12.
- Dansgaard, W., Johnson, S.J., Clausen, H.B., Dahl-Jensen, D., Gundestrup, N., Hammer, C.H., and H. Oeschger. 1984. North Atlantic oscillations revealed by deep Greenland ice cores. *Climate Processes and Climate Sensitivity, Geophys. Monogr.*, No. 29. Amer. Geophys. Union, 288-298.
- Dansgaard, W., White, J.W.C., and S.J. Johnsen. 1989. The abrupt termination of the Younger Dryas climate event. *Nature*. 339; 532- 534.
- Davis, B.A.S., Brewer, S., Stevenson, A.C., Guiot, J., and Data Contributors. 2003. The temperature of Europe during the Holocene reconstructed from pollen data. *Quaternary Science Reviews*. 22; 1701-1716.
- Davis, O.K.. 1984. Multiple Thermal Maximum During the Holocene. *Science*. 225; 617-619.
- deMenocal, P., Ortiz, J., Guilerson, T., Adkins, J., Sarnthein, M., Baker, L., and M. Yarusinsky. 2000. Abrupt onset and termination of the African Humid Period: rapid climate responses to gradual insolation forcing. *Quaternary Science Reviews*. 19; 347-361.
- Denton, G.H., Alley, R.B., Comer, G.C., and W.S. Broecker. 2005. The role of seasonality in abrupt climate change. *Quaternary Science Reviews*. 24; 1159-1182.
- Duplessy, J.-C., Shackleton, N.J., Fairbanks, R.G., Labeyrie, L., Oppo, D., and N. Kallel. 1988. Deepwater source variations during the last climate cycle and their impact on the global deepwater circulation. *Paleoceanography*. 3; 343-360.
- Ebbesen, H. and M. Hald. 2004. Unstable Younger Dryas Climate in the Northeast North Atlantic. *Geology*. 32 (8); 673-676.
- Elliot, M., Labeyrie, L., and J.C. Duplessy. 2002. Changes in North Atlantic deepwater formation associated with the Dansgaard-Oeschger temperature oscillations (60-10 ka). *Quaternary Science Reviews*. 21; 1153-1165.

- Ellison, C.R.W., Chapman, M.R., and I.R. Hall. 2006. Surface and Deep Ocean Interactions During the Cold Climate Event 8200 Years ago. *Science*. 312; 1929-1933.
- Elliot, M., Labeyrie, L., and J.-C. Duplessy. 2002. Changes in North Atlantic deepwater formation associated with the Dansgaard-Oeschger temperature oscillations (60-10ka). *Quaternary Science Reviews*. 21; 1153-1165.
- Eltgroth, S.F., Adkins, J.F., Robinson, L.F., Southon, J., and M. Kashgarian. 2006. A deep-sea coral record of the North Atlantic radiocarbon through the Younger Dryas: Evidence for intermediate water/deepwater reorganization. *Paleoceanography*. 21; 1-12.
- Evans, H.K. and I.R. Hall. 2008. Deepwater circulation on Blake Outer Ridge (western North Atlantic) during the Holocene, Younger Dryas, and Last Glacial Maximum. *Geochemistry, Geophysics, Geosystems*. 9 (3); 1-19.
- Fagel, N., Innocent, C., Gariepy, C. and C. Hillaire-Marcel. 2002. Sources of Labrador Sea sediments since the last glacial maximum inferred from Nd-Pb isotopes. *Geochimica et Cosmochimica Acta*. 66 (14); 2569-2581.
- Fairbanks, R.G.. 1989. A 17,000-year glacio-eustatic sea level record: influence of glacial melting rates on the Younger Dryas event and deep-ocean circulation. *Nature*. 342; 637-642.
- Fairbanks, R.G., Mortlock, R.A., Chiu, T.-C., Cao, L., Kaplan, A., Guilderson, T.P., Fairbanks, T.W., and A.L. Bloom. 2005. Marine Radiocarbon Calibration Curve Spanning 0 to 50,000 Years B.P. Based on Paired $^{230}\text{Th}/^{234}\text{U}/^{238}\text{U}$ and ^{14}C Dates on Pristine Corals. *Quaternary Science Reviews*. 24; 1781-1796.
- Fanning, A.F. and A.J. Weaver. 1997. Temporal-geographical meltwater influences on the North Atlantic Conveyor: Implications for the Younger Dryas. *Paleoceanography*. 12 (2); 307-320.
- Firestone, R.B., West, A., Kennett, J.P., Becker, L., Bunch, T.E., Revay, Z.S., Schultz, P.H., Belgia, T., Kennett, D.J., Erlandson, J.M., Dickenson, O.J., Goodyear, A.C., Harris, R.S., Howard, G.A., Kloosterman, J.B., Lechler, P., Mayewski, P.A., Montgomery, J., Poreda, R., Darrah, T., Que Hee, S.S., Smith, A.R., Stich, A., Topping, W., Wittke, J.H., and W.S. Wolbach. 2007. Evidence for an extraterrestrial impact 12,900 years ago that contributed to the megafaunal extinctions and the Younger Dryas cooling. *PNAS*. 104 (41); 16016-16021.
- Gherardi, J.-M., Labeyrie, L., McManus, J.F., Francois, R., Skinner, L.C., and E. Cortijo. 2005. Evidence from the Northeastern Atlantic basin for variability in the rate of

- the meridional overturning circulation through the last deglaciation. *Earth and Planetary Science Letters*. 240 (3-4); 710-723.
- Graham, D.W., Corliss, B.H., Bender, M.L., and L.D. Keigwin. 1981. Carbon and oxygen isotopic disequilibria of recent deep-sea benthic foraminifera. *Marine Micropaleontology*. 6; 483-479.
- Godwin, H.. 1962. Half-life of Radiocarbon. *Nature*. 195; 984.
- Goslar, T., Arnold, M., Bard, E., Kuc, T., Pazdur, M.F., Ralska- Jasiewiczowa, M., Rozanski, K., Tisnerat, N., Walanus, A., Wicik, B., and K. Wieckowski. 1995. High concentration of atmosphere ^{14}C during the Younger Dryas. *Nature*. 377; 414-417.
- Gosse, J.C., Evenson, E.B., Klein, J., Lawn, B., and R. Middleton. 1995. Precise cosmogenic ^{10}Be measurements in western North America: Support for a global Younger Dryas cooling event. *Geology*. 23 (10); 877-880.
- Haflidason, H., Sejrup, H.P., Kristensen, D.K., and S. Johnsen. 1995. Coupled response of the late glacial climatic shifts of northwest Europe reflected in Greenland ice cores: Evidence from the northern North Sea. *Geology*. 23 (12); 1059-1062.
- Hays, J.D., Imbrie, J., and N.J. Shackleton. 1976. Variations in the Earth's Orbit: Pacemaker of the Ice Ages. *Science*. 194; 1121-1132.
- Henderson, S.S., Wright, J.D., Mountain, G.S., and P. Manley. 2009. Characterizing the Early Holocene Establishment of Deep North Atlantic Circulation. *IN PREP*.
- Hughen, K.A., Overpeck, J.T., Lehman, S.J., Kashgarian, M., Southon, J., Peterson, L.C., Alley, R., and D.M. Sigman. 1998. Deglacial changes in ocean circulation from an extended radiocarbon calibration. *Nature*. 391; 65-69.
- Huizhong, W. and I.N. McCave. 1990. Distinguishing climatic and current effects in mid-Pleistocene sediments of Hatton and Gardar Drifts, NE Atlantic. *Journal of the Geological Society, London*. 147; 373-383.
- Imbrie, J. and N.G. Kipp. 1971. A new micropaleontological method for Quantitative Paleoclimatology: Application to a late Pleistocene Caribbean Core, in *The Late Cenozoic Glacial Ages*. ed. K.K. Turekian, Yale Univ. Press, New Haven, CT. pp. 71-181.
- Ivy-Ochs, S., Schluchter, C., Kubik, P.W., and G.H. Denton. 1999. Moraine exposure dates imply synchronous Younger Dryas glacier advances in the European Alps and in the southern Alps of New Zealand. *Geografiska Annaler*. 81A; 313-324.
- Jensen, K.. 1938. Some west Baltic pollen diagrams. *Quartar*. 1; 124-139.

- Johnson, R.G. and B.T. McClure. 1976. A model for northern hemisphere continental ice sheet variation. *Quaternary Research*. 6; 325.
- Karlen, I., Olsson, I.U., Kallberg, P., and S. Kilicci. 1966. Absolute determination of the activity of two C^{14} dating standards. *Arkiv Geofysik*. 6; 465-471.
- Kaufman, D.S., Ager, T.A., Anderson, N.J., Anderson, P.M., Andrews, J.T., Bartlein, P.J., Brubaker, L.B., Coats, L.L., Cwynar, L.C., Duvall, M.L., Dyke, A.S., Edwards, M.E., Eisner, W.R., Gajewski, K., Geirsdottir, A., Hu, F.S., Jennings, A.E., Kaplan, M.R., Kerwin, M.W., Lozhkin, A.V., MacDonald, G.M., Miller, G.H., Mock, C.J., Oswalt, W.W., Oppt-Cliesner, B.L., Porinchu, D.F., Ruhland, K., Smol, J.P., Steig, E.J., and B.B. Wolf. 2004. Holocene thermal maximum in the western Arctic (0-180 W). *Quaternary Science Reviews*. 23; 519-560.
- Keigwin, L.D.. 2004. Radiocarbon and stable isotope constraints on Last Glacial Maximum and Younger Dryas ventilation in the western North Atlantic. *Paleoceanography*. 19; 1-15.
- Kleiven, H.F., Kissel, C., Laj, C., Ninnemann, U.S., Richter, T.O., and E. Cortijo. 2008. Reduced North Atlantic Deepwater Coeval with the Glacial Lake Agassiz Fresh Water Outburst. *Science*. 319; 60-65.
- Kohfeld, K., Anderson, R.F., and J. Lynch-Stieglitz. 2000. Carbon isotopic disequilibrium in polar planktonic foraminifera and its impact on modern and Last Glacial Maximum reconstructions. *Paleoceanography*. 15 (1); 53-64.
- Kroopnick, P.. 1980. The Distribution of ^{13}C in the Atlantic Ocean. *Earth and Planetary Science Letters*. 49; 469-484.
- Lagerklint, I.M. and J.D. Wright. 1999. Late glacial warming prior to Heinrich event 1: The influence of ice rafting and large ice sheets on the timing of initial warming. *Geology*. 27 (12); 1099-1102.
- Libby, W.F.. 1955. Radiocarbon Dating. Second Ed. University of Chicago Press.
- Licciardi, J., Teller, J.T., and P.U. Clark. 1999. Freshwater Routing by the Laurentide Ice Sheet During the Last Deglaciation. *Mechanisms of Global Climate Change at Millennial Time Scales*. 112; 177-201.
- Lynch-Stieglitz, J., Stoker, T.F., Broecker, W.S., and R.G. Fairbanks. 1995. The influence of air-sea exchange on the isotopic composition of oceanic carbon: Observations and modeling. *Global Biogeochemical Cycles*. 9 (4); 653-665.
- Marchitto, T.M., Jr., Curry, W.B., and D.W. Oppo. 2000. Zinc concentrations in benthic foraminifera reflect seawater chemistry. *Paleoceanography*. 15(3); 299-306.

- Mangerud, J., Andersen, S.T., Berglund, B.E., and J.J. Donner. 1974. Quaternary stratigraphy of Norden, a proposal for terminology and classification. *Boreas*. 3; 109-128.
- Mayewski, P.A., Meeker, L.D., Whitlow, S., Twickler, M.S., Morrison, M.C., Alley, R., Bloomfield, P., and K. Taylor. 1993. The Atmosphere During the Younger Dryas. *Science*. 261; 195-197.
- McManus, J.F., Francois, R., Gherardi, J.-M., Keigwin, L.D., and S. Brown-Leger. 2004. Collapse and rapid resumption of Atlantic meridional circulation linked to deglacial climate changes. *Nature*. 428; 834-837.
- Meland, M.Y., Dokken, T.M., Jansen, E., and K. Hevroy. 2008. Water mass properties and exchange between the Nordic seas and the northern North Atlantic during the period 23-6 ka: Benthic oxygen isotopic evidence. *Paleoceanography*. 23; 1210-1229.
- Mercer, J.H.. 1969. The Allerod Oscillation: A European Climatic Anomaly? *Arctic and Alpine Research*. 1 (4); 227-234.
- Millo, C., Sarnthein, M., Voelker, A., and H. Erlenkeuser. 2006. Variability of the Denmark Strait Overflow during the Last Glacial Maximum. *Boreas*. 35; 50-60.
- Oppo, D.W. and R.G. Fairbanks. 1987. Variability in the deep and intermediate water circulation of the Atlantic Ocean during the past 25,000 years; Northern Hemisphere modulation of the Southern Ocean. *Earth and Planetary Science Letters*. 86 (1); 1-15.
- Pahnke, K., Hemming, S., and S. Goldstein. 2008. Abrupt changes in Antarctic Intermediate Water circulation over the past 25,000 years. *Nature Geoscience*. 1; 870-875.
- Pak, D.K and J.P. Kennett. 2002. A Foraminiferal isotopic proxy for upper water mass stratification. *Journal of Foraminiferal Research*. 32 (3); 319-327.
- Peteet, D.. 1995. Global Younger Dryas? *Quaternary International*. 28; 93-104.
- Piotrowski, A.M., Goldstein, S.L., Hemming, S.R., and R.G. Fairbanks. 2005. Temporal relationships of carbon cycling and ocean circulation at glacial boundaries. *Science*. 307; 1933-1938.
- Praetorius, S.K., McManus, J.F., Oppo, D.W., and W.B. Curry. 2008. Episodic reductions in bottom-water currents since the last ice age. *Nature Geoscience*. 1; 449-452.

- Raymo, M.E., Ruddiman, W.F., Backman, J., Clement, B.M., and D.G. Martinson. 1989. Late Pliocene variation in Northern Hemisphere ice sheets and North Atlantic deep circulation. *Paleoceanography*. 4; 413-446.
- Robinson, L.F., Adkins, J.F., Keigwin, L.D., Southon, J., Fernandez, D.P., Wang, S.-L., and D.S. Scheirer. 2005. Radiocarbon Variability in the Western North Atlantic During the Last Deglaciation. *Science*. 310; 1469-1473.
- Rohling, E.J. and H. Palikey. 2005. Centennial-scale climate cooling with a sudden cold even around 8,200 years ago. *Nature*. 434; 975-979.
- Rooth, C.. 1982. Hydrology and ocean circulation. *Progress in Oceanography*. 11; 131.
- Ruddiman, W.F. and A. McIntyre. 1981. The North Atlantic Ocean during the last deglaciation. *Paleogeography, Paleoclimatology, Paleoecology*. 35; 145-214.
- Rutherford, E.. 1905. Radio-activity. Cambridge University Press.
- Seager, R., Battisti, D.S., Yin, J., Gordon, N., Naik, N., Clement, A.C., and M.A. Cane. 2002. Is the Gulf Stream responsible for Europe's mild winters? *Q. J. R. Metereol. Soc.*. 128; 2563–2586.
- Shackleton, N.J., Hall, M.A., and E. Vincent. 2000. Phase relationships between millennial-scale events 64,000 to 24,000 years ago. *Paleoceanography*. 15; 565-569.
- Smith, D.G. and T.G. Fisher. 1993. Glacial Lake Agassiz: The northwestern outlet and paleoflood. *Geology*. 21; 9-12.
- Streeter, S.S. and N.J. Shackleton. 1979. Paleocirculation of the deep North Atlantic: 150,000- year record of benthic foraminifera and oxygen-18. *Science*. 203; 168-171.
- Stuiver, M. and H.A. Polach. 1977. Discussion and reporting of ^{14}C data. *Radiocarbon*. 19; 355-363.
- Stuiver, M., P.M. Grootes, and T.F. Braziunas. 1995. The GISP2 ^{18}O climate record of the past 16,500 years and the role of the sun, ocean and volcanoes. *Quaternary Research*. 44; 341-354.
- Tarasov, L., and W.R. Peltier. 2005. Arctic freshwater forcing of the Younger Dryas cold reversal. *Nature*. 435; 662-665.
- Thomson, J., Brown, L., Nixon, S., Cook, G.T., and A.B. MacKenzie. 2000. Bioturbation and Holocene sediment accumulation fluxes in the north-east Atlantic Ocean (Benthic Boundary Layer experiment sites). *Marine Geology*. 169; 21-39.

- Toggweiler, J.R. and J. Russell. 2008. Ocean circulation in a warming climate. *Nature*. 451; 286-288.
- de Vernal, A., Hillaire-Marcel, C., and G. Bilodeau. 1996. Reduced meltwater outflow from the Laurentide ice margin during the Younger Dryas. *Nature*. 381; 774-777.
- Vidal, L., Labeyrie, L., Cortijo, E., Arnold, M., Duplessy, J.C, Michel, E., Becque, S., and T.C.E. van Weering. 1997. Evidence for changes in the North Atlantic Deepwater linked to meltwater surges during the Heinrich events. *Earth and Planetary Science Letters*. 146; 13-27.
- Wold, C.N.. 1994. Cenozoic Sediment Accumulation on Drifts in the Northern North Atlantic. *Paleoceanography*. 9 (6); 917-941.
- Worthington, L.V.. 1969. An attempt to measure the volume transport of Norwegian Sea overflow water through the Denmark Strait. *Deep-Sea Research*. 16; 421-432.
- Wunsch, C.. 2003. Determining paleoceanographic circulations, with emphasis on the Last Glacial Maximum. *Quaternary Science Reviews*. 22; 371-385.
- Wunsch, C.. 2006. Abrupt climate change: An alternative view. *Quat. Res*. 65; 191–203.

Table 2.1: Locations of cores used in this study.

Site	Water Depth (m)	Latitude	Longitude
KN166-14 11JPC	2707	56°15'N	27°40'W
ODP site 984	1984	60°24'N	23°38'W
KNR140-2 JPC 37	3000	31°41'N	75°29'W
EN120 GGC1	450	33°40'N	57°37'W
KN166-14 15JPC	2230	58°12'N	45°34'W
VM29-191	2370	54°16'N	16°47'W
OCE326-GGC5	4550	33°42'N	57°35'W

Table 2.2: Age model for the top of core 11JPC including AMS ^{14}C dates and 1 chronostratigraphic tie point (blue). AMS ^{14}C dates in red were not included in the age model as they caused slight age reversals. AMS ^{14}C dates were corrected by 400 years to account for the reservoir correction and calibrated to calendar years using the Fairbanks 0805 calibration (Fairbanks et al., 2005). Activity of ^{14}C , bioturbated activity, corrected activity (Corr. Act.), and final calendar ages were determined according to the methods outlined above in section 2.2.2. All ages are given in years.

Depth (cm)	^{14}C Age	Reservoir Cor.	\pm	Calendar Age	\pm	Activity	Bioturbated Activity	Corr. Act.	Final Calendar Age
0	1105	705	15	665	5	12.51	1.91E-11	12.51	665
45	3135	2735	45	2821	46	9.64	1.72E-9	9.64	2821
105	5670	5270	15	6014	35	6.55	6.95E-7	6.55	6014
127	6545	6145	15	7020	41	5.80	6.27E-6	5.80	7020
143	7940	7540	20	8367	12	4.93	3.11E-5	4.93	8367
145	6525	6125	25	6992	42	5.82	3.80E-5	5.82	6992
147	8175	7775	20	8556	20	4.82	4.64E-5	4.82	8556
149	8375	7975	30	8864	92	4.64	5.66E-5	4.64	8864
153	8345	7945	30	8783	94	4.69	8.45E-5	4.69	8783
163	9085	8685	25	9611	39	4.24	2.30E-4	4.24	9611
183				11450		3.40	1.70E-3	3.40	11446
198	10600	10200	25	11922	66	3.21	7.61E-3	3.22	11902
213	11825	11425	30	13278	58	2.72	3.41E-2	2.76	13175
220	12100	11700	35	13563	54	2.63	6.86E-2	2.70	13350
227	28810	28410	220	33795	273	0.23			

Table 2.3: Summary of Results

Proxy		Younger Dryas		Holocene	
		Values	Significance	Values	Significance
Surface Water	<i>N. pachyderma</i> (s) abundance	40-60%	Polar	0-10%	Subpolar
	<i>G. bulloides</i> abundance	5-15%	Polar	40-60%	Subpolar
	<i>N. pachyderma</i> (d) abundance	0-5%	Polar	10-20%	Subpolar
	$\delta^{18}\text{O}$ <i>N. pachyderma</i> (s)	3.5-4.0‰	Cold	1.5-2.0‰	Warmer
	$\delta^{18}\text{O}$ <i>G. bulloides</i>	2.5-3.0‰	Cold	1.5-2.0‰	Warmer
	Lithics/gram sediment	> 400	IRD	< 50	No IRD
Bottom	$\delta^{18}\text{O}$ <i>P. wuellerstorfi</i>	3.0-3.5‰	Cold	2.5-3.0‰	Warmer
	$\delta^{13}\text{C}$ <i>P. wuellerstorfi</i>	0.4-1.0‰	2 pronged NCW reduction	~1.0‰	Strong NCW formation

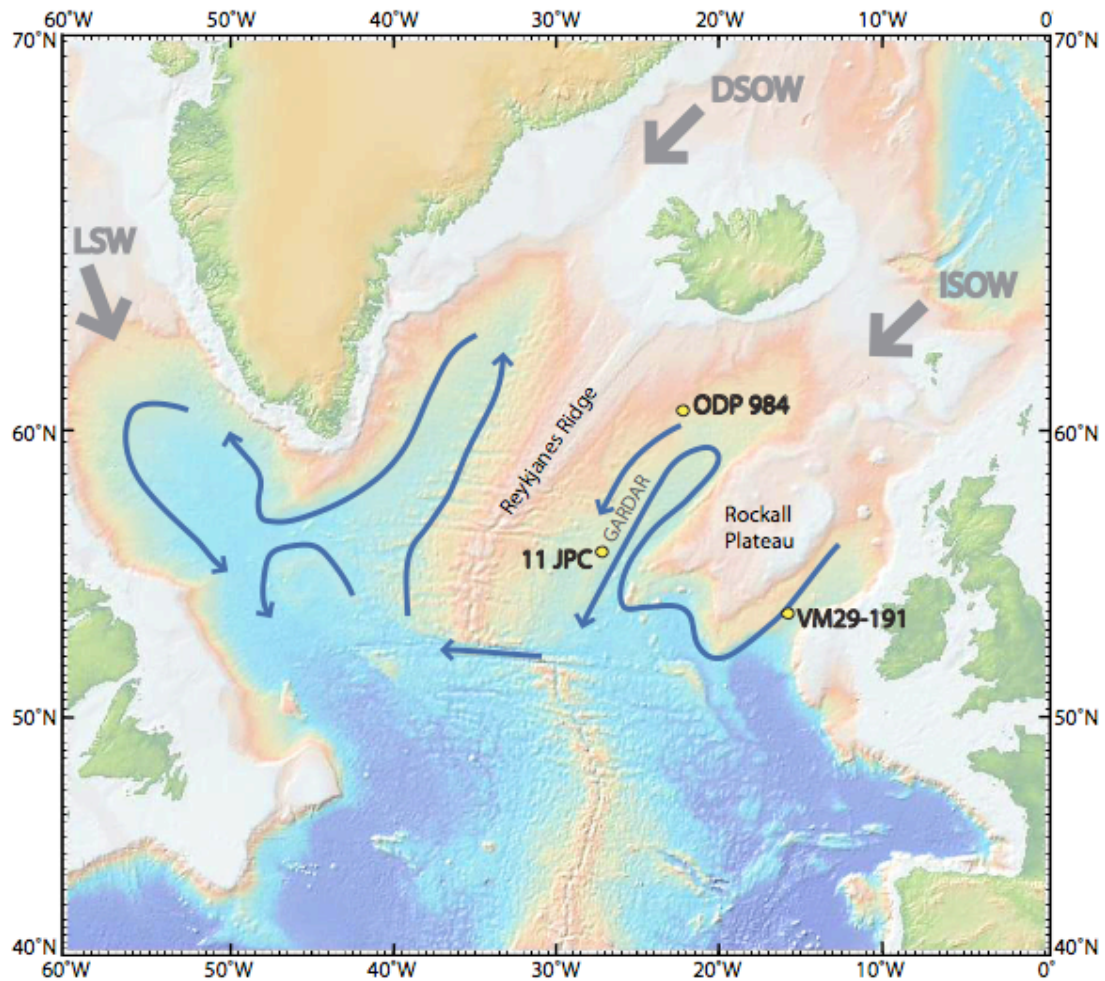


Figure 2.1: Bathymetric map of the North Atlantic showing generalized bottom water currents. The location of KN166 11JPC on Gardar Drift from this study, and ODP 984 (Praetorius et al., 2008) and VM29-191 (Bond et al., 1997), are also shown.

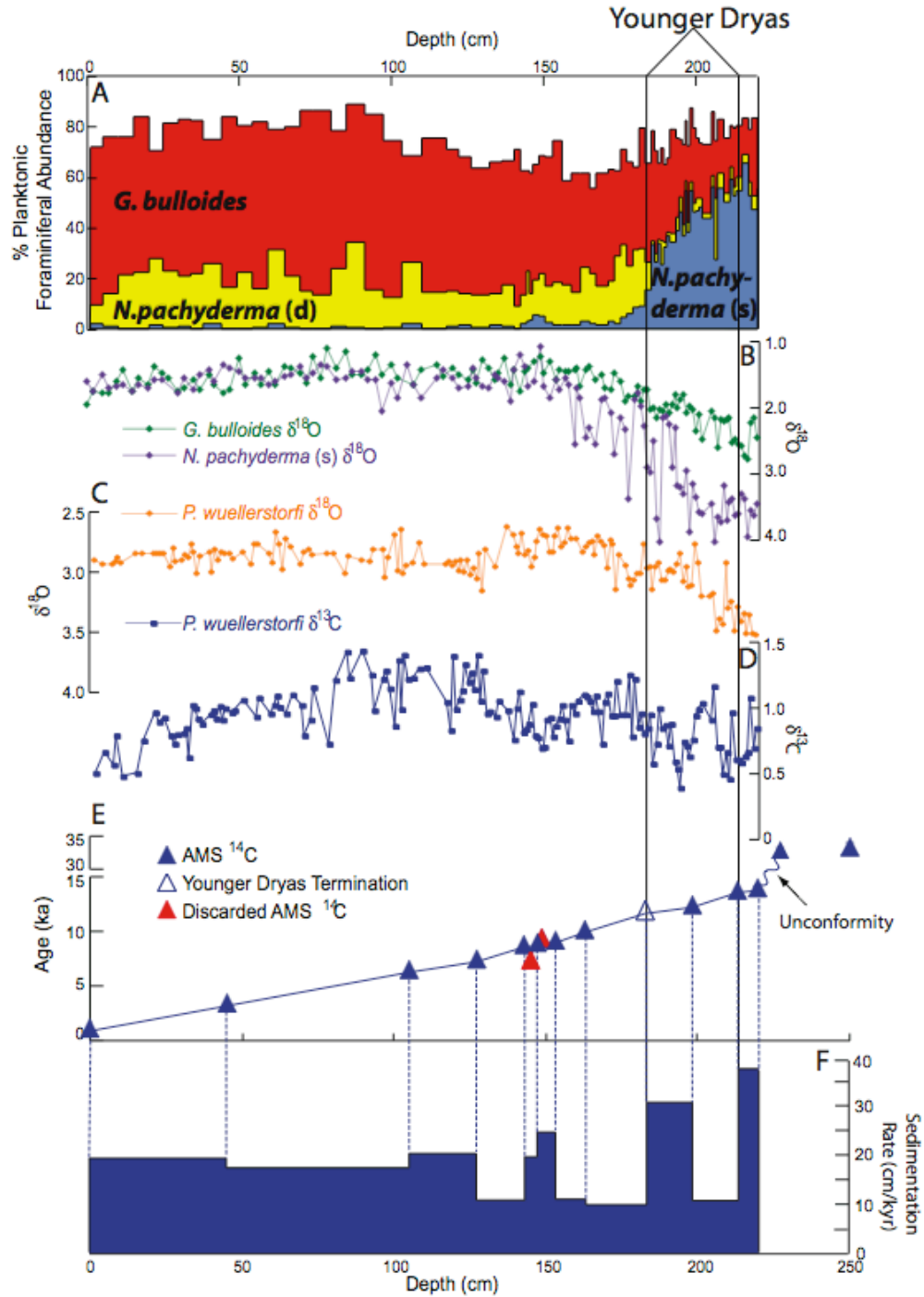


Figure 2.2: Proxy records from core 11JPC plotted versus sediment depth. (A) planktonic foraminiferal abundances, (B) $\delta^{18}\text{O}$ *G. bulloides*, $\delta^{18}\text{O}$ *N. pachyderma*, (C) $\delta^{18}\text{O}$ *P. wuellerstorfi*, (D) $\delta^{13}\text{C}$ *P. wuellerstorfi*, (E) the age model, and (F) sedimentation rates are shown.

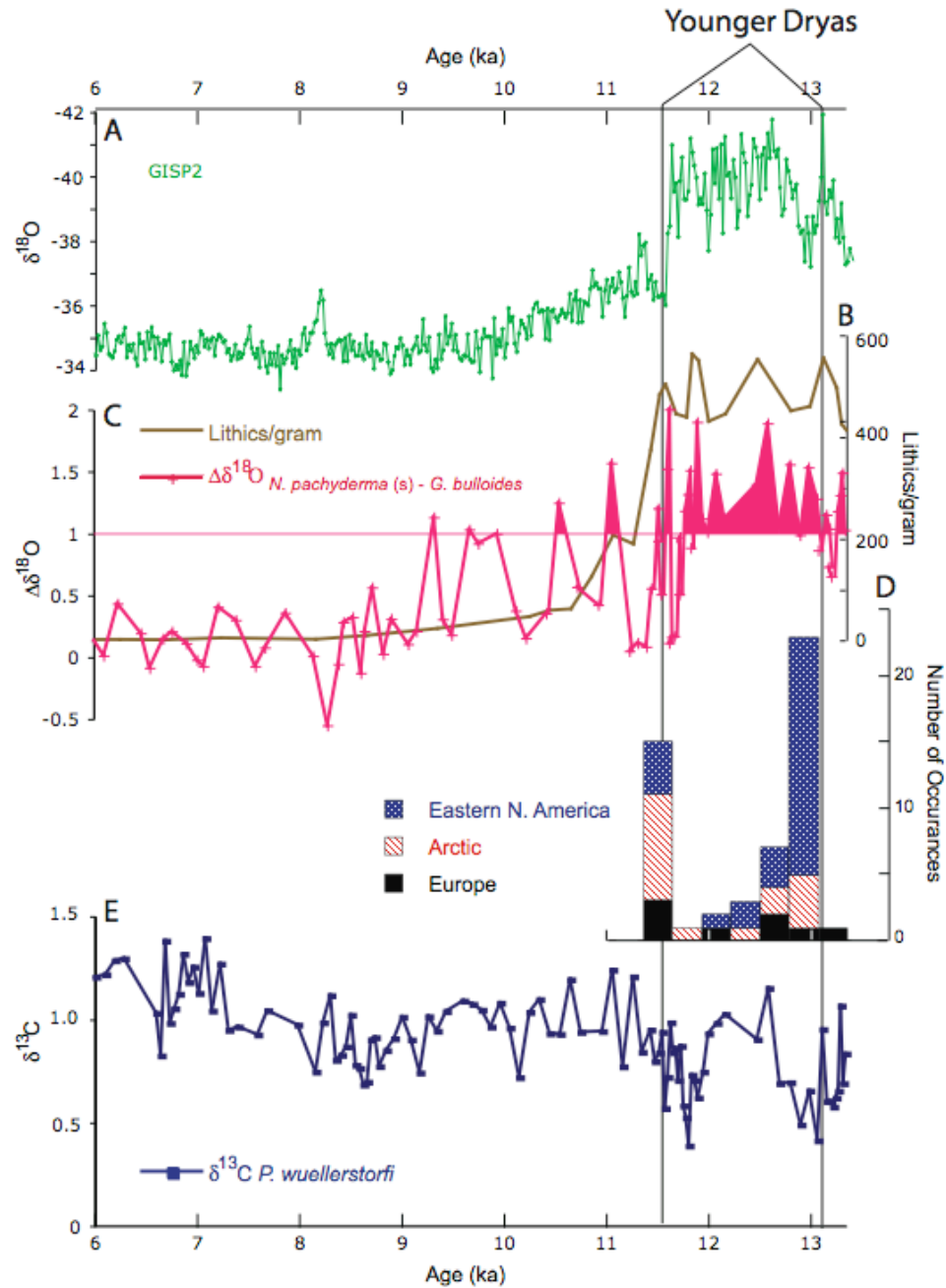


Figure 2.3: Proxy records from core 11JPC shown versus age from 6 to 13.5 ka plotted with (A) the $\delta^{18}\text{O}$ record of ice from a Greenland ice core (GISP2; Stuiver et al., 1995). (B) Lithics/gram (brown), (C) $\Delta\delta^{18}\text{O}_{G.bulloides - N.pachyderma}$ (pink), (D) a histogram of published meltwater occurrence (see Appendix 2), and (E) $\delta^{13}\text{C}$ *P. wuellerstorfi*.

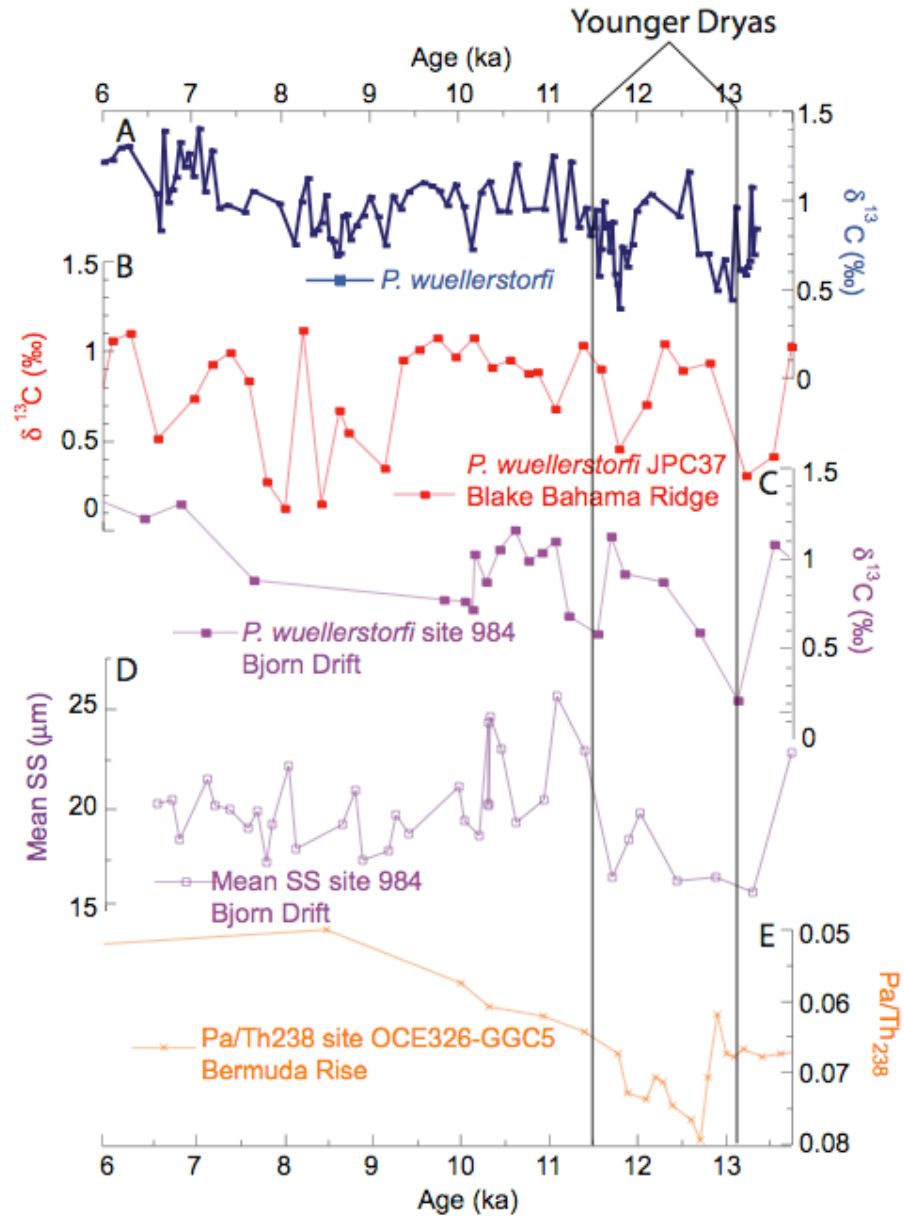


Figure 2.4: Comparison of (A) the $\delta^{13}\text{C}$ *P. wuellerstorfi* from 11JPC plotted with other North Atlantic deepwater proxy records. (B) $\delta^{13}\text{C}$ *P. wuellerstorfi* from core JPC37 (Hagen and Keigwin, 2002), (C) *P. wuellerstorfi* from ODP site 984 (Pretorius et al., 2008), (D) sortable silt from ODP site 984 (Pretorius et al., 2008), and (E) Pa/Th from core OCE326-GGC5 (McManus et al., 2004).

3.0 Precession-driven Changes in Iceland-Scotland Overflow Water Density and Bottomwater Circulation on Gardar Drift Since ~ 200 ka

3.1 Abstract

Benthic foraminiferal stable isotopic records from a transect of sediment cores south of the Iceland-Scotland Ridge reveal that the density of Iceland-Scotland Overflow Water (ISOW) varied on orbital timescales with a pronounced precessional signal over the past 200 kyr. High benthic foraminiferal $\delta^{13}\text{C}$ values ($\sim 1.0\text{‰}$) were recorded at all transect sites downstream of the Iceland-Scotland Ridge during interglacial periods, indicating a deeply penetrating ISOW (Marine Isotope Chrons 5e-5a, and 1). During glacial periods (Marine Isotope Chrons 6, 4, and 2), $\delta^{13}\text{C}$ values from the deeper (2700-3300 m), southern portion of this transect were significantly lower ($\sim 0.5\text{‰}$) than values from the northern transect ($\sim 1.0\text{‰}$), reflecting greater influence of Southern Component Water (SCW). In addition to the large-scale glacial-interglacial ISOW variability, ISOW strength is driven by precessional cycles, particularly during intermediate climate states. Millennial-scale variability in the density of ISOW, likely caused by high-frequency Heinrich and Dansgaard/Oeschger Events, is superimposed on the orbital-scale variations and is most pronounced during intermediate climate states.

3.2 Introduction

Variability in the formation of deep Northern Component Water (NCW; analogous to modern North Atlantic Deep Water) is linked to regional and global climate changes on orbital time-scales (e.g., Broecker and Denton, 1989; Raymo et al., 1989). Causal mechanisms for NCW variability are thought to be associated with incoming solar

radiation (insolation), fresh-water input, and/or sea ice extent (Broecker and Denton, 1989; Rind et al., 2001; Stanford et al., 2006). During the late Pleistocene, insolation variability in the high northern latitudes resulted from longer-scale (~ 400 kyr) eccentricity modulation of the shorter eccentricity (~ 100 kyr) and obliquity (~ 40 kyr) cycles, as well as precession (~ 23 kyr) variations (Laskar et al., 1993). Since past variations in NCW production are tied to climatic conditions (including surface water temperature and wind strength), studies have linked particular NCW circulation patterns to different climate states, notably the glacial and interglacial end members (e.g., Broecker et al., 1985; Imbrie et al., 1993; Liseicki et al., 2008). However, insolation changes are not simply sinusoidal because the total insolation received is derived from distinct orbital periodicities (Laskar et al., 1993); and therefore, the deep-water circulation states may be unique for each glacial and interglacial period, as well as for intermediate climate states. Neitzke and Wright (2007) showed that the density of NCW varied on the orbital scale, suggesting that multiple states of climate produced varying densities of NCW over the past ~ 150 kyr.

Modern North Atlantic Deep Water (NADW) is produced by the interplay between five intermediate to deep components, Iceland-Scotland Overflow Water (ISOW; 5 Sv), Denmark Strait Overflow Water (DSOW; 5 Sv), Antarctic Bottom Water (AABW; 1 Sv), Labrador Sea Water (1 Sv), and Mediterranean Outflow Water (1 Sv) (Mann, 1969; Worthington, 1976). While variability in each of the components of NADW is not fully understood, it has been proposed that changes in these components have contributed to the orbital-scale climate variability (Hillaire-Marcel et al., 2001, Raymo et al., 2004; Millo et al., 2006).

Iceland-Scotland Overflow Water and DSOW form by convection in the Norwegian and Greenland Seas, respectively, and are the largest components of NADW contributing ~ 5 Sverdrups each (Worthington, 1972; 1976). The total contribution of these water masses is related to surface temperature and salinity in the Nordic Seas (Duplessy et al., 1988a), as well as to surface inflow (Worthington, 1972), sill depth (Millo et al., 2006), sea ice cover (Prins et al., 2002; Raymo et al., 2004) and tectonics (Wright and Miller, 1996). Thus, researchers suggested that overflow strength has varied on time-scales of millions of years (Wright and Miller, 1996), tens of thousands of years (i.e. orbital scale; Duplessy et al., 1988a; Raymo et al., 2004), thousands of years (i.e. millennial; Oppo et al., 1995; Dokken and Hald, 1996; McManus et al., 1999), hundreds of years (Bianchi and McCave, 1999), years (Turrell et al., 1999), or seasons (Hatun et al., 2004).

Iceland-Scotland Overflow Water formation was vigorous during interglacial Marine Isotope Chron (MIC) 1 and 5e (Duplessy et al., 1988a,b; Kissel et al., 1997) and weak during the Last Glacial Maximum (LGM; MIC 2; Duplessy et al., 1998a; Kissell et al., 1997); however, the history of ISOW is unclear for other glacial and intermediate climate states. For instance, Kuijpers et al. (1998) argued for enhanced formation of ISOW during MIC 6, while Kissel et al. (1997) and Rasmussen et al. (1996) considered it minimal. Kissel et al. (1997) presumed ISOW was vigorous during MIC 5d, while Kuijpers et al. (1998) and Rasmussen et al. (1996) suggest it was minimal. Additionally, several studies suggest ISOW was vigorous during MIC 3 (Duplessy et al., 1998b; Sarnthein et al., 1994; Kissel et al., 1997; Kuijpers et al., 1998), while others suggest a variable ISOW due to higher-frequency Heinrich Events and Dansgaard/Oeschger Cycles

(Rasmussen et al., 1996; Kissel et al., 1999; Prins et al., 2001; 2002; Rasmussen and Thomsen, 2009). Because ISOW is such a large contributor to NCW (Schmitz and McCartney, 1993; Kissel et al., 1997), variations in ISOW strength have been proposed to exert a large control over NCW circulation patterns (Kuijpers et al., 1998).

Most studies indicate that convection in the Nordic Seas was reduced or absent during the LGM in part due to sea ice cover (Duplessy et al., 1988a; 1988b; Kissel et al., 1997). In the absence of vigorous ISOW formation, subpolar convection has been proposed south of the Greenland-Scotland Ridge (Duplessy et al., 1988b; Oppo and Lehman, 1993; Sarnthein et al., 1994; Revel et al., 1996; Kuijpers et al., 1998; Cortijo et al., 2000; Gherardi et al., 2005). The southward displacement of deepwater formation during the LGM can be reconciled with both the proposed increased circulation vigor (Wunsch, 2002; Toggweiler and Rusell, 2008) and decreased circulation vigor (Broecker et al., 1990; Lynch-Stieglitz et al., 1999; Piotrowski et al., 2005), as well as with a shoaling of the current axis during the LGM (Sarnthein et al., 1988; Curry et al., 1988; Lehman and Keigwin, 1992; Oppo and Lehman, 1995).

Deepwater circulation patterns in the North Atlantic have been reconstructed using geochemical records from benthic foraminiferal $\delta^{13}\text{C}$ (e.g., Boyle and Keigwin, 1987; Oppo and Fairbanks, 1987), Cd/Ca (Boyle and Keigwin, 1987), Zn/Ca (Marchitto et al., 2002), and bulk sediment ϵNd (Piotrowski et al., 2005). Benthic foraminiferal $\delta^{13}\text{C}$ values have been the most extensively used to track variability in NCW production (e.g., Boyle and Keigwin, 1987; Oppo and Fairbanks, 1987; Duplessy et al., 1988a; Sarnthein et al., 1988; Raymo et al., 1990; Oppo and Lehman, 1995; Oppo et al., 1995; Flower et al., 2000; Curry and Oppo, 2005). North Atlantic deep waters are nutrient depleted, and

thus, have high $\delta^{13}\text{C}$ values (1 – 1.5 ‰; Kroopnick, 1985). In contrast, the Southern Ocean, which is higher in nutrients, is vertically well mixed due to the strong West Wind Drift ($\delta^{13}\text{C} \sim 0.4\text{‰}$; Kroopnick, 1985). Deep Pacific Ocean $\delta^{13}\text{C}$ values are $\sim 0.0\text{‰}$, reflecting the long residence time of these waters (Kroopnick, 1985). As such, measured $\delta^{13}\text{C}$ values of biogenic calcite in the deep Southern Ocean reflect the relative inputs of deepwater masses from the Pacific, Indian, and Atlantic Oceans (Oppo and Fairbanks, 1987; Charles and Fairbanks, 1992; Lynch-Stieglitz, 2007).

Geochemical studies, including benthic foraminiferal $\delta^{13}\text{C}$ studies, determined that the large-scale patterns of deepwater circulation vary between glacial and interglacial climate states (Boyle and Keigwin, 1987; Oppo and Fairbanks, 1987; Duplessy et al., 1988a; Oppo and Lehman, 1995; Piotrowski et al., 2005). Cross sections of benthic foraminiferal $\delta^{13}\text{C}$ values of the Atlantic (GEOSECS; Curry et al., 1988; Oppo and Horowitz, 2000; Venz and Hodell, 2002; Raymo et al., 2004; Curry and Oppo, 2005) show that a shoaling of NCW currents allowed for the northward intrusion of Antarctic Bottom Water (AABW) into the northern North Atlantic, up to 60 °N, during the LGM. Studies have suggested that the core of NCW shoaled by as much as ~ 2 km during the LGM (Sarthein et al., 1988; Curry et al., 1988; Duplessy et al., 1988a; Oppo and Lehman, 1995), coincident with a weakened ISOW (Duplessy et al., 1988b; Kissel et al., 1997). Kuijpers et al. (1998) suggested that ISOW is the most important water mass for forming NCW; however, uncertainty remains as to the historical fluxes and density of ISOW, particularly during intermediate climate states.

The objective of this study is to determine variability in deep-water circulation

patterns in the eastern North Atlantic over the past 200 kyr on orbital and millennial time-scales. Determining the variability in ISOW is important to understanding the interactions between circulation and climate because ISOW is one of the largest components to NADW (Worthington, 1976). Herein, new $\delta^{13}\text{C}$ records from sediment cores 11JPC and 3GGC, from the southern end of Gardar Drift, are presented for the past 200 ka (Figure 3.1). Records from these two cores are combined with published records from seven other cores to form my “Gardar Drift Transect” (Table 3.1; Figure 3.1; Figure 3.2). This transect provides a unique opportunity to track variations in the influence of ISOW. Transect cores, combined with cores from the South Atlantic (ODP site 1090) and mid-latitude North Atlantic (DSDP site 607), allow for the examination of southern sourced waters in the eastern northern North Atlantic in a similar method to the Atlantic cross sections (e.g., Curry and Oppo, 2005), but on a smaller scale (Figure 3.2). To examine the density structure of ISOW, benthic foraminiferal $\delta^{13}\text{C}$ was compared along a depth transect south of the Iceland-Scotland Ridge; the occurrence of southern sourced water on southern Gardar Drift is indicative of a shoaling of ISOW.

3.3. Methods

3.3.1 Site Locations

As ISOW flows south along the Reykjanes Ridge, a drift forms along each edge of the current, with Bjorn Drift to the north and Gardar Drift to the South (Figure 3.1; Davies and Laughton, 1972). Contourite drifts, like Gardar and Bjorn, are found throughout the North Atlantic where large quantities of sediments are ‘plastered’ against already existing bathymetric features (Hollister et al., 1978); these regions provide an excellent location for paleoceanographic reconstructions due to the high sedimentation

rates (Figure 3.1; e.g., McCave et al., 1980; McCave and Tucholke, 1986; Channell et al., 1997; Hall et al., 1998; Bianchi and McCave, 1999; Faugers et al., 1999; Manley et al., 2004; Praetorius et al., 2008). Gardar and Bjorn Drifts are in key locations for paleoceanographic studies since they lie within the flow of modern-day ISOW (Figure 3.1; e.g., Oppo and Lehman, 1995; Bianchi and McCave, 1999).

The *R/V Knorr* collected jumbo piston core, 11JPC, and giant gravity core, 3GGC, from southern Gardar Drift on cruise 166, leg 14 (2707 and 3305 m water depth, respectively; Table 3.1; Figure 3.1). Seismic data from site 11JPC were generated using the hull-mounted 3.5 kHz sub-bottom profiler and recorded with the shipboard Knudsen 320B/R digital data logger. Profiles were generated along a track and while drifting on the core site, and were then displayed with Knudsen software. Conversions from two-way travel time to depth were made by using velocities of 1500 m/s in water and 1505 m/s in sediment (G. Mountain, personal communication).

3.3.2 Data Collection

Cores 11JPC and 3GGC were sampled at 5 cm intervals for the entire length of both cores. Samples were split roughly in half and each half was dried overnight in a 50 °C oven. One half of each sample was weighed (Dry Wt. _{initial}) and combined with ~ 40 ml of 1.0 N acetic acid in a 50 ml centrifuge tube for 24 hours. Each sample was agitated during the process to ensure complete removal of all of the carbonate from the sample. The vials were centrifuged for 1 minute to separate the sample from the acid, which was then decanted. Samples were reprocessed in acetic acid, and then rinsed with 40 ml of deionized water three times, centrifuging for one minute before each decanting. Samples were then oven-dried and weighed again (Dry Wt. minus $-CaCO_3$). Weight

percent calcium carbonate (Wt. % CaCO₃) was then determined using the following equation:

$$[1] \quad \text{Wt. \% CaCO}_3 = (1 - \text{Dry Wt. minus } \text{CaCO}_3 / \text{Dry Wt. initial}) * 100$$

Weight percent coarse fraction (Wt. % CF), was determined by weighing the other half of the dried sample before (wt._{unwashed}) and after (wt._{washed}) being washed through a 63 µm sieve. Dry samples were soaked in a dilute calgon solution to prevent flocculation during washing. Wt. % CF was then calculated using the following equation:

$$[2] \quad \text{Wt. \% CF} = (\text{wt.}_{\text{washed}} / \text{wt.}_{\text{unwashed}}) * 100$$

For stable isotopic analyses, up to fifteen tests of the planktonic foraminifera, *Globigerina bulloides* and/or *Neoglobobadrina pachyderma* (sinistral; s), were handpicked under a binocular microscope from the 250 – 350 µm size fraction of the washed samples. Up to five tests of the benthic foraminifera, *Planulina wuellerstorfi*, were similarly selected. Only *P. wuellerstorfi* tests were chosen for analysis since our own work shows that some *Cibicidoides* taxa (e.g., *C. robertsoniensis*) do not record equilibrium values and may be up to 1 ‰ lower in δ¹³C values (Elmore and Wright, unpublished data). The samples were analyzed using a Micromass Optima Mass Spectrometer equipped with an automated Multiprep at the Rutgers University Stable Isotope Laboratory. Samples were reacted in phosphoric acid for 15 minutes at 90 °C. Measured values are reported using standard δ-notation and are compared to Vienna

PeeDee Belemnite using an internal lab standard that is routinely calibrated with NBS-19 (1.95 ‰ $\delta^{13}\text{C}$, -2.20 ‰ $\delta^{18}\text{O}$; Coplen et al., 1983). The internal lab standard is offset from NBS-19 by 0.1 ‰ for $\delta^{13}\text{C}$ and 0.04 ‰ for $\delta^{18}\text{O}$. The 1- σ precision of standards is typically 0.05 ‰ for $\delta^{13}\text{C}$ and 0.09 ‰ for $\delta^{18}\text{O}$.

The number of lithic grains larger than 150 μm was counted under a binocular microscope and divided by the sample weight to determine the lithic grains per gram of sediment (Bond and Lotti, 1995). The location of 11JPC is too far from any terrestrial source to have lithic grains transported to the site by means other than ice rafting, thus the lithic grains per gram are assumed to be ice-rafted detritus (IRD).

3.3.3 Age Models

The age model for the top 220 cm of 11JPC is constrained by fifteen AMS ^{14}C ages (Table 3.2). For each AMS ^{14}C analysis, 4 - 6 mg of planktonic foraminifera *Globigerina bulloides* were selected using a binocular microscope and sonified in deionized water. Samples were analyzed at the Keck Center for Accelerator Mass Spectrometry at the University of California, Irvine. The radiocarbon ages were converted to calendar ages according to the Fairbanks0805 calibration, and a 400-year reservoir correction was applied (Fairbanks et al., 2005). The Younger Dryas termination (11.5 ka) at 183 cm, as recorded in % *N. pachyderma* (s) was used as additional chronostratigraphic tie point (See section 2.3.2; Ellison et al., 2006, Alley et al., 1995; Table 3.2). Two AMS dates (at 145 and 149 cm) were not included in the age model because they produced slight age reversals (Figure 3.3; Table 3.1). The resulting age model revealed an ~ 18 kyr hiatus constrained by ^{14}C dates and placed at 222 cm in the core based on a change in color. AMS ^{14}C dates immediately above the hiatus (at 220 and 213

cm) were corrected for the bioturbation of older, sub-hiatus material (see Chapter 2 of this dissertation for these calculations; Table 3.2).

Three AMS ^{14}C dates from the 1 meter interval just below the unconformity yielded similar ages of ~ 33.5 ka (Table 3.2). This meter of sediment is interpreted to represent a mass transport event and thus data from this meter-long interval were not interpreted as part of this study.

The AMS date of ~ 34 ka at 350 cm is considered to be below the mass transport event because it conforms to the linear sedimentation rate defined by the chrono-stratigraphic tie points below the event. The Lachamp Event (40 ka) was identified at 430 cm (H. Evans, personal communication; Table 3.2). Additional chrono-stratigraphic tie points were determined by comparing measured foraminiferal $\delta^{18}\text{O}$ values to a stacked, benthic foraminiferal $\delta^{18}\text{O}$ record by Lisiecki and Raymo (2005; Figure 3.3; Table 3.2).

An age model for 3GGC was established based on correlation of benthic and planktonic $\delta^{18}\text{O}$ records to the Lisiecki and Raymo LR04 stack and correlation of records of benthic and planktonic $\delta^{18}\text{O}$, benthic $\delta^{13}\text{C}$, % Coarse Fraction, and % CaCO_3 to the proximal core, 11JPC (Figure 3.4; Table 3.3). All previously published benthic foraminiferal $\delta^{13}\text{C}$ records were kept on their published chronologies (Table 3.1).

3.3.4 Transect Construction

The range in length (1600 km), range in depth (1600 m), and confined geographic area of the transect sites allows for the detection of ISOW density changes by monitoring variations in benthic foraminiferal $\delta^{13}\text{C}$ values (Table 3.1). To assess this variability in $\delta^{13}\text{C}$ gradients on Gardar Drift, data from each of the transect sites were treated in two

ways. First, benthic foraminiferal $\delta^{13}\text{C}$ data from all sites were binned into 2 kyr intervals, and an average benthic foraminiferal $\delta^{13}\text{C}$ value and the standard deviation of the data were calculated for each bin (Appendix 5). Second, a composite record was generated for sites in the northern portion of the transect (ODP site 984, ODP site 983, EW9302 JPC8, and V29-202) by compiling all data from these sites and interpolating the data every 200 years, and then smoothing using a 21-point gaussian curve. A composite record for the sites in the southern portion of the transect (11JPC, 3GGC, and Neap 18k) was determined using the same method. The difference between the smoothed north transect benthic foraminiferal $\delta^{13}\text{C}$ record and the smoothed south transect benthic foraminiferal $\delta^{13}\text{C}$ record was then determined.

Time-series analyses were completed on the average and standard deviation of the benthic foraminiferal $\delta^{13}\text{C}$ transect data using the AnalySeries 2.0.4.2 program (Paillard et al., 1996) to identify recurring features. The AnalySeries program is available online at <http://www.ncdc.noaa.gov/paleo/softlib/softlib.html>. Spectral analyses were completed using the Blackman-Tukey method (Blackman and Tukey, 1958). A 95 % confidence interval of the spectra was also determined.

The $\delta^{13}\text{C}$ value of the Southern Component Water (SCW) end member was determined by using ODP Site 1090 from the Atlantic sector of the Southern Ocean (Table 3.1). As an additional monitor of the intrusion of SCW into the North Atlantic, benthic foraminiferal $\delta^{13}\text{C}$ data was included from ODP Site 607, located below the subtropical North Atlantic (Ruddiman et al., 1989; Raymo et al., 1989). Core locations and depths for each site are provided in Table 3.1.

3.4. Results

3.4.1 Core KN166-14 11JPC

Marine Isotope Chronozones (MIC) 1 through 9a were defined in core 11JPC using the planktonic and benthic oxygen isotope records which show the typical saw-toothed pattern that characterized the late Pleistocene oxygen isotope curves (Lisiecki and Raymo, 2005; Figure 3.3; Appendix 3). The $\delta^{18}\text{O}$ values range from 0.8 to 3.8 ‰ for *G. bulloides*, and from 2.5 to 4.5 ‰ for *P. wuellerstorfi* (Figure 3.3). Sharp decreases in $\delta^{18}\text{O}$ are recorded at transitions from glacial to interglacial chronozones (MIC 8 – 7.5, MIC 6 – 5e; Figure 3.3). Both planktonic and benthic $\delta^{18}\text{O}$ records are variable during MIC 3, indicating variable temperatures, likely caused by high-frequency climate events (Figure 3.3).

Benthic foraminiferal $\delta^{13}\text{C}$ records from core 11JPC record orbital scale variability, with values from -0.3 to 1.5 ‰ for *P. wuellerstorfi* (Figure 3.3). The lowest values in benthic $\delta^{13}\text{C}$ are recorded in MIC 8, 6, 4, and 3 (Figure 3.3). Values of benthic $\delta^{13}\text{C}$ are highly variable during MIC 3, likely due to the high frequency Heinrich or Dansgaard/Oeschger Events (Figure 3.3).

The record of Wt. % CF varies on glacial-interglacial timescales with values ranging from 0 – 35 % for core 11JPC (Figure 3.3; Figure 3.5). Low Wt. % CF (< 15 %) values are recorded in interglacial MICs 7.5, 7.3-7.1, 5e-5c, 5a, and 1 (Figure 3.3; Figure 3.5). The highest Wt. % CF values are recorded from 1700 to 1550 cm, corresponding to MIC 6 (Figure 3.3; Figure 3.5b). Variability in Wt. % CF values indicates either: an increase in fine particles during interglacials, an increase of large particles during glacials, or both (Figure 3.3; Figure 3.5b). Increased ice rafted detritus (IRD) abundances during glacial periods are a well-documented feature of North Atlantic sediment records

(Ruddiman, 1977; Bond and Lotti, 1995; McManus et al., 1999; Venz et al., 1999; Andrews, 2000); this suggests that higher glacial Wt. % CF is due, mainly, to an increase in IRD (Figure 3.3; Figure 3.5b). The MIC 3 section is characterized by Wt. % CF values that are highly variable and range from 0 to 25 %; this is likely caused by increased IRD during Heinrich and Dansgaard/Oeschger Events (Bond and Lotti, 1995; Figure 3.3; Figure 3.5b). Intervals with the highest Wt. % CF correspond to the brightest reflectors in the 3.5 kHz seismic profile (Figure 3.5a; Figure 3.5b).

Weight percent carbonate also varies on glacial-interglacial time-scales in core 11JPC (Figure 3.5b), as has been shown in other cores (McManus et al., 1998). Low Wt. % CaCO_3 values (20 to 30 %) are recorded in the sections from 2200 to 2100, 1900 to 1800, 1600 to 1500 and 500 to 300 cm (Figure 3.5b). These low % CaCO_3 values are coincident with elevated % Coarse Fraction suggesting that the record of % CaCO_3 is determined mainly by the dilution of carbonate by larger IRD during glacial periods (Figure 3.3; Figure 3.5b). Highest values in % CaCO_3 are recorded in the core from 2100 to 2050, 1500 to 1450, 1275 to 1225, 950 to 800, and 150 to 0 cm (Figure 3.5b). These zones of high % CaCO_3 correspond to interglacial periods with high productivity (Figure 3.3). Percent CaCO_3 is variable during MIC 3 (Figure 3.3; McManus et al., 1998).

3.4.2 Core KN166-14 3GGC

Core 3GGC was subdivided into chronozones of the upper MIC 3, Last Glacial Maximum (LGM), Bolling/Allerod, Younger Dryas, and Holocene, using the benthic and planktonic $\delta^{18}\text{O}$ records (Figure 3.4; Appendix 4). Oxygen isotope values for *G. bulloides*, *N. pachyderma* (s), and *P. wuellerstorfi* are highest (~3.5, 4.5, and 4.5 ‰, respectively) in the LGM section (~ 25 to 15 ka; Figure 3.4). Termination 1 is recorded

by a decrease in the $\delta^{18}\text{O}$ values in all species, marking the Bolling/Allerod section. Increasing $\delta^{18}\text{O}$ values reflect the cooler conditions during the Younger Dryas section (~13.1 to 11.5 ka; Figure 3.4). The lowest $\delta^{18}\text{O}$ values in 3GGC represent the Holocene section (~11.5 to 0 ka; Figure 3.4).

Benthic and planktonic $\delta^{13}\text{C}$ records from core 3GGC also vary between these chronozones (Figure 3.4). Values of $\delta^{13}\text{C}$ decrease in the upper MIC3 and LGM sections for *G. bulloides*, *N. pachyderma* (s), and *P. wuellerstorfi* (from 0.0 to -1.0, from 0.5 to -0.3, and from 1.2 to 0.4 ‰, respectively); values of each species are similar in these sections (Figure 3.4). *Neoglobquadrina pachyderma* (s) and *P. wuellerstorfi* $\delta^{13}\text{C}$ values increase in the Bolling/Allerod, Younger Dryas, and lower Holocene to values of 1.0 and 0.5 ‰, respectively (Figure 3.4). Unlike *N. pachyderma* (s) and *P. wuellerstorfi*, *G. bulloides* $\delta^{13}\text{C}$ values decrease in the Bolling/Allerod, Younger Dryas, and lower Holocene to a value of -1.0 (Figure 3.4).

The record of Wt. % CF is variable for core 3GGC, with values ranging from 0 to 35 % (Figure 3.4). Low Wt. % CF (< 10 %) is observed in the upper MIC 3 and throughout MIC 1 (Figure 3.4). Higher Wt. % CF (> 20 %) is observed during the LGM, likely due to an increase in IRD (Figure 3.4; McManus et al., 1999).

3.4.3 Transect Results

A comparison of benthic foraminiferal $\delta^{13}\text{C}$ records from sites downstream of the Iceland-Scotland Ridge reveals a large degree of variability, indicating changes in watermasses (Figure 3.6). The sites in the southern portion of the transect show greater variability than those in the northern part (Figure 3.6; Figure 3.7). This is reflective of the greater influence of SCW, with low $\delta^{13}\text{C}$ values, recorded from sites that are more distal

from the Iceland-Scotland Ridge (Figure 3.6). Lower variability in $\delta^{13}\text{C}$ values in the northern sites, or sites proximal to the ridge, indicates that they were almost always bathed by a watermass of unchanging composition, which is likely ISOW (Figure 3.6). The difference in benthic foraminiferal $\delta^{13}\text{C}$ values between all transect sites is minimal ($< 0.5\text{‰}$) during the full interglacials, MIC 5e and the Holocene, indicating that all transect sites were bathed by a similar water mass during interglacial periods (Figure 3.6). The benthic foraminiferal $\delta^{13}\text{C}$ values of the northern transect compilation and southern transect compilation are similar during interglacial periods, also indicating that all of the transect sites were bathed by a similar watermass, likely ISOW (Figure 3.7).

The standard deviation of all benthic foraminiferal $\delta^{13}\text{C}$ data is less than 0.25‰ during interglacial periods, providing statistical representations of the small gradient in benthic foraminiferal $\delta^{13}\text{C}$ values within the transect sites (Figure 3.8). The difference between the northern and southern transect composite benthic foraminiferal $\delta^{13}\text{C}$ records is also lower during interglacials ($< 0.2\text{‰}$) indicating a small gradient in benthic foraminiferal $\delta^{13}\text{C}$ (Figure 3.8). The small increase in standard deviation values in the earliest portion MIC 5e is likely due to differences within the age models for individual records over the abrupt transition from MIC 6 to 5e (Figure 3.8). Since the northernmost cores used in this comparison (ODP site 984 and ODP site 983) lie northward of the maximum extent of AABW (Curry and Oppo, 2005), they always record the $\delta^{13}\text{C}$ signature of a northern source. The low variability in the benthic foraminiferal $\delta^{13}\text{C}$ records during the interglacial periods indicates that all sites are recording a northern sourced watermass during interglacial periods (Figure 3.6). Additionally, while benthic

foraminiferal $\delta^{13}\text{C}$ values at DSDP site 607 are very similar to southern Gardar values during interglacial periods, benthic foraminiferal $\delta^{13}\text{C}$ values from the South Atlantic site (ODP site 1090) are significantly lower, suggesting that southern sourced waters were not prevalent in the northern North Atlantic during these periods (Figure 3.6). Thus, a small benthic foraminiferal $\delta^{13}\text{C}$ gradient during MIC 5e and the Holocene indicates that a deep penetrating ISOW bathed all sites on Gardar Drift (Figure 3.6).

The gradient in benthic foraminiferal $\delta^{13}\text{C}$ values between the transect sites is large (up to ~ 1.5 ‰) during glacial periods MIC 6, 4, and 2; this suggests that different water masses bathed the north and south regions of this transect during each of these glacial periods (Figure 3.6; Figure 3.7). The standard deviation of the binned benthic foraminiferal $\delta^{13}\text{C}$ data show greater variability in bins that are in MIC 6, 4 and the LGM (> 0.25 ‰) relative to the bins in MIC 5e and 1; this suggests that the southern portion of the transect is bathed by a different watermass than the northern portion. The difference between the northern and southern transect composite benthic foraminiferal $\delta^{13}\text{C}$ records are both also larger (> 0.5 ‰) during these glacial periods, suggesting two water masses (Figure 3.8). During MIC 6, 4 and the LGM, benthic foraminiferal $\delta^{13}\text{C}$ values from southern Gardar Drift are more similar to values at ODP 607 and ODP 1090 than the benthic foraminiferal $\delta^{13}\text{C}$ values at northernmost transect sites, indicating that SCW waters invaded the North Atlantic, reaching the southern flanks of Gardar Drift (Figure 3.6; Figure 3.7). Because of the location of this transect, the intrusion of SCW onto southern Gardar Drift is evidence for the shoaling of ISOW during glacial periods.

The warmer substages of MIC 5, 5e, 5c, and 5a, are characterized by low (< 0.5 ‰) benthic foraminiferal $\delta^{13}\text{C}$ variability on Gardar Drift (Figure 3.6; Figure 3.7). The standard deviation of the benthic foraminiferal $\delta^{13}\text{C}$ bins during MIC 5 is generally < 0.25 ‰ (Figure 3.8). The difference between the northern and southern composite benthic foraminiferal $\delta^{13}\text{C}$ records is also lower during MIC 5e, 5c, 5a (Figure 3.8). The gradient is slightly larger during the cooler substages of MIC 5, MIC 5d and 5b (~ 0.5 ; Figure 3.6). Increased difference between the northern and southern composite benthic foraminiferal $\delta^{13}\text{C}$ records and increased standard deviation of benthic foraminiferal $\delta^{13}\text{C}$ values during MIC 5d and 5b signify a greater range in benthic foraminiferal $\delta^{13}\text{C}$ values within the transect (Figure 3.8). This suggests that ISOW was less vigorous or less dense during MIC 5d and 5b than during the other sub-stages of MIC 5 (Figure 3.6; Figure 3.8). However, MIC 5d and 5b are characterized by ISOW that was only slightly weakened or shoaled.

Higher frequency variability is superimposed on the longer-term trends during MIC 4 and 3 in core 11JPC records of % Coarse Fraction, IRD/gram, *G. bulloides* $\delta^{18}\text{O}$, *P. wuellerstorfi* $\delta^{13}\text{C}$, and % CaCO_3 (Figure 3.10). Percent Coarse Fraction and IRD/gram records decreased from 70 to 60 ka and reached minimum values at ~ 58 ka, followed by a general increase from 58 to 35 ka (Figure 3.10). Percent Carbonate and *P. wuellerstorfi* $\delta^{13}\text{C}$ records increased from 70 to 60 ka and reached maximum values at ~ 58 ka, followed by a general decrease in value from 58 to 35 ka (Figure 3.10). The period from 70 to 60 ka was characterized by a general decrease in the standard deviation of the benthic foraminiferal $\delta^{13}\text{C}$ values in the transect, followed by an increase in standard deviation from 58 to 35 ka, suggesting a decrease in ISOW strength (Figure 3.10).

Globigerina bulloides $\delta^{18}\text{O}$ values became increasingly variable during the period from 58 to 35 ka, suggesting changing surface water conditions that are attributed to increased freshwater inputs (Figure 3.10). Together, these records indicate an overarching change in circulation and climate whereby a general decrease in ice rafting and freshwater input leads to an increase in ISOW strength from 70 to 60 ka, and a general increase in ice rafting is linked to a decrease in ISOW strength from 58 to 35 ka (Figure 3.10).

Spectral analysis of the standard deviation of the benthic foraminiferal $\delta^{13}\text{C}$ values for the transect sites, which indicates the size of the gradient between northern and southern transect sites, reveals a strong precessional signal (Figure 3.9). The precessional control on the north-south gradient indicates that the density of ISOW is controlled by this orbital forcing (Figure 3.9).

3.5 Discussion

3.5.1. Orbital Scale ISOW Strength Variability

Variability in NCW formation is often linked to changes in insolation, known as Milankovich Cycles (Hays, 1976; Imbrie and Imbrie, 1980; Imbrie et al., 1993; Raymo et al., 1997; Raymo et al., 2004; Lisiecki and Raymo, 2005). Between 3 and 1 Ma, the 41-kyr obliquity cycles dominated benthic foraminiferal $\delta^{13}\text{C}$ records (Raymo et al., 1989; 1997; Shackleton et al. 1990; Lisiecki and Raymo, 2005). Following the Mid-Pleistocene Climate Transition, the 100-kyr eccentricity cycle dominated ice volume trends through the late Pleistocene (Hays, 1976; Raymo et al., 2004; Lisiecki et al., 2008). Northern Component Water strength has been shown to follow these orbital-scale climate changes (e.g., Raymo et al., 2004). The strength of ISOW also follows orbital-scale climate cycles with a strong 100-kyr periodicity (Figure 3.8; Duplessy et al., 1988a; Kissel et al., 1997).

In addition to the longer eccentricity and obliquity cycles, the ~ 23 -kyr precession cycle is also visible in climate records, most notably through the sub-stages of MIC 5 (Raymo et al., 2004), as well as in the Mediterranean sapropels (Hilgen, 1991); however, precession is considered to be a weak driver of large-scale ice volume changes (Lisiecki et al., 2008). Precession-driven peaks in high-latitude northern hemisphere insolation can be seen at ~ 50 and ~ 60 ka (Figure 3.8; Laskar et al., 2004); however, previous studies of NCW strength do not show corresponding changes during MIC 3 (Raymo et al., 2004). Similarly, an insolation peak at ~ 150 and ~ 170 ka caused by the precessional forcing occur during MIC 6, which is generally presumed to be a prolonged glacial period of decreased NCW formation (Raymo et al., 2004).

Benthic foraminiferal $\delta^{13}\text{C}$ records (Figure 3.6; Figure 3.8) indicate that ISOW was deeply flowing during interglacial periods, consistent with modern observations (Worthington, 1979) and other paleoceanographic reconstructions (Duplessy et al., 1988a; 1988b; Kissel et al., 1997). During glacial periods, ISOW shoaled according to our records (Figure 3.6; Figure 3.8), consistent with proxy evidence for weakened ISOW (Rasmussen et al., 1996; Kissel et al., 1997), and with observations of the intrusion of AABW into the northern North Atlantic (Boyle and Keigwin, 1987; Curry et al., 1988; Duplessy et al., 1988; McManus et al., 1999; Oppo and Horowitz, 2000; Marchitto et al., 2002; Curry and Oppo, 2005). This suggests that the general patterns of ISOW variability are driven by the 100-kyr eccentricity forcing. However, the variability in the benthic foraminiferal $\delta^{13}\text{C}$ values from the sites within the Gardar Drift transect also indicates that ISOW strength and/or density varied in concert with the precessional cycles (Figure 3.8; Figure 3.9). These cycles are easily seen during the precession minima at ~ 185 and \sim

145 ka during MIC 6, which are both associated with increased benthic foraminiferal $\delta^{13}\text{C}$ gradients from the standard deviation data, indicating weakened ISOW due to decreased insolation (Figure 3.8). These results are in opposition to those of Kuijpers et al. (1998) who suggested that ISOW formation was enhanced during MIC 6.

Additionally, the precessionally driven insolation minima at ~ 70 and ~ 25 ka, and slight minima at ~ 45 ka, have corresponding maxima in benthic foraminiferal $\delta^{13}\text{C}$ gradients (Figure 3.8; Figure 3.10).

The mechanism that links precession cycles and ISOW strength must not be strictly temperature dependent since neither ice core (Alley et al., 2004) nor paleoceanographic temperature records have a pronounced precessional signal (Raymo et al., 2004; Liseicki et al., 2009). However, I propose that, high northern latitude summer insolation minima, driven mainly by precession cycles, led to increased low-elevation glaciers and sea-ice, which in turn provided the fresh water necessary to impede convection in the Nordic Seas, and hinder the formation of ISOW. Additionally, the precessional forcing strongly effects low latitude climate variations (McIntyre and Molino, 1996) and thus precessionally-driven changes in the tropical carbon cycle may be driving the precessional variability seen in the Gardar Drift benthic foraminiferal $\delta^{13}\text{C}$ records.

A strong precessional control on ISOW strength (Figure 3.9) is especially interesting considering that ISOW is a large contributor to NCW (Worthington, 1976), and precession is not considered to exert a strong control on NCW production strength (Raymo et al., 2004; Lisiecki et al., 2008). This apparent difference may be due to the Gardar Drift transect is in a confined special location that is sensitive to even subtle

changes in NCW, making it highly sensitive. One possible explanation for the apparent disagreement between ISOW variations and NCW variations is that many NCW strength records do not have the temporal resolution to decipher precession-scale variability.

Another possible explanation is that other NCW contributors compensate for decreased ISOW production during some precession minima; such orbital-scale variability has been seen in records of Denmark Straits Overflow Water (e.g., Fagel et al., 2004; Millo et al., 2006) and Labrador Sea Water (Hillaire-Marcel et al., 2004).

3.5.2 Millennial Scale ISOW Variability

Higher-frequency variability is superimposed on the general trend from 70 to 35 ka (Figure 3.10). The % Coarse Fraction record shows several periods with a higher proportion of larger grains, from 68 to 66 ka, 64 to 59 ka, 53 to 48 ka, 45 to 40 ka, and 36.5 to 35.5 ka (Figure 3.10). Periods with elevated % Coarse Fraction are coincident with higher IRD/gram values suggesting that most coarse material is IRD, and with high *G. bulloides* $\delta^{18}\text{O}$ values, suggesting cold sea surface temperatures (Figure 3.10). These periods are characterized by low *P. wullerstorfi* $\delta^{13}\text{C}$ values and high standard deviation of transect benthic foraminiferal $\delta^{13}\text{C}$, indicating changes in bottom water masses. The most obvious way to induce these changes is by having a highly variable ISOW during MIC 3. While the age model for 11JPC is constrained by oxygen isotope stratigraphy and the Lachamp paleomagnetic event in this interval, these changes in ISOW strength may be linked to higher frequency Heinrich Events 4 thorough 6 and Dansgaard/Oeschger Events. These records are consistent with records that have shown variable ISOW due to Heinrich and Dansgaard/Oeschger Events (Oppo and Lehman, 1995; Dokken and Hald, 1996; Rasmussen et al., 1996; Kissell et al., 1999; McManus et al., 1999; Prins et al.,

2001; Prins et al., 2002; Rasmussen and Thomsen, 2009), and in contrast with records that suggest that ISOW was vigorous throughout MIC 3 (Duplessy et al., 1998b; Sarnthein et al., 1994; Kissel et al., 1997; Kuijpers et al., 1998).

3.6 Conclusions

Benthic foraminiferal $\delta^{13}\text{C}$ records from Gardar Drift reveal that the density and/or vigor of ISOW varied on orbital time-scales. Similar benthic foraminiferal $\delta^{13}\text{C}$ values were recorded along the transect during MIC 5e and 1, indicating that ISOW was deeply penetrating during interglacial periods (Figure 3.6; Figure 3.7). During MIC 6, 4, and 2, ISOW shoaled significantly allowing the intrusion of SCW into the southern region of Gardar Drift (Figure 3.6; Figure 3.10b). This relationship is consistent with previous studies linking NCW variation with the 100-kyr climate cycles of the late Pleistocene (e.g., Hays, 1976; Raymo et al., 1990; 2004). However, the Gardar Drift transect reveals a strong imprint of the precession component of insolation on ISOW production, particularly during intermediate climate states, such as MIC 3, and during the glacial states of MIC 6 and 4 (Figure 3.8; Figure 3.9). The expression of precession in MIC 5 is strong in the climate signal (*c.f.*, benthic foraminiferal $\delta^{18}\text{O}$ changes from MIC 5a to 5e) but muted in the $\delta^{13}\text{C}$ gradient on Gardar Drift. This suggests that, during the substages of MIC 5: 1) ISOW production remained strong and dense such that the mixing zone between NCW and SCW lay south of Gardar, and therefore Gardar Drift was insensitive to precession-driven changes; or 2) the smaller ice sheets in the northern hemisphere did not contribute substantial meltwater to the Norwegian Sea, and therefore could not affect ISOW production through either flux or density variations. On shorter

time-scales, high-frequency changes in ISOW strength are also linked to freshwater inputs, likely due to Heinrich or Dansgaard/Oeschger Events.

3.7 References

- Alley, R.B., Gow, A.J., Johnsen, S.J., Kipfstuhl, J., Messe, D.A., T. Thorsteinsson. 1995. Comparison of Deep Ice Cores. *Nature*. 373; 393-394.
- Andrews, J.T.. 2000. Icebergs and iceberg rafted detritus (IRD) in the North Atlantic: facts and assumptions. *Oceanography*. 13 (3); 100-108.
- Bé, A.W.H.. 1977. An ecological, zoogeographic and taxonomic review of recent planktonic foraminifera, in Ramsay, A.T.S. (ed.), Oceanic Micropaleontology, Academic Press, London. 1; 1-100.
- Bé, A.W.H. and D.S. Tolderlund. 1971. Distribution and ecology of living planktonic foraminifera in surface waters of the Atlantic and Indian Oceans, in Funnel, B.M. and Riedel, W.R. (eds.), The Micropaleontology of Oceans. 105-149.
- Berger, A.. 1992. Orbital Variations and Insolation Database. IGBP PAGES/World Data Center-A for Paleoclimatology Data Contribution Series # 92-007. NOAA/NGDC Paleoclimatology Program, Boulder CO, USA.
- Bianchi, G.G. and N. McCave, 1999. Holocene periodicity in North Atlantic climate and deep-ocean flow south of Iceland. *Nature*. 397; 515-517.
- Blackman, R. B. and J. W. Tukey. 1958. The Measurement of Power Spectra From the Point of View of Communication Engineering. Dover Publications, New York. 190 pp.
- Bond, G.C. and R. Lotti. 1995. Iceberg Discharges into the North Atlantic on Millennial Time Scales During the Last Glaciation. *Science*. 267; 1005-1010
- Boyle, E.A. and L.D. Keigwin, 1987. North Atlantic thermohaline circulation during the past 20,000 years linked to high-latitude surface temperature. *Nature*. 330; 35-40.
- Broecker, W.S., Peteet, D.M., and D. Rind. 1985. Does the ocean-atmosphere system have more than one stable mode of operation? *Nature*. 315; 21-26.
- Broecker, W.S. and G.H. Denton. 1989. The role of ocean-atmosphere reorganizations in glacial cycles. *Geochimica et Cosmochimica Acta*. 53; 2465-2501.
- Broecker, W.S., Bond, G., Klas, M., Bonani, G., and W. Wolfli. 1990. A Salt Oscillator in the Glacial Atlantic? *Paleoceanography*. 5(4); 469-477.

- Chapman, M.R. and N.J. Shackleton. 1999. Global ice-volume fluctuations, North Atlantic ice-rafting events, and deep-ocean circulation changes between 130 and 70 ka. *Geology*. 27 (9); 795-798.
- Charles, C.D. and R.G. Fairbanks. 1992. Evidence from Southern Ocean sediments for the effect of North Atlantic deep-water flux on climate. *Nature*. 355; 416-419.
- Channell, J.E.T., Hodell, D.A., and B. Lehman. 1997. Relative geomagnetic paleointensity and $\delta^{18}\text{O}$ at ODP Site 983 (Gardar Drift, North Atlantic) since 350ka. *Earth and Planetary Science Letters*. 153; 103-118.
- Coplen, T.B., Kendall, C., and J. Hopple. 1983. Comparison of stable isotope reference samples. *Nature*. 302; 236-238.
- Cortijo, E., Labeyrie, L., Vidal, L., Vautravers, M., Chapman, M., Duplessy, J.-C., Elliot, M., Arnold, M., Turon, J.-L., and G. Auffret. 1997. Changes in sea surface hydrology associated with Heinrich Event 4 in the North Atlantic Ocean between 40 and 60N. *Earth and Planetary Science Letters*. 146; 29-45.
- Curry, W.B., Duplessy, J.C., Labeyrie, L.D., and N.J. Shackleton. 1988. Changes in the distribution of $\delta^{13}\text{C}$ of deep water ΣCO_2 between the last glaciation and the Holocene. *Paleoceanography*. 3(3); 317-341.
- Curry, W.B. and D.W. Oppo. 2005. Glacial water mass geometry and the distribution of $\delta^{13}\text{C}$ and ΣCO_2 in the western Atlantic Ocean. *Paleoceanography*. 20; 1-12.
- Davies, T.A. and A.S. Laughton. 1972. Sedimentary processes in the North Atlantic. In: Laughton, A.S., Berggren, W.A. et al. (Eds.), Initial Reports of Deep Sea Drilling Project, Vol. 12. U.S. Government Printing Office, Washington, D.C., pp. 905-934.
- de Menocal, P.B., Oppo, D.W., and R.G. Fairbanks. 1992. Pleistocene $\delta^{13}\text{C}$ Variability of North Atlantic Intermediate Water. *Paleoceanography*. 7 (2); 229-250.
- de Vernal, A., Hillaire-Marcel, C., Peltier, W.R., and A.J. Weaver. 2002. Structure of the upper water column in the Northwest North Atlantic: modern versus last glacial maximum conditions. *Paleoceanography*. 17(4); 1050-1065.
- de Vernal, A., Eynaud, F., Henry, M., Hillaire-Marcel, C., Londeix, L., Mangin, S., Matthiessen, J., Marret, F., Radi, T., Rochon, A., Solignac, S., and J.-L. Turon. 2005. Reconstruction of sea-surface conditions at middle to high latitudes to the Northern hemisphere during the Last Glacial Maximum (LGM) based on dinoflagellate cyst assemblages. *Quaternary Science Reviews*. 24; 897-924.
- Dokken, T. and M. Hald. 1996. Rapid climatic shifts during isotopes stages 2-4 in the Polar North Atlantic. *Geology*. 24 (7); 599-602.

- Duplessy, J.C., Shackleton, N.J., Fairbanks, R.G., Labeyrie, L., Oppo, D.W., and N. Kallel. 1988a. Deepwater source variations during the last climatic cycle and their impact on the global deep-water circulation. *Paleoceanography*. 3(3); 342-360.
- Duplessy, J.C., Labeyrie, L., and P.L. Blanc. 1988b. Norwegian Sea Deep Water Variations Over the Last Climatic Cycle: Paleo-oceanographical Implications. *Long and Short Term Variability of Climate*. 16; 86-116.
- Ellison, C.R.W., Chapman, M.R., and I.R. Hall. 2006. Surface and Deep Ocean Interactions During the Cold Climate Event 8200 Years ago. *Science*. 312; 1929-1933.
- Fagel, N., Innocent, C., Gariépy, C. and C. Hillaire-Marcel. 2002. Sources of Labrador Sea sediments since the last glacial maximum inferred from Nd-Pb isotopes. *Geochimica et Cosmochimica Acta*. 66 (14); 2569-2581.
- Fairbanks, R.G., Mortlock, R.A., Chiu, T.-C., Cao, L., Kaplan, A., Guilderson, T.P., Fairbanks, T.W., Bloom, A.L., Grootes, P.M., and M.-J. Nadeau. 2005. Radiocarbon calibration curve spanning 0 to 50,000 years BP based on paired ^{230}Th , $^{234}\text{U}/^{238}\text{U}$ and ^{14}C dates on pristine corals. *Quaternary Science Reviews*. 24; 1781-1796.
- Faugers, J.C., Stow, D.A.C., Imbert, P., and A. Viana. 1999. Seismic features diagnostic of contourite drifts. *Marine Geology*. 162; 1-38.
- Flower, B.P., Oppo, D.W., McManus, J.F., Venz, K.A., Hodell, D.A., and J.L. Cullen. 2000. North Atlantic intermediate to deep water circulation and chemical stratification during the past 1 Myr. *Paleoceanography*. 15; 388-403.
- Ganopolsi, A., Rahmstorf, S., Petoukhov, V., and M. Claussen. 1998. Simulation of modern and glacial climates with a coupled global model of intermediate complexity. *Nature*. 391; 351-356.
- Gherardi, J.-M., Labeyrie, L., McManus, J.F., Francois, R., Skinner, L.C., and E. Cortijo. 2005. Evidence from the Northeastern Atlantic basin for variability in the rate of meridional overturning circulation through the last deglaciation. *Earth and Planetary Science Letters*. 240; 710-723.
- Hall, I.R., McCave, I.N., Chapman, M.R., and N.J. Shackleton. 1998. Coherent deep flow variation in the Iceland and American basins during the last interglacial. *Earth and Planetary Science Letters*. 164; 15-21.
- Hatun, H., Sando, A.B., Drang, H., and M. Bentsen. 2004. Seasonal to Decadal Temperature Variations in the Faroe-Shetland Inflow Water. *Geophysical Monograph- American Geophysical Union*.

- Hays, J.D., Imbrie, J., and N.J. Shackleton. 1976. Variations in the Earth's Orbit: Pacemaker of the Ice Ages. *Science*. 194 (4270); 1121-1134.
- Hemming, S.R., Broecker, W.S., Sharp, W.D., Bond, G.C., Gwiazda, R.H., McManus, J.F., Klas, M., and I. Hajdas. 1998. Provenance of Heinrich layers in core V28-82, northeastern Atlantic: $^{40}\text{Ar}/^{39}\text{Ar}$ ages of ice-rafted hornblende, Pb isotopes in feldspar grains and Nd-Sr-Pb isotopes in the fine sediment fraction. *Earth and Planetary Science Letters*. 164; 317-333.
- Hilgen, F.J.. 1991. Astronomical calibration of Gauss to Matuyama sapropels in the Mediterranean and implication for the Geomagnetic Polarity Time Scale. *Earth and Planetary Science Letters*. 104; 226-244.
- Hillaire-Marcel, C., A. de Vernal, M. Lucotte, and A. Mucci. 1994. The Labrador Sea during the late Quaternary. *Canadian Journal of Earth Sciences*. 31; 1-4.
- Hillaire-Marcel, C., de Vernal, A., Bilodeau, G., and A.J. Weaver. 2001. Absence of deep-water formation in the Labrador Sea During the last interglacial period. *Nature*. 410; 1073-1078.
- Hodell, D., Gersonde, R., and P. Blum. 2002. Leg 177 synthesis: insights into the Southern Ocean paleoceanography on tectonic to millennial timescales. In Gersonde, R., Hodell, D., and P. Blum (Eds.), *Proc.ODP, Sci. Results*. 177; 1-54.
- Hollister, C.D., Flood, R.D., and I.N. McCave. 1978. Plastering and decorating in the North Atlantic. *Oceanus*. 21 (1); 5-13.
- Imbrie, J. and J.Z. Imbrie. 1980. Modeling the Climatic Response to Orbital Variations. *Science*. 207 (4434); 943-953.
- Imbrie, J., A., Berger, E.A. Boyle, S.C. Clemens, A. Duffy, W.R. Howard, G. Kulka, J. Kitzbach, D.G. Martinon, A. McIntyre, A.C. Mix, B. Molfino, J.J. Morley, L.C. Peterson, N.G. Pisias, W.L. Prell, M.E. Raymo, N.J. Shackleton, and J. R. Toggweiler. 1993. On the structure and origin of major glaciation cycles 2. The 100,000-year cycle. *Paleoceanography*. 8 (6); 699-736.
- Jansen, E., Raymo, M.E., Blum, P., et al., 1996. Site 983. In *Proceedings of Ocean Drilling Program, Initial Reports*. 162; 139-167.
- Kissel, C., Laj, C., Lehman, B., Labyrie, L., and V. Bout-Roumazielles. 1997. Changes in the strength of the Iceland-Scotland Overflow Water in the last 200,000 years: Evidence from magnetic anisotropy analysis of core SU90-33. *Earth and Planetary Science Letters*. 152; 25-36.

- Kissel, C., Laj, C., Labeyrie, L., Dokken, T., Voelker, A., and D. Blamart. 1999. Rapid climatic variations during marine isotopic stage 3: magnetic analysis of sediments from Nordic Seas and North Atlantic. *Earth and Planetary Science Letters*. 171; 489-502.
- Kleiven, H.F., Jansen, E., Curry, W.B., Hodell, D.A., and K. Venz. 2003. Atlantic Ocean thermohaline circulation changes on orbital to sub-orbital timescales during the mid-Pleistocene. *Paleoceanography*, 18 (1); 1-13.
- Kohler, P. and R. Bintanja. 2008. The carbon cycle during the Mid Pleistocene Transition: the Southern Ocean Decoupling Hypothesis. *Climate of the Past*. 4; 311-332.
- Knorr, G. and G. Lohmann. 2003. Southern Ocean origin for the resumption of Atlantic thermohaline circulation during deglaciation. *Nature*. 424; 532-536.
- Kroopnick, P.. 1985. The Distribution of ^{13}C in the Atlantic Ocean. *Earth and Planetary Science Letters*. 49; 469-484.
- Kuijpers, A., Troelstra, S.R., Wisse, M., Nielsen, S.H., and T.C.E. van Weering. 1998. Norwegian Sea overflow variability and NE Atlantic surface hydrography during the past 150,000 years. *Marine Geology*. 152; 75-99.
- Lagerklint, I.M. and J.D. Wright. 1999. Late glacial warming prior to Heinrich Event 1: The influence of ice rafting and large ice sheets on the timing of initial warming. *Geology*. 27 (12); 1099-1102.
- Laskar, J., Joutel, F., and F. Boudin. 1993. Orbital, precessional, and insolation quantities for the Earth from -20 Myr to +10 Myr. *Astronomy and Astrophysics*. 270; 522-533.
- Lazier, J.R.N.. 1973. The renewal of Labrador Sea Water. *Deep Sea Research*. 21; 341-353.
- Lehman, S.J. and L.D. Keigwin. 1992. Sudden changes in North Atlantic Circulation during the Last Deglaciation. *Nature*. 356; 757-762.
- Lisiecki, L.E. and M.E. Raymo. 2005. A Pliocene-Pleistocene stack of 57 globally distributed benthic $\delta^{18}\text{O}$ records. *Paleoceanography*. 20 (1003); 1-17.
- Lisiecki, L.E., Raymo, M.E., and W.B. Curry. 2008. Atlantic overturning responses to Late Pleistocene climate forcings. *Nature*. 456 (6); 85-88.
- Lynch-Stieglitz, J., Adkins, J.F., Curry, W.B., Dokken, T., Hall, I.R., Herguera, J.C., Hirschi, J.J.M., Ivanova, E.V., Kissell, C., Marchal, O., Marchitto, T.M., McCave, I.N., McManus, J.F., Mulitza, S., Ninnemann, U., Peeters, F., Yu, E.-F., and R.

- Zahn. 2007. Atlantic Meridonal Overturning Circulation During the Last Glacial Maximum. *Science*. 316; 66-69.
- Manley, P.L., Manley, T.O., Kelly, L.C., Wright, J.D., and G.S. Mountain. 2004. Mudwaves on the South Gardar Drift: North Atlantic. *Eos Trans. AGU* 85(17), Jt. Assem. Supp., Abstract GC21A-05.
- Mann, C.R.. 1969. Temperature and salinity characteristics of the Denmark Strait overflow. *Deep-Sea Research*. 16; 125-137.
- Marchitto, T.M., Oppo, D.W., and W.B. Curry. 2002. Paired benthic foraminiferal Cd/Ca and Zn/Ca evidence for a greatly increased presence of Southern Ocean Water in the glacial North Atlantic. *Paleoceanography*. 17 (3); 1-16.
- McCave, I.N, Lonsdale P.F., Hollister C.D., and W.D. Gardner. 1980. Sediment Transport over the Hatton and Gardar Contourite Drifts. *Journal of Sedimentary Petrology*. 50 (4); 1049-1062.
- McCave, I.N. and B.E. Tucholke. 1986. Deep current-controlled sedimentation in the western North Atlantic. In Vogt, P.R. and B.E. Tucholke (Eds.), *The Geology of North America, Vol. M, The Western North Atlantic Region*. Geological Society of America, Boulder, CO; 451-468.
- McIntyre, A. and B. Molino. 1996. Forcing of Atlantic Equatorial and Subpolar Millennial Cycles by Precession. *Science*. 274; 1867-1870.
- McIntyre, K., Ravelo, A.C., and M.L. Delaney. 1999. North Atlantic Intermediate Waters in the late Pliocene to early Pleistocene. *Paleoceanography*. 14; 324-335.
- McManus, J.F., Oppo, D.W., and J.L. Cullen. 1999. A 0.5-Million-Year Record of Millennial-Scale Climate Variability in the North Atlantic. *Science*. 283; 971-975.
- Millo, C., Sarnthein, M., Voelker, A., and H. Erlenkeuser. 2006. Variability of the Denmark Strait Overflow during the Last Glacial Maximum. *Boreas*. 1; 50-60.
- Neitzke, L.C. and J.D. Wright. 2007. The Imprint of NADW on the Eirik Drift during the Younger Dryas. *Eos Trans. AGU* 87(52), Fall Meet. Suppl.; Abstract PP23C-1766.
- Oppo, D.W. and R.G. Fairbanks. 1987. Variability in the deep and intermediate water circulation of the Atlantic Ocean during the past 25,000 years; Northern Hemisphere modulation of the Southern Ocean. *Earth and Planetary Science Letters*. 86 (1); 1-15.
- Oppo, D.W. and S.J. Lehman. 1995. Suborbital timescale variability of North Atlantic Deep Water during the past 200,000 years. *Paleoceanography*. 10(5); 901-910.

- Oppo, D.W., Raymo, M.E., Lohmann, G.P., Mix, A.C., Wright, J.D., and W.L. Prell. 1995. A $\delta^{13}\text{C}$ record of Upper North Atlantic Deep Water during the past 2.6 million years. *Paleoceanography*. 10 (3); 373-394.
- Oppo, D.W., Horowitz, M., and S.J. Lehman. 1997. Marine Core Evidence for Reduced Deep Water Production During Termination II Followed By a Relatively Stable Substage 5e (Eemian). *Paleoceanography*. 12; 51-63.
- Oppo, D.W. and M. Horowitz. 2000. Glacial deep water geometry: South Atlantic benthic foraminiferal Cd/Ca and $\delta^{13}\text{C}$ evidence. *Paleoceanography*. 15 (2); 147-160.
- Oppo, D.W., Keigwin, L.D., McManus, J.F., and J.L. Cullen. 2001. Persistent suborbital climate variability in marine isotope stage 5 and Termination II. *Paleoceanography*. 16(3); 280.
- Oppo, D.W., McManis, J.F., and J.L. Cullen. 2003. Deepwater variability in the Holocene epoch. *Nature*. 422; 277-278.
- Paillard, D. and E. Cortijo. 1999. A simulation of the Atlantic meridional circulation during Heinrich Event 4 using reconstructed sea surface temperatures and salinities. *Paleoceanography*. 14(6); 716-724.
- Paillard, D., Labeyrie, L., and P. Yiou. 1996. Macintosh program performs time-series analysis. *Eos Trans. AGU*. 77; 379.
- Philanderer, S.G. and A.V. Fedorov. 2003. Role of tropic in changing the response to Millankovich forcing some three million years ago. *Paleoceanography*. 18 (2); 1-12.
- Piotrowski, A.M., Goldstein, S.L., Hemming, S.R., and R.G. Fairbanks. 2005. Temporal relationships of carbon cycling and ocean circulation at glacial boundaries. *Science*. 307; 1933-1938.
- Prins, M.A., Troelstra, S.R., Kruk, R.W., van der Borg, K., de Jong, A.F.M., and G.J. Weltje. 2001. The Late Quaternary Sediment Record of the Reykjanes Ridge, North Atlantic. *Radiocarbon*. 43 (2B); 939-947.
- Prins., M.A., Bouwer, L.M., Beets, C.J., Troelstra, S.R., and G.J. Weltje. 2002. Ocean circulation and iceberg discharge in the glacial North Atlantic: Inferences from unmixing of sediment size distribution. *Geology*. 30 (6); 555-558.
- Rasmussen, T.L., Thomson, E., van Weering, T.C.E., and L. Labeyrie. 1996. Rapid changes in surface and deep water conditions at the Faeroe Margin during the last 58,000 years. *Paleoceanography*. 11(6); 757-771.

- Rasmussen, T.L Thomson, E., Labeyrie, L., and T.C.E. van Weering. 1996. Circulation changes in the Faeroe-Shetland Channel correlating with cold events during the last glacial period (58-10 ka). *Geology*. 24; 937-940.
- Rasmussen, T.L. and E. Thomson. 2009. Ventilation changes in intermediate water on millennial time scales in the SE Nordic seas, 65-11 kyr BP. *Geophysical Research Letters*. 36l; 1-5.
- Raymo, M.E., Ruddiman, W.F., Backman, J., Clement, B.M., and D.G. Martinson. 1989. Late Pliocene variation in Northern Hemisphere ice sheets and North Atlantic deep water circulation. *Paleoceanography*. 4; 413-446.
- Raymo, M.E., Ruddiman, W.F., Backman, J., Clemet, B.M., and D.G. Martinson. 1990. Evolution of Atlantic-Pacific $\delta^{13}\text{C}$ gradients over the last 2.5 my. *Earth and Planetary Science Letters*. 97; 353-368.
- Raymo, M.E.. 1997. The timing of major climate terminations. *Paleoceanography*. 12; 577-585.
- Raymo, M.E., Oppo, D.W., and W.B. Curry. 1998. The Mid-Pleistocene Climate Transition: A Deep Sea Carbon Isotopic Perspective. *Paleoceanography*. 12 (4); 546-559.
- Raymo, M.E., Ganley, K., Carter, S., Oppo, D.W., and J. McManus. 1998. Millennial-scale climate instability during the early Pleistocene epoch. *Nature*. 392; 699-702.
- Raymo, M.E., Oppo, D.W., Flower, B.P., Flower, Hodell, D.A., McManus, J.F., Venz, K.A., Kleiven, K.F., and K. McIntyre. 2004. Stability of North Atlantic Water Masses in Face of Pronounced Climate Variability During the Pleistocene. *Paleoceanography*. 19; 1-13.
- Revel, M., Cremer, M., Grousset, F.E., and L. Labeyrie. 1996. Grain-size and Sr-Nd isotopes as tracer of paleo-bottom current strength, Northeast Atlantic Ocean. *Marine Geology*. 131; 233-249.
- Rind, D., Demenocal, P., Russel, G.L., Sheth, S., Collins, D., Schmidt, G.A., and J. Teller. 2001. Effects of glacial meltwater in the GISS Coupled Atmosphere-Ocean Model: Part 1: North Atlantic Deep Water response. *Journal Geophysical Research Letters*. 106; 27335-27354.
- Ruddiman, W.F.. 1977. Late Quaternary deposition of ice-rafted sand in the subpolar North Atlantic (lat 40 to 65N). *Geological Society of America Bulletin*. 88; 1813-1827.

- Ruddiman, W.F., Raymo, M.E., Martinson, D.G., Clement, B.M., and J. Backman, 1989. Mid-Pleistocene evolution of Northern Hemisphere climate, *Paleoceanography*, 4; 353-412.
- Sarnthein, M., Winn, K., Jung, S.J.A., Duplessy, J.-C., Labeyrie, L., Erienkeuser, H., and G.Ganssen. 1994. Changes in east Atlantic deepwater circulation over the last 30,000 years: Eight time slice reconstructions. *Paleoceanography*. 9 (2); 209-267.
- Schmitz, W.J. and M.S. McCartney. 1993. On the North Atlantic Circulation. *Reviews of Geophysics*. 31 (1); 29-49.
- Seidenkrantz, M.-S., Bornmalm, L., Johnsen, S.J., Knudsen, K.L., Kuijpers, A., Lauritzen, S.-E., Leroy, S.A.G., Mergeal, I., Schweger, C., and B. Van Vliet-Lanoe. 1996. Two-step deglaciation at the oxygen isotope stage 6/5e transition: the Zeifen-Kattegat Climate Oscillation. *Quaternary Science Reviews*. 55; 63-75.
- Shipboard Scientific Party. 1999. Site 1090. In: Gersonde, R., Hodell, D.A., Blum, P., et al. (Eds.), *Proc. ODP Init. Rep.* 177; 1-101.
- Stanford, J.D., Rohling, E.J., Hunter, S.E., Roberts, A.P., Rasmussen, S.O., Bard, E., McManus, J., and R.G. Fairbanks. 2006. Timing of meltwater pulse 1a and climate responses to meltwater injections. *Paleoceanography*. 21; PA4103.
- Turrell, W.R., Slessor, G., Adams, R.D, Payne, R., and P.A. Gillibrand. 1999. Decadal variability in the composition of Faroe Shetland Channel bottom Water. *Deep-Sea Research I*. 46; 1-25.
- Venz, K.A. and D.A. Hodell. 2002. New evidence for changes in Plio-Pleistocene deep circulation from Southern Ocean ODP Leg 177 Site 1090. *Paleogeography, Paleoclimatology, Paleoecology*. 182; 197-220.
- Worthington, L.V.. 1969. An attempt to measure the volume transport of Norwegian Sea overflow water through the Denmark Strait. *Deep-Sea Research*. 16; 421-432.
- Worthington, L.V.. 1976. On the North Atlantic Circulation. Johns Hopkins University Press; Baltimore, MD.
- Wright, J.D. and K.G. Miller. 1996. Control of North Atlantic Deep Water circulation by the Greenland-Scotland Ridge. *Paleoceanography*. 11(2); 157-170.

Table 3.1: Locations and water depths of cores used in this study.

Core	Lat	Lon	Water Depth (m)	Reference
ODP site 984	61.43	-24.08	1660	Raymo et al., 2004
EW9302 JPC8	61.00	-25.00	1915	Oppo et al., 2001; Oppo et al., 1997
ODP site 983	60.40	-23.63	1995	Jansen et al., 1996; McIntyre et al., 1999; Raymo et al., 1998; Kleiven et al., 2003; Raymo et al., 2004;
V29-202	61.00	-21.00	2658	Oppo and Lehman, 1995
KN166-14 11JPC	56.24	-27.65	2707	This Study
KN166-14 3GGC	55.52	-26.53	3305	This Study
Neap 18k	52.77	-30.35	3275	Chapman & Shackleton, 1999
DSDP site 607	41.00	-32.96	3427	Raymo et al., 2004
ODP site 1090	42.91	-8.90	3702	Venz and Hodell, 2002

Table 3.2: Age model for core KN166-14 11JPC. Tie points were determined by AMS ^{14}C (white boxes), magneto-stratigraphy (orange box) or chrono-stratigraphic comparison to a stacked benthic foraminiferal $\delta^{18}\text{O}$ record by Liseicki and Raymo (2005; blue boxes). AMS ^{14}C ages in red were not included in the age model. AMS ^{14}C dates were corrected to calendar ages and those designated by asterisks were further corrected to account for the bioturbation of sub-hiatus material (see section 2.3.2).

Depth (cm)	Age (ka)
0	0.67
45	2.87
105	6.05
127	7.06
143	8.38
145	6.99
147	8.58
149	8.86
153	8.88
163	9.65
183	11.45
198	11.99
213	13.34 *
220	13.62 *
227	34.07
250	33.71
282	31.91
333	33.81
430	40.00
626	62.70
779.7	74.50
1003	88.00
1260	103.00
1394	110.00
1518	129.30
1558	138.20
1636	174.50
1795	201.00
1929	226.00
2083	254.00
2290	295.00

Table 3.3: Age model for core KN166-14 3GGC was determined based on chrono-stratigraphic comparison to a stacked benthic foraminiferal $\delta^{18}\text{O}$ record by Liseicki and Raymo (2005).

Depth (cm)	Age (ka)
0	0
82	11.5
94	13.3
102	15
184	30

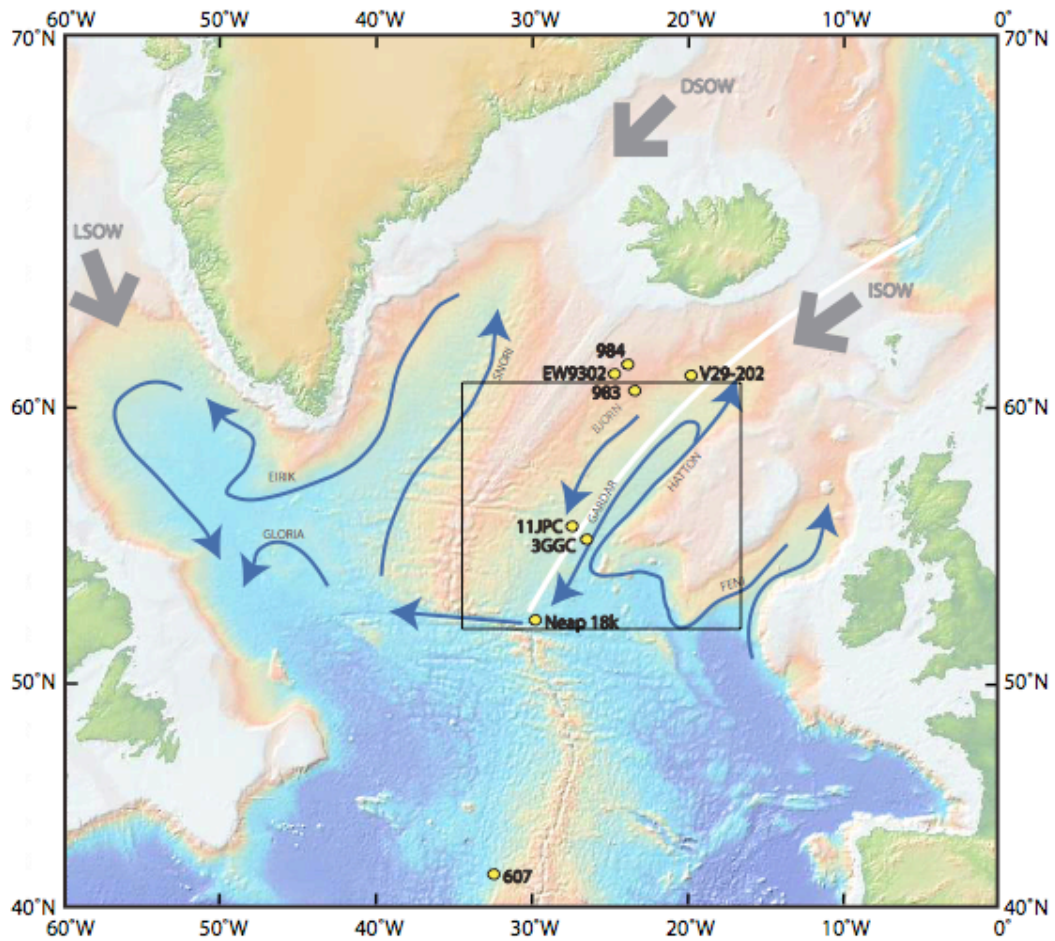


Figure 3.1: Bathymetric map of the North Atlantic, including bottom water currents (blue), contourite drifts (uppercase lettering), and the northern components of NADW (grey arrows). Core locations from this study and previously published studies are shown (yellow). The location of the cross section of Figure 3.2 is shown by the white line. The location of map inset for Figure 3.5a is designated by the black box.

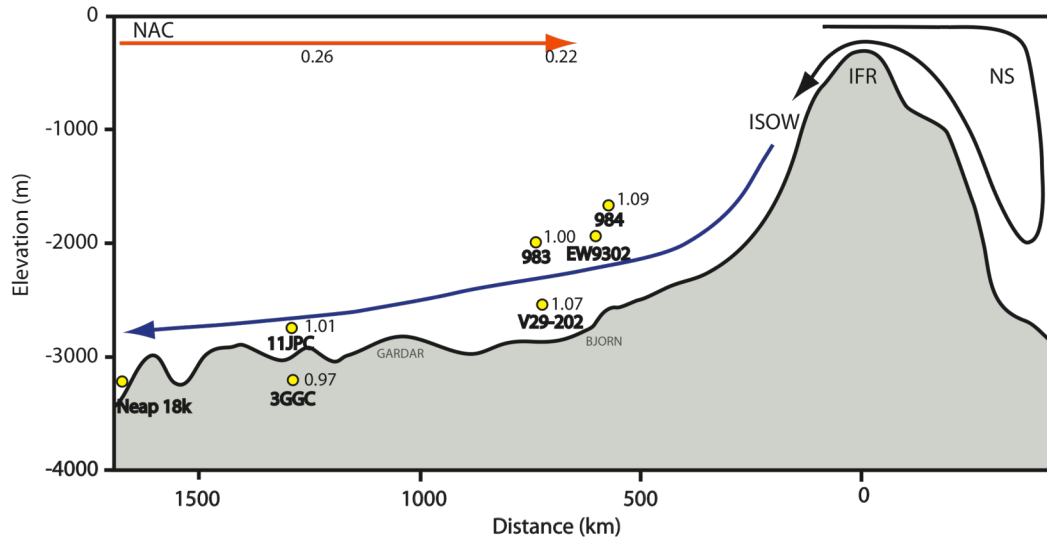


Figure 3.2: Bathymetric cross section of the southern Norwegian Sea (NS) and the region south of the Iceland-Scotland Ridge (IFR), as shown by the white line on Figure 3.1. The location of Bjorn and Gardar Drifts are shown, as are the projected locations of all cores used in this study (yellow circles). Bold lines show idealized directions of the major water masses, North Atlantic Current (NAC) and Iceland-Scotland Overflow Water (ISOW). Late Holocene *P. wuellerstorfi* and *N. Pachyderma* $\delta^{13}\text{C}$ values are shown.

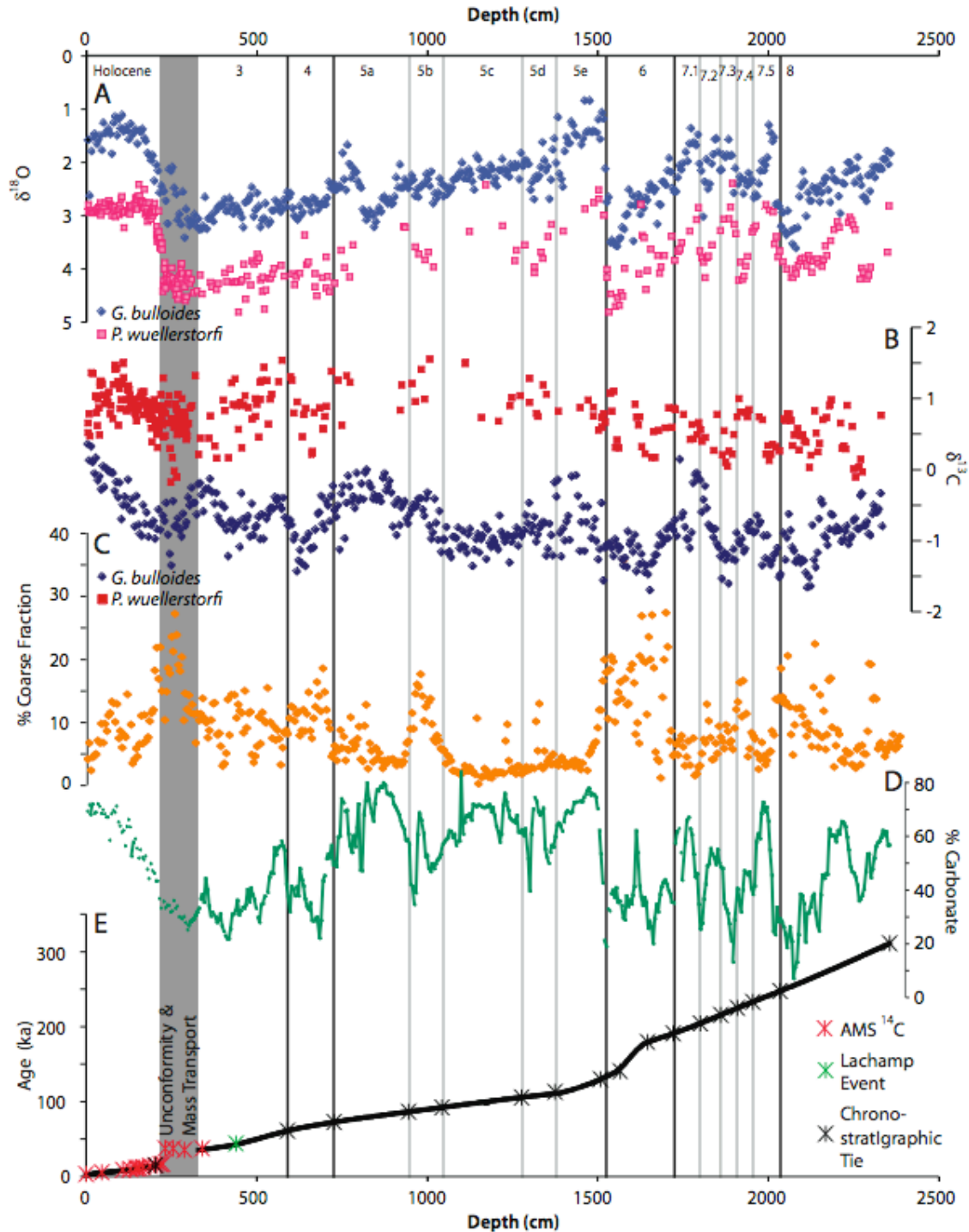


Figure 3.3: Proxy records from core 11JPC plotted versus sediment depth. (A) $\delta^{18}\text{O}$ *G. bulloides* (pink) and $\delta^{18}\text{O}$ *P. wuellerstorfi* (red), (B) $\delta^{13}\text{C}$ *G. bulloides* (blue) and $\delta^{13}\text{C}$ *P. wuellerstorfi* (navy), (C) % coarse fraction (orange), (D) % carbonate, and (E) the age model are shown. Marine Isotope Chrons 1 through 8 are also shown.

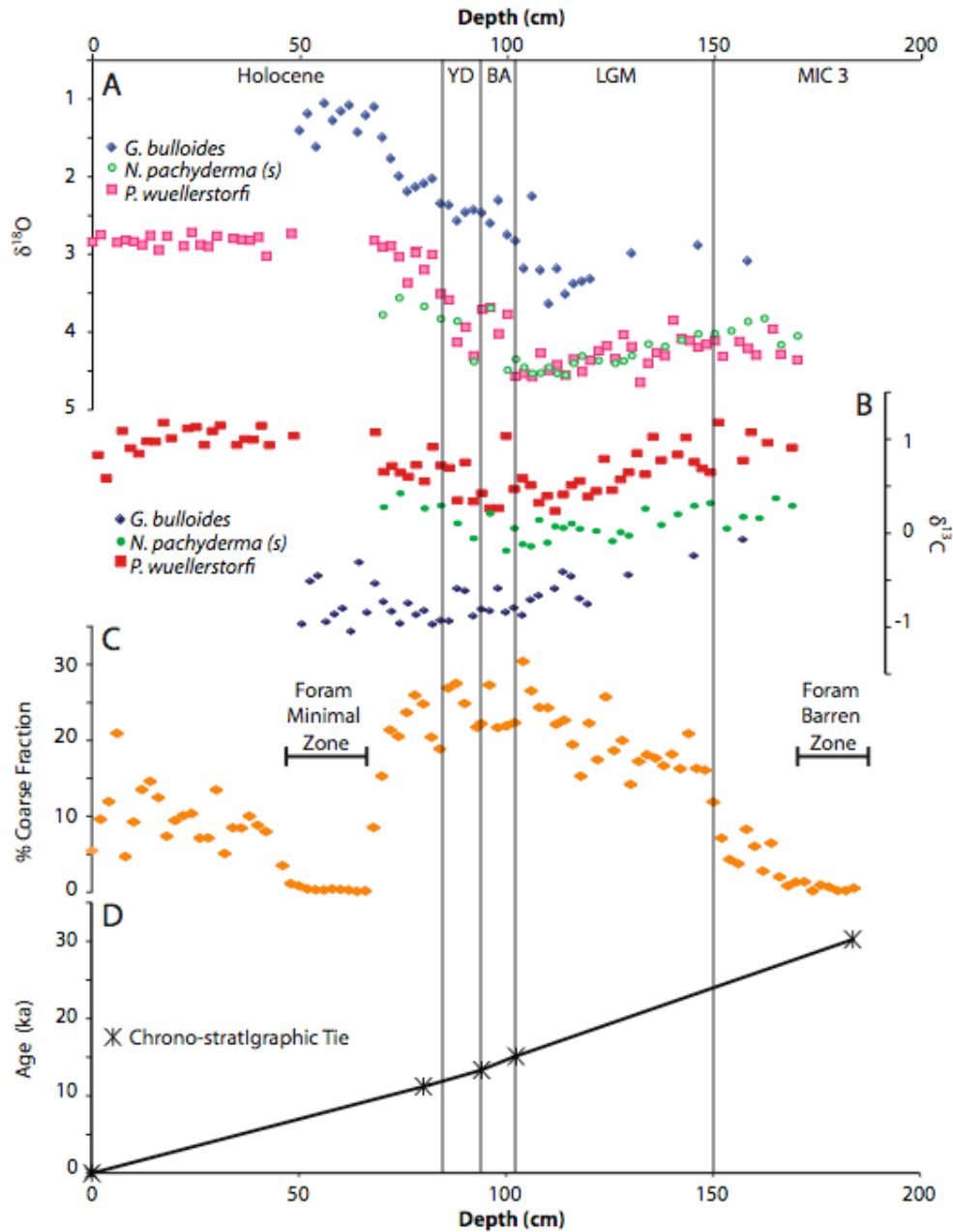


Figure 3.4: Proxy records for core 3GGC plotted versus sediment depth. **(A)** $\delta^{18}\text{O}$ *G. bulloides* (pink), $\delta^{18}\text{O}$ *N. pachyderma* (s; light green), and $\delta^{18}\text{O}$ *P. wuellerstorfi* (red), **(B)** $\delta^{13}\text{C}$ *G. bulloides* (blue), $\delta^{13}\text{C}$ *N. pachyderma* (s; green), and $\delta^{13}\text{C}$ *P. wuellerstorfi* (navy), **(C)** % coarse fraction (orange), **(D)** the age model are shown. The Holocene, Younger Dryas (YD), Bolling/Allerod (BA), Last Glacial Maximum (LGM) and MIC 3 are also shown.

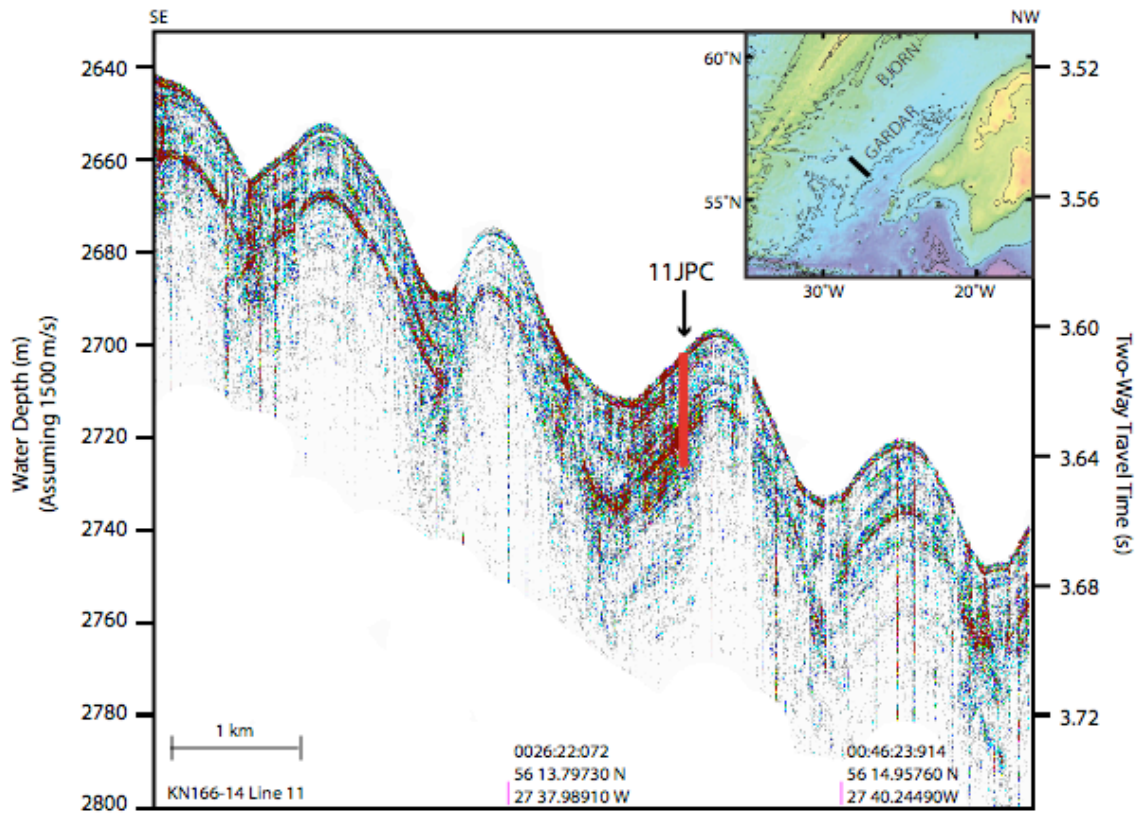


Figure 3.5a: 3.5 kHz seismic image of the cruise track over the mudwave field on southern Gardar Drift showing the location of core KN166-14 11JPC. The location of the cruise track is given by the black line in the map inset. Two-way travel time and approximate water depth assuming 1500 m/s velocity through water are shown.

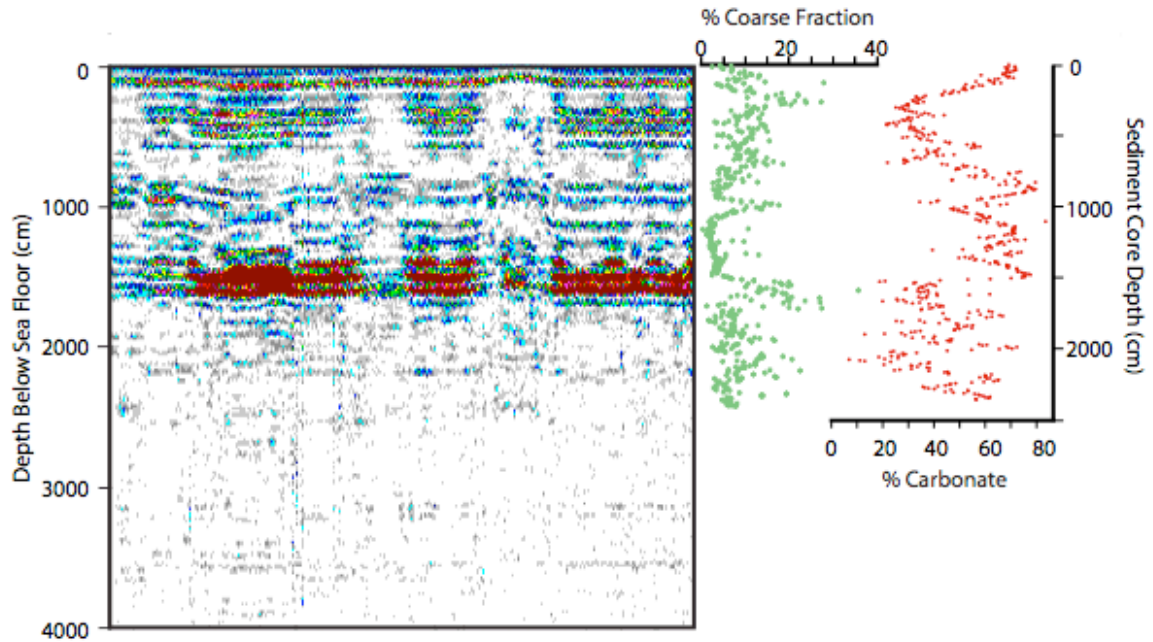


Figure 3.5b: 3.5 kHz seismic image while hove to at the site of core KN166-14 11JPC (See Figure 3.5a), depth below sea floor was determined by assuming a sediment velocity of 1505 m/s (G. Mountain, personal communication). Percent coarse fraction and % carbonate for the core are also shown plotted with depth.

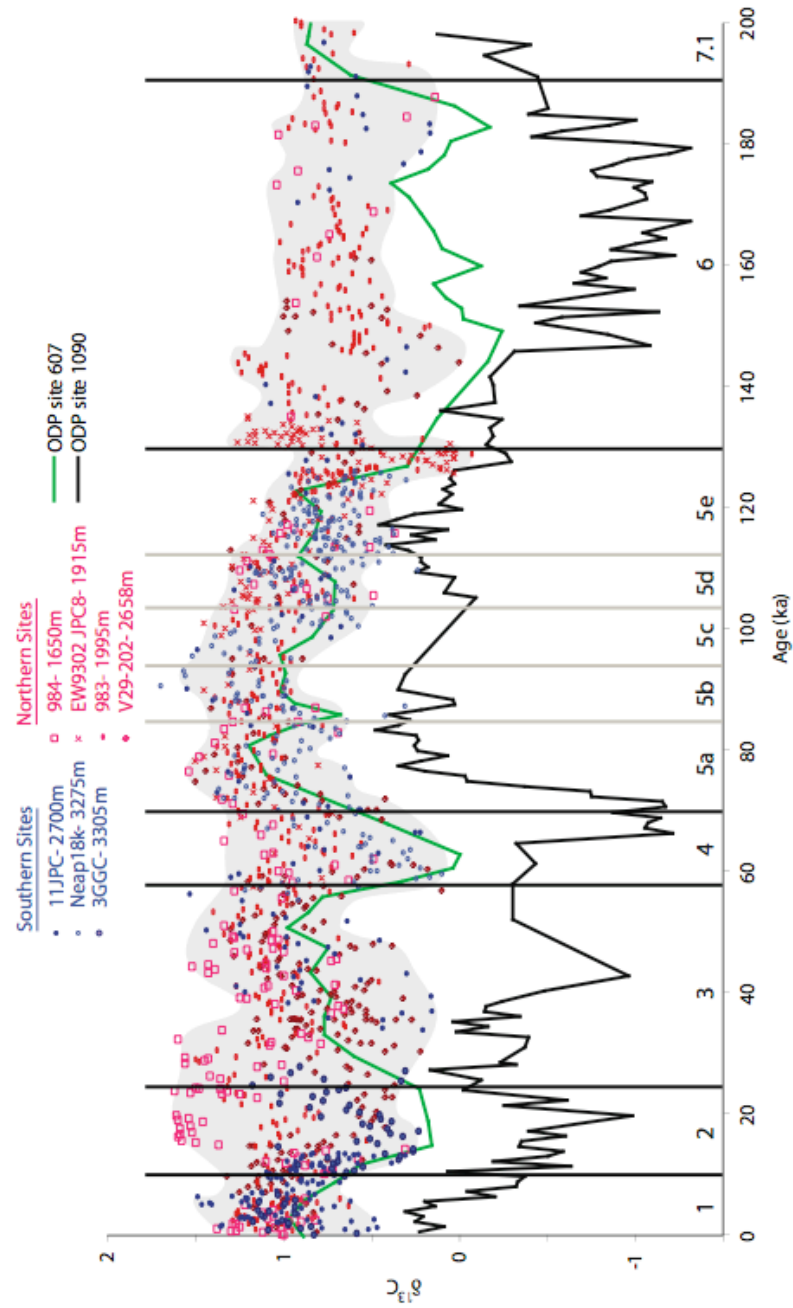


Figure 3.6: Records of $\delta^{13}\text{C}$ *P. wuellerstorfi* from the northern portion of the depth transect (red), the southern portion of the transect (blue), the mid-latitude North Atlantic (DSDP site 607; green line) and South Atlantic (ODP site 1090; black line). The grey shading is a non-statistical representation of the maximum and minimum benthic foraminiferal $\delta^{13}\text{C}$ values of the transect.

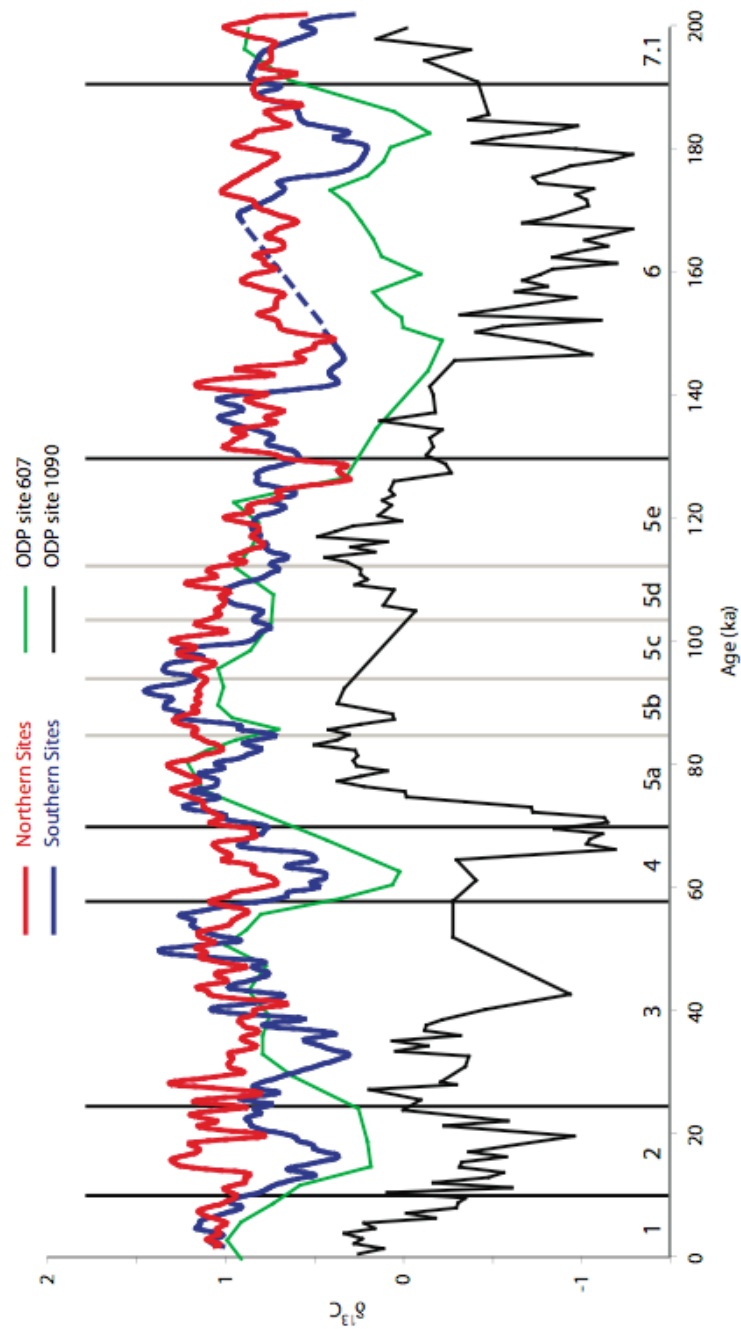


Figure 3.7: Interpolated $\delta^{13}\text{C}$ *P. wuellerstorfi* records from the northern transect sites (red; ODP site 984, EW9302 JPC8, ODP site 983, and V29-202), the southern transect sites (blue; 11JPC, 3GGC, and Neap18k), the mid-latitude North Atlantic (DSDP site 607; green line) and South Atlantic (ODP site 1090; black line).

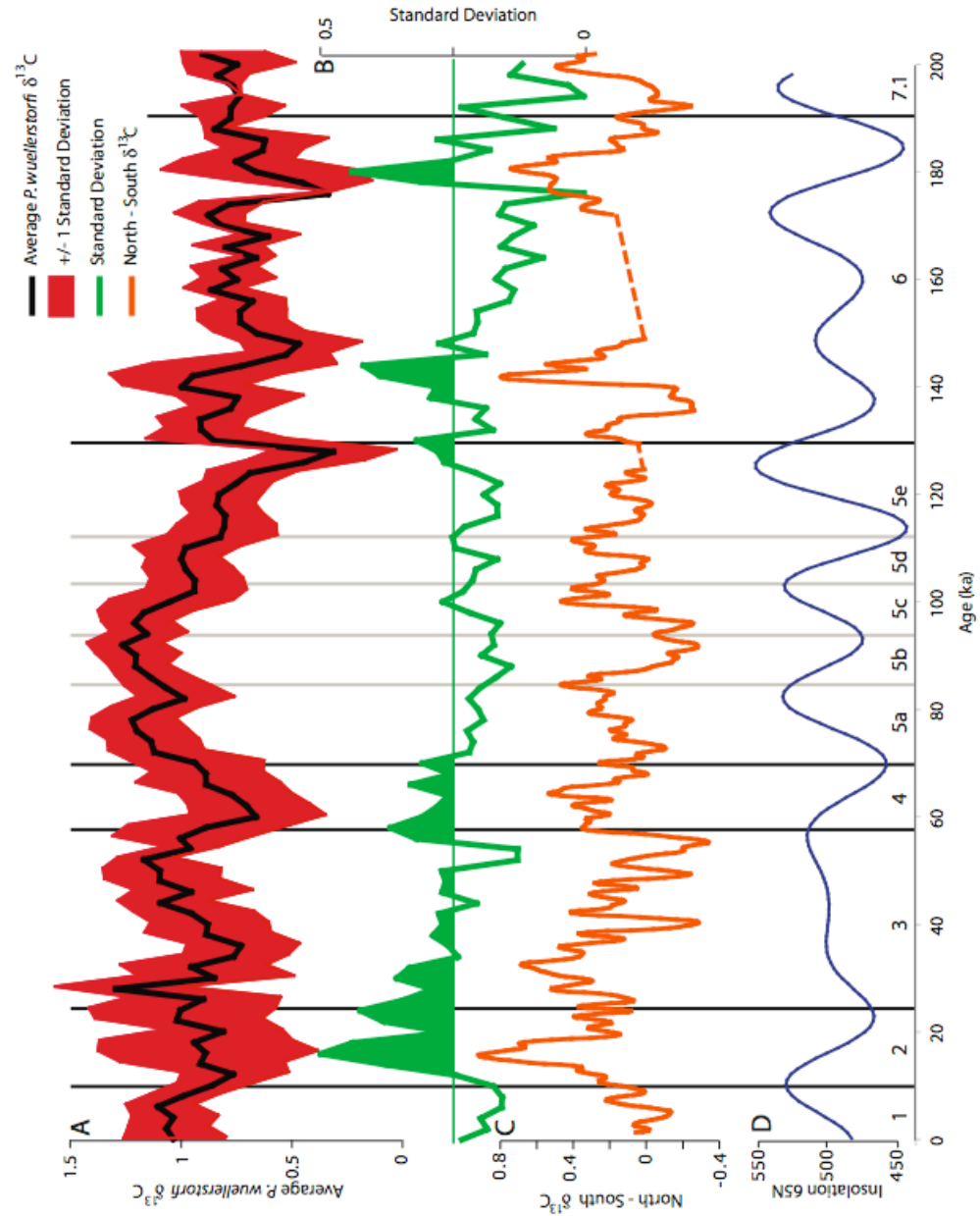


Figure 3.8: (A) Average of transect *P. wuellerstorfi* $\delta^{13}\text{C}$ values interpolated in 2-kyr intervals (black line) plotted with ± 1 standard deviation is shown versus age from 0 to 200 ka. (B) Standard deviation of transect *P. wuellerstorfi* $\delta^{13}\text{C}$ values interpolated in 2-kyr intervals (green), (C) difference between *P. wuellerstorfi* $\delta^{13}\text{C}$ values of the smoothed northern and southern transects (orange), and (D) northern hemisphere summer insolation at 65°N (Laskar et al., 2004) are also shown.

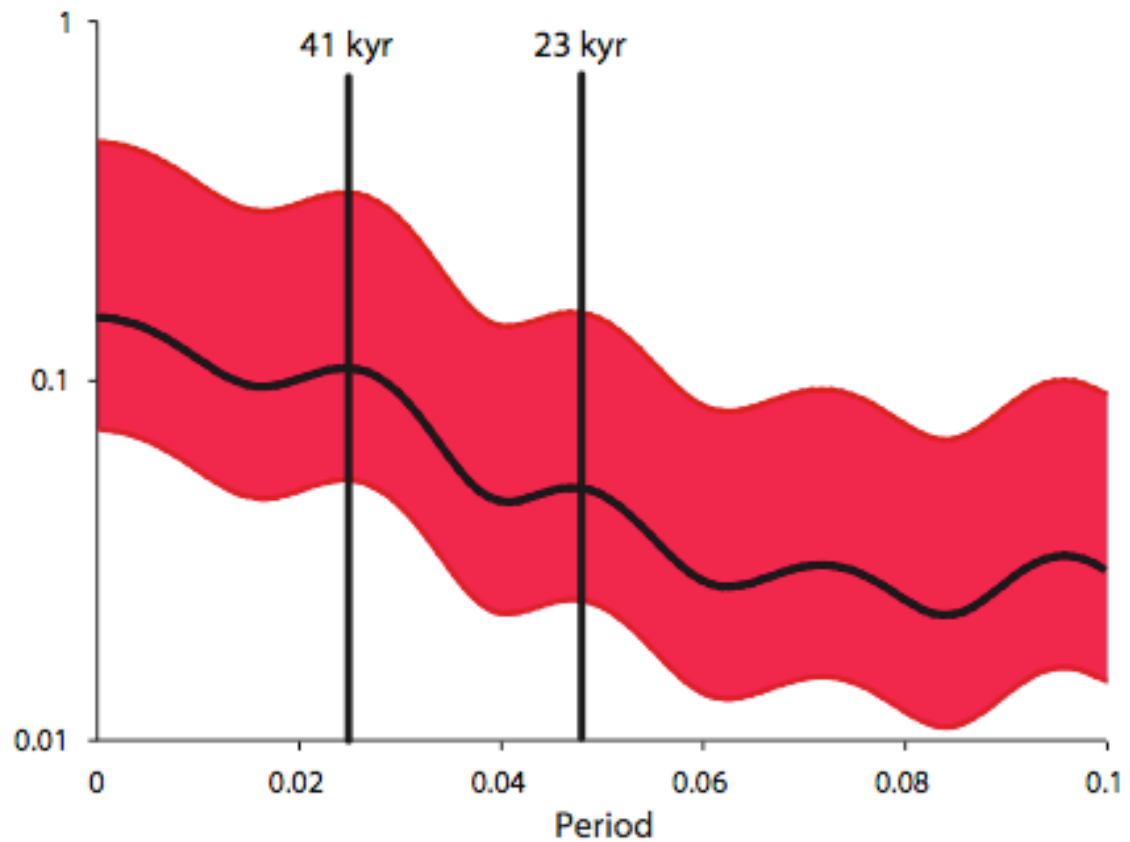


Figure 3.9: Spectral analysis of the standard deviation benthic foraminiferal $\delta^{13}\text{C}$ values for the Gardar Drift transect from 0 to 200 ka (black line) determined using AnalySeries. 95 % confidence intervals are shown (red window). Power can be seen in the obliquity (41 kyr) and precession (23 kyr) bands.

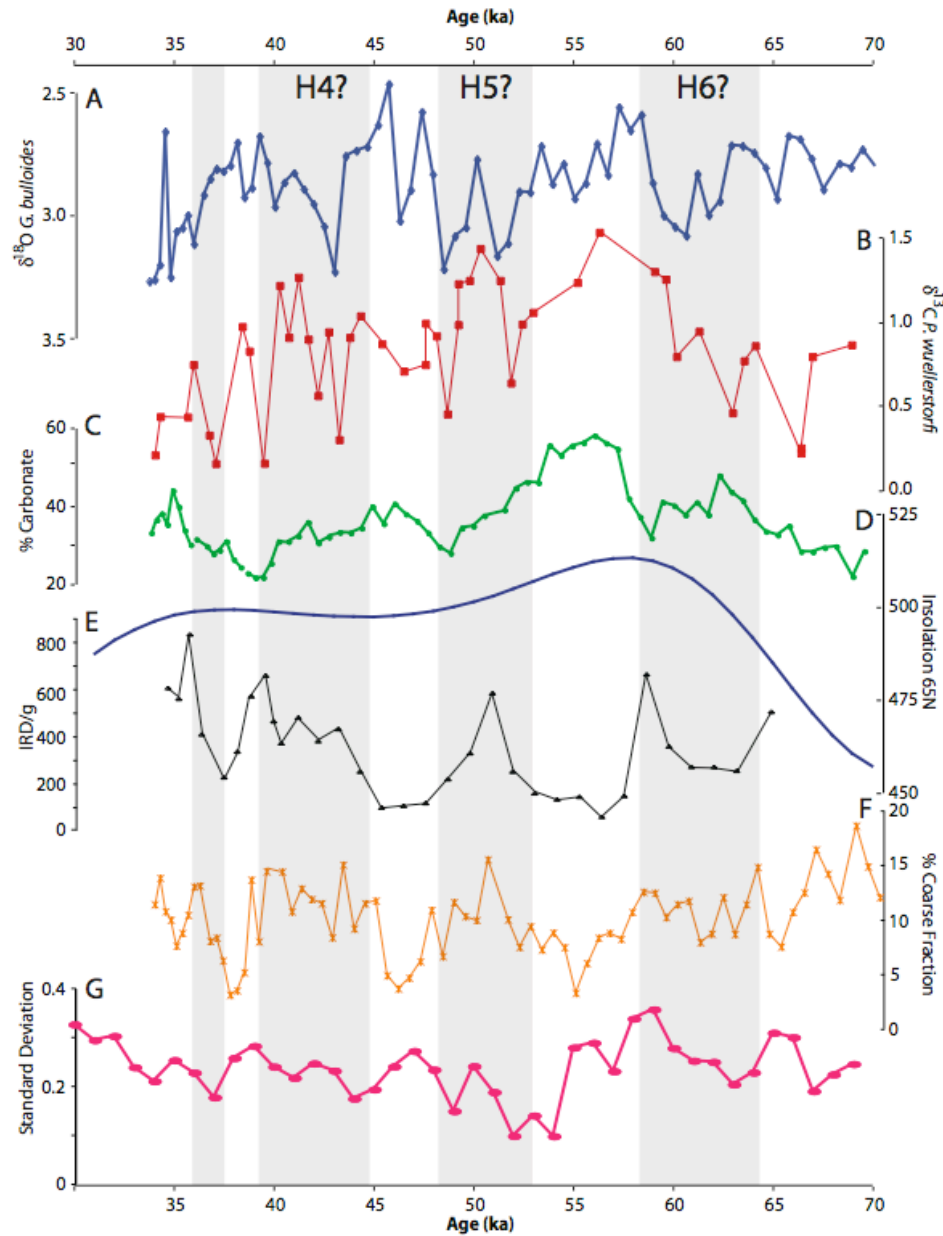


Figure 3.10: Proxy records for core 11JPC plotted versus age from ~ 30 to 70 ka. **(A)** *G. bulloides* $\delta^{18}\text{O}$ (blue), **(B)** *P. wuellerstorfi* $\delta^{13}\text{C}$ (red), **(C)** % Carbonate (green), **(D)** insolation at 65°N (Laskar et al., 2004), **(E)** and IRD/gram (black), **(F)** % Coarse Fraction (orange), **(G)** Standard deviation of the average of *P. wuellerstorfi* $\delta^{13}\text{C}$ values in 1-kyr intervals (pink) are also shown. Shaded areas mark periods of increased ice rafting, likely caused by Heinrich Events.

4.0 Examination of Temperature and Carbonate Ion Effects on Mg/Ca Ratios of Ostracoda Genus *Krithe*

4.1 Abstract

The magnesium/calcium (Mg/Ca) ratios of carapaces of the benthic ostracod genus *Krithe* were determined from core top samples from the Norwegian Sea, Cape Hatteras shelf, Gulf of Mexico, Sulawesi Margin (Indonesia), New Zealand shelf, Ceara Rise, and the North Atlantic. A linear regression of the *Krithe* Mg/Ca ratios and bottom water temperature (BWT) reveals a strong correlation for locations where temperature during calcification was above 3 °C, which can be described by the equation; $\text{Mg/Ca} = 0.928 \pm 0.041 * \text{BWT} + 5.137 \pm 0.231$. For locations where carapace calcification occurred at or below 3 °C, the incorporation of magnesium into ostracodal calcite is secondarily controlled by changes in carbonate ion concentration; a linear regression also describes this relationship; $\text{Mg/Ca} = 0.928 \pm 0.041 * \text{BWT} + 0.094 \pm 0.014 * \Delta[\text{CO}_3^{2-}] + 4.466 \pm 0.671$. When combined with an independent proxy for paleo-carbonate ion concentration, such as benthic foraminiferal boron/calcium ratios, benthic foraminiferal boron isotopes, or planktonic foraminiferal shell weight, *Krithe* Mg/Ca ratios provide a useful proxy for determining paleo-temperatures down core.

4.2 Introduction

The determination of oceanic paleotemperatures is integral to the understanding of past climate (CLIMAP, 1981; CLIMAP, 1984). One important application is the coupling of paleotemperature estimates with the measured oxygen isotopic composition of biogenic calcite ($\delta^{18}\text{O}_{\text{calcite}}$), which records both calcification temperature and isotopic

composition of ambient seawater ($\delta^{18}\text{O}_{\text{SW}}$; e.g., Urey, 1947; Epstein et al., 1953; Emiliani, 1955). Shackleton (1967) argued that changes in Pleistocene benthic foraminiferal $\delta^{18}\text{O}_{\text{calcite}}$ largely reflect ice-volume changes, and therefore global benthic foraminiferal $\delta^{18}\text{O}$ records can be scaled to reflect the $\delta^{18}\text{O}_{\text{SW}}$ due to ice volume changes. Hence, $\delta^{18}\text{O}_{\text{calcite}}$ is often utilized as an indirect proxy for glacio-eustatic changes, since ^{16}O is preferentially stored in continental ice sheets (e.g., Shackleton, 1967; Martinson et al., 1987; Miller et al., 2005).

Magnesium cations have a long residence time in the global oceans and are therefore considered to be conservative (Chester, 1990). During calcification, microfossils (e.g., planktonic foraminifera, benthic foraminifera, and benthic ostracods) partition elements from ambient seawater into their carbonate shells (Chave, 1954). Magnesium is similar in size to calcium and readily substitutes for calcium in the calcite lattice (Chave, 1954). Studies have shown a positive correlation between the calcification temperature and the concentration of magnesium in the calcium carbonate lattice of barine biogenic calcite (Chave, 1954). Thus, the incorporation of magnesium into biogenic calcite has been used as a paleotemperature proxy (e.g., Chave, 1954; Rosenthal et al., 1997; Elderfield and Ganssen, 2000; Lear et al., 2000). Thus, elemental ratios in marine biogenic calcite can be exploited to better understand past oceanic surface and deepwater hydrography (e.g., Boyle and Keigwin, 1987; Russell et al., 1994; Dwyer et al., 1995; Lea et al., 1999; McConnell and Thunell, 2005).

Foraminifera are the most commonly used microfossil group in paleoceanographic studies; chemical analyses of their tests can yield information about water characteristics during calcification. It was recognized early that different taxa

incorporate magnesium differently, requiring species-specific paleotemperature equations (e.g., Chave, 1954; Izuka, 1988; Russell et al., 1994; Rosenthal et al., 1997; Lear et al., 2002; Martin et al., 2002; McConnell et al., 2005; Marchitto et al., 2007). Core top calibrations of benthic foraminiferal Mg/Ca ratios versus bottom water temperature showed an exponential relationship (Chave, 1954; Rosenthal et al., 1997; Lear et al., 2002), apparently in agreement with thermodynamic calculations (Lea et al., 1999) and inorganic precipitation experiments (Katz, 1973).

In addition to temperature, other effects on foraminiferal Mg/Ca ratios have been proposed for foraminifera, including salinity (Nurnberg et al., 1996; Lea et al., 1999; Arbuszewski et al., 2008) and pH (Lea et al., 1999; Russell et al., 2004). Martin et al. (2002) noted a large degree in scatter and elevated Mg/Ca ratios at low temperatures, which led to the proposal of a carbonate ion effect (Elderfield et al., 2006; Rosenthal et al., 2006). Recent studies that have incorporated carbonate ion effects have expressed the Mg/Ca versus temperature relationship as linear (Elderfield et al., 2006; Marchitto et al., 2007; Healey et al., 2008).

The effect of carbonate ion variations on the incorporation of trace metals in benthic foraminiferal calcite is unclear as to whether CO_3^{2-} variations are a post-mortem dissolution process (McCorkle et al., 1995) or represent changing saturation during calcification (e.g., Boyle and Rosenthal, 1996; Elderfield et al., 2006; Rosenthal et al., 2006). Studies comparing the Mg/Ca ratio of benthic tests stained by Rose-Bengal (i.e., un-altered by dissolution) to unstained individuals from the same locations showed no significant difference, and interpreted the lack of a difference to indicate that carbonate ion concentration affects the incorporation of magnesium during test formation, rather

than post-deposition (Marchitto et al., 2000; Elderfield et al., 2006; Rosenthal et al., 2006). The carbonate ion effect on benthic foraminiferal Mg/Ca ratios remains uncertain with arguments that this effect is non-linear (Marchitto et al., 2005), dependent on threshold values of $\Delta[\text{CO}_3^{2-}]$ (the difference between concentration and saturation of CO_3^{2-} , see section 4.3.2 for this calculation; Marchitto et al., 2005; Rosenthal et al., 2006; Jordan, 2008), or dependent on a threshold values of temperature (Elderfield et al., 2006; Raitzsch et al., 2008).

Ostracods, another microfossil group, are also used for paleoceanographic studies (Dwyer et al., 1995). Ostracods are microscopic bi-valved crustaceans, typically ~ 1 mm in length, that live in lacustrine, brackish, estuarine, and marine environments. Every 1 to 3 days, they molt their calcitic carapace and secrete a new one (Turpen and Angell, 1971); thus, their carapaces record a snapshot of geochemical conditions, rather than intra-seasonal variability (Okada, 1982; Dwyer et al., 2002). Ostracods are ideal for paleoclimate studies because they are widely abundant, have thick carbonate shells, and maintain their chemical compositions post-mortem (e.g., Holmes et al., 1995; Cronin et al., 2005). Their carapaces are analyzed for both stable isotopic (e.g., Didie and Bauch, 2002) and trace metal composition (e.g., Dwyer et al., 1995).

Chave (1954) first showed that a positive linear relationship exists between bottom water temperature and the magnesium concentration in the calcitic carapaces of mixed-species benthic ostracods from the marine realm. Subsequent studies established that the relationship between Mg/Ca ratios and temperature differed among several ostracod superfamily groups (Cadot et al., 1972; Cadot and Kaesler, 1977), emphasizing the need for mono-generic paleotemperature equations.

Krithe (Brady et al., 1874) is a ubiquitous ostracod genus found from 150 m to abyssal water depths (Whatley and Quanghong, 1993; Yasuhara et al., 2008). *Krithe* incorporates Mg into its carapace homogeneously (Cadot et al., 1972; Dwyer et al., 2002) and is resistant to dissolution (Swanson and van der Lingen, 1994). Carapaces of *Krithe* have a smooth texture with few pores, minimizing the potential for contamination, making *Krithe* ideal for paleoceanographic reconstructions (e.g., Bodergat, 1983; Corregge, 1993a; Corregge, 1993b; Corregge and De Deckker, 1997; Cronin and Raymo, 1997; Zhao and Whatley, 1997; Dwyer et al., 1995; Cronin et al., 1996; Swanson and van der Lingen, 1997; Rodriguez-Lazaro and Cronin, 1999; Cronin et al., 2000; Dwyer et al., 2000).

Previous studies have described a linear relationship between *Krithe* Mg/Ca and bottom water temperature (BWT; Cadot and Kaesler, 1997; Corregge and DeDeckker, 1997; Dwyer et al., 1995; Cronin et al., 1996; Dwyer et al., 2002), although Dwyer et al. (2002) argued that the relationship may be exponential (Table 4.1). Temperature has been the main factor investigated with respect to magnesium incorporation in *Krithe* carapaces, though salinity has been shown to exert some effect on the Mg/Ca ratio in other ostracod genera from marine (Bodergat et al., 1993), lacustrine (Guang et al., 2008), and estuarine environments (Cronin et al., 2002). A previous study suggested that carbonate ion concentration did not affect magnesium incorporation in *Krithe* (Dwyer et al., 2002).

The understanding of elemental ratios in ostracod calcite has followed foraminiferal studies in generating species-specific paleotemperature equations. Now, similar to the elevated Mg/Ca ratios at low temperatures noted for benthic foraminiferal (e.g., Martin et al., 2002), which led to the proposal of the carbonate ion effect (Elderfield

et al., 2006; Rosenthal et al., 2006), Cronin et al. (1996) noted elevated *Krithe* Mg/Ca ratios at low temperatures. Cronin et al. (1996), and subsequent studies (Dwyer et al., 2002; Dwyer et al., 2005), excluded samples from the deep Arctic Ocean from their calibrations because of their elevated Mg/Ca ratios. Given this similarity and the other factors that have been suggested to affect the Mg/Ca ratio in other microfossils, this study aims to reevaluate how temperature and carbonate ion concentration influence magnesium incorporation into the calcite lattice of *Krithe* carapaces. Additionally, this study will address whether the relationship between Mg/Ca and BWT is linear or exponential, a topic which is still debated for foraminiferal studies (Rosenthal et al., 1997; Billups and Shrag, 2002; Lear et al., 2002; Martin et al., 2002; Elderfield et al., 2006; Marchitto et al., 2007; Healey et al., 2008).

Here, I present *Krithe* Mg/Ca ratios from globally dispersed core top locations to elucidate primary and secondary controls on the Mg incorporation in the ostracod carapace. Previously published *Krithe* paleotemperature equations have been iterative but were mainly comprised of a few locations (Cadot and Kaesler, 1997; Corregge and DeDeckker, 1997; Dwyer et al., 1995; Cronin et al., 1996; Dwyer et al., 2002). Using a globally distributed collection of core tops, and previously published core top data, I will determine the Mg/Ca sensitivity to temperature and examine the effects of carbonate ion concentration during calcification and post-depositional carbonate dissolution. Finally, I discuss the implications of this calibration on down core records. An improved *Krithe* paleotemperature equation will be a useful paleoceanographic tool, since some sediment cores are deficient in commonly studied benthic foraminifera taxa. For example, drift sites like KN166-14 11JPC, have sacrificed abundance of benthic foraminifera for

increased sedimentation rates due to advective processes (Elmore and Wright, unpublished data; Appendix 6).

4.3 Methods

4.3.1 Core Top Locations

Core top samples for this study were obtained predominantly from multi- and box cores from five depth transects, designed to sample a large range of water depths, bottom water temperatures (BWT), salinities, and carbonate ion concentrations. In this dissertation, the difference between *in situ* carbonate ion saturation and concentration, $\Delta[\text{CO}_3^{2-}]$ (see section 4.3.2 for this calculation) is used instead of $[\text{CO}_3^{2-}]$ concentration because benthic foraminiferal Mg/Ca studies have shown that the degree of undersaturation is the key parameter when assessing the control of carbonate ion on Mg/Ca ratios (Elderfield et al., 2006; Rosenthal et al., 2006). Samples came from the Norwegian Sea, Gulf of Mexico, Cape Hatteras shelf, New Zealand shelf, and Sulawesi Margin, Indonesia (Figure 4.1; Table 4.2). Core top samples from gravity and piston cores from the North Atlantic and Ceara Rise were also analyzed (Figure 4.1; Table 4.2).

Norwegian Sea samples were collected from water depths of 418 to 2799 m in the Norway Basin (Figure 4.1; Table 4.2). These sites are bathed by Norwegian Sea Bottom Water, which forms from winter convection of cold surface water originating from the North Atlantic Drift and Arctic inflow. These samples represent nearly homothermal (-0.8 to 0.8 °C) and homohaline (~ 34.91 PSU) conditions, and are considered to be oversaturated with respect to calcite ($\Delta[\text{CO}_3^{2-}] = 30.43$ to 78.86 $\mu\text{mol/kg}$; Table 4.2). Norwegian Sea sites provide excellent samples to examine possible carbonate ion effects at low temperatures. The samples were collected by the *R/V Knorr* on Cruise 177-2.

Samples from the northern Gulf of Mexico were collected from water depths of 1026 to 3150 m (Table 4.2). These sites are bathed by the Yucatan Current, which becomes the Loop Current that exits the Florida Strait to join the Gulf Stream. The Gulf of Mexico sites also represent nearly homothermal (4.3 to 4.9 °C) and homohaline (34.94 to 35.00 PSU), but have a range of $\Delta[\text{CO}_3^{2-}]$ values (23.94 to 57.47 $\mu\text{mol/kg}$). These locations allow for the examination of carbonate ion effects at temperatures > 3 °C. The Gulf of Mexico samples were sub-sampled from the Deepwater Program: Northern Gulf of Mexico Continental Slope Habitats and Benthic Ecology (DGoMB; Gilbert T. Rowe, TAMU, 2000).

Samples from the Cape Hatteras shelf were collected from water depths of 2214 to 3979 m (Table 4.2). Southward flowing North Atlantic Deep Water bathes these sites, which range in bottom water temperature from 2.2 to 3.4 °C, salinity from 34.88 to 34.94 PSU, and $\Delta[\text{CO}_3^{2-}]$ from 17.39 to 44.12 $\mu\text{mol/kg}$ (Table 4.2). These samples were collected by the *R/V Knorr* on Cruise 178, and were chosen to represent a supersaturated environment.

New Zealand shelf samples were collected from water depths from 663 to 2472 m in waters bathed by Antarctic Intermediate Water (Table 4.2). The sites have bottom water temperatures of 1.9 to 4.9 °C, salinities of 34.29 to 34.72 SU, and $\Delta[\text{CO}_3^{2-}]$ values of 13.87 to 57.23 $\mu\text{mol/kg}$ (Table 4.2). The New Zealand shelf samples were collected by the *R/V Roger Revelle* Cruise 05-03, and represent an undersaturated environment.

Northern North Atlantic, mid-latitude North Atlantic, and Ceara Rise samples were collected by *R/V Knorr*, Cruise 166-14, and by the Ocean Drilling Program Legs 94 and 154, respectively (Table 4.2). Cores KN166-14 11JPC, 8GGC, and 3GGC were

collected from 2707 to 3305 m water depth on Gardar Drift (Table 4.2) and are bathed by modern Iceland Scotland Overflow Water (Worthington, 1976; Bianchi and McCave, 1999). Cores 11JPC, 8GGC, and 3GGC have Holocene sedimentation rates of ~ 20 cm/kyr (see Chapter 2 of this dissertation), ~ 8 cm/kyr (Elmore and Wright, unpublished data), and ~ 10 cm/kyr (see Chapter 4 of this dissertation), respectively. Core KN166-14 12JPC was collected from 3078 m water depth near the Charlie Gibbs Fracture Zone (Table 4.2); the location is also currently bathed by Iceland Scotland Overflow Water (Worthington, 1976). Core KN166-14 15JPC was collected from 2300 m on Eirik Drift and also has a high sedimentation rate (~ 15 cm/kyr), though late Holocene sediments have been winnowed from this location (Neitzke and Wright, 2007). The location of 15JPC is bathed by modern Northeast North Atlantic Deep Water, which is comprised of Iceland Scotland Overflow Water and Denmark Straights Overflow Water (Worthington, 1976). Deep Sea Drilling Project (DSDP) Leg 94, site 607 was occupied at a water depth of 3427 m in the central North Atlantic (Table 4.2). This site is bathed by modern North Atlantic Deep Water (Raymo et al., 1990).

Ceara Rise cores ODP sites 926, 928, and 989 were collected from a water depth range of 3589 to 4355 m from the western equatorial Atlantic (Table 4.2; Bickert et al., 1997). Ocean Drilling Program sites 926, 928, and 929 have Holocene sedimentation rates of ~ 4.5 , ~ 4.8 , and ~ 5 cm/kyr, respectively (Bickert et al., 1997). Ceara Rise is bathed by modern North Atlantic Deep Water (Bickert et al., 1997).

Site information for samples from the Sulawesi Margin in Indonesia, which were collected by the *R/V Baruna Jaya* on cruise 08-03, was published in Rosenthal et al. (2006; Table 4.2).

4.3.2 Core Top Hydrography

For each site, hydrographic parameters of bottom water temperature and bottom water salinity were either measured on the cruise from a conductivity-temperature-depth (CTD) cast or found from online databases, including the World Ocean Circulation Experiment (WOCE; <http://cdiac.ornl.gov>), Transient Tracers in the Oceans (TTO; http://gcmd.nasa.gov/records/GCMD_CDIAAC_NDP4.html), or Carina cruise summary data (CARINA; http://cdiac.ornl.gov/oceans/CARINA/Carina_table.html). Total phosphorous, total silicate, total dissolved inorganic carbon, and total alkalinity were measured shipboard for Indonesia (Rosenthal et al., 2006) and found from online databases for the other locations. All hydrographic information for the sites discussed in this chapter is listed in Appendix 7. In addition to the core tops discussed herein, hydrographic data have been compiled for as many previously published core top locations as possible (Appendix 8). For some of the core top sites discussed in this work, and some previously published core top sites, a correction was required to account for the difference between the presumed late Holocene calcification environment and the measured modern hydrographic conditions caused by the invasion of anthropogenic CO₂ into the subsurface waters in regions of deep water formation (e.g., Orr et al., 1995). Where applicable, TCO₂ has been corrected to pre-industrial values by subtracting the estimated anthropogenic CO₂ contribution, according to the region and water depth (Table 4.2; Appendix 7; Appendix 8). Estimated anthropogenic CO₂ inputs for northern North Atlantic, Norwegian Sea, and Arctic samples were found in Sabine et al. (2004), Jutterstrom et al. (2008), and Jutterstrom and Jeanson (2008), respectively. This correction was only applied for sites where the predicted concentration of anthropogenic

CO₂ is greater than 5 µmol/kg, otherwise the anthropogenic effect was considered negligible (Elderfield et al., 2006).

Hydrographic parameters were entered into the CO₂Sys program (Lewis and Wallace, 1994) to calculate *in situ* carbonate ion concentration ($[\text{CO}_3^{2-}]_{in\ situ}$; Table 4.2; Appendix 7; Appendix 8). Equilibrium constants K_1 and K_2 were calculated using Dickson and Millero (1987) after Mehrbach et al. (1973), and K_{SO_4} was calculated according to Dickson (1990). Carbonate ion saturation ($[\text{CO}_3^{2-}]_{\text{saturation}}$) was determined by:

$$[1] \quad [\text{CO}_3^{2-}]_{\text{saturation}} = 90 * e^{[0.16 * (z - 4)]}$$

where z is the water depth in kilometers (Broecker and Peng, 1982). Seawater calcite saturation state ($\Delta[\text{CO}_3^{2-}]$) was then calculated by:

$$[2] \quad \Delta[\text{CO}_3^{2-}] = [\text{CO}_3^{2-}]_{in\ situ} - [\text{CO}_3^{2-}]_{\text{saturation}}$$

4.3.3 Core Top Sample Processing

Following collection, core top samples from the Norwegian Sea, Cape Hatteras shelf, New Zealand shelf, and Sulawesi Margin, Indonesia were refrigerated at 4 °C, preserved in a 4 % buffered formalin-seawater solution, then processed with Rose Bengal stain (1 g/L of 4% formalin-seawater solution; Walton, 1952) for 1 week to separate the recently alive (stained) from the unstained carapaces according to the procedure outlined in Corliss and Emerson (1990). Stained carapaces indicate the occurrence of protoplasm;

these carapaces were assumed to be recently living and thus unaltered by any effects of post-mortem dissolution (Walton, 1952). Unstained specimens, with no remaining protoplasm, may have been altered post-depositionally (Walton, 1952). Core tops from other regions were not stained due to a delay in processing.

4.3.4 Core KN166-14 11JPC

Jumbo piston core KN166-14 11JPC (11JPC) was collected by the *R/V Knorr* on cruise 166-14 from 2707 m on southern Gardar Drift, in the northern North Atlantic (56°W, 27°W). Following collection, the core was refrigerated at 5 °C at the Rift/Drift Core Repository at Rutgers University and later sampled at 5 cm intervals, yielding a ~ 600 year sampling resolution. An age model was generated from 15 AMS ¹⁴C dates and chrono-stratigraphic comparison to a stacked benthic record by Lisiecki and Raymo (2005; see Chapter 3 of this dissertation). The core top age is estimated to be ~ 600 years.

4.3.5 Analytical Methods

Each sample was washed through a 63 µm sieve to remove silts and clays, and then dried. *Krithe* carapaces were hand picked under a binocular microscope from the > 250 µm size fraction from each sample. Previous studies have shown that there is no systematic offset in the Mg/Ca ratio between the left and right valves or between male and female individuals for *Krithe* (Dwyer et al., 2002). *Krithe reversa* and *K. minima* were excluded from this study because they have been shown to record elevated magnesium concentrations and thus are expected to co-precipitate magnesium differently from other species in the *Krithe* genus (Correge 1993a, b; Dwyer et al., 2002). All adult and A-1 (in their final stage of molting before adulthood) carapaces were collected for analyses to test the hypothesis that they incorporate Mg similarly (Dwyer et al., 2002). A

‘Visual Preservation Index’ (VPI) was used to determine the quality of preservation of the carapaces (Dwyer et al., 1995; Cronin et al., 1996; Cronin et al., 2000). On a scale of 1, signifying clear and unaltered, to 6, crusty and brittle (Dwyer et al., 1995), carapaces used in this study were typically very well preserved (VPI 1-3; Table 4.2; Appendix 9).

One to three *Krithe* carapaces ($\sim 200 \mu\text{g}$) were selected using a binocular microscope for trace metal geochemical analysis at the Rutgers Inorganic Analytical Laboratory (RIAL) at the Institute of Marine and Coastal Sciences at Rutgers University (Rosenthal et al., 1999). The carapaces were manually cleaned with a fine-hair brush to remove surficial clays (Holmes, 1992; Jin et al., 2006). Samples were then chemically cleaned to remove any remaining clays, organic matter and metal oxides, according to the procedure outlined in Rosenthal et al. (1999), modified from Boyle and Keigwin (1985; 1986). Cleaned samples were dissolved in trace metal clean 0.065 N HNO_3 , and diluted to 400 ml with 0.5 N HNO_3 . Diluted solutions were then analyzed by Thermo Element Sector Field Inductively Coupled Plasma Mass Spectrometer (SF-ICP-MS). All samples were routinely compared to consistency standards according to Rosenthal et al. (1999) and modified by Lear et al. (2002). The long-term reproducibility of Mg/Ca analysis was $\sim 1\%$, as determined by repeated measurements of three consistency standards. The precision of consistency standards with Mg/Ca ratios of 1.25, 3.32 and 7.51 mmol/mol was $\pm 1.24\%$, $\pm 1.16\%$ and $\pm 0.57\%$ (r.s.d), respectively. Mn/Ca, Fe/Ca, Al/Ca, and Ti/Ca were used to screen samples for contamination due to diagenetic coatings or lingering detrital material.

Stable oxygen and carbon isotopic analyses were performed on one to five tests of the benthic foraminifera *Planulina wuellerstorfi*. These specimens were handpicked under a binocular microscope from the 250 – 350 μm size fraction of the washed samples from core 11 JPC. All stable isotope measurements were made using an Optima Mass

Spectrometer with an attached multiprep at the Rutgers University Stable Isotope Laboratory. Measured values were reported using standard δ - notation as compared to V-PDB using NBS-19 and an internal lab standard. The 1- σ laboratory precision of an internal lab standard was 0.08 ‰ for $\delta^{18}\text{O}$ and 0.05 ‰ for $\delta^{13}\text{C}$.

4.4 Results and Discussion

4.4.1 Post Depositional Dissolution

Seven core tops from 2 regions (Cape Hatteras shelf and New Zealand shelf) contained both stained and unstained carapaces for direct comparison of Mg/Ca ratios between recently living and non-recently living specimens (Figure 4.2; Appendix 9). Ratios of Mg/Ca in these samples range from 4 to 11 mmol/mol (Figure 4.2). An assessment of the Mg/Ca ratio of stained and unstained carapaces reveals that the samples fall close to a 1:1 relationship, and the average of each difference between stained and unstained carapace Mg/Ca values was 0.10 mmol/mol. This indicates that post-depositional dissolution did not alter the Mg/Ca ratios at these locations (Figure 4.2). Rose Bengal stain has also been shown to react with dead protoplasm in foraminifera (Bernhard, 1988); however, ostracod carapaces do not have chambers like foraminifera, therefore dead protoplasm may not be as easily preserved in ostracod carapaces, increasing the validity of using staining as a test for recent calcification in *Krithe*. The staining comparison was not available at all locations used in this study; however, another means of determining post-depositional dissolution, the Visual Preservation Index (VPI; Dwyer et al., 1995), was determined prior to the analysis of each sample (Appendix 9). Each analyzed carapace had a VPI of less than 4, and typically 1 to 2, indicating that they were all well preserved, with no visible signs of post-depositional

dissolution (Table 4.2). Both the staining comparison, and VPI data are consistent with previous studies that suggested that there is no relationship between the degree of preservation or post-depositional dissolution and Mg/Ca ratios when $VPI < 4$ (Dwyer et al., 1995; Cronin et al., 1996; Dwyer et al., 2000; Dwyer et al., 2002).

4.4.2 Adult and A-1 Juvenile Carapaces

The Mg/Ca ratios of adult carapaces and A-1, late stage juvenile, carapaces were compared from 8 different core top samples (Figure 4.2; Appendix 9). There was no systematic difference between adult and A-1 carapaces at each site, and thus, comparison of the data reveals a nearly 1:1 relationship (Figure 4.2; Appendix 9). The average of the difference between the Mg/Ca values of Adult and A-1 juveniles from each sample is 0.07 mmol/mol; this indicates that adults and A-1 juveniles co-precipitate magnesium similarly, confirming results of Dwyer et al. (2002) for marine ostracods and Wansard and Metzquita (2001) for lacustrine ostracods. Thus, Mg/Ca ratios of A-1 juvenile carapaces are used in addition to adult carapaces in this study.

4.4.3 The Mg/Ca – Depth Relationship

The 52 core tops analyzed in this study come from water depths of 200 to 4000 m, and cover a wide range of bottom water temperatures (-0.85 to 11.50 °C) and $\Delta[CO_3^{2-}]$ values (9.95 to 78.86 $\mu\text{mol/kg}$; Table 4.2). The Mg/Ca ratios for the entire set of core top samples range from 4.26 to 16.59 mmol/mol (Table 4.2; Figure 4.3; Appendix 7). For samples in water depths greater than 1000 m, Mg/Ca ratios are between 5 and 12 mmol/mol, and show a general relationship of increasing Mg/Ca with increasing water depth (Figure 4.3). Ratios of Mg/Ca from shallow sites (< 400 m) from the Sulawesi Margin, Indonesia have higher values than deeper sites (up to 15 mmol/mol), possibly

due to increased water temperatures, as these samples were collected from within the thermocline (Figure 4.3). New Zealand shelf samples from ~ 600 m water depth have the lowest Mg/Ca Ratios (~ 4 mmol/mol; Figure 4.3). A trend of increasing Mg/Ca ratios with increasing water depth was also noted for benthic foraminifera, but was shown to be caused by changes in $\Delta[\text{CO}_3^{2-}]$ (McCorkle et al., 1995; Elderfield et al., 1996; Marchitto et al., 2000). Below the thermocline, core top Mg/Ca ratios show low correspondence with bottom water salinity (Appendix 7; Appendix 9). This indicates that depth and salinity are not dominant factors affecting Mg/Ca ratios in *Krithe* (Figure 4.3). The concentration of Mg in the *Krithe* carapaces analyzed in this study (4.26 to 16.59 mmol/mol) is nearly an order of magnitude higher than the concentration of Mg/Ca in benthic foraminiferal calcite, which is ~ 0.5 to 2.5 mmol/mol over a similar range of temperatures (Elderfield et al., 2006; Jordan, 2008).

4.4.4 The Mg/Ca - Temperature Relationship

Core top Mg/Ca ratios from this study range from ~ 3 to 17 mmol/mol over a BWT range of -1 to 12 °C (Figure 4.4; Appendix 9). A linear regression of these data reveals that Mg/Ca and BWT have a weak, but positive correlation ($R^2 = 0.17$; slope = 0.38 mmol/mol/°C; intercept = 7.85 mmol/mol Figure 4.4). When examined by region, distinct Mg/Ca vs. BWT relationships emerge (Figure 4.4). Samples from the cold, carbonate saturated Norwegian Sea sites have elevated Mg/Ca ratios with respect to the general trend (Figure 4.4b). Warm Sulawesi Margin, Indonesia sites also have elevated Mg/Ca ratios (Figure 4.4c). Mg/Ca ratios from New Zealand shelf sites, particularly the shallowest New Zealand shelf sites, are lower than the general Mg/Ca trend (Figure 4.4). Additionally, the scatter around this regression, particularly at low temperatures, suggests

that there may be secondary, non-temperature controls on the incorporation of magnesium into the calcitic carapace of *Krithe*.

4.4.5 Secondary Effects on Mg/Ca Ratios

A weak positive linear relationship is observed between core top *Krithe* Mg/Ca ratios and $\Delta[\text{CO}_3^{2-}]$ for samples analyzed in this study, but the trend is insignificant ($R^2 = 0.193$; Figure 4.5a). The two homothermal, homohaline transects, from the Norwegian Sea and Gulf of Mexico, allow the opportunity to examine the effect of $\Delta[\text{CO}_3^{2-}]$ independent of temperature and salinity changes (Figure 4.5b, Figure 4.5c). Samples from the Norwegian Sea transect have a positive linear relationship between Mg/Ca and $\Delta[\text{CO}_3^{2-}]$ at temperatures from -1.0 to 0.5 °C ($R^2 = 0.701$; Figure 4.5b). Samples from the Gulf of Mexico transect do not have a positive trend between Mg/Ca and $\Delta[\text{CO}_3^{2-}]$ at temperatures of ~ 4.3 °C (Figure 4.5c). The observation that $\Delta[\text{CO}_3^{2-}]$ values affect Mg/Ca ratios at cold temperatures but not at warmer temperatures indicates that there is a ‘carbonate ion effect’ on *Krithe* that only occurs at low temperatures (Figure 4.5b; Figure 4.5c).

4.4.6 Temperature Calibration

Previously published core top calibrations of *Krithe* Mg/Ca ratios have identified temperature as the main control on magnesium incorporation (e.g., Dwyer et al., 1995). Core top Mg/Ca ratios from this study were combined with previously published core top data in order to more completely examine factors that may affect the incorporation of magnesium into the carapaces of ostracods. A comparison between data generated for this study and previously published data from Cadot (1977), Dwyer et al. (1995), Cronin et al. (1996), Corregge and DeDeckker (1997), and Dwyer et al. (2002) reveals an offset

between the data sets; thus, a correction is required to compare the data (Figure 4.6). Examinations of cleaning protocols on the Mg/Ca ratios of foraminifera (Rosenthal et al., 2004; Greaves et al., 2008) and lacustrine ostracods (Holmes, 1992; Jin et al., 2006) have identified that oxidatively and reductively cleaning of biogenic calcite prior to elemental analysis results in lower Mg/Ca ratios. The effect of different cleaning procedures on marine ostracods has not been determined. Samples for this study were oxidatively and reductively cleaned while previous studies of *Krithe* did not chemically clean their specimens; therefore, I propose that the offset between data from this study and previous studies reflect analytical offsets (Figure 4.6). A simple correction, described below, has been made to account for the differences in cleaning, though the effect of different cleaning methodologies on *Krithe* carapaces should be systematically evaluated.

A correction factor was determined by comparing the linear regression of Mg/Ca ratios and temperature data from this study with the linear regression of Mg/Ca ratios and temperature data from all previously published studies (Figure 4.6). Only data above 3 °C were used in order to avoid any possible variability due to carbonate ion effects at low temperatures (Elderfield et al., 2006), and data from *Krithe reversa* have been removed from the Dwyer et al. (2002) data set (Correge, 1993a; Correge, 1993b). The linear regressions of data from this study and previously published studies have slopes of 0.85 ± 0.04 and 0.93 mmol/mol/°C, and intercepts of 5.19 ± 0.23 and 8.59 mmol/mol, respectively (Figure 4.6). The similarity in these slopes suggests that a uniform offset can be applied (Figure 4.6). The difference between the intercepts of the two regressions is 3.40 mmol/mol, which is assumed to be a generalized correction factor between data from this study and previously published studies. This difference between cleaned and

uncleaned samples is reasonable when compared to the maximum difference due to cleaning protocols shown for lacustrine ostracods (~ 3.0 mmol/mol; Jin et al., 2006).

A compilation of core top data from this study and adjusted published core top data yields a positive linear regression between Mg/Ca ratios and temperature, defined by the equation, $\text{Mg/Ca} = (0.69 \text{ mmol/mol/}^{\circ}\text{C} * \text{BWT}) + 6.72 \text{ mmol/mol}$ ($R^2 = 0.47$; Figure 4.7). Scatter is prevalent at low temperatures, particularly from Norwegian Sea data from this study, and from the Arctic Ocean data from Cronin et al. (1996), as was noted by those authors (Figure 4.7). Deep Pacific sites have Mg/Ca ratios that are lower than the global regression (Figure 4.4; Figure 4.7). Because some of this scatter at low temperatures may result from secondary calcification effects, the initial paleotemperature equation was generated by compiling data from this study and published data from locations with bottom water temperatures above 3°C (Figure 4.7). This temperature is the threshold below which carbonate ion effects have been observed in benthic foraminifera, and below which carbonate ion decreases rapidly (Elderfield et al., 2006). A linear regression of all core top data above 3°C yields the equation:

$$[3] \quad \text{Mg/Ca}_{\text{Krithe}} = (0.93 * \text{BWT}) + 5.14$$

where Mg/Ca is in mmol/mol and BWT is in $^{\circ}\text{C}$ ($R^2 = 0.48$). Extrapolation of this regression to lower temperatures also reveals that the Mg/Ca ratios of Norwegian Sea samples from this study and in Arctic Ocean samples from Cronin et al. (1996) fall consistently above the trend line (Figure 4.7). The Mg/Ca temperature sensitivity for *Krithe*, $0.93 \text{ mmol/mol/}^{\circ}\text{C}$, is higher than published temperature sensitivities for benthic

foraminifera that range from 0.11 to 0.50 mmol/mol/°C (Healey and Thunell, 2008), which is reasonable given that the concentration of Mg/Ca found in *Krithe* is an order of magnitude higher than benthic foraminiferal concentrations.

4.4.7 Carbonate Ion Effects

Results from this study and published studies suggest that temperature is the primary control on Mg/Ca incorporation in *Krithe* carapaces (Figure 4.7; Dwyer et al., 1995; Cronin et al., 1996), but results of this study indicate that carbonate ion concentration controls Mg incorporation at low temperatures (Figure 4.5a, Figure 4.5c). Therefore, the dominant temperature effect must be removed to better understand the secondary relationship between Mg/Ca and $\Delta[\text{CO}_3^{2-}]$ (Elderfield et al., 2006). To determine if parameters other than temperature affect Mg/Ca ratios, a predicted Mg/Ca ratio was calculated for each location using the measured bottom water temperature and Equation 3. The difference between the measured Mg/Ca ratio and the predicted Mg/Ca ratio ($\Delta\text{Mg/Ca}$) quantifies the Mg/Ca variability not explained by the Mg/Ca-temperature relationship.

A linear regression of $\Delta\text{Mg/Ca}$ ratio and $\Delta[\text{CO}_3^{2-}]$ from all of the sites in this study reveals a poor correlation ($R^2 = 0.025$); this suggests that the carbonate ion effect for *Krithe* may not be linear (Figure 4.8). Since the largest deviation from the temperature-expected Mg/Ca ratio is observed in the Norwegian Sea sites ($\Delta\text{Mg/Ca} > 4$ mmol/mol), which cover a wide range of $\Delta[\text{CO}_3^{2-}]$ values (30 to 80 $\mu\text{mol/kg}$; Figure 4.8), I follow Elderfield et al. (2006) and suggest that the carbonate ion effect particularly occurs at low temperatures. Thus, I re-examined the relationship between $\Delta[\text{CO}_3^{2-}]$ and

$\Delta\text{Mg}/\text{Ca}$ for sites where bottom water temperature was less than or equal to 3 °C, and found a strong linear correlation defined by the equation (Figure 4.8):

$$[4] \quad \Delta\text{Mg}/\text{Ca} = (0.094 \pm 0.014) * \Delta[\text{CO}_3^{2-}] - (0.671 \pm 0.014)$$

where Mg/Ca has units of mmol/mol and $\Delta[\text{CO}_3^{2-}]$ has units of $\mu\text{mol}/\text{kg}$ ($R^2 = 0.593$).

This equation suggests that $\Delta[\text{CO}_3^{2-}]$ is a significant factor in the incorporation of magnesium into *Krithe* carapaces at temperatures at or below 3 °C. The $\Delta[\text{CO}_3^{2-}]$ sensitivity of 0.094 mmol/mol/ $\mu\text{mol CO}_3^{2-}/\text{kg}$ from Equation 4 is 10 times the published $\Delta[\text{CO}_3^{2-}]$ sensitivities for benthic foraminifera of 0.0086 mmol/mol/ $\mu\text{mol CO}_3/\text{kg}$ (Elderfield et al., 2006), 0.0090 mmol/mol/ $\mu\text{mol CO}_3/\text{kg}$ (Yu and Elderfield, 2008), and 0.0083 mmol/mol/ $\mu\text{mol}/\text{kg}$ (Healey and Thunell, 2008); this order of magnitude difference is consistent with the 10 fold higher Mg/Ca ratios in *Krithe* compared to benthic foraminifera.

I then applied Equation 4 to all of the cold temperature ($\text{BWT} \leq 3$ °C) core top sites within the compilation and found a strong correlation between $\Delta[\text{CO}_3^{2-}]$ corrected Mg/Ca ($\text{Mg}/\text{Ca}_{\Delta[\text{CO}_3]}$) and BWT ($R^2 = 0.74$; Figure 4.9). This correlation is improved from the initial correlation between Mg/Ca and BWT for core top sites with bottom water temperatures above 3 °C ($R^2 = 0.48$; Figure 4.7). The application of this correction factor to the Norwegian sites, which were previously enriched in Mg/Ca with respect to the initial linear regression (Figure 4.7), greatly reduces the difference between the corrected Mg/Ca and the general Mg/Ca core top relationship (Figure 4.9). Mg/Ca ratios from Arctic Ocean sites, even those below 900 m water depth that were previously excluded

from calibrations, were also much improved by the application of this correction factor (Figure 4.9).

4.4.8 Global Paleotemperature Equation

A revised paleotemperature equation for *Krithe* Mg/Ca ratios can be generated that takes into account the secondary carbonate ion saturation effects. For this equation, data from this study was combined with previously published data that were adjusted by 3.40 mmol/mol for cleaning offsets (see Section 4.4.6; Figure 4.6). The Mg/Ca values then were corrected for carbonate ion effects according to Equation 4 for sites where bottom water temperature during calcification was less than or equal to 3 °C, to yield $Mg/Ca_{carb.cor}$. Since error may exist in both the Mg/Ca ratio and bottom water temperature measurement, a geometric mean regression (Model II) was used to calculate the relationship between $Mg/Ca_{carb.cor}$ and bottom water temperature (Laws, 1997). The regression normalized the data to a zero intercept and accounts for errors in both Mg/Ca and bottom water temperature (e.g., Rosenthal and Lohman, 2002; Anand et al., 2003). This method was then used to generate a new equation to explain Mg/Ca incorporation in *Krithe*:

For bottom water temperatures above 3 °C:

$$[5] \quad Mg/Ca_{Krithe} = (1.308 \pm 0.041) * BWT + (2.836 \pm 0.231)$$

where Mg/Ca has units of mmol/mol and $\Delta[CO_3^{2-}]$ has units of $\mu\text{mol/kg}$ ($R^2 = 0.813$). The combination of equations 4 and 5 yields:

For bottom water temperatures at or below 3 °C:

$$[6] \quad \text{Mg/Ca}_{\text{Krithe}} = (1.308 \pm 0.041) * \text{BWT} + (0.094 \pm 0.014) * \Delta[\text{CO}_3^{2-}] + (2.165 \pm 0.671)$$

where Mg/Ca has units of mmol/mol, BWT has units of °C, and $\Delta[\text{CO}_3^{2-}]$ has units of $\mu\text{mol/kg}$.

Analytical error ($\sim 1\%$) yields an error of ~ 0.0817 mmol/mol at 3 °C, a typical deep ocean temperature; propagating this error in Equation 4, without accounting for carbonate ion effects, yields an uncertainty of ± 0.08 °C. However, at 3 °C, an error in temperature of ± 0.21 °C exists in the calibration, according to the 95 % confidence interval (Figure 4.9). Larger errors in the calibration are observed at low and high temperatures (± 0.55 °C at -1.36 °C and ± 0.67 °C at 14.5 °C; Figure 4.9). Analytical error explains only a small fraction of the scatter observed in this global calibration; other possible errors, including: post-depositional dissolution, non-modern Holocene core tops, vital effects, and differences in cleaning procedure, have been identified for benthic foraminiferal paleotemperature calibrations (e.g., Rosenthal et al., 2000; Elderfield et al., 2006; Greaves et al., 2008). A full discussion of other possible sources of error is given in Appendix 10.

4.4.9 Comparison to Published Calibration Studies

Contrary to the results of this core top calibration that suggest a $\Delta[\text{CO}_3^{2-}]$ control on *Krithe* Mg/Ca ratios at low temperatures, a preliminary study by Dwyer et al. (2002) suggested that carbonate ion concentration does not affect *Krithe* Mg/Ca ratios; however,

a re-evaluation of this data reveals that $\Delta[\text{CO}_3^{2-}]$ is an important control on *Krithe* Mg/Ca ratios. Dwyer et al. (2002) drew this conclusion because the measured *Krithe* Mg/Ca ratios from 4 core top sites on the Ontong Java Plateau were consistent with the expected Mg/Ca ratios calculated from *in situ* bottom water temperatures (1.5 to 2.8 °C) using their Mg/Ca-temperature equation (equating to $\Delta\text{Mg/Ca}$ near 0 mmol/mol; Appendix 8). However, following the inter-laboratory offset correction, the reported Mg/Ca ratios from Ontong Java Plateau have slightly lower Mg/Ca ratios than the expected Mg/Ca ratios according to Equation 5. Thus the Ontong Java Plateau samples have a small negative $\Delta\text{Mg/Ca}$ (-0.04 to - 3.66 mmol/mol; Figure 4.9). The $\Delta[\text{CO}_3^{2-}]$ range of these samples, -3.3 to 8.8 $\mu\text{mol/kg}$, is close to the x-intercept of Equation 4 ($\Delta\text{Mg/Ca} = 0$ at $\Delta[\text{CO}_3^{2-}] = 7.14 \mu\text{mol/kg}$), and thus only small changes in Mg/Ca would be expected for these samples due to carbonate ion effects. The $\Delta[\text{CO}_3^{2-}]$ correction slightly increased the Mg/Ca values from the Ontong Java Plateau sites, which then conform to the linear Mg/Ca-temperature relationship (Equation 5). Therefore, even the previously published Ontong Java Plateau data are consistent with the carbonate ion effect identified by this study (Figure 4.9).

Whether the proposed paleotemperature calibration equation is linear or exponential is particularly important for paleoceanographic reconstructions. Inorganic, empirical, culture, and core top foraminiferal studies have shown that the Mg/Ca – temperature relationship could be either linear (Mucci, 1987; Toyofuku et al., 2000; Healey et al., 2008) or exponential (Katz, 1973; Rosenthal et al., 1997; Lea et al., 1999). However, the *Krithe* paleotemperature equation has typically been described as linear (Cadot, 1977; Cadot and Kaesler, 1979; Dwyer, 1995; Cronin et al., 1996; Correge and

De Deckker, 1997; Dwyer et al., 2000; Dwyer et al., 2002), though an improved statistical representation from an exponential relationship was suggested (Dwyer et al., 2002). Prior to correcting for carbonate ion effects, an exponential regression of the entire data set yielded an R^2 value of 0.423 (not shown), whereas a linear regression of the data yielded an improved R^2 value of 0.469 (Figure 4.7). Similarly, an exponential regression of the data from sites where temperature is above 3 °C yielded an R^2 values of 0.485 (not shown), whereas linear regressions of the same data yielded an improved R^2 value of 0.483 (Figure 4.7). Thus, before accounting for secondary calcification effects, initial statistical analysis suggests that a linear relationship best describes the relationship between Mg/Ca and temperature (Figure 4.7). The identification of a carbonate ion effect on *Krithe* Mg/Ca at low temperatures has the added result of decreasing the apparent Mg/Ca ratios at many cold temperature sites (Figure 4.9); these elevated Mg/Ca ratios at cold temperatures may have contributed to why Dwyer et al. (2002) described the paleotemperature equation as exponential. Since many of the low temperature, high Mg/Ca values are now explained by $\Delta[\text{CO}_3^{2-}]$ effects, instead of by temperature effects, there is no statistical reason to describe the Mg/Ca-temperature relationship as exponential (Figure 4.9). This indicates that *Krithe* may be particularly useful as a paleothermometer, when combined with an independent $\Delta[\text{CO}_3^{2-}]$ proxy.

In addition to explaining much of the variability in Mg/Ca ratios at low temperatures, applying the $\Delta[\text{CO}_3^{2-}]$ correction to sites with bottom water temperatures at or below 3 °C changes both the slope (i.e., the temperature sensitivity of Mg/Ca) and the intercept of the paleotemperature equation (Table 4.1). The y-intercept of the paleotemperature equation from this study (5.137 mmol/mol; Equation 5) is higher than

the intercepts published by Cadot and Kaesler (1977), Corregge and DeDecker (1997), and Dwyer et al. (1995), which have been adjusted for differences in cleaning protocols (see Section 4.46; Figure 4.10). Equations that were generated using data only from the Arctic Ocean core tops (Cronin et al., 1996), or from a compilation of sites that included the Arctic Ocean (Cronin et al., 1996; Dwyer et al., 2002) were found to have higher y-intercepts than the equation generated by this study, since a $\Delta[\text{CO}_3^{2-}]$ correction had not been applied (Figure 4.10; Table 4.1). The y-intercept defined by this study is similar to that defined by Dwyer et al. (2002), since the majority of their locations have BWT > 3 °C and therefore a $\Delta[\text{CO}_3^{2-}]$ correction factor was not needed (Table 4.1; Figure 4.7; Figure 4.10). Additionally, the Dwyer et al. (2002) calibration is similar to the equation from this study due in part to the small carbonate ion effect on the cold temperature Ontong Java Plateau, as mentioned above (Figure 4.10). The y-intercept of the Corregge and De Deckker (1997) equation is the lowest of all published equations (Table 4.1); however, within the temperature range of their data (2.3 – 5.9 °C), their equation is similar to the equation generated by this study (Figure 4.10).

Paleotemperature equations from Dwyer et al. (1995), Cronin et al. (1996), and Dwyer et al. (2002) have similar Mg/Ca versus temperature relationships at the warmer end (BWT = 13 – 15 °C) because the Mg/Ca ratios for this temperature range is determined from core top locations on the Little Bahama Bank. Little Bahama Bank samples used in benthic foraminiferal Mg/Ca vs. temperature calibrations have been shown to be contaminated by high Mg-calcite overgrowths (Lear et al., 2002; Marchitto et al., 2007); this could be an additional complication of the Dwyer et al., (1995) calibration, which did not oxidatively and reductively clean specimens. However, the

core tops presented here from Sulawesi Margin, Indonesia (BWT = 9 to 12 °C) support this portion of the paleotemperature equation (Figure 4.10).

4.5 Paleooceanographic Applications

The paleotemperature equation generated by this study is similar to many published equations because those equations were generated mainly for sites with bottom water temperatures above 3 °C, thus a $\Delta[\text{CO}_3^{2-}]$ correction was not required. However, many modern deep ocean sites have bottom water temperatures at or below 3 °C, with glacial temperatures of 0 to 1 °C (Labeyrie et al., 1987). Given this cold temperature range, the use of a paleotemperature equation that also incorporates carbonate ion effects is important for paleooceanographic reconstructions.

The determination of paleotemperatures is critical to the understanding of past oceans and climate; however, the suggestion of carbonate ion effects in addition to the temperature effects on Mg/Ca ratios of *Krithe* poses a problem for the use of *Krithe* as paleothermometer since few paleo-carbonate ion concentration records exist.

Foraminiferal shell weights (Lohmann, 1995; Broecker and Clark, 2001; Broecker and Clark, 2002), benthic foraminiferal boron to calcium ratios (B/Ca; e.g., Yu and Elderfield, 2007), and benthic foraminiferal boron isotopes (e.g., Sanyal et al., 1995; Rae et al., 2008) provide proxies for estimating paleo-carbonate ion concentrations; however, these proxies have shown that the carbonate ion system is highly complex (Yu and Elderfield, 2008; Yu et al., 2008).

Here, I calculate paleotemperatures according to three different methods for comparison, using measured Mg/Ca ratios only, using measured Mg/Ca ratios and estimated paleo-carbonate ion concentrations, and using paleotemperature estimates from

benthic foraminiferal $\delta^{18}\text{O}$ values. Since Last Glacial Maximum sediments are missing from 11JPC (see Chapter 3 of this dissertation), average values of *Krithe* Mg/Ca and *P. wuellerstorfi* $\delta^{18}\text{O}$ were calculated for the Holocene (Mg/Ca = 10.02 mmol/mol; $\delta^{18}\text{O}$ = 3.50 ‰ V-PDB) and for the late MIC 3 (~ 33 – 43 ka; Mg/Ca = 8.95 mmol/mol; $\delta^{18}\text{O}$ = 4.95 ‰ V-PDB; Table 4.3).

Paleotemperatures from Mg/Ca ratios were estimated for the Holocene and late MIC 3, without taking carbonate ion concentrations into account, according to Equation 5 (Table 4.3). This method yielded unreasonably high bottom water temperatures of 4.8 and 3.8 °C for the Holocene and Late MIC 3, respectively (Table 4.3).

Taking into account carbonate ion concentrations, paleotemperatures were estimated from Mg/Ca ratios for the Holocene and late MIC 3 according to Equation 6 (Table 4.3). The modern $\Delta[\text{CO}_3^{2-}]$ value of 38.8 $\mu\text{mol/kg}$ was used for the Holocene and an estimated $\Delta[\text{CO}_3^{2-}]$ change of ~ 25 $\mu\text{mol/kg}$ from late Marine Isotope Stage 3 to the Holocene was used according to estimates of $\Delta[\text{CO}_3^{2-}]$ for this period from a similar water depth in the northeastern North Atlantic, calculated from B/Ca ratios (Yu and Elderfield, 2008; Yu et al., 2008). Yu et al. (2008) suggested that waters shallower than 2400 m had higher $\Delta[\text{CO}_3^{2-}]$ during the Last Glacial Maximum than during the Holocene; a site at 2777 m also appears to show elevated glacial $\Delta[\text{CO}_3^{2-}]$, though to a lesser degree than at the shallower sites (Yu et al., 2008). Higher LGM $\Delta[\text{CO}_3^{2-}]$ at sites shallower than 2800 m may be due to lower atmospheric CO_2 and an increased biologic pump (Barker and Elderfield, 2002; Bertram et al., 1995; Curry and Oppo, 2005; Petit et al., 1999; Yu and Elderfield, 2008; Yu et al., 2008). By correcting for the $\Delta[\text{CO}_3^{2-}]$ effect, temperatures

of 2.21 and -0.69 °C were calculated for the Holocene and Late MIC 3, respectively (Table 4.3).

Paleotemperatures were independently calculated from average benthic foraminiferal $\delta^{18}\text{O}$ for both time periods according to Shackleton (1974):

$$[7] \quad \text{BWT} = 16.9 - 4.0 (\delta^{18}\text{O}_{\text{calcite}} - (\delta^{18}\text{O}_{\text{SW}} - 0.27 \text{‰}))$$

where $\delta^{18}\text{O}_{\text{calcite}}$ is the measured value benthic foraminiferal calcite, in units of ‰ V-PDB, corrected by 0.64 ‰ to adjust to equilibrium seawater (Shackleton and Hall, 1984), $\delta^{18}\text{O}_{\text{SW}}$ is the oxygen isotopic composition of the overlying sea water, in units of ‰ V-SMOW (0.3 ‰ for the Holocene and 0.6 ‰ for late MIC 3; Waelbroeck et al., 2002, after Shackleton, 2000), and 0.27 ‰ is the correction factor between V-SMOW and V-PDB (Bemis et al., 1998). The $\delta^{18}\text{O}_{\text{SW}}$ value for late MIC 3 was estimated assuming that Antarctic Bottom Water did not bathe this site during late MIC 3 (see Chapter 3 of this dissertation). This method yielded temperatures of 3.02 and -1.58 °C for the Holocene and late MIC 3, respectively (Table 4.3).

Paleotemperatures generated by the carbonate ion concentration corrected Mg/Ca and benthic foraminiferal $\delta^{18}\text{O}$ methods yield Holocene temperatures that are within error limits of each other, and are consistent with modern bottom water temperature measurements (3.06 °C, Table 4.2; Table 4.3), indicating that our calibration is effective in characterizing modern temperatures (Table 4.3). The carbonate corrected Mg/Ca and $\delta^{18}\text{O}$ methods yield late MIC 3 paleotemperatures that are also within error limits of each other (Table 4.3). The paleotemperatures generated from Mg/Ca by Equation 5, which

does not include carbonate ion effects, are significantly warmer than paleotemperatures generated according to the other two methods, and do not effectively characterize modern bottom water temperatures (Table 4.3); this demonstrates that carbonate ion effects must be accounted for when using *Krithe* Mg/Ca as a paleothermometer. Additionally, the modern BWT at this site of 3.06 °C (Table 4.2), is likely higher than the MIC 3 BWT at this site, and therefore, following this core top calibration study, carbonate ion effects must be taken into account throughout the record.

A published downcore record from CHN82 4PC, in the mid-latitude North Atlantic, identified a change in *Krithe* Mg/Ca ratios from ~ 7.5 to 10.5 mmol/mol from the LGM to the Holocene (Dwyer et al., 1995). When interpreted without carbonate ion effects, this Mg/Ca record was proposed to represent a change of ~ 3 °C and a > 1.5 ‰ change in $\delta^{18}\text{O}_{\text{SW}}$ due to ice volume changes (Dwyer et al., 1995). However, it has been estimated that $\Delta[\text{CO}_3^{2-}]$ was 12 $\mu\text{mol/kg}$ higher at this site during the LGM than during Holocene (Sosdian, 2008), consistent with previous estimates of 10 to 15 $\mu\text{mol/kg}$ (Marchitto et al., 2002). Reanalysis of the CHN82 4PC data incorporating carbonate ion effects, using Equation 6 from this study, suggests that Dwyer et al. (1995) overestimated this temperature change by up to 1 °C, and therefore underestimated the change in $\delta^{18}\text{O}_{\text{SW}}$. A higher $\delta^{18}\text{O}_{\text{SW}}$ value would make this record more consistent with other records that suggest a larger change in $\delta^{18}\text{O}_{\text{SW}}$ from the LGM to Holocene of 1.1 ‰ (Labeyrie et al., 1987) or 1.2 ‰ (Fairbanks, 1989), rather than 1.0 ‰ (Waelbroeck et al., 2002; Shrag et al., 1996). Thus, the development of a paleotemperature equation that includes carbonate ion effects affords the ability to generate reasonable estimates of ice

volume variations and shows the usefulness of this proxy for paleoceanographic reconstructions for deep oceans.

4.6 Conclusions

Mg/Ca ratios of ostracods from globally distributed core tops indicate that the incorporation of magnesium into the calcium carbonate lattice of *Krithe* carapaces is not strictly temperature dependent, as was previously suggested. Just as benthic foraminiferal Mg/Ca calibration studies have identified carbonate ion effects at temperatures below 3 °C (Elderfield et al., 2006), this study has shown that $\Delta[\text{CO}_3^{2-}]$ concentration exerts a role on *Krithe* Mg/Ca ratios below the same temperature threshold. Based on these results a new temperature calibration is proposed that incorporates a carbonate ion effect. It is also evident from this study that other published Mg/Ca paleotemperature equations are offset from the measurements made in this study, likely due to a difference in cleaning methodology, which should be systematically studied in *Krithe* ostracods.

The acknowledgement of a carbonate ion effects on the Mg/Ca ratios of *Krithe* below 3 °C, creates previously unknown problems in the interpretation of most down core *Krithe* Mg/Ca records since BWT is less than 3 °C in much of the global oceans. In order to use Mg/Ca as a paleotemperature proxy, $\Delta[\text{CO}_3^{2-}]$ must first be carefully considered, through the use of foraminiferal shell weights (Lohmann, 1995; Broecker and Clark, 2001; Broecker and Clark, 2002), benthic foraminiferal B/Ca ratios (e.g., Yu and Elderfield, 2007), benthic foraminiferal boron isotopes in benthic foraminifera (e.g., Sanyal et al., 1995; Rae et al., 2008), or other means. Alternatively, Mg/Ca of *Krithe* may be useful in conjunction with an independent temperature proxy such as benthic oxygen isotopes or by using pore-water fluid analysis (Adkins et al., 2002) to calculate paleo-

carbonate ion saturation (e.g., Elderfield et al., 2006). In summary, *Krithe* Mg/Ca may be useful in warmer locations, or when combined with an independent proxy for temperature or carbonate ion concentration. This calibration provides an alternate method for estimating paleotemperatures in sediment cores that do not have a sufficient quantity of benthic foraminifera for trace metal analysis, such as some North Atlantic drift sites (Elmore and Wright, unpublished data).

4.7 References

- Adkins, J.F., McIntyre, K., and D.P. Schrag. 2002. The salinity, temperature and $\delta^{18}\text{O}$ of the glacial deep ocean. *Science*. 298; 1773.
- Anand, P., Elderfield, H., and M.H. Conte. 2003. Calibration of Mg/Ca thermometry in planktonic foraminifera from a sediment trap time series. *Paleoceanography*. 18 (2); 1-15.
- Arbuszewski, J., deMenocal, P., and A. Kaplan. 2008. Toward a global calibration and validation of the *G. ruber* (white) Mg/Ca paleothermometer. American Geophysical Union Abstracts and Programs. PP41F-02.
- Barker, S. and H. Elderfield. 2002. Foraminiferal calcification response to glacial–interglacial changes in atmospheric CO_2 . *Science*. 297; 833-836.
- Bemis, B.E., Spero, H.J., Bjima, J., and D.W. Lea. 1998. Reevaluation of the oxygen isotopic composition of planktonic foraminifera: Experimental results and revised paleotemperature equations. *Paleoceanography*. 13; 150-160.
- Bertram, C.J., Elderfield, H., Shackleton, N.J., and J.A. Macdonald. 1995. Cadmium/calcium and carbon isotope reconstructions of the glacial Northeast Atlantic Ocean. *Paleoceanography*. 10; 563-578.
- Bernhard, J.M.. 1988. Postmortem vital staining in benthic foraminifera: duration and importance in population and distributional studies. *Journal of Foraminiferal Research*. 18; 143-146.
- Bianchi G.G., and N. McCave, 1999. Holocene periodicity in North Atlantic climate and deep-ocean flow south of Iceland. *Nature*. 397, 515-517.
- Bickert, T., Curry, W.B., and G. Wefer. 1997. Late Pliocene to Holocene (2.6-0 MA) Western Equatorial Atlantic Deep-Water Circulation: Inferences from Benthic Stable Isotopes. In Shackleton, N.J., Curry, W.B., Richter, C., and T.J. Bralower,

- eds. *Proceedings of the Ocean Drilling Program, Scientific Results*, Vol. 154. 239-254.
- Billups, K. and D.P. Shrag. 2002. Paleotemperatures and ice volume of the past 27 Myr revisited with paired Mg/Ca and $^{18}\text{O}/^{16}\text{O}$ measurements on benthic foraminifera. *Paleoceanography*. 17 (1); 1-11.
- Bodergat, A.M.. 1983. Les ostracods, temoins de leur environnement. Approche chimique et ecologie en milieu lagunaire et oceanique. *Docums Lab. Geol. Fac. Sci. Lyon H. Ser.* 88; 1-246.
- Bodergat, A.M., Carbonnel, G., Rio, M., and D. Keyser. 1993. Chemical composition of *Leptocythere psammophila* (Crustacea: Ostracoda) as influenced by winter metabolism and summer supplies. *Marine Biology*. 117; 53-62.
- Boyle, E.A. and L.D. Keigwin. 1985. Comparison of Atlantic and Pacific paleochemical records for the last 215,000 years: changes in deep ocean circulation and chemical inventories. *Earth and Planetary Science Letters*. 76 (1-2); 135-150.
- Boyle E.A. and L.D. Keigwin. 1986. Glacial North Atlantic hydrography and atmospheric carbon dioxide. *Transactions of the American Geophysical Union*. 67; 868-869.
- Boyle, E.A. and L.D. Keigwin. 1987. North Atlantic thermohaline circulation during the past 20,000 years linked to high-latitude surface temperature. *Nature*, 330, 35-40.
- Boyle, E.A. and Y. Rosenthal. 1996. Chemical hydrography of the South Atlantic during the Last Glacial Maximum: Cd vs. $\delta^{13}\text{C}$, in: G. Wefer, W.H. Berger, G. Sielder, D. Webb (Eds.), *The South Atlantic: Present and Past Circulation*, Springer-Verlag, Berlin; 423-443.
- Brady, G.S., Crossey, H.W., and D. Robertson. 1874. A monograph of the Post-Tertiary *Entomostraca* of Scotland Including Species from England and Ireland. *Palaeontographical Society of London*. 274 pp.
- Broecker, W.S. and Peng. 1982. Tracers in the Sea. Lamont-Doherty Geological Observatory Press. New York.
- Broecker, W.S. and E. Clark. 2001. Glacial-to-Holocene redistribution of carbonate ion in the deep sea. *Science*. 294; 2152-2155.
- Broecker, W.S. and E. Clark. 2002. Carbonate ion concentration in glacial-age deep waters of the Caribbean Sea. *Geochemistry, Geophysics, Geosystems*. 3 (3); 1-14.
- Cadot, H.M., Van Schmus, W.R., and R.L. Kaesler. 1972. Magnesium in Calcite of Marie Ostracoda. *Geological Society of America Bulletin*. 83; 3519-3522.

- Cadot, H.M. and R.L. Kaesler. 1977. Magnesium content of calcite in carapaces of benthic marine ostracoda. *University of Kansas Paleontological Contributions*. 87; 1-23.
- Chave, K.E.. 1954. Aspects of the Biogeochemistry of Magnesium 1: Calcareous Marine Organisms. *Journal of Geology*. 62; 266-283.
- Chester, R.. 1990. Marine Geochemistry. Unwin Hyman, London. 698 pp.
- CLIMAP Project Members. 1981. Seasonal reconstructions of the Earth's surface at the last glacial maximum in Map Series, Technical Report MC-36. Boulder, Colorado: Geological Society of America.
- CLIMAP Project Members. 1984. The last Interglacial Ocean. *Quaternary Research*. 21; 123-224.
- Corliss, B.H. and S. Emerson. 1990. Distribution of Rose Bengal stained deep-sea benthic foraminifera from the Nova Scotian continental margin and Gulf of Maine. *Deep Sea Research Part A: Oceanographic Research Papers*. 37; 381-400.
- Correge, T.. 1993a. Late Quaternary Paleoceanography of the Queensland Trough (western Coral Sea) based on Ostracoda and the chemical composition of their shells. Dissertation at Australia National University.
- Correge, T.. 1993b. Preliminary results of paleotemperature reconstruction using the magnesium to calcium ratio of deep-sea ostracode shells from the late Quaternary of Site 822, Leg 133, (western Coral Sea), *Proceedings of the Ocean Drilling Program, Scientific Results*, 133; 175-180.
- Correge, T. and P. De Deckker. 1997. Faunal and geochemical evidence for changes in intermediate water temperature and salinity in the western Coral Sea (northeast Australia) during the Late Quaternary. *Paleogeography, Paleoclimatology, Paleoecology*. 133; 183-205.
- Cronin, T.M., Dwyer, G.S, Baker, P.A., Rodriguez-Lazaro, J., and W.M. Briggs, Jr.. 1996. Deep-sea ostracode shell chemistry (Mg:Ca ratios) and Late Quaternary Arctic Ocean history. *In*; Late Quaternary Paleoceanography of the North Atlantic Margins (Andrews, Austin, Bergsten, & Jennings, eds.) Geological Society of London Special Publication No. 111. 117-134
- Cronin, T.M. and M.E. Raymo, 1997. Orbital forcing of deep-sea benthic species diversity. *Letters to Nature*, 385, 624-627.

- Cronin, T.M., Dwyer, G.S., Schwede, S.B., Vann, C.D., and H. Dowsett. 2002. Climate variability from the Florida Bay sedimentary record: possible teleconnections to ENSO, PNA and CNP. *Climate Research*. 19; 233-245.
- Cronin, T.M., T. Kamiya, G.S. Dwyer, H. Belkin, C.D. Vann, S. Schwede, and R. Wagner. 2005. Ecology and shell chemistry of *Loxoconcha matagordensis*. *Paleoceanography, Paleoclimatology, Paleoecology*, 225, 14-67.
- Curry, W.B. and D. Oppo, D. 2005. Glacial water mass geometry and the distribution of $\delta^{13}\text{C}$ of ΣCO_2 in the western Atlantic Ocean. *Paleoceanography*. 20.PA1017. doi:10.1029/2004PA001021.
- Dickson, A.G.. 1990. Thermodynamics of the dissociation of boric-acid in synthetic seawater from 273.15-k to 318.15-k. *Deep-Sea Research Part A-Oceanographic Research Papers*. 37; 755-766.
- Dickson, A.G. and F.J. Millero. 1987. A comparison of the equilibrium constants for the dissociation of carbonic acid in seawater media. *Deep-Sea Research*. 34; 1733–1743.
- Didie, C. and H.A. Bauch. 2002. Implications of upper Quaternary stable isotope records of marine ostracods and benthic foraminifers for paleoecological and paleoceanographical investigations. Pp 279-299. *In* Holmes, J.A. and A.R. Chivas (eds.), *The Ostracoda: Applications in Quaternary Research*. American Geophysical Union Monograph. 131.
- Dwyer, G.S., T.M. Cronin, P.A. Baker, M.E. Raymo, J.S. Buzas, and T. Corregge. 1995. North Atlantic Deepwater Temperature Change During Late Pliocene and Late Quaternary Climatic Cycles. *Science*, 270, 1347-1351.
- Dwyer, G.S., Cronin, T.M., Baker, P.A., and J. Rodriguez-Lazaro. 2000. Changes in North Atlantic deep-sea temperature during climatic fluctuations of the last 25,000 years based on ostracode Mg/Ca ratios. *Geochemistry, Geophysics, Geosystems*. 1; 1-17.
- Dwyer, G.S., Cronin, T.M., and P.A. Baker. 2002. Trace elements in marine ostracods. *Geophysical monograph*. 131; 205-225.
- Elderfield, H., Bertram, C.J., and J. Erez. 1996. A biomineralization model for the incorporation of trace elements into foraminiferal calcium carbonate. *Earth and Planetary Science Letters*. 142 (3-4); 409-423.
- Elderfield, H., and G. Ganssen. 2000. Past temperature and $\delta^{18}\text{O}$ of surface ocean waters inferred from foraminiferal Mg/Ca ratios. *Nature*; 405, 442-445.

- Elderfield, H., Yu, J., Anand, P., Kiefer, T., and B. Nyland. 2006. Calibrations for benthic foraminiferal Mg/Ca paleothermometry and the carbonate ion hypothesis. *Earth and Planetary Science Letters*. 250; 633-649.
- Emiliani, C.. 1955. Tropical Paleotemperatures. *Science*. 268; 1264.
- Epstein, S., Buchsbaum, R., Lowenstam, H.A., and H.C. Urey. 1953. Revised carbonate-water isotopic temperature scale. *Geological Society of America Bulletin*. 64; 1315-1326.
- Fairbanks, R.G.. 1989. A 17,000- year glacio-eustatic sea level record: influence of glacial melting rates on the Younger Dryas event and deep-ocean circulation. *Nature*. 342; 637-640.
- Greaves, M., Caillon, N., Rebaubier, H., Bartoli, G., Bohaty, S., Cacho, I., Clarke, L., Cooper, M., Daunt, C., Delaney, M., deMenocal, P., Dutton, A., Eggins, S., Elderfield, H., Garbe-Schoenberg, D., Goddard, E., Green, D., Groeneveld, J., Hastings, D., Hathorne, E., Kimoto, K., Klinkhammer, G., Labeyrie, L., Lea, D.W., Marchitto, T., Martinez-Boti, M.A., Mortyn, P.G., Ni, Y., Nuerberg, D., Paradis, G., Pena, L., Quinn, T., Rosenthal, Y., Russel, A., Sagaway, T., Sosdian, S., Stott, L., Tachikawa, K., Tappa, E., Thunell, R., and P.A. Wilson. 2008. Interlaboratory comparison study of calibration standards for foraminiferal Mg/Ca thermometry. *Geochemistry, Geophysics, Geosystems*. 9 (8); 1-27.
- Guang, H., ZhangDong, J., and F. Zhang. 2008. Constraints of authigenic carbonates on trace elements (Sr, Mg) of lacustrine ostracod shells in paleoenvironment reconstruction and its mechanism. *Science in China Series D: Earth Sciences*; 51 (5); 654-664.
- Healey, S.L., Thunell, R.C., and B.H. Corliss. 2008. The Mg/Ca-temperature relationship of benthic foraminiferal calcite: New core-top calibrations in the <4°C temperature range. *Earth and Planetary Science Letters*. 272; 523-530.
- Holmes, J.A. 1992. Micropaleontology notebook. Trace element chemistry of non-marine ostracod shells: A preliminary evaluation of cleaning methods. *Journal of Micropaleontology*. 11; 36.
- Holmes, J.A., Street-Perrott, F.A., Ivanovich, M., and R.A. Perrott. 1995. A late Quaternary paleolimnological record from Jamaica based on trace-element chemistry of ostracod shells. *Chemical Geology*. 124; 143-160.
- Homes, J.A.. 2008. Sample-size implications of the trace-element variability of ostracod shells. *Geochimica et Cosmochimica Acta*. 72; 2934-2945.

- Izuka, S.K. 1988. Relation of magnesium and other minor elements in the test of *Cassidulina subglobosa* and *Cassidulina orianguilata* to physical oceanic properties. *Journal of Foraminiferal Research*. 18. 151-157.
- Jin, Z., Bickle, M., Chapman, H., Yu, J., Greaves, M., Wang, S., and S. Chen. 2006. An Experimental evaluation of cleaning methods for fossil ostracod Mg/Ca and Sr/Ca determination. *Journal of Paleolimnology*. 36; 211-218.
- Jordan, K.. 2008. Evaluating carbonate saturation effects on magnesium calcium core top calibration in benthic foraminifera. Masters Thesis at Rutgers University.
- Jutterstrom, S., and E. Jeansson. 2008. Anthropogenic carbon in the East Greenland Current. *Progress in Oceanography*. 78; 29-36.
- Jutterstrom, S., Jeansson, E., Anderson, L.G., Bellerby, R., Jones, E.P., Smethie, W.M., Jr., and J.H. Swift. 2008. Evaluation of anthropogenic carbon in the Nordic Seas using observed relationships of N, P and C versus CFCs. *Progress in Oceanography*. 78; 78-84.
- Katz, A. 1973. The interaction of magnesium with calcite during crystal growth at 25-90°C and one atmosphere. *Geochimica et Cosmochimica Acta*. 37; 1563-1586.
- Labeyrie, L.D., Duplessy, J.C., and P.L. Blanc. 1987. Variations in mode of formation and temperature of oceanic deep waters of the past 125,000 years. *Nature*. 327; 447-482.
- Laws, E.. 1997. Mathematical Methods for Oceanographers. John Wiley, New York. 343 pp.
- Lea, D.W., Mashiotta, T.A., and H.J. Spero. 1999. Controls on magnesium and strontium uptake in planktonic foraminifera determined by live culturing. *Geochimica et Cosmochimica Acta*. 63; 2369-2379.
- Lear, C.H., Elderfield, H., and P.A. Wilson. 2000. Cenozoic deep-sea temperatures and global ice volumes from M/Ca in benthic foraminiferal calcite. *Science* 287, 269-272.
- Lear, C.H., Rosenthal, Y., and N. Slowey. 2002. Benthic foraminiferal Mg/Ca paleothermometry: a revised core-top calibration. *Geochimica et Cosmochimica Acta*. 66(19); 3375-3387.
- Lewis, E. and D.W.R. Wallace. 1998. Program Developed for CO₂ System Calculations. ORNL/CDIAC-105. Carbon Dioxide Information Analysis Center, Oak Ridge National Laboratory, U.S. Department of Energy, Oak Ridge, Tennessee.

- Lisiecki, L.E. and M.E. Raymo, 2005. A Pliocene-Pleistocene stack of 57 globally distributed benthic $\delta^{18}\text{O}$ records. *Paleoceanography*. 20 (1003), 1-17.
- Lohmann, G.P.. 1995. A model for variation in the chemistry of planktonic foraminifera due to secondary calcification and selective dissolution. *Paleoceanography*. 10; 445-457.
- Marchitto, T.M., Curry, W.B., and D.W. Oppo. 2000. Zinc concentration in benthic foraminifera reflect seawater chemistry. *Paleoceanography*. 15; 299-306.
- Marchitto, T.M., Oppo, D.W., and W.B. Curry. 2002. Paired benthic foraminiferal Cd/Ca and Zn/Ca evidence for a greatly increased presence of Southern Ocean Water in the glacial North Atlantic. *Paleoceanography*. 17 (3); 1-16.
- Marchitto, T.M., Lynch-Stieglitz, J., and S. R. Hemming. 2005. Deep Pacific CaCO_3 compensation and glacial-interglacial atmospheric CO_2 , *Earth Planet. Sci. Lett.*, 231; 317-336.
- Marchitto, T.M. Bryan, S.P., Curry W.B., and D.C. McCorkle. 2007. Mg/Ca temperature calibration for the benthic foraminifer *Cibicides pachyderma*. *Paleoceanography*. 22; 1-9.
- Martin, P.A., Lea, D.W., Rosenthal, Y., Shackleton, N.J., Sarnthein, M., and T. Papefuss. 2002. Quaternary deep sea temperature histories derived from benthic foraminiferal Mg/Ca. *Earth and Planetary Science Letters*. 198; 193-209.
- Martinson, D.G., Pisias, N.G., Hays, J.D., Imbrie, J., Moore Jr., T.C., and N.J. Shackleton. 1987. Age dating and the orbital theory of the ice ages; development of a high-resolution 0 to 300,000-year chronostratigraphy. *Quaternary Research*. 27 (1); 1-29.
- McCorkle, D.C., Martin, P.A., Lea, D.W., and G.P. Klinkhammer. 1995. Evidence of a dissolution effect on benthic foraminiferal shell chemistry from the Ontong Java Plateau. *Paleoceanography*. 10; 699-714.
- McConnell, M.C. and R.C. Thunell. 2005. Calibration of the planktonic foraminiferal Mg/Ca paleothermometer: Sediment trap results from the Guaymas Basin, Gulf of California. *Paleoceanography*. 20; 1-18.
- Mehrbach, C., Culberso, C.H., Hawley, J.E., and R.M. Pytkowic. 1973. Measurement of apparent dissociation-constants of carbonic-acid in seawater at atmospheric-pressure. *Limnological Oceanography*. 18; 897-907.
- Miller, K.G., Kominz, M.A., Browning, J.V., Wright, J.D., Mountain, G.S., Katz, M.E., Sogerman, P.J., Cramer, B.S., Christie-Blick, N., and S.F. Pekar. 2005. The

- Pahnerozoic Record of Global Sea-Level Change. *Science*. 310 (5752); 1293-1298.
- Mucci A.. 1987. Influence of temperature on the composition of magnesian calcite overgrowths precipitated from seawater. *Geochimica et Cosmochimica Acta*. 51; 1977-1984.
- Neitzke, L.C. and J.D. Wright. 2007. Variations in Deep-Water Circulation on Eirik Drift from the Last Glacial Maximum to early Holocene. Geological Society of America, GSA 2007 Annual Meeting, Vol. 39(6); Paper 114-20.
- Nurnberg, D., Bijma, J., and C. Hemleben. 1996. Assessing the reliability of magnesium in foraminiferal calcite as a proxy for water mass temperature. *Geochimica et Cosmochimica Acta*. 60; 803-814.
- Okada, Y.. 1982. Structure and cuticle formation of the reticulated carapace of the ostracode *Bicornucythere bisanesis*. *Lethaia*. 15; 85-101.
- Orr, J.C., Fabry, V.J., Aumont, O., Bopp, L., Doney, S.C., Feely, R.A., Gnanadesikan, A., Gruber, N., Ishida, A., Joos, F., Key, R.M., Lindsay, K., Maier-Reimer, E., Mearns, R., Monfray, P., Mouchet, A., Najjar, R.G., Plattner, G.-K., Rodgers, K.B., Sabine, C.L., Sarmiento, J.L., Schlitzer, R., Slater, R.D., Totterdell, I.J., Weirig, M.-F., Yamanaka, Y., and A. Yool. 1995. Anthropogenic ocean acidification over the twenty-first century and its impact on calcifying organisms. *Nature*. 437; 681-686.
- Petit, J.R., Jouzel, J., Raynaud, D., Barkov, N.I., Barnola, J.M., Basile, I., Bender, M., Chappellaz, J., Davis, M., Delaygue, G., Delmotte, M., Kotlyakov, V.M., Legrand, M., Lipenkov, V.Y., Lorius, C., Pepin, L., Ritz, C., Saltzman, E., and M. Stievenard. 1999. Climate and atmospheric history of the past 420,000 years from the Vostok ice core, Antarctica. *Nature*. 399; 429-436.
- Rae, J.W., Foster, G.L., Schmidt, D.N., and T.R. Elliot. 2008. Boron Isotopes in Benthic Foraminifera by MC-ICPMS: Unlocking the Ocean's Carbon Cycle. American Geophysical Union Fall Meeting Abstracts # PP41D-1480.
- Raitzsch, M., Kuhnert, H., Groenveld, J., and T. Bickert. 2008. Benthic foraminifer Mg/Ca anomalies in South Atlantic core top sediments and their implications for paleothermometry. *Geochemistry Geophysics Geosystems*. 9 (5); 1-15.
- Raymo, M.E., Ruddiman, W.F., Shackleton, N.J., and D.W. Oppo. 1990. Evolution of Atlantic-Pacific $\delta^{13}\text{C}$ gradients over the last 2.5 m.y.. *Earth and Planetary Science Letters*. 97; 353-368.

- Rodriguez-Lazaro, J. and T.M. Cronin. 1999. Quaternary glacial and deglacial Ostracoda in the thermocline of the Little Bahama Bank (NW Atlantic): paleoceanographic implications. *Paleogeography, Paleoclimatology, Paleoecology*, 152, 339-364.
- Rosenthal, Y., Boyle, E.A., and N. Slowey. 1997. Temperature control on the incorporation of Mg, Sr, F, and Cd into benthic foraminiferal shells from Little Bahama Bank: prospects for thermocline Paleoceanography. *Geochimica et Cosmochimica Acta*. 61; 3363-3643.
- Rosenthal, Y., P. Field, and R.M. Sherrell. 1999. Precise determination of element/calcium ratios in calcareous samples using Sector Field Inductively Coupled Plasma Mass Spectrometry. *Analytical Chemistry*, 71, 3248-3253.
- Rosenthal, Y. and G. P. Lohman. 2002. Accurate estimation of sea surface temperatures using dissolution-corrected calibrations for Mg/Ca paleothermometry. *Paleoceanography*; 17(4).
- Rosenthal, Y., Perron-Cashman, S., Lear, C.H., Bard, E., Barker, S., Billups, K., Bryan, M., Delany, M.L., deMenocal, P.B., Dwyer, G.S., Elderfield, H., German, C.R., Greaves, M., Lea, D.W., Marchitto, Jr., T.M., Pak, D.K., Paradis, G.L., Russell, A.D., Schneider, R.R., Scheiderich, K. Stott, L., Tachikawa, K., Tappa, E., Thunell, R.C., Wara, M., Weldeab, S. and P.A. Wilson. 2004. Interlaboratory comparison study of Mg/Ca and Sr/Ca measurements in planktonic foraminifera for paleoceanographic research. *Geochemistry Geophysics Geosystems*. 5 (4); 1-29.
- Rosenthal, Y., Lear, C.H., Oppo, D.W., and Linsley, B.K. 2006. Temperature and carbonate ion effects on Mg/Ca and Sr/Ca ratios in benthic foraminifera: aragonitic species *Hoeglundia elegans*. *Paleoceanography*. 21; 1-14.
- Ross, D.A. and W.R. Riedel. 1967. Comparison of upper parts of some piston cores with simultaneously collected open-barrel cores. *Deep-Sea Research*. 14; 285-294.
- Russell, A.D., Emerson, S., Nelson, B.K., Erez, J. and D.W. Lea. 1994. Uranium in foraminiferal calcite as a recorder of seawater uranium concentration. *Geochimica et Cosmochimica Acta*. 58; 671-681.
- Russell, A.D., Hoenisch, B., Spero, H.J., and D.W. Lea. 2004. Effects of seawater carbonate ion concentration and temperature on shell U, Mg, and Sr in cultured planktonic foraminifera. *Geochimica et Cosmochimica Acta*. 68, 4347-4361.
- Sabine, C.L., Feely, R.A., Gruber, N., Key, R.M., Lee, K., Bullister, J.L., Wanninkhof, R., Wong, C.S., Wallace, D.W.R., Tilbrook, B., Millero, F.J., Peng, T.-H., Kozyr, A., Onon, T., and A.F. Rios. 2004. The Oceanic Sink for Anthropogenic CO₂. *Science*. 305; 367-371.

- Sanyal, A., Hemming, N.G., Hanson, G.N., and W.S. Broecker. 1995. Evidence for a higher pH in the glacial ocean from boron isotopes in foraminifera. *Nature*. 373; 234-236.
- Shackleton, N.J.. 1967. Oxygen Isotope Analyses and Pleistocene Temperatures Re-assessed. *Nature*. 215; 15-17.
- Shackleton, N.J.. 1974. Attainment of isotopic equilibrium between ocean water and the benthonic foraminifera genus *Uvigerina*: isotopic changes in the ocean during the last glacial. *Les. Meth. Quant. D'étude Var. Clim. Au Cours du Pleist., Coll. Int. CNRS*, 219:203–209.
- Shackleton, N.J. and M.A. Hall.. 1984. Oxygen and carbon isotope stratigraphy of Deep Sea Drilling Project Hole 552A: Plio-Pleistocene glacial history. In Roberts, D.G., Schnitker, D., et al., *Init. Repts. DSDP*, 81: Washington (U.S. Govt. Printing Office), 599–609.
- Shackleton, N.J.. 2000. The 100,000-year Ice-Age cycle identified and found to lag temperature, carbon dioxide, and orbital eccentricity. *Science*. 289; 1897-1902.
- Shrag, D.P., Hampt, G., and D.W. Murray. 1996. Pore Fluid Constraints on the Temperature and Oxygen Isotopic Composition of the Glacial Ocean. *Science*. 272; 1930-1932.
- Skinner, L.C. and I.N. McCave. 2003. Analysis and modeling of gravity- and piston coring based on soil mechanics. *Marine Geology*. 199; 181-204.
- Sosdian, S.M. 2008. Climate Transitions Across the Cenozoic: Insights from Elemental Ratios in Benthic Foraminifera and Marine Gastropods. Ph.D. Dissertation, Rutgers University. 255 pp.
- Swanson, K.M. and G.J. van der Lingen. 1994. Podocopid ostracod dissolution description of a new paleoenvironmental tool, with examples from the eastern Tasman Sea. In: G.J. van der Kingen, K.M. Swanson and R.J. Muir (Eds), *Evolution of the Tasman Sea Basin*. Balkema. Rotterdam. pp. 245-260.
- Swanson, K.M. and G.J. van der Lingen. 1997. Late Quaternary ostracod and planktonic foraminiferal dissolution signals from the eastern Tasman Sea—palaeoenvironmental implications. *Paleogeography, Palaeoclimatology, Palaeoecology*. 131; 303-314.
- Turpen, J.B. and R.W. Angell. 1971. Aspects of molting and calcification in the ostracod *Heterocypris*. *Biological Bulletin*; 140, 331-338.
- Urey, H.C..1947. The thermodynamic properties of isotopic substances. *Journal of the Chemical Society London*; 562-581.

- Waelbroeck, C., Labeyrie, L., Michel, E., Duplessy, J.C., McManus, J.F., Lambeck, K., Balbon, E., and M. Labracherie. 2002. Sea-level and deep water temperature changes derived from benthic foraminifera isotopic records. *Quaternary Science Reviews*. 21; 295-305.
- Walton, W.. 1952. Techniques for recognition of living foraminifera. *Cushman Foundation for Foraminiferal Research Contributions*. 2; 56-60.
- Whatley, R. and Z. Quanhong. 1993. The *Krithe* problem: a case history of the distribution of *Krithe* and *Parakrithe* (Crustacea, Ostracoda) in the South China Sea. *Palaeogeography, Palaeoclimatology, Palaeoecology*. 103 (3-4); 281-297.
- Worthington, L.V., 1976. On the North Atlantic Circulation. Johns Hopkins University Press; Baltimore, MD.
- Yasuhara, M., Cronin, T.M., and P.M. Arbizu. 2008. Abyssal ostracods from the South and Equatorial Atlantic Ocean: Biological and paleoceanographic implications. *Deep-Sea Research*. 55; 490-497.
- Yu, J.M. and H. Elderfield. 2007. Benthic foraminiferal B/Ca ratios reflect deep water carbonate saturation state. *Earth and Planetary Science Letters*. 258; 73-86..
- Yu, J.M. and H. Elderfield. 2008. Mg/Ca in the benthic foraminifera *Cibicidoides wuellerstorfi* and *Cibicidoides mundulus*: Temperature versus carbonate saturation. *Earth and Planetary Science Letters*. 276; 129-139.
- Yu, J.M., Elderfield, H., and A.M. Piotrowski. 2008. Seawater carbonate ion- $\delta^{13}\text{C}$ systematics and application to glacial–interglacial North Atlantic Ocean circulation. *Earth and Planetary Science Letters*. 271; 209–220.
- Zhao, Q. and R. Whatley. 1997. Distribution of the ostracod genera *Krithe* and *Parakrithe* in bottom sediments of the East China and Yellow seas. *Marine Micropaleontology*. 32; 195-207.

Table 4.1: Previously published paleotemperature equations for *Krithe* Mg/Ca. Location abbreviations are; South Coral Sea (SCS), Little Bahama Bank (LBB), Shallow Arctic less than 900 m (SA), Ontong Java Plateau (OJP), and Chilean Fjords (CF). Units for the equations are mmol/mol for Mg/Ca, °C for BWT, and $\mu\text{mol/kg}$ for $\Delta[\text{CO}_3^{2-}]$. Intercepts from previously published equations were corrected for inter-laboratory differences by 3.40 mmol/mol (*) according to section 4.4.6.

BWT (°C)	Location	Equation	Author
1-6	8 Global Sites	$\text{Mg/Ca} = 1.466 * \text{BWT} + 1.789$	Cadot & Kaesler, 1977*
2-6	SCS	$\text{Mg/Ca} = 1.923 * \text{BWT} + 3.030$	Correge & De Deckker, 1997*
3-14	LBB	$\text{Mg/Ca} = 1.172 * \text{BWT} + 3.329$	Dwyer et al., 1995*
-2-2	SA	$\text{Mg/Ca} = 2.667 * \text{BWT} + 6.010$	Cronin et al., 1996*
-2-14	LBB, SA	$\text{Mg/Ca} = 0.96 * \text{BWT} + 5.2113$	Cronin et al., 1996*
4-9	SCS, LBB, SA, OJP, CF	$\text{Mg/Ca} = 0.931 * \text{BWT} + 4.84$; $\text{Mg/Ca} = 9.353 * 10^{0.025 * \text{BWT}}$	Dwyer et al., 2002*
-2-14	Global Calibration	For BWT > 3°C: $\text{Mg/Ca} = 0.928 \pm 0.041 * \text{BWT} + 5.137 \pm 0.231$ For BWT < 3°C: $\text{Mg/Ca} = 0.928 \pm 0.041 * \text{BWT} + 0.094 \pm 0.014 * \Delta[\text{CO}_3^{2-}] + 4.466 \pm 0.671$	This study

Table 4.2: Hydrographic information for sites used in this core top calibration including; region, core, water depth, bottom water temperature (BWT), bottom water salinity (BWS), $\Delta[\text{CO}_3^{2-}]$, and Mg/Ca. Asterisks indicate $\Delta[\text{CO}_3^{2-}]$ values that were corrected for anthropogenic CO_2 input according to Section 4.3.2. Extended hydrographical information is given in Appendix 7.

Region	Core	Water Depth (m)	BWT (°C)	BWS (psu)	$\Delta[\text{CO}_3^{2-}]$ ($\mu\text{mol/kg}$)	Mg/Ca (mmol/mol)
Cape Hatteras shelf	KN178 16MCB	2214	3.37	34.94	44.12	8.32
Cape Hatteras shelf	KN178 16MCB	2214	3.37	34.94	44.12	8.59
Cape Hatteras shelf	KN178 14MCD	2602	3.03	34.93	39.59	9.19
Cape Hatteras shelf	KN178 8MCE	2997	2.51	34.91	34.16	9.35
Cape Hatteras shelf	KN178 5MCD	3382	2.20	34.88	26.91	7.71
Cape Hatteras shelf	KN178 1MCD	3979	2.20	34.88	17.39	8.61
Cape Hatteras shelf	KN178 1MCD	3979	2.20	34.88	17.39	7.74
Gulf of Mexico	DGOMB S36-3	1026	5.07	34.94	50.48	8.73
Gulf of Mexico	DGOMB W4-5	1406	4.33	34.97	57.47	8.26
Gulf of Mexico	DGOMB W4-5	1406	4.33	34.97	57.47	9.66
Gulf of Mexico	DGOMB S38-4	2630	4.30	34.99	35.22	8.60
Gulf of Mexico	DGOMB S38-4	2630	4.30	34.99	35.22	7.96
Gulf of Mexico	DGOMB W5-4	2745	4.31	34.99	32.57	9.39
Gulf of Mexico	DGOMB S39-2	3000	4.33	35.00	26.61	8.90
Gulf of Mexico	DGOMB W6-3	3150	4.35	35.00	23.94	8.48
Indonesia	BJ8-03 40MCF	251	11.50	34.47	60.60	16.59
Indonesia	BJ8-03 61MCD	292	10.85	34.45	57.80	15.06
Indonesia	BJ8-03 16MCC	409	8.75	34.47	31.33	12.68
New Zealand	RR05-03 86MCF	663	4.88	34.29	57.23	5.27
New Zealand	RR05-03 86MCF	663	4.88	34.29	57.23	4.26
New Zealand	RR05-03 82MCG	1623	2.45	34.54	16.30	8.37
New Zealand	RR05-03 22MCB	1682	2.40	34.56	16.09	8.79
New Zealand	RR05-03 22MCC	1682	2.40	34.56	16.09	7.45
New Zealand	RR05-03 22MCC	1682	2.40	34.56	16.09	7.69
New Zealand	RR05-03 92MCG	1818	2.29	34.60	15.72	6.78
New Zealand	RR05-03 102MCA	2055	2.12	34.66	13.87	8.17

New Zealand	RR05-03 102MCA	2055	2.12	34.66	13.87		6.22
New Zealand	RR05-03 118MCF	2252	2.04	34.69	15.71		7.41
New Zealand	RR05-03 118MCF	2252	2.04	34.69	15.71		7.89
New Zealand	RR05-03 118MCF	2252	2.04	34.69	15.71		7.17
New Zealand	RR05-03 26MCF	2418	1.91	34.71	15.08		6.75
New Zealand	RR05-03 26MCF	2418	1.91	34.71	15.08		8.25
New Zealand	RR05-03 106MCF	2472	1.87	34.72	14.47		8.46
North Atlantic	KN166-14 15JPC	2300	2.91	34.90	25.43	*	10.03
North Atlantic	KN166-14 15JPC	2300	2.91	34.90	25.43	*	8.95
North Atlantic	KN166-14 15JPC	2300	2.91	34.90	25.43	*	9.27
North Atlantic	KN166-14 11JPC	2707	3.00	34.93	38.82		10.36
North Atlantic	KN166-14 8GGC	2707	3.00	34.93	38.82		10.36
North Atlantic	KN166-14 8GGC	2707	3.00	34.93	38.82		8.85
North Atlantic	KN166-14 12JPC	3078	2.75	34.94	30.05		8.90
North Atlantic	KN166-14 3GGC	3305	2.56	34.92	25.27		8.87
North Atlantic	KN166-14 3GGC	3305	2.56	34.92	25.27		9.38
North Atlantic	DSDP Site 607	3427	2.57	34.92	21.77		10.07
Ceara Rise	ODP Site 926	3598	2.45	34.91	23.85		10.88
Ceara Rise	ODP Site 928	4010	1.52	34.90	16.45		11.33
Ceara Rise	ODP Site 929	4355	1.80	34.89	9.95		5.00
Norwegian Sea	KN177-2 4MC-E	418	0.84	34.91	78.86	*	11.65
Norwegian Sea	KN177-2 4MC-E	418	0.84	34.91	78.86	*	11.39
Norwegian Sea	KN177-2 11MC-C	1285	-0.71	34.91	58.89	*	11.31
Norwegian Sea	KN177-2 50MC-B	1906	-0.84	34.91	47.50	*	10.94
Norwegian Sea	KN177-2 50MC-B	1906	-0.84	34.91	47.50	*	9.04
Norwegian Sea	KN177-2 45MC-D	2799	-0.85	34.91	30.43	*	8.68

Table 4.3: *Krithe* Mg/Ca and *P. wuellerstorfi* $\delta^{18}\text{O}$ data from Holocene and late MIC 3 sections of core 11JPC used for independent paleotemperature estimates. Average Mg/Ca and estimated $\Delta[\text{CO}_3^{2-}]$ values for modern (Table 4.2) and glacial (Yu et al., 2008) were used to determine bottom water temperatures from Mg/Ca with and without carbonate ion effects using Equations 5 and 6, respectively. *Planulina wuellerstorfi* $\delta^{18}\text{O}$ data has been corrected by 0.64 ‰ to account for disequilibrium from sea water during calcification (Adj. $\delta^{18}\text{O}$ *P. wuell.*; Shackleton, 1974). Temperatures based on *P. wuellerstorfi* $\delta^{18}\text{O}$ (BWT $\delta^{18}\text{O}$) and $\delta^{18}\text{O}_{\text{SW}}$ (Waelbroeck et al., 2002) were estimated using equation 7.

Depth (cm)	Age (ka)	Mg/Ca (mmol/ mol)	BWT (°C) Mg/Ca	$\Delta[\text{CO}_3^{2-}]$ ($\mu\text{mol/kg}$)	BWT (°C) Mg/Ca, $\Delta[\text{CO}_3^{2-}]$	Adj. $\delta^{18}\text{O}$ <i>P. wuell.</i> (‰ V-PDB)	$\delta^{18}\text{O}_{\text{SW}}$ (‰ V- SMOW)	BWT (°C) $\delta^{18}\text{O}$
HOLOCENE								
10	1.14	10.36				3.56		
35	2.36	8.85				3.48		
55	3.38	10.21				3.40		
100	5.80	10.53				3.52		
105	6.05	9.71				3.59		
120	6.73	11.01				3.55		
165	9.82	9.54				3.40		
175	10.75	9.95				3.50		
Average		10.02	4.8	38.8	2.21	3.50	0.03	3.02
St. deviation		0.67				0.07		
LATE MIC 3								
333	33.81	9.15				4.76		
348	34.60	9.19				5.11		
363	35.44	8.93				4.90		
368	35.72	9.09				4.98		
431	40.09	9.10				4.90		
431	40.09	9.26				4.90		
431	40.09	9.50				4.90		
441	41.01	8.35				4.89		
441	41.01	8.70				4.89		
446	41.48	8.25				5.45		
471	44.17	8.95				4.78		
Average		8.95	3.8	63.8	-0.69	4.95	0.60	-1.58
St. deviation		0.38				0.19		

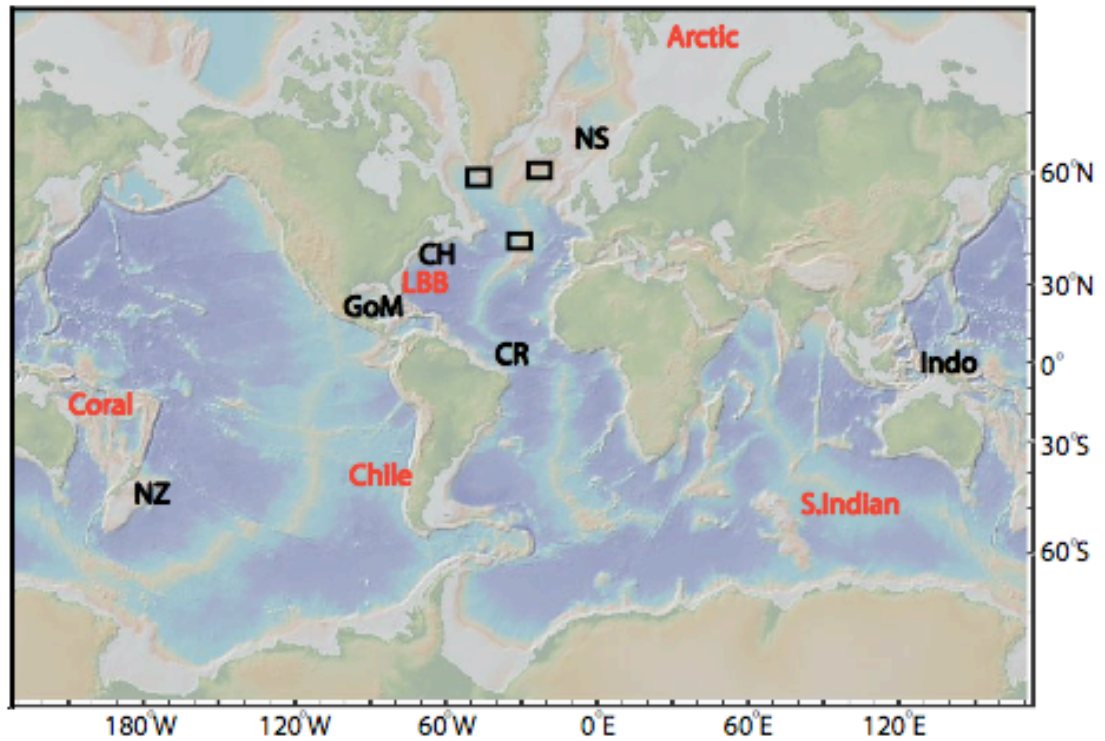


Figure 4.1: Map showing the global distribution of core tops used in this study. Location abbreviations from this study (black) are; Norwegian Sea (NS), Cape Hatteras shelf (CH), Gulf of Mexico (GoM), Ceara Rise (CR), Sulawesi Margin, Indonesia (Indo), and New Zealand shelf (NZ). Location abbreviations for locations used in previous studies (red) are; Little Bahama Bank (LBB), Coral Sea (Coral), Chilean Fjords (Chile), and Southern Indian Ocean (SI).

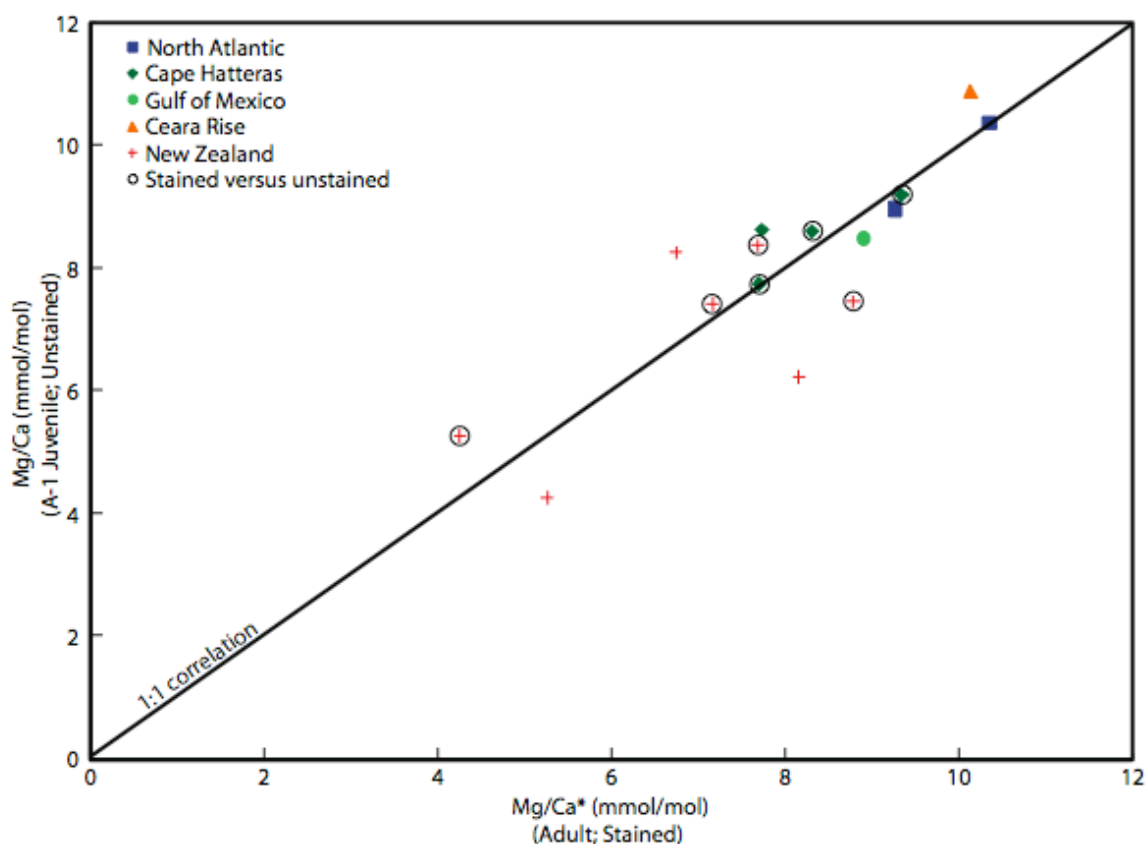


Figure 4.2: A comparison of the Mg/Ca of adult *Krithe* carapaces and the Mg/Ca of A-1 juvenile *Krithe* carapaces from the same locations falls close to the 1:1 relationship suggesting similar Mg-incorporation mechanisms. The Mg/Ca of Rose Bengal stained carapaces versus unstained carapaces of *Krithe* also shows a 1:1 relationship, indicating no discernible post-mortem dissolution effects. Adult and stained carapaces are plotted on the x-axis as Mg/Ca*. Samples are from the North Atlantic Ocean (blue), Cape Hatteras shelf (dark green), Gulf of Mexico (green), Ceara Rise (orange), or New Zealand shelf (red).

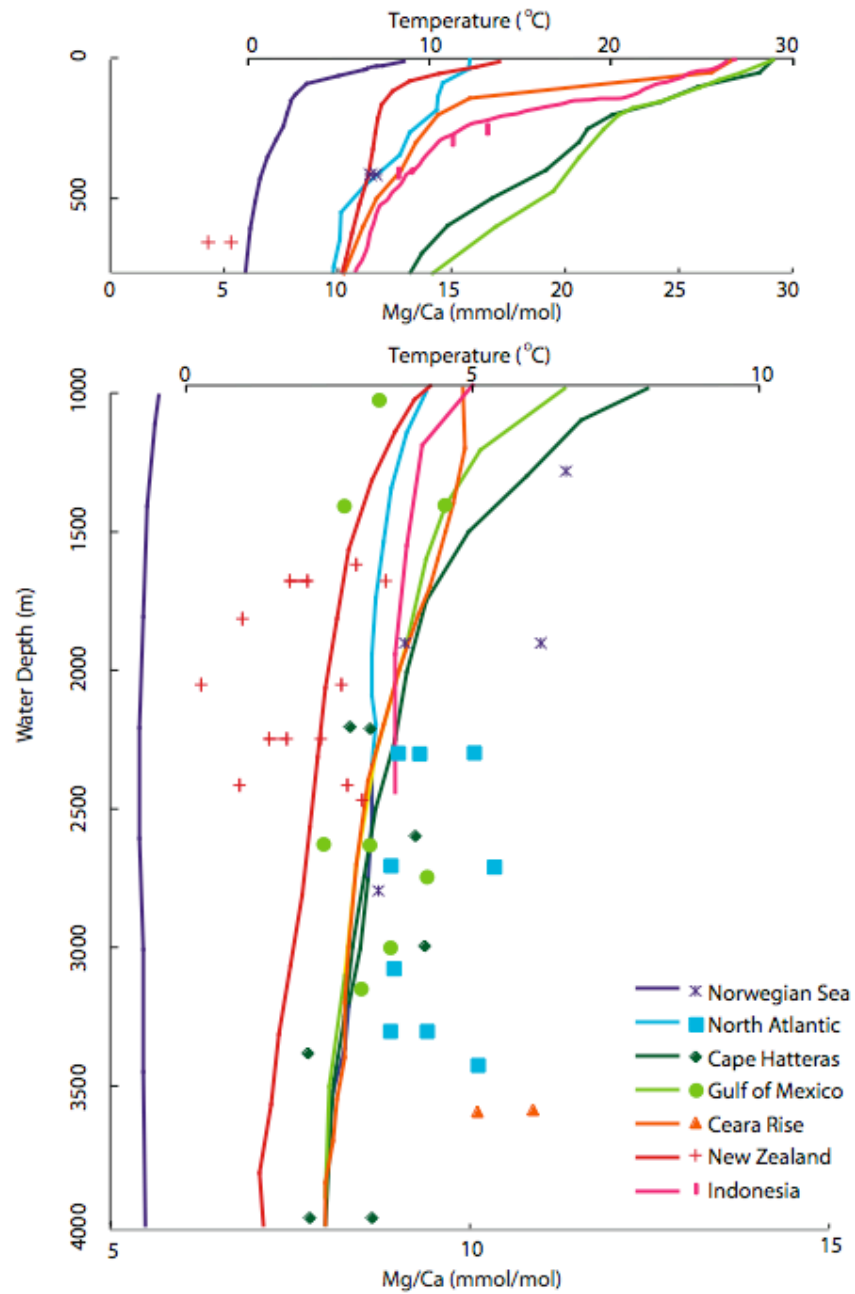


Figure 4.3: *Krithe* Mg/Ca and bottom water temperature versus water depth for sites from the Norwegian Sea (purple), North Atlantic Ocean (blue), Cape Hatteras shelf (dark green), Gulf of Mexico (light green), Ceara Rise (orange), New Zealand shelf (red), and Sulawesi Margin, Indonesia (pink).

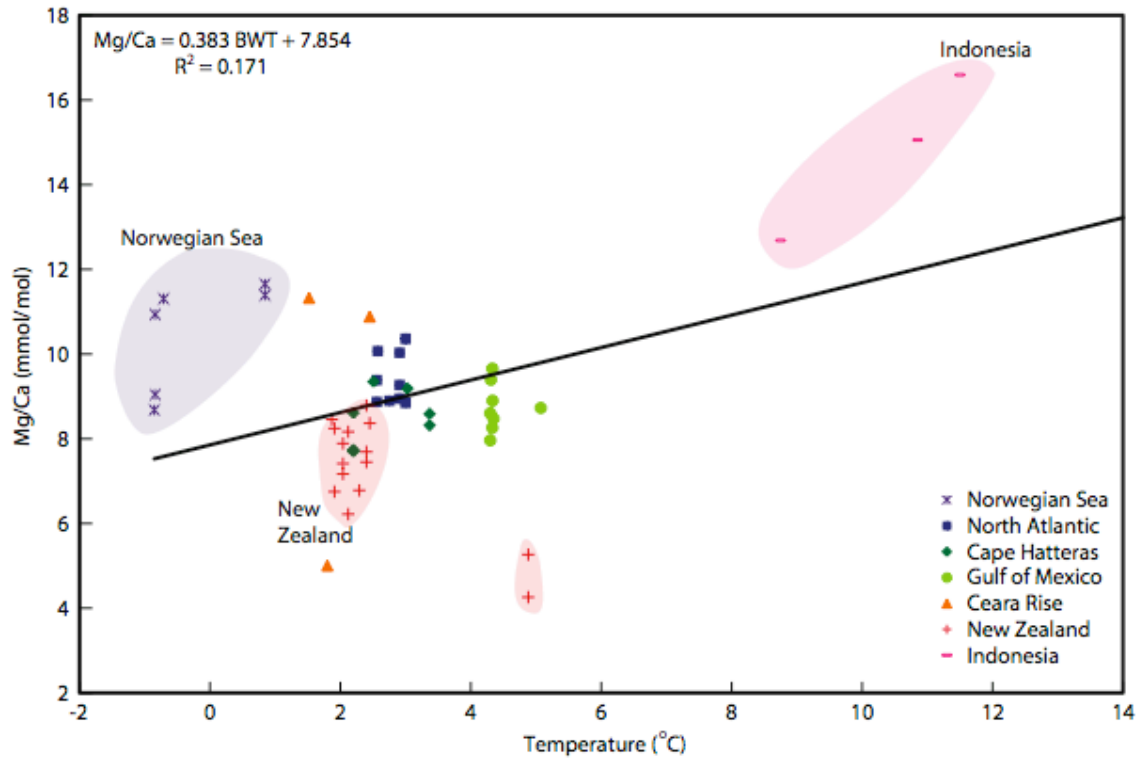


Figure 4.4: Comparison of *Krithe* Mg/Ca ratios and bottom water temperature for core tops from the Norwegian Sea (purple), North Atlantic Ocean (blue), Cape Hatteras shelf (dark green), Gulf of Mexico (light green), Ceara Rise (orange), New Zealand shelf (red), and Sulawesi Margin, Indonesia (pink). A linear regression is shown. Shaded regions represent a non-statistical grouping of data of data from Norwegian Sea (purple), New Zealand (red), and Indonesia (pink).

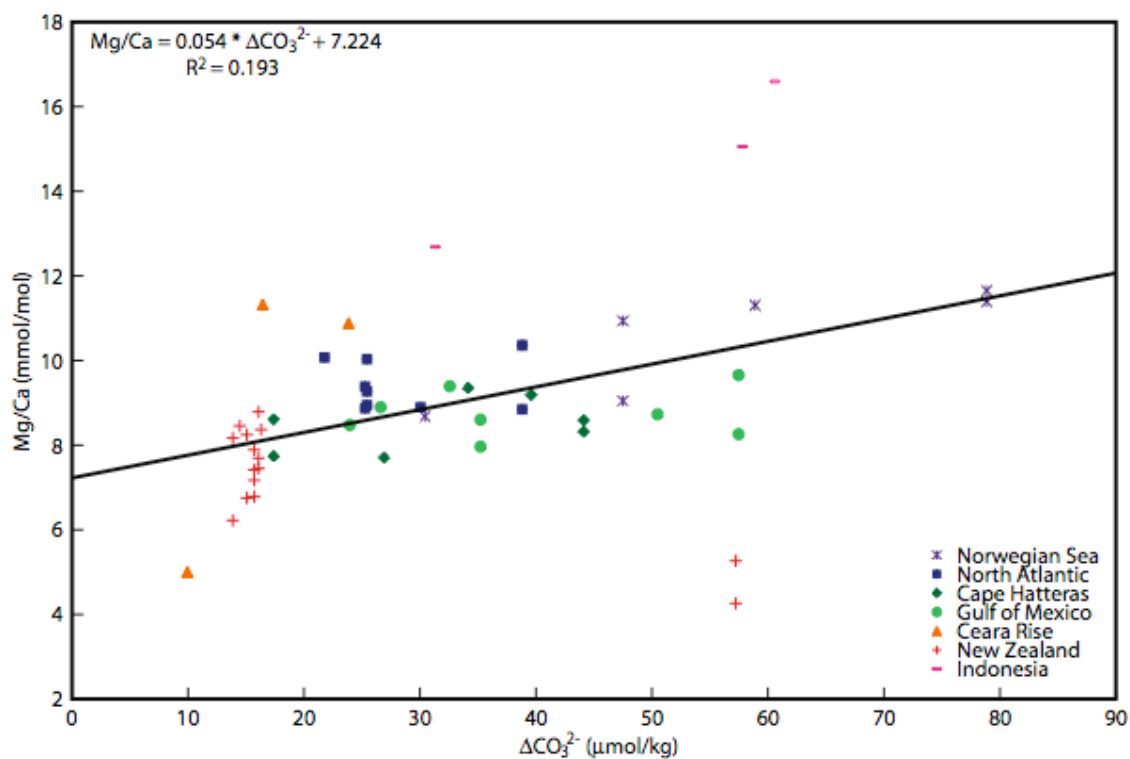


Figure 4.5a: Core top Mg/Ca data versus $\Delta[\text{CO}_3^{2-}]$ from this study; Norwegian Sea (purple), North Atlantic Ocean (blue), Cape Hatteras shelf (dark green), Gulf of Mexico (light green), Ceara Rise (orange), New Zealand shelf (red), and Sulawesi Margin, Indonesia (pink) sites plotted versus $\Delta[\text{CO}_3^{2-}]$. A linear regression for all the data is shown in black.

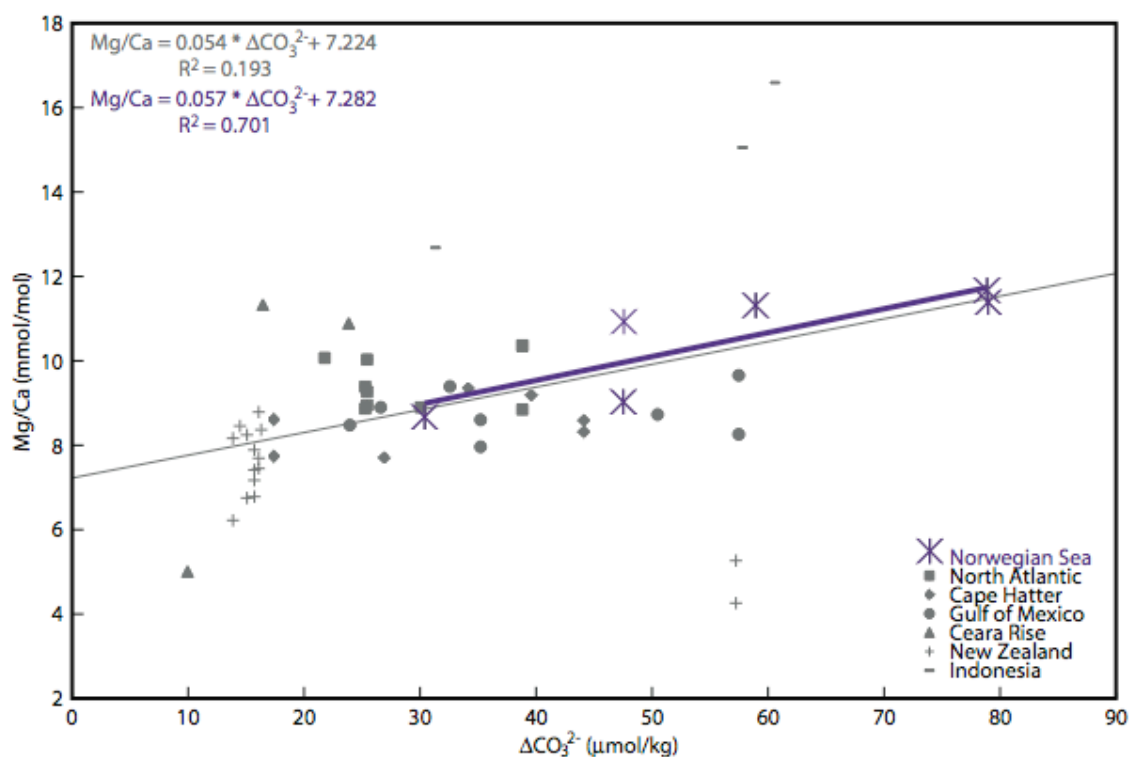


Figure 4.5b: Core top Mg/Ca data versus $\Delta[\text{CO}_3^{2-}]$ from this study; Norwegian Sea (purple), North Atlantic Ocean, Cape Hatteras shelf, Gulf of Mexico, Ceara Rise, New Zealand shelf, and Sulawesi Margin, Indonesia (grey) sites plotted. A linear regression for all the data is shown in grey; a linear regression for the homo-thermal, homo-haline transect of the Norwegian Sea (purple) is also shown.

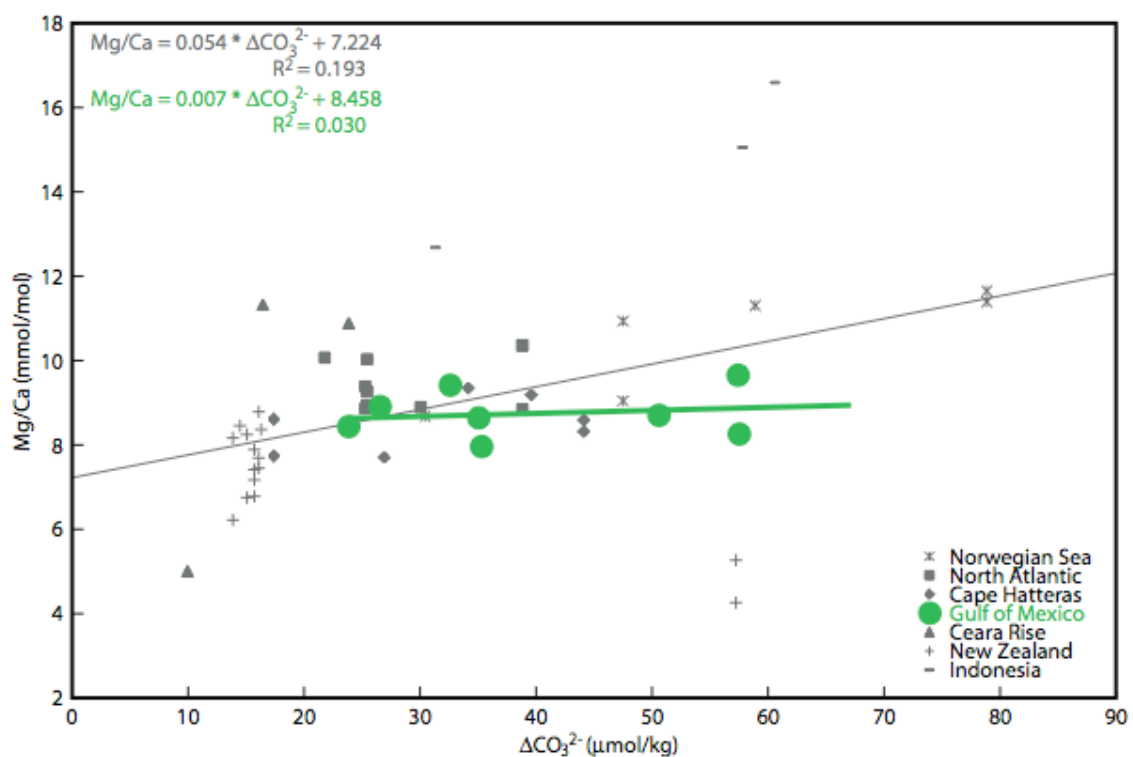


Figure 4.5c: Core top Mg/Ca data versus $\Delta[\text{CO}_3^{2-}]$ from this study; Norwegian Sea, North Atlantic Ocean, Cape Hatteras shelf, Gulf of Mexico (light green), Ceara Rise, New Zealand shelf, and Sulawesi Margin, Indonesia (grey). A linear regression for all the data is shown in grey; a linear regression for the homo-thermal, homo-haline transect of the Gulf of Mexico (light green) is also shown.

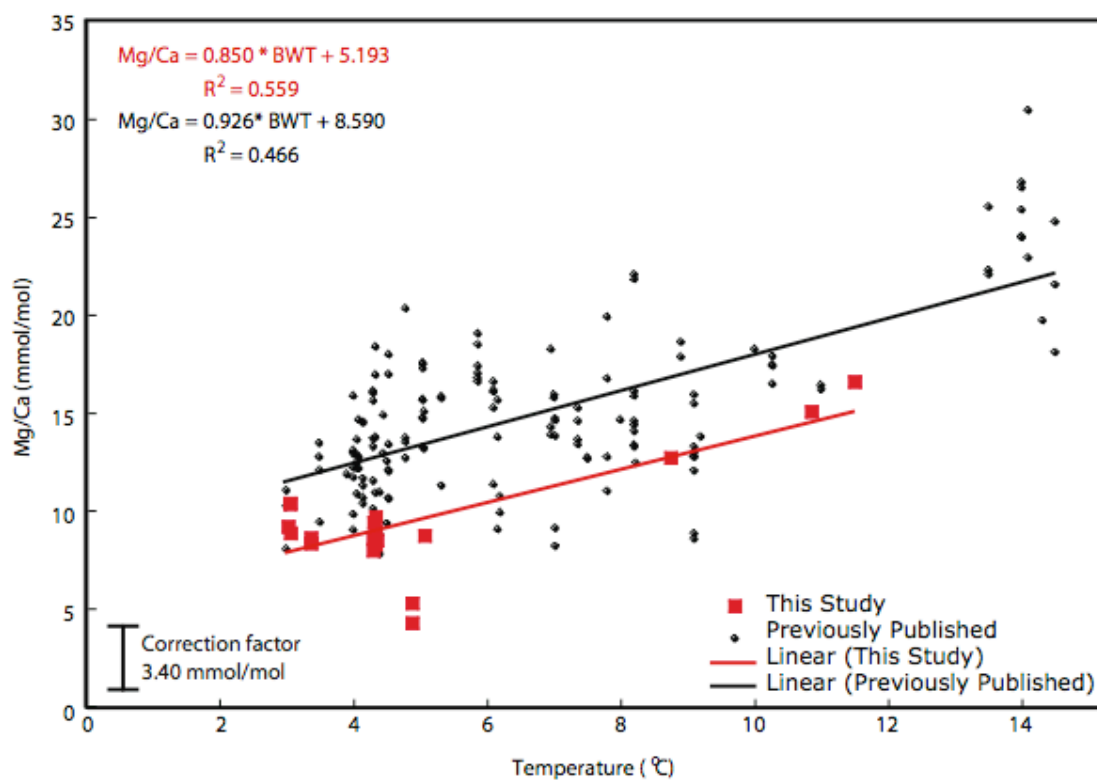


Figure 4.6: Mg/Ca data from core top sites from this study (red squares) plotted against temperature for bottom water temperatures above 3 °C. Data from previously published studies (black diamonds) are also plotted against temperatures. The correction factor due to differences in cleaning protocols calculated by the difference between the linear regression intercepts, 3.40 mmol/mol is shown.

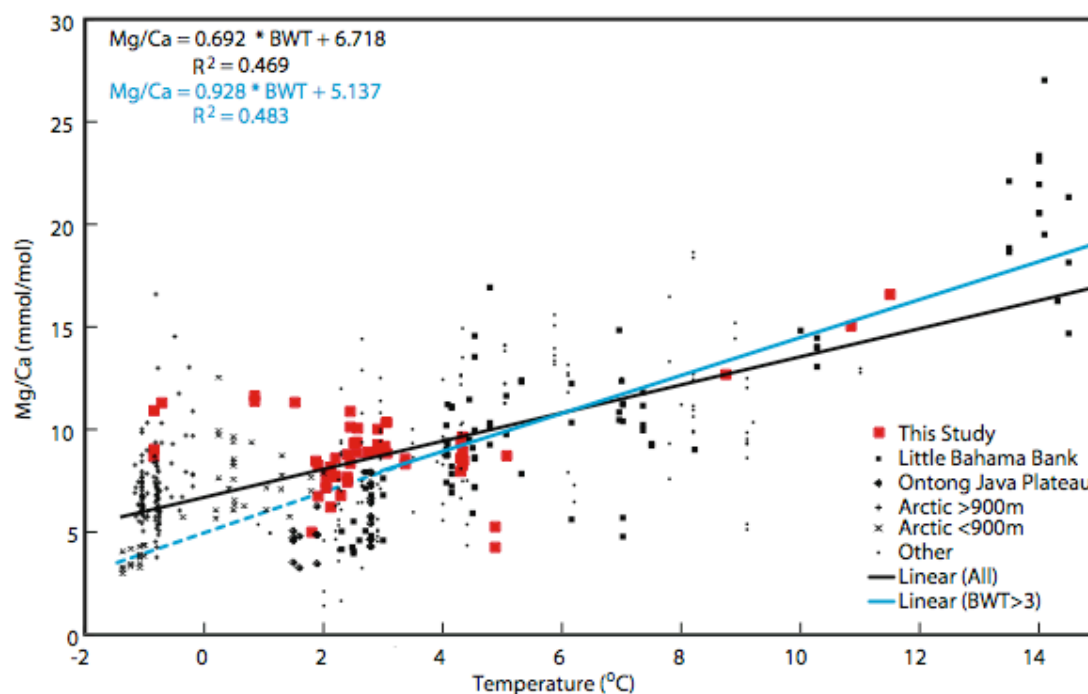


Figure 4.7: Mg/Ca data from core top sites from this study (red squares) plotted against temperature. Data from Little Bahama Bank (Dwyer et al., 1995; black squares), Ontong-Java Plateau (Dwyer et al., 2002; black diamonds), Arctic Ocean < 900 m (Cronin et al., 1996; black x-s), the Arctic Ocean > 900 m (Cronin et al., 1996; black crosses), and all other sources (Cadot et al., 1972; Cadot and Kaesler, 1977; Corregge et al., 1993b; Corregge and DeDecker, 1997; small black circles) have all been corrected to account for differences in cleaning. The black line represents a linear regression of all of the data, and the blue line represents a linear regression of data from sites where temperature > 3 °C. Data tables are given in Appendices 6 and 7.

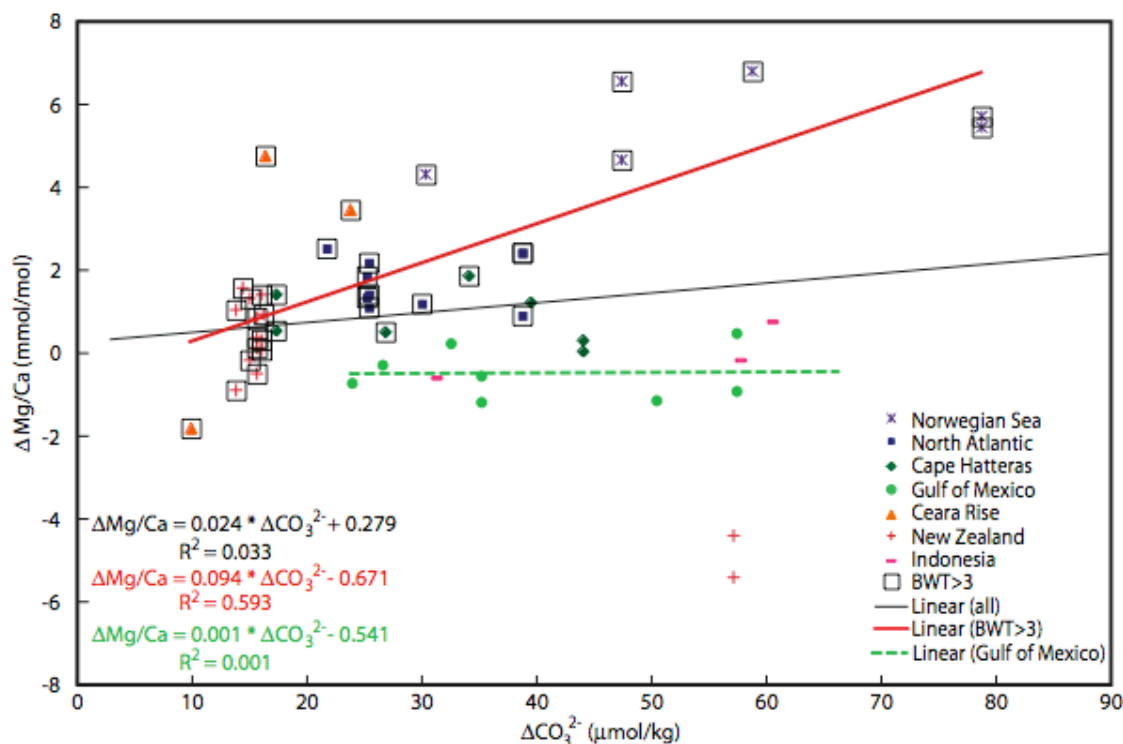


Figure 4.8: The deviation between measured Mg/Ca and temperature based upon expected Mg/Ca ($\Delta \text{Mg/Ca}$) from Equation 4 plotted versus $\Delta[\text{CO}_3^{2-}]$ for core top sites from the Norwegian Sea (purple), North Atlantic Ocean (blue), Cape Hatteras shelf (dark green), Gulf of Mexico (light green), Ceara Rise (orange), New Zealand shelf (red), and Sulawesi Margin, Indonesia (pink). The black line represents a linear regression of all of the data. Core top sites with $\text{BWT} \leq 3$ °C are identified by outer squares, and defined by the red linear regression.

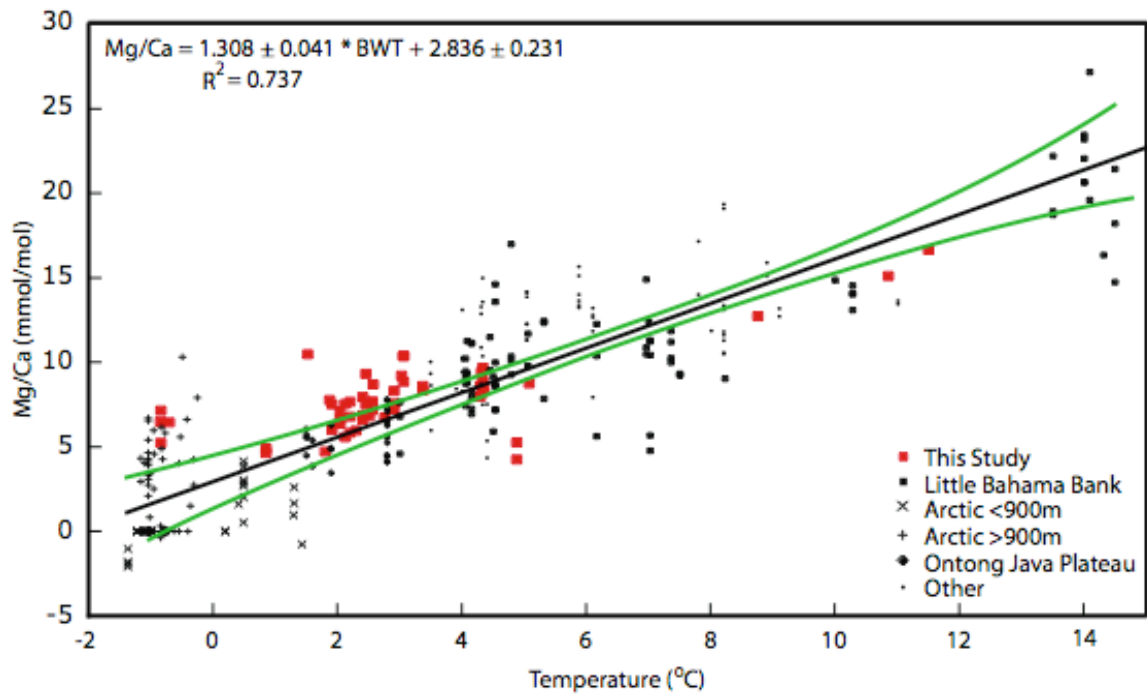


Figure 4.9: Mg/Ca data corrected for carbonate ion effects from this core top study (red squares) plotted against temperature. Data from Little Bahama Bank (Dwyer et al., 1995; black squares), Ontong-Java Plateau (Dwyer et al., 2002; black diamonds), Arctic Ocean < 900 m (Cronin et al., 1996; black x-s), and the Arctic Ocean > 900 m (Cronin et al., 1996; black crosses) have been corrected to account for differences in cleaning. The black line represents a linear regression of all data, and the green lines represent the 95% confidence intervals.

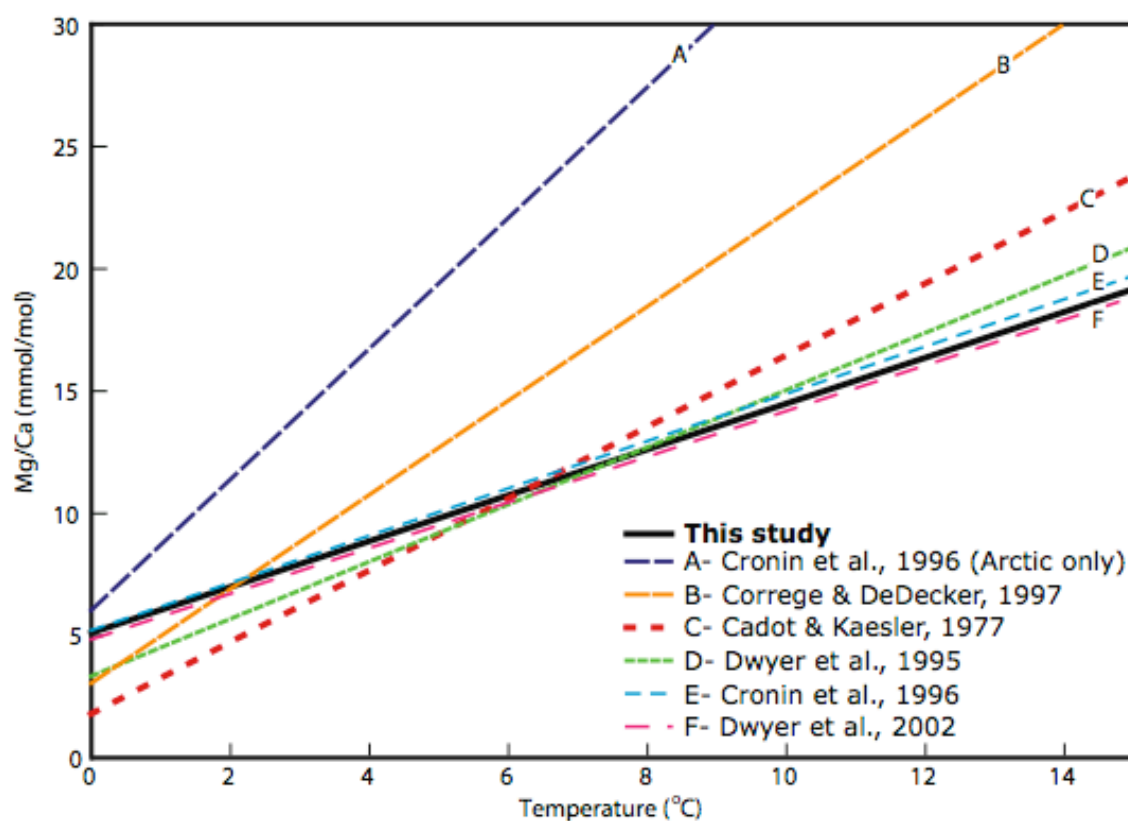


Figure 4.10: Comparison of published Mg/Ca-temperature calibrations (Table 4.1) with the calibration proposed by this study (Equation 4).

5.0 Dissertation Conclusions and Future Work

5.1 Summary of Results

In this dissertation, I used multiple paleoceanographic proxies in multiple locations of the world's oceans in an effort to better understand oceanic circulation on orbital and millennial time-scales. Much of this dissertation focused on the variability in Iceland-Scotland Overflow Water (ISOW), which is one of the largest components of Northern Component Water (NCW). I have utilized well-established geochemical (benthic foraminiferal $\delta^{13}\text{C}$ and $\delta^{18}\text{O}$, and planktonic foraminiferal $\delta^{18}\text{O}$) and sedimentological proxies (Ice Rafted Detritus/ gram, % Carbonate, % Coarse Fraction) to examine orbital- and millennial-scale ISOW variability since ~ 200 ka. I have also examined the potential of using the benthic ostracod *Krithe* as a paleotemperature proxy. The sediment cores analyzed in this study come from southern Gardar Drift (11JPC and 3GGC) as well as from a globally distributed collection of core tops (Norwegian Sea, North Atlantic, Cape Hatteras shelf, Ceara Rise, Gulf of Mexico, Sulawesi Sea, Indonesia, and the New Zealand shelf); numerous published results of sediment cores were also incorporated for comparison to the data generated herein.

Understanding the nature of abrupt climate change, including tempo and cause(s), is not only important for the past 150 kyr, when millennial-scale changes were prevalent, but is also crucial for determining how climate may respond to future increases in greenhouse gases. The Younger Dryas (~ 12.9 to 11.5 ka) was a return to cold temperatures that interrupted the climate warming associated with the most recent deglaciation. While previously published studies have suggested decreased NCW

formation during the entire Younger Dryas (e.g., Broecker et al., 1989), the benthic foraminiferal $\delta^{13}\text{C}$ record from 11JPC suggests an increase in southern sourced waters in the northern North Atlantic during the early and late Younger Dryas, but not during the mid Younger Dryas. Lower $\delta^{13}\text{C}$ values coincide with proxy evidence for increased meltwater delivery and ice rafting during the early and late Younger Dryas, suggesting that early and late Younger Dryas meltwater events led to a shoaling of NCW. My records support recent studies that identified deepwater variability within the Younger Dryas chron, and provide a mechanistic link between the oceans, cryosphere, and atmosphere during this period of abrupt climate change.

Another key area in paleoceanographic research is the interaction between individual water mass components that combine to form NCW. In the third chapter of this dissertation, benthic stable isotopic records from southern Gardar Drift sediment cores were compared with records from northern Gardar and Bjorn Drifts to examine the variability in ISOW density on orbital time-scales. An increase in the benthic foraminiferal $\delta^{13}\text{C}$ gradient (north- south) during glacial periods indicates that the axis of ISOW shoaled relative to the modern ISOW current. This orbital scale variability is similar to other studies, which show that Pleistocene variations were paced by insolation changes with the 40- and 100-kyr cyclicity. The study demonstrates that the Gardar $\delta^{13}\text{C}$ transect records significant changes related to the precessional forcing. The precessional variability in ISOW is strongest in MIC 6, but is also prevalent during MIC3 and 4. While the precessional-scale climate signal is strong in MIC 5a to 5e, the ISOW variations are small within this period. This reflects either that: the overall vigor of ISOW was strong throughout MIC 5, such that the mixing zone between ISOW and SCW

remained south of Gardar; or that smaller ice sheets during MIC 5 did not have a significant impact on the production of ISOW in the Norwegian Sea. Superimposed on the orbital scale variability in ISOW were higher frequency changes that are most pronounced in MIC 3 and 4. These changes are associated with the Heinrich and Dansgaard-Oeschger climate cycles.

In the fourth chapter of this dissertation, I reexamined the potential for *Krithe* Mg/Ca ratios as a paleoceanographic proxy. This study involved a revised core top calibration for the incorporation of magnesium into the calcitic carapaces of benthic ostracods within the genus, *Krithe*. Mg/Ca ratios were determined for core tops from the Norwegian Sea, Cape Hatteras shelf, Gulf of Mexico, Sulawesi margin (Indonesia), New Zealand Shelf, and North Atlantic Ocean, and a compilation drawn from previous studies (e.g., Dwyer et al., 2002). Results from this study show that temperature is the primary control on Mg/Ca ratios, with carbonate ion concentration as a secondary control at low calcification temperatures (below 3 °C). The identification of a ‘Carbonate Ion Effect’ on the magnesium incorporation in ostracodal calcite below 3 °C is identical to the threshold identified for benthic foraminifera (Elderfield et al., 2006), suggesting a common calcification mechanism. This reevaluation of *Krithe* Mg/Ca ratios provides an additional paleotemperature proxy in locations where benthic foraminifera are not abundant.

5.2 Future Work

This research focuses on variability of ISOW on orbital and millennial time-scales. The influence of eccentricity, obliquity and particularly precession in driving ISOW variability may be related to the production and distribution of meltwater, which is controlled by the overall cryospheric state (i.e., large vs. small ice sheets). The

millennial-scale changes in ISOW are shown to be similarly forced by freshwater but respond to stochastic outbursts of meltwater and/or icebergs into the Norwegian Sea. The ISOW variability during the Younger Dryas, and MIC 3 are good examples of this higher-frequency variability. However, in addition to during the Younger Dryas, excess meltwater has also been recorded at ~ 14.2 ka (Meltwater Pulse 1a; Fairbanks, 1999), ~ 11.4 ka (Meltwater Pulse 1b; Fairbanks, 1999), and ~ 8.4 ka (Kleiven et al., 2008) suggesting that location of the meltwater input, rather than the quantity of meltwater, is the determining factor in the ability of meltwater to affect ISOW vigor. In addition to the importance of the location of meltwater, meltwater may be restricted to only perturbing ISOW during intermediate or cold climate states. In order to test this hypothesis, a more detailed examination of some of these events should determine if ISOW has a similar response to all Heinrich Events and the 8.2 ka Event; the current age model does not allow for this level of analysis. Interestingly, another proposed period of meltwater, the transition from MIC 6 to 5e (Seidenkrantz et al., 1996) may also be characterized by a reduction in ISOW strength according to benthic foraminiferal $\delta^{13}\text{C}$ gradients; this may be a relic of age model differences or ISOW changes, and thus should be studied further.

Another avenue of further research is the link between ISOW strength and overall NCW strength, as it has been proposed that ISOW drives NCW variability (e.g., Kuijpers et al., 2004) since ISOW is a large contributor to NCW (Worthington, 1976). Thus the strong precessional control on ISOW strength is especially interesting considering that precession is not considered to exert a strong control on NCW production strength (Hays et al., 1976; Raymo et al., 2004; Lisiecki et al., 2008). One possible explanation for this is that many NCW strength records do not have the temporal resolution to decipher

precession-scale variability or that the sites that monitored the NCW variability were not positioned to record the smaller NCW variations. Another possible explanation is that other NCW contributors compensate for decreased ISOW production during some precession minima. Orbital-scale variability has been noted in records of Denmark Straits Overflow Water (e.g., Fagel et al., 2004) and Labrador Sea Water (Hillaire-Marcel et al., 2004). Variations in the components of NCW should be systematically examined using sites in the western North Atlantic that are downstream of ISOW and Denmark Straits Overflow Water (e.g., Eirik Drift). Neodymium isotopes, a new paleoceanographic proxy, have the capability to examine changes in the relative components to NCW. For instance, ISOW, which originates near the Iceland mantle plume, has a radiogenic neodymium isotopic signature, whereas Labrador Sea Water, which is sourced near the old North American craton, has a highly unradiogenic neodymium isotopic signature; Antarctic Bottom Water and Denmark Straits Overflow Water neodymium isotopic values are also distinct (Lacan and Jeandell, 2004). Thus, by measuring neodymium isotopes in a location downstream of the mixing of these components, the relative abundance of these components can be determined.

The spatial extent of the hiatus observed in 11JPC, which was only discovered because of AMS ^{14}C dates, is also an outstanding issue. Prior to AMS ^{14}C dating, all proxy records in 11JPC were interpreted to contain Last Glacial Maximum sediments due to the similarities in each of these records to proximal cores. However, many of these proximal cores (e.g., ODP 983, ODP 984) do not have ^{14}C AMS dates, and therefore, it is important to determine whether or not they, in fact, contain pure Last Glacial Maximum sediments, or if the unconformity in 11JPC is a larger, regional feature.

Another outstanding question this research leaves unsolved involves the separation of ISOW strength and density. The transect of cores from Bjorn and Gardar Drifts allows for the observation of whether ISOW was deeply flowing or shoaled at periods in the past; however, the flux of ISOW remains unclear. Grain size of sortable silt has been used as a proxy for ISOW flow strength for the Holocene on Gardar Drift (Bianchi and McCave, 1999). An alternate technique for determining bottom water flow velocity of ISOW may be possible by employing the dynamics of migrating, asymmetrical mudwaves (Flood and Giosan, 2004), which characterize southern Gardar Drift (Manley et al., 2004). A sister core to 11JPC, 9JPC was collected from the opposite side of the same mudwave. Following a thorough determination of an age model for 9JPC, a comparison of the relative sedimentation rates of 11JPC vs. 9JPC may reveal further information about the history of deep water circulation strength on southern Gardar Drift.

5.3 References

- Bianchi G.G., and N. McCave, 1999. Holocene periodicity in North Atlantic climate and deep-ocean flow south of Iceland. *Nature*. 397, 515-517.
- Broecker, W.S., Kennett, J.P., Flower, B.P., Teller, J.T., Trumbore, S., Bonani, G., and W. Wolfi. 1989. Routing of meltwater from the Laurentide Ice Sheet during the Younger Dryas cold episode. *Nature*. 341; 318-321.
- Dwyer, G.S., Cronin, T.M., and P.A. Baker. 2002. Trace elements in marine ostracods. *Geophysical monograph*. 131; 205-225.
- Elderfield, H., Yu, J., Anand, P., Kiefer, T., and B. Nyland. 2006. Calibrations for benthic foraminiferal Mg/Ca paleothermometry and the carbonate ion hypothesis. *Earth and Planetary Science Letters*. 250; 633-649.
- Fagel, N., Innocent, C., Gariépy, C. and C. Hillaire-Marcel. 2002. Sources of Labrador Sea sediments since the last glacial maximum inferred from Nd-Pb isotopes. *Geochimica et Cosmochimica Acta*. 66 (14); 2569-2581.

- Fairbanks, R.G. 1989. A 17,000-year glacio-eustatic sea level record: influence of glacial melting rates on the Younger Dryas event and deep-ocean circulation. *Nature*. 342; 637-642.
- Flood, R.D. and L. Giosan, 2002. Migration history of a fine-grained abyssal sediment wave on Bahama Outer Ridge. *Marine Geology*. 192, 259-273.
- Hemming, S.R., Broecker, W.S., Sharp, W.D., Bond, G.C., Gwiazda, R.H., McManus, J.F., Klas, M., and I. Hajdas. 1998. Provenance of Heinrich layers in core V28-82, northeastern Atlantic: $^{40}\text{Ar}/^{39}\text{Ar}$ ages of ice-rafted hornblende, Pb isotopes in feldspar grains and Nd-Sr-Pb isotopes in the fine sediment fraction. *Earth and Planetary Science Letters*. 164; 317-333.
- Hillaire-Marcel, C., de Vernal, A., Bilodeau, G., and A.J. Weaver. 2001. Absence of deep-water formation in the Labrador Sea During the last interglacial period. *Nature*. 410; 1073-1078.
- Kleiven, H.F., Kissel, C., Laj, C., Ninnemann, U.S., Richter, T.O., and E. Cortijo. 2008. Reduced North Atlantic Deepwater Coeval with the Glacial Lake Agassiz Fresh Water Outburst. *Science*. 319; 60-65.
- Lacan F. and C. Jeandel. 2004. Neodymium isotopic composition and rare earth element concentrations in the deep and intermediate Nordic Seas: Constraints on the Iceland Scotland Overflow Signature. *Geochemistry Geophysics Geosystems*. 5(11); 1- 10.
- Lisiecki, L.E., Raymo, M.E., W.B. Curry. 2008. Atlantic overturning responses to Late Pleistocene climate forcings. *Nature*. 456 (6); 85-88.
- Manley, P.L., Manley, T.O., Kelly, L.C., Wright, J.D., and G.S. Mountain. 2004. Mudwaves on the South Gardar Drift: North Atlantic. *Eos Trans. AGU 85(17)*, Jt. Assem. Supp., Abstract GC21A-05.
- Raymo, M.E., Oppo, D.W., Flower, B.P., Flower, Hodell, D.A., McManus, J.F., Venz, K.A., Kleiven, K.F., and K. McIntyre. 2004. Stability of North Atlantic Water Masses in Face of Pronounced Climate Variability During the Pleistocene. *Paleoceanography*. 19; 1-13.
- Seidenkrantz, M.-S., Bornmalm, L., Johnsen, S.J., Knudsen, K.L., Kuijpers, A., Lauritzen, S.-E., Leroy, S.A.G., Mergeal, I., Schweger, C., and B. Van Vliet-Lanoe. 1996. Two-step deglaciation at the oxygen isotope stage 6/5e transition: the Zeifen-Kattegat Climate Oscillation. *Quaternary Science Reviews*. 55; 63-75.
- Worthington, L.V., 1976. On the North Atlantic Circulation. Johns Hopkins University Press; Baltimore, MD.

6.0 Appendices

Appendix 1: Stable isotope, planktonic foraminiferal assemblage, and lithics/gram data from core KN166-14 11JPC (0 to 222 cm). $\Delta\delta^{18}\text{O}$ is the difference between the $\delta^{18}\text{O}$ value of *N. pachyderma* (s) and the $\delta^{18}\text{O}$ value of *G. bulloides*. Stable isotope values are reported as ‰ with respect to V-PDB.

Depth (cm)	Age (ka)	$\delta^{13}\text{C}$ <i>G. bulloides</i>	$\delta^{18}\text{O}$ <i>G. bulloides</i>	$\delta^{13}\text{C}$ <i>N. pachyderma</i> (s)	$\delta^{18}\text{O}$ <i>N. pachyderma</i> (s)	$\delta^{13}\text{C}$ <i>P. wuellerstorfi</i>	$\delta^{18}\text{O}$ <i>P. wuellerstorfi</i>	$\Delta\delta^{18}\text{O}$	% <i>N. pachyderma</i> (s)	% <i>N. pachyderma</i> (d)	% <i>G. bulloides</i>	Lithics/gram
0	0.67	-0.21	1.96	0.58	1.59							
1	0.71								2.1	7.1	62.7	15.78
2	0.76	-0.11	1.74	0.84	1.75	0.50	2.90	0.01				
3	0.80											
4	0.85											
5	0.90	-0.09	1.78	0.50	1.50	0.65	2.93	-0.29	0.9	12.9	62.1	18.48
6	0.94											
7	0.99	0.00	1.77	0.88	1.71			-0.06				
8	1.04					0.56	2.93					
9	1.08					0.78	2.92					
10	1.13	-0.03	1.60	0.70	1.68		2.88	0.08	0.0	21.1	54.4	0.00
11	1.18					0.47	2.92					
12	1.22	-0.22	1.43	0.80	1.65			0.22				
13	1.27											
14	1.32											
15	1.36	0.14	1.74	0.74	1.76			0.02	0.0	22.2	61.4	8.45
16	1.41					0.50	2.85					
17	1.46	-0.19	1.54	0.37	1.66			0.12				
18	1.51					0.74	2.84					
19	1.55											
20	1.60	-0.16	1.66	0.85	1.71			0.05	1.5	26.1	42.6	32.82
21	1.65											
22	1.70	-0.15	1.37	0.65	1.56	0.96	2.85	0.19				
23	1.74					0.88	2.85					
24	1.79						2.85					
25	1.84	-0.06	1.47	0.65	1.56	0.92	2.85	0.09	0.6	22.1	58.4	5.81
26	1.89											
27	1.94	-0.08	1.54	0.60	1.55	0.78	2.95					

77	4.53	-0.38	1.54	0.22	1.34			-0.20				
78	4.58											
79	4.64	-0.14	1.09	-0.23	1.37	0.71	2.84	0.28				
80	4.69								0.7	22.8	54.8	0.00
81	4.75					1.20	2.85					
82	4.81	-0.26	1.39	0.77	1.57			0.18				
83	4.86											
84	4.92											
85	4.97	-0.31	1.15	0.34	1.55	1.41	3.01	0.40	0.3	33.6	54.8	
86	5.03					1.22	2.87					
87	5.08	-0.18	1.49	0.62	1.46			-0.03				
88	5.13											
89	5.19											
90	5.24	-0.18	1.50	0.64	1.46	1.42	2.91	-0.04				
91	5.30								0.0	15.2	69.3	3.43
92	5.35	-0.25	1.43	0.57	1.56			0.13				
93	5.40					1.24	2.91					
94	5.46					0.97	2.81					
95	5.51	-0.40	1.19	0.49	1.58			0.39				
96	5.56											
97	5.62	-0.29	1.50	0.42	1.74	1.21	2.81	0.54	0.4	11.9	61.7	
98	5.67					1.27	3.05					
99	5.72					1.14	2.88					
100	5.77	-0.19	1.36	0.55	1.62			0.26				
101	5.82					0.85	2.69					
102	5.87	-0.45	1.56	0.91	1.86	1.35	2.99	0.30				
103	5.92					0.98	2.65		2.1	23.9	42.6	1.91
104	5.97					1.39	3.01					
105	6.01			0.33	1.51	1.21	2.95					
106	6.06											
107	6.11	-0.39	1.64	0.79	1.65	1.22	2.93	0.01				
108	6.15											
109	6.20					1.29	2.76					
110	6.25	-0.51	1.43	0.85	1.86			0.43	0.0	14.2	61.3	1.58
111	6.29					1.29	2.94					
112	6.34											
113	6.38											
114	6.43											
115	6.47	-0.39	1.36	0.67	1.55			0.19				
116	6.52											
117	6.56	-0.70	1.52	0.27	1.43			-0.09				
118	6.61					1.03	2.93		0.7	13.8	56.3	
119	6.65					0.82	2.91					
120	6.69	-0.51	1.41	0.89	1.55	1.38	2.95	0.14				
121	6.74					0.98	2.92					
122	6.78	-0.41	1.51	0.76	1.71	1.05	2.99	0.20	1.3	12.4	54.0	0.94
123	6.83					1.12	2.90					
124	6.87					1.32	3.00					
125	6.92	-0.42	1.56	0.74	1.67	1.18	2.91	0.10				

126	6.97					1.25	3.03		0.5	12.8	49.7	
127	7.02	-0.58	1.42	0.59	1.39	1.13	2.97	-0.03				
128	7.09	-0.53	1.62	0.45	1.54	1.39	3.06	-0.08				
129	7.15					1.04	2.85					
130	7.23	-0.58	1.28	0.39	1.68	1.27	3.16	0.40				
131	7.31					0.95	2.82					
132	7.41	-0.71	1.40	0.63	1.69	0.96	2.88	0.29	1.4	12.0	52.3	4.63
133	7.50											
134	7.59	-0.37	1.57	0.10	1.49	0.93	2.96	-0.08				
135	7.69	-0.43	1.48	0.55	1.55	1.04	2.94	0.07				
136	7.79								0.8	16.6	49.0	
137	7.89	-0.62	1.24	0.62	1.59			0.35				
138	7.99					0.97	2.63					
139	8.08	-0.33	1.66	0.19	1.90							
140	8.17	-0.58	1.43	0.54	1.43	0.75	2.69	0.00	0.0	8.7	61.9	
141	8.24					0.98	2.79					
142	8.31	-0.77	1.75	0.39	1.33	1.12	2.85	-0.56	1.7	11.7	49.0	2.28
143	8.36					0.80	2.67					
144	8.41	-0.30	1.44	0.26	1.38	0.83	2.86	-0.06	2.8	20.0	39.6	
145	8.46	-0.81	1.39	1.01	1.67	0.87	2.82	0.28	3.1	10.8	47.5	
146	8.50					1.02	2.95		5.3	14.0	45.7	
147	8.54	-0.83	1.29	0.08	1.61	0.78	2.88	0.32				
148	8.57					0.76	2.74		4.8	16.6	46.7	
149	8.61	-0.56	1.22	0.25	1.24	0.68	2.65	-0.13				
150	8.65	-0.59	1.48	0.33	1.69	0.70	2.69	0.20	2.2	14.4	51.4	
151	8.69					0.90	2.71					
152	8.74	-0.69	1.29	0.39	1.56	0.91	2.84	0.56				
153	8.79					0.77	2.84		1.3	16.9	56.3	9.84
154	8.86	-0.61	1.56	0.53	1.58	0.85	2.70	0.02				
155	8.93	-0.78	1.42	0.57	1.73	0.91	2.63	0.31				
156	9.02					1.01	2.79		1.3	15.9	41.2	
157	9.10	-0.69	1.46	0.31	1.56	0.90	2.76	0.10				
158	9.18	-0.58	1.45	0.59	1.66	0.74	2.64	0.20				
159	9.27					1.01	2.73		1.1	13.2	46.7	
160	9.35	-0.91	1.43	0.50	2.55	0.94	2.80	1.12				
161	9.44	-0.70	1.41	0.45	1.71	1.04	2.72	0.30				
162	9.53	-0.83	1.68	0.58	1.85			0.17	1.2	22.8	37.6	23.49
163	9.61					1.09	2.83					
164	9.70	-0.59	1.42	0.48	2.45	1.07	2.79	1.03				
165	9.79	-0.94	1.38	0.25	2.29	1.05	2.76	0.91	1.6	19.9	33.9	
166	9.87					0.96	2.74					
167	9.96	-0.95	1.57	0.36	2.56	1.08	2.85	0.99	1.3	15.5	44.4	
168	10.06					0.96	2.70					
169	10.15	-0.75	1.51	0.03	1.88	0.72	2.75	0.37				
170	10.24	-0.82	1.71	0.62	1.86	1.03	2.78	0.15				
171	10.34					1.10	2.96		2.7	15.9	44.3	46.88
172	10.43	-0.76	1.73	-0.09	2.08	0.93	2.74	0.35				
173	10.53	-0.76	1.47	0.51	2.71	0.93	2.77	1.24	1.8	26.9	33.8	58.93
174	10.63					1.19	3.15					

175	10.73	-0.77	1.60	0.32	2.16	0.94	2.86	0.56	4.1	29.1	37.7	61.89
176	10.83											
177	10.93	-0.68	1.90	0.43	2.32	0.94	2.94	0.42	5.8	19.1	40.7	125.29
178	11.03	-0.85	1.82			1.24	3.05					
179	11.12					0.77	3.11		8.4	22.8	32.6	206.75
180	11.22	-0.61	1.83	0.51	1.87	1.21	3.07	0.04				
181	11.31	-0.93	1.68	0.55	1.79	0.84	3.01	0.11	8.6	23.2	47.5	189.59
182	11.39	-0.56	1.89	0.68	1.97	0.95	3.02	0.08				
183	11.44	-0.74	1.74	0.47	2.29	0.80	2.76	0.55	15.3	11.5	39.7	373.75
184	11.48	-0.77	1.72	0.45	2.91	0.84	2.96	1.20				
185	11.52	-0.83	2.03	0.23	2.97	0.94	2.96	0.93	32.9	1.9	43.5	482.99
186	11.55	-0.78	2.01	0.50	2.51	0.57	3.14	0.50	26.4	3.1	40.7	
187	11.58	-0.72	2.15	0.28	3.58	0.72	2.96	1.51	33.6	1.6	30.2	503.07
188	11.61	-0.60	2.03	0.29	3.83	0.99	2.92	2.00	25.3	9.5	36.3	
189	11.64	-0.69	2.04	0.67	2.15	0.84	3.07	0.11	32.1	2.1	30.7	
190	11.67	-0.78	1.96	0.67	2.12	0.86	3.07	0.16	36.5	1.7	28.9	
191	11.70	-0.69	2.08	0.49	2.24	0.71	2.99	0.16	34.1	3.3	41.1	445.01
192	11.73	-0.91	1.94	0.31	2.91	0.87	2.98	0.97				
193	11.76	-0.92	1.81	0.12	2.31	0.58	3.00	0.50	38.5	5.7	30.9	
194	11.79	-0.84	1.99	0.41	3.17	0.52	2.93	1.18	45.9	6.1	22.6	438.26
195	11.82	-0.78	1.88	0.18	3.19	0.39	2.84	1.31	36.7	4.5	31.4	
196	11.85	-1.03	1.81	0.42	3.31	0.73	3.07	1.50	54.6	4.0	23.7	562.35
197	11.89	-0.91	2.07	0.44	2.95	0.70	2.95	0.88	38.0	3.8	30.7	
198	11.93	-0.70	1.97	0.09	3.87	0.62	3.13	1.89	54.2	3.6	29.1	549.81
199	11.98	-0.71	2.03	0.35	3.14	0.75	3.11	1.11	45.9	3.7	29.7	
200	12.04	-0.73	2.35	0.34	3.35	0.93	2.77	1.00	46.6	4.7	24.0	430.18
201	12.13	-0.91	2.09	0.24	3.57	0.98	2.92	1.48	48.0	3.5	21.7	
202	12.22	-0.87	2.48	0.28	3.60	1.02	3.20	1.12	43.3	2.2	27.2	444.62
205	12.54	-0.98	2.05	0.36	3.44	0.90	3.21	1.39	55.7	4.7	25.1	551.46
206	12.66	-0.80	2.14	0.03	4.03	1.15	3.18	1.88	46.9	4.4	22.7	
207	12.77	-0.69	2.60	0.20	3.65	0.69	3.49	1.05	55.3	6.2	21.1	
208	12.88	-0.88	2.18	0.36	3.73	0.69	3.39	1.55				450.91
209	12.98	-0.86	2.19	0.46	3.17	0.49	3.43	0.98	49.8	3.4	21.8	
210	13.07	-0.85	2.17	0.35	3.70	0.89	2.92	1.53				459.29
211	13.16	-0.89	2.16	0.35	3.43	0.31	3.30	1.27	59.0	5.0	16.3	
212	13.22	-0.77	2.52	0.37	3.38	0.95	3.24	0.86	52.2	3.7	23.3	554.49
213	13.27	-0.87	2.47	0.14	3.61	0.60	3.49	1.15	54.5	5.2	20.7	
214	13.32	-0.43	2.56	0.16	3.60	0.60	3.29	1.03				
215	13.37	-0.57	2.58	0.19	3.30	0.58	3.42	0.72	65.2	3.4	14.7	
216	13.41	-0.16	2.73	0.13	3.38	0.62	3.34	0.64				496.13
217	13.45	-0.73	2.77	0.30	3.94	0.65	3.52	1.17	52.4	5.5	20.9	
218	13.49	-0.81	2.24	0.23	3.54	1.07	3.36	1.30	46.9	5.4	30.7	424.52
219	13.53	-0.84	2.14	0.32	3.63	0.69	3.51	1.49				
220	13.56	-0.86	2.44	0.19	3.46	0.83	3.53	1.02	54.4	3.4	24.4	412.75
221	13.60					1.05	3.64					

Appendix 2: Compilation of Published Meltwater Events

A2.1 Methods

To compare timing of meltwater events, the age of each published event was converted to a calibrated calendar age using the Fairbanks 0805 calibration (Fairbanks et al., 2005) following the application of an appropriate reservoir correction, typically found within the reference (Table 2.A1.1). Due to uncertainties in individual age models, errors in measuring ^{14}C (~ 50 years during the Younger Dryas; Fairbanks et al., 2005), and the observed ^{14}C - age plateau during this period (Goslar et al., 1995), bins of 400 years were chosen for the histogram displayed in Figure 2.2.3. The histogram shows an increase in meltwater from all sources during the early Younger Dryas, from $\sim 13.2 - 12.4$ ka, and during the late Younger Dryas, from $\sim 11.6 - 11.2$ ka (Figure 2.2.3).

A2. Table 1 Published references of meltwater occurrences during the Younger Dryas.

Reported Age (ka)	Reported Res. Cor. (y)	Applied Res. Cor. (y)	Calibrated Calendar Years (ka)	Age (ka)	Observation	Reference
ARCTIC						
9.9 ¹⁴ C	0		11.31	11.31	Lake Agassiz overflow to Arctic	Rayburn & Teller, 2007
9.9 ¹⁴ C	0		11.31	11.31	Lake Agassiz flood through the Clearwater- Lower Athabasca Spillway	Smith & Fisher, 1993
9.9 ¹⁴ C	0		11.31	11.31	Lake Agassiz outflow to the northwest	Teller et al., 2002
9.93 ¹⁴ C	0		11.36	11.36	Glacial Meadow Lake drainage through Athabasca Spillway	Schreiner, 1983
9.94 ¹⁴ C	0		11.37	11.37	Lake Agassiz flood through the Clearwater- Lower Athabasca Spillway	Fisher et al., 2002
10 ¹⁴ C	800		11.48	11.48	Freshwater spike in Beaufort Sea	Andrews & Dunhill, 2004
10 ¹⁴ C	400		11.48	11.48	Whale bones show meltwater to the Canadian Arctic	Dyke et al., 1996
10 ¹⁴ C		400	11.48	11.48	Lake Agassiz outburst to the Arctic	Licciardi et al., 1999
10.1 ¹⁴ C	0		11.69	11.69	Agassiz outflow to the northwest	Teller et al., 2002
10.5 ¹⁴ C	400		12.43	12.43	Distal glacio-marine environment in the Barents Sea with some Atlantic inflow	Polyak & Mikhailov, 1996
12.5 cal	500			12.5	Foraminiferal stable isotopes and assemblages evidence for fresh water pulse	Ebbesen & Hald, 2004
10.9 ¹⁴ C	0		12.79	12.79	Opening of northern outlets of Lake Agassiz, draining the Southern Basin	Brophy and Bluemle, 1983
10.9 ¹⁴ C	0		12.79	12.79	Arctic routing of Lake Agassiz because lake level dropped but no eastward exit	Teller et al., 2005
11 ¹⁴ C		0	12.88	12.88	Lake Agassiz watershed routed to the Mackenzie River Basin	Christiansen, 1979
11 ¹⁴ C		400	12.88	12.88	Glacier disintegration in the Arctic	Hodgson & Vincent, 1984
11 ¹⁴ C		0	12.88	12.88	Lake Agassiz watershed routed to the Mackenzie River Basin	Klassen, 1989
Eastern North America						
11.3 cal				11.30	Glacial Lake Algonquin overflows to Glacial Lake Vermont, which overflows to the east	Cronin et al., 2008
9.9 ¹⁴ C		0	11.31	11.31	Spillover of the entire Lake	Smith, 1989

					Agassiz	
10 ^{14}C		400	11.48	11.48	Isotopic and faunal evidence for freshening on Labrador shelf and Hudson Strait	Andrews et al., 1987
10 ^{14}C	0		11.48	11.48	Lake Agassiz outburst through St. Lawrence	Licciardi et al., 1999
11.9 cal				11.90	Mg and Sr evidence for increased St. Lawrence overflow	Carlson et al., 2007
12.4 cal				12.40	Increase in detrital carbonate in Baffin Bay derived from distal icebergs or meltwater	Andrews et al., 1996
10.5 ^{14}C	440		12.43	12.43	Lake Agassiz outflow to the east	Lewis et al., 1994
10.9 ^{14}C	0		12.79	12.79	Lake Agassiz outflow to the east	Leverington et al., 2000
10.9 ^{14}C	0		12.79	12.79	Lake Agassiz outflow to the east	Teller et al., 2002
10.9 ^{14}C		400	12.79	12.79	Drainage of Lake Agassiz to the east through Lake Superior	Teller et al., 1996
12.81 cal				12.81	Earliest fall in Lake Algonquin	Moore et al., 2000
12.83 cal				12.83	Lake Agassiz flowed east	Fisher, 2003
11 ^{14}C	400		12.88	12.88	Abrupt increase in detrital carbonate	Andrews et al., 1995b
11 ^{14}C	450		12.88	12.88	Iceberg armadas in the western North Atlantic	Andrews et al., 1995a
11 ^{14}C	400		12.88	12.88	Terrestrial grains on Orphan Knoll indicate increased iceberg flux from St. Lawrence	Bond & Lotti, 1995
11 ^{14}C	400		12.88	12.88	Terrestrial grains on Rockall Drift indicate increased iceberg flux	Bond et al., 1993
11 ^{14}C	440		12.88	12.88	Eastward flow following termination in Mississippi River drainage	Broecker et al., 1988
11 ^{14}C	0		12.88	12.88	Lake Agassiz drains eastward through the Nipigon basin to Lake Superior	Clayton, 1983
11 ^{14}C	0		12.88	12.88	Lake Agassiz discharge diverted to Superior Basin, then through an eastern outlet	Drexel et al., 1983
11 ^{14}C		0	12.88	12.88	Lake Agassiz eastern outlet to Great Lakes opened	Fenton et al., 1983
11 ^{14}C	0		12.88	12.88	Lake Agassiz flow through the Superior Basin	Lewis & Anderson, 1992
11 ^{14}C	440		12.88	12.88	Lake Agassiz flow to the east	Lewis et al., 1994
11 ^{14}C	0		12.88	12.88	Lake Agassiz outburst through St. Lawrence	Licciardi et al., 1999
11 ^{14}C		0	12.88	12.88	Lake Agassiz eastern outlet to Great Lakes opened	Thorleifson, 1996
11 ^{14}C		400	12.88	12.88	Rapid draw down of Lake Agassiz in the Thunder Bay region	Warman, 1991
12.9 cal				12.90	Mg and Sr evidence for	Carlson et al.,

					increased St. Lawrence overflow	2007	
12.91	cal			12.91	Lake Agassiz draw down	Moore et al., 2000	
12.95	cal			12.95	Glacial Lake Vermont drainage	Cronin et al., 2008	
Europe							
10	^{14}C	440		11.48	11.48	Benthic foraminiferal oxygen isotopes show freshening near Baltic Ice Lake	Boden et al., 1997
10	^{14}C	440		11.48	11.48	Iceberg calving through deep troughs bordering the Barents Sea	Forman et al., 1996.
10	^{14}C	440		11.48	11.48	Freshwater in the Barents Sea	Lubinski et al., 2001
10.3	^{14}C		0	12.09	12.09	Terrestrial macrofossils show drainage of Baltic Ice Lake	Wohlfarth, 1993
10.9	^{14}C	440		12.79	12.79	Benthic foraminiferal oxygen isotopes show freshening near Baltic Ice Lake	Boden et al., 1997
10.9	^{14}C	400		12.79	12.79	Baltic Ice Lake drainage	Jiang & Nordberg, 1996
11	^{14}C	0		12.88	12.88	Freshwater peak from melting of the Scandinavian Ice Sheet	Bjorck et al., 1996
11.5	^{14}C	440		13.36	13.36	Freshwater in the Barents Sea	Lubinski et al., 2001

A2.2 References

- Andrews, J.T. and G. Dunhill. 2004. Early to mid-Holocene Atlantic water influx and deglacial meltwater events, Beaufort Sea slope, Arctic Ocean. *Quaternary Science Reviews*. 61;14-21.
- Andrews, J.T., Jennings, A.E, Kerwin, M., Kirby, M., Manley, W., and G.H. Miller. 1995. A Heinrich-like event, H-0 (DC-0): Source(s) for detrital carbonate in the North Atlantic during the Younger Dryas chronozone. *Paleoceanography*. 10 (5); 943-952.
- Andrews, J.T., Maclean, B., Kerwin, M., Manley, W., Jennings, A.E., and F. Hall. 1995. Final Stages in the Collapse of the Laurentide ice sheet, Hudson Strait, Canada, NWT: 14C AMS Dates, Seismic Stratigraphy, and Magnetic Susceptibility logs. *Paleoceanography*. 10 (5); 943-952.
- Andrews, J.T., Matthews, R.K., Osterman, L.E., Miller, G.H., Hillaire-Marcel, C., and K.M. Williams. 1987. Deglaciation and meltwater events in Hudson Strait and the Eastern Canadian arctic. *Geo Marine Letters*. 7; 23-30.
- Andrews, J.T., Osterman, L.E., Jennings, A.E., Syvitski, J.P.M., Miller, G.H., & N. Weiner. 1996. Abrupt changes in marine conditions, Sunshine Fiord, eastern Baffin Island, NWT (ca.66 N) during the last deglacial transition: Younger Dryas and H-0 events. In Late Quaternary Paleooceanography of the North Atlantic Margins (Andrews, J.T., Austin, W.E.N., Bergsten, H. & A.E. Jennings, eds.) *Geological Society of London Special Publication No. 111*; 11-27.
- Bjorck, S., Kromer, B., Johnsen, S., Bennike, O., Hammarlund, D., Lemdahl, G., Possnert, G., Rasmussen, T.L., Wohlfarth, B., Hammer, C.U., and M. Spurk. 1996. Synchronized Terrestrial-Atmospheric Deglacial Records Around the North Atlantic. *Science*. 274; 1155-1160.
- Boden, P., Fairbanks, R.G., Wright, J.D., and L.H. Burkle. 1997. High-resolution stable isotope records from southwest Sweden: The drainage of the Baltic Ice Lake and Younger Dryas ice margin oscillations. *Paleoceanography*. 12(1); 39-49.
- Bond, G. and R. Lotti. 1995. Iceberg discharges into the North Atlantic on millennial time scales during the last deglaciation. *Science*. 267; 1005-1010.
- Bond, G., Broecker, W., Johnsen, S., McManus, J., Labeyrie, L., Jouzel, J., and G. Bonani. 1993. Correlations between climate records from North Atlantic sediments and Greenland ice. *Nature*. 365; 143-147.
- Broecker, W.S., Andree, M., Wolfli, W., Oeschger, H., Bonani, G, Kennett, J., and D. Peteet. 1988. The Chronology of the Last Deglaciation: Implications to the Case of the Younger Dryas Event. *Paleoceanography*. 3(1); 1-19.

- Brophy, J.A. and J.P. Bluemle. 1983. The Sheyenne River: Its Geological History and Effects on Lake Agassiz. In Glacial Lake Agassiz (J.T. Teller and L. Clayton, eds) *Geological Association of Canada Special Publication* 26; 173-186.
- Carlson, A.E., Clark, P.U., Haley, B.A., Klinkhammer, G.P., Simmons, K., Brook, E.J., and K.J. Meissner. 2007. Geochemical proxies of North American freshwater routing during the Younger Dryas cold event. *Proceedings of the National Academy of Sciences*. 104(16); 6556-6561.
- Christiansen, E.A.. 1979, The Wisconsinian deglaciation of southern Saskatchewan and adjacent areas. *Canadian Journal of Earth Sciences*. 16; 913-938.
- Clayton, L.. 1983. Chronology of Lake Agassiz Drainage to Lake Superior. In Glacial Lake Agassiz (J.T. Teller and L. Clayton, eds) *Geological Association of Canada Special Publication* 26; 291-307.
- Cronin, T.M., Manley, P.L., Brachfeld, S., Manley, T.O., Willard, D.A., Guilbault, J.-P., Rayburn, J.A., Thunell, R.C., and M. Berke. 2008. *Palaeogeography, Palaeoclimatology, Palaeoecology*. 262; 46-60.
- Drexel, C.W., Ferrand, W.R., and J.D. Hughes. 1983. In Glacial Lake Agassiz (J.T. Teller and L. Clayton, Eds) *Geological Association of Canada Special Publication* 26; 291-307.
- Dyke, A.S., Hooper, J., and J.M. Savelle. 1996. A History of Sea Ice in the Canadian Arctic Archipelago Based on Postglacial Remains of the Bowhead Whale (*Balaena mysticetus*). *Arctic*. 49(3); 235-255.
- Ebbesen, H. and M. Hald. 2004. Unstable Younger Dryas Climate in the Northeast North Atlantic. *Geology*. 32 (8); 673-676.
- Fenton, M.M., Moran, S.R., Teller, J.T., and L. Clayton. 1983. Quaternary stratigraphy and history in the southern part of the Lake Agassiz basin. In "Glacial Lake Agassiz" (J.T. Teller and L. Clayton, Eds) *Geological Association of Canada Special Paper* 26; 49-74.
- Fisher, T.G.. 2003. Chronology of glacial Lake Agassiz meltwater routed to the Gulf of Mexico. *Quaternary Research*. 59; 271-276.
- Fisher, T.G., Smith, D.G., and J.T. Andrews. 2002. Preboreal oscillation caused by a glacial Lake Agassiz Flood. *Quaternary Science Reviews*. 21; 873-878.
- Forman, S.L., Lubinski, D., Miller, G.H., Matishov, G.G., Korsun, S., Snyder, J., Herlihy, F., Weihe, R., and V. Myslivets. 1996. Postglacial Emergence of western Franz

- Josef Land, Russia, and retreat of the Barents Sea Ice Sheet. *Quaternary Science Reviews*. 15; 77-90.
- Hodgson, D.A. and J.-S. Vincent. 1984. A 10,000 yr. BP extensive ice shelf over Viscount Melville Sound, Arctic Canada. *Quaternary Research*. 22; 18-30.
- Jiang, H. and K. Nordberg. 1996. Late Weichselian environmental changes of the southern Kattegat, Scandinavia, inferred from diatom records. in Late Quaternary Paleooceanography of the North Atlantic Margins (Andrews, J.T., Austin, W.E.N., Bergsten, H. & A.E. Jennings, eds.) *Geological Society Special Publication No. 111*; 245-260.
- Klassen, R.W.. 1989. Quaternary geology of the southern Canadian Interior Plains. in The geology of North America Vol. K-1, Quaternary Geology of Canada and Greenland, ed. R.J. Fulton. Geological Society of America, Boulder, Colorado. p 138-173.
- Leverington, D.W., Mann, J.D., and J.T. Teller. 2000. Changes in the Bathymetry and Volume of Glacial Lake Agassiz Between 11,000 and 9,300 ^{14}C yr BP. *Quaternary Research*. 54; 174-181
- Lewis, C.F.M. and T.W. Anderson. 1992. Stable isotope (O and C) and pollen trends in eastern Lake Erie, evidence for a locally induced climatic reversal of Younger Dryas age in the Great Lakes Basin. *Climate Dynamics*. 6; 241-250.
- Lewis, C.F.M., Moore Jr., T.C. Rea, D.K., Dettman, D.L., Smith, A.J., and L.A. Mayer. 1994. Lakes of the Huron basin: their record of runoff from the Laurentide Ice Sheet. *Quaternary Science Reviews* 13; 891-922.
- Licciardi, J.M, Teller, J.T., and P.U. Clark. 1999. Freshwater routing by the Laurentide Ice Sheet During the Last Deglaciation. in: Mechanisms of Global Climate Change at Millennial Time Scales Geophysical Monograph 112; 177-201.
- Lubinski, D.J., Polyak, L, and S.L., Forman. 2001. Freshwater and Atlantic water inflows to the deep northern Barents and Kara seas since ca 13 ^{14}C ka: foraminifera and stable isotopes. *Quaternary Science Reviews*. 20; 1851-1879.
- Moore, T.C., Jr., Walker, J.C.G., Rea, D.K., Lewis, C.F.M., Shane, L.C.K., and A.J. Smith. 2000. Younger Dryas Interval and Outflow from the Laurentide Ice Sheet. *Paleoceanography*. 15(1); 4-18.
- Polyak, L. and V. Mikhailov. 1996. Post-glacial environments o the southeastern Barents Sea: foraminiferal evidence. In Late Quaternary Paleooceanography of the North Atlantic Margins (Andrews, J.T., Austin, W.E.N., Bergsten, H. & A.E. Jennings, eds.) *Geological Society Special Publication No. 111*; 323-337.

- Rayburn, J.A. and J.T. Teller. 2007. Isostatic rebound in the northwestern part of the Lake Agassiz basin: Isobase changes and overflow. *Palaeogeography, Palaeoclimatology, Palaeoecology*. 247; 23-30.
- Schreiner, B.T.. 1983. Lake Agassiz in Saskatchewan. In Glacial Lake Agassiz (J.T. Teller and L. Clayton, Eds) *Geological Association of Canada Special Publication* 26; 75-96.
- Smith, D.G. and T.G. Fisher. 1993. Glacial Lake Agassiz: The northwestern outlet and paleoflood. *Geology*. 21; 9-12.
- Smith, D.G.. 1989. Catastrophic paleoflood from glacial Lake Agassiz 9900 years ago in the Ft. McMurray region, NE Alberta. *Canadian Quaternary Association Program Abstract*. 47.
- Teller, J.T., Boyd, M., Yang, Z., Kor, P.S.G., and A.M. Fard. 2005. Alternative routing of Lake Agassiz overflow during the Younger Dryas: new dates, paleotopography, and a re-evaluation. *Quaternary Science Reviews*. 24; 1890-1905.
- Teller, J.T., Leverington, D.W., and J.D. Mann. 2002. Freshwater outbursts to the oceans from glacial Lake Agassiz and their role in climate change during the last deglaciation. *Quaternary Science Research*. 21; 879-887.
- Teller, J.T., Thorleifson, L.H., Matile, G., and W.C. Brisbin. 1996. Sedimentology, Geomorphology and History of the Central Lake Agassiz Basin (Field Trip B2). Publication of the Geological Association of Canada/Mineralogical Association of Canada Joint Annual Meeting, Winnipeg, Manitoba, 27-29 May, 1996.
- Thorleifson, L.H.. 1996. Review of Lake Agassiz History. In "Sedimentology, Geomorphology, and History of the Central Lake Agassiz Basin" (J.T. Teller, L.H. Throleifson, G. Matile, and W.C. Brisbin, Eds.) pp. 55-84. Geological Association of Canada Field Trip Guidebook for GA/MAC Joint Annual Meeting.
- Warman, T.A.. 1991. Sedimentology and history of deglaciation in the Dryden, Ontario area, and their bearing on the history of Lake Agassiz. M.Sc. Thesis, University of Manitoba, Winnipeg, 248 pp.
- Wohlfarth, B., Bjorck, S., Possnert, G., Lemdhal, G., Brunnberg, L., Ising, J., Olsson, S., and N.-O. Svensson. 1993. AMS dating Swedish varved clays of the last glacial/interglacial transition and the potential/difficulties of calibrating Late Weichselian "absolute" chronologies, *Boreas*. 22; 113-128.

Appendix 3: Stable isotope, percent carbonate (% CaCO₃), and percent coarse fraction data for core KN166-14 11JPC. Methodologies for stable isotopes, percent coarse fraction, and % CaCO₃ are given in sections 2.3.1 and 3.3.2. Stable isotope values are reported as ‰ with respect to V-PDB.

Depth (cm)	Age (ka)	% CaCO ₃	% Coarse Fraction	$\delta^{13}\text{C}$ <i>G.bulloides</i>	$\delta^{18}\text{O}$ <i>G.bulloides</i>	$\delta^{13}\text{C}$ <i>P.wuellerstorfi</i>	$\delta^{13}\text{C}$ <i>P.wuellerstorfi</i>
3	0.81						
5	0.91	69.17	4.10	0.35	1.59		
5	0.91					0.52	2.80
5	0.91					0.65	2.93
9	1.10					0.78	2.92
10	1.14	71.54	6.72	0.12	2.63		
11	1.19					0.47	2.92
15	1.38	67.96	2.37	0.32	1.80	1.36	2.95
20	1.63	71.84	4.44	0.10	1.53	1.35	2.95
23	1.77						
25	1.87	68.51	4.83	-0.06	1.47		
27	1.97					1.03	2.95
29	2.07					1.04	2.91
30	2.12	68.87	4.93	0.16	1.66		
31	2.17					0.80	2.90
33	2.27					0.62	2.88
35	2.36	71.90	7.07	-0.16	1.58		
35	2.36					0.99	2.84
37	2.46					0.87	2.87
39	2.56					0.49	2.96
40	2.61	71.00	6.72	-0.10	1.51		
40	2.61					1.19	2.77
41	2.67					1.22	3.00
43	2.77					1.25	2.90
45	2.87	68.36	9.75	-0.29	1.77		
45	2.87					1.23	2.84
47	2.97					1.21	2.84
49	3.07						
50	3.12	69.71	6.76	0.04	1.26		
51	3.17					1.05	2.83
53	3.28						
55	3.38	68.18	9.76	-0.25	1.47		
55	3.38					0.92	2.76

57	3.49						
59	3.59						
60	3.65	67.01	8.61	0.02	1.44		
61	3.70					1.01	2.93
65	3.91	67.06	11.03	-0.02	1.38		
65	3.91					0.95	2.72
67	4.02					1.09	2.79
70	4.19	58.36	11.46	-0.03	1.47		
71	4.24					0.78	2.83
73	4.35					0.90	2.81
75	4.46	68.27	13.27	-0.05	1.85	1.71	3.00
77	4.57						
79	4.68					0.71	2.84
80	4.73	69.48	13.04	-0.05	1.26		
81	4.79					1.20	2.85
85	5.00	68.86	10.03	-0.31	1.15	1.41	3.01
85	5.00					1.47	3.02
90	5.28	71.07	12.92	-0.18	1.50	1.42	2.91
93	5.44					1.24	2.91
95	5.54	65.17	7.46	-0.40	1.19		
95	5.54					0.62	2.98
97	5.65					1.21	2.81
99	5.75					1.14	2.88
100	5.80	63.79	8.59	-0.19	1.36		
101	5.85					0.85	2.69
103	5.95					0.98	2.65
105	6.05	61.37	5.98	-0.70	1.12		
105	6.05					1.21	2.95
107	6.14					1.22	2.93
110	6.28	61.99	8.00	-0.51	1.43	1.49	3.23
111	6.33					1.29	2.94
115	6.51	56.34	7.62	-0.39	1.36		
119	6.69					0.82	2.91
120	6.73	63.46	14.44	-0.51	1.41		
121	6.77					0.98	2.92
123	6.86					1.12	2.90
125	6.96	66.10	27.85	-0.15	1.58		
125	6.96					1.18	2.91
125	6.96					0.86	2.81
127	7.06					1.13	2.97
129	7.20					1.04	2.85
130	7.29	63.43	9.60	-0.58	1.28		
131	7.37					0.95	2.82
135	7.72	52.43	3.46	-0.43	1.48		
140	8.17	57.53	4.06	-0.58	1.43		
141	8.24					0.984	2.791
143	8.37					0.803	2.673
145	8.48	58.96	5.84	-0.81	1.39		
145	8.48					0.868	2.820

147	8.58					0.779	2.882
149	8.68					0.683	2.645
150	8.73	55.40	4.56	-0.38	1.66		
151	8.77					0.903	2.706
153	8.88					0.836	2.417
155	9.02	51.71	6.51	-0.78	1.42		
155	9.02					0.907	2.635
157	9.17					0.901	2.759
159	9.33					1.014	2.728
160	9.41	54.86	11.01	-0.91	1.43		
161	9.49					1.039	2.723
163	9.65					1.091	2.828
165	9.82	51.98	6.60	-0.94	1.38		
165	9.82					1.045	2.756
167	9.99					1.079	2.852
169	10.17					0.766	2.507
170	10.27	51.20	11.15	-0.51	1.55		
171	10.36					1.098	2.964
173	10.55					0.929	2.772
175	10.75	52.47	7.07	-0.77	1.60		
175	10.75					0.96	2.77
175	10.75					0.939	2.861
177	10.94					0.943	2.944
179	11.13					0.772	3.110
180	11.22	47.58	7.64	-0.61	1.83		
181	11.30					0.842	3.009
183	11.44					0.796	2.765
185	11.55	44.13	10.16	-0.96	1.87		
185	11.55					0.938	2.961
187	11.62					0.721	2.958
189	11.67					0.839	3.067
190	11.70	49.66	11.49	-0.78	1.96		
191	11.72					0.705	2.988
193	11.77					0.582	3.001
195	11.83	46.99	11.98	-0.78	1.88	0.39	2.84
195	11.83					0.791	2.947
197	11.92					0.705	2.952
199	12.04						
200	12.10	46.11	18.22	-0.73	2.35	0.93	2.77
201	12.18					0.982	2.919
205	12.55	43.24	21.81	-0.98	2.05	0.90	3.21
205	12.55					0.628	3.362
207	12.74					0.69	3.49
209	12.93					0.49	3.43
210	13.01	43.19	16.89	-0.85	2.17	0.89	2.92
211	13.10					0.31	3.30
213	13.22					0.60	3.49
215	13.31	36.64	21.91	-0.57	2.58	0.85	3.60
215	13.31					0.58	3.42

217	13.38					0.65	3.52
219	13.44					0.69	3.51
220	13.46	33.12	14.94	-0.86	2.44	0.83	3.53
221						1.05	3.64
223						0.75	4.42
225						0.89	4.29
227						0.63	4.22
228		35.62	10.35	-0.65	2.55	1.29	4.00
229						0.46	3.89
231						0.80	4.36
233		33.20	14.83	-0.73	2.73		
233						0.48	4.12
235						0.79	4.20
238		34.23	18.56	-0.48	3.16		
241						0.65	4.17
243		34.11	17.78	-0.92	2.14		
243							
243						0.92	4.15
245						1.04	4.21
247							
248		31.70	23.54	-1.19	2.17		
249						0.30	3.99
251						-0.18	4.18
253		32.02	21.24	-1.35	2.10		
253						0.71	4.31
255						0.17	4.33
257						0.71	4.29
258		35.96	27.19	-0.45	2.49		
259						0.60	4.37
261						-0.02	4.50
263		33.03	23.88	-0.81	2.60		
263						0.66	4.37
265						0.92	4.24
267						0.85	4.27
268		33.90	19.05	-0.80	3.09	-0.11	4.57
269						0.49	4.20
271						1.05	4.48
273		29.85	18.14	-0.69	2.98		
273						0.76	4.14
275						0.73	4.01
277						0.58	4.18
278		29.62	20.36	-0.86	3.17	0.65	3.92
279						0.50	3.91
281						0.66	4.09
283		29.05	10.30	-0.95	2.56		
283						1.00	4.28
287						0.81	4.34
288		30.00	14.55	-0.63	3.42	0.62	4.55
289						0.55	4.60

291							
293		27.69	12.02	-0.80	2.89		
293						0.66	4.53
293						0.75	4.18
295						0.56	4.13
297						0.42	4.22
298		25.09	14.30	-0.75	3.07		
299						0.47	4.08
303		26.56	11.51	-0.40	3.19	0.65	4.27
308		27.93	12.81	-0.51	3.12	0.87	4.20
313		28.61	11.28	-0.26	3.13	0.90	4.45
318		28.87	6.71	-0.47	2.98		
323		30.37	11.44	-0.47	3.21	1.32	4.42
328		31.50	10.25	-0.64	3.07		
333	33.81	33.08	11.33	-0.21	3.27		
333	33.81					0.21	4.12
338	34.07	36.43	13.76	-0.19	3.27	0.44	4.47
343	34.33	37.97	10.70	-0.37	3.20		
348	34.60	35.17	9.92	-0.59	2.66		
353	34.86	43.91	7.53	-0.28	3.26		
358	35.15	39.76	8.70	-0.29	3.07		
363	35.44	33.74	10.37	-0.28	3.06	0.44	4.26
368	35.72	30.05	12.96	-0.14	3.00		
368	35.72					0.75	4.34
373	36.01	31.39	13.06	-0.32	3.12		
381	36.52	29.70	7.99	-0.48	2.92	0.33	4.39
386	36.84	27.74	8.29	-0.34	2.85	0.16	4.28
391	37.15	28.64	6.19	-0.67	2.81		
396	37.49	30.88	3.06	-0.73	2.82		
401	37.84	26.30	3.45	-0.49	2.80		
406	38.19	24.32	5.10	-0.78	2.71		
406	38.19					0.98	4.07
411	38.54	22.67	13.60	-0.54	2.93	0.83	4.24
416	38.92	21.61	7.95	-0.86	2.89		
421	39.31	21.67	14.35	-1.23	2.68	0.16	4.01
426	39.70	25.30		-0.75	2.79		
431	40.09	30.92	14.33	-0.72	2.97	1.22	4.26
431	40.09						
436	40.54	30.89	10.68	-0.86	2.87	0.91	4.25
441	41.01	32.24	12.79	-0.81	2.83	1.27	4.25
446	41.48	35.83	11.81	-0.79	2.90	0.90	4.81
451	41.96	30.51	11.45	-0.76	2.96	0.56	4.24
456	42.50	32.04	8.31	-1.09	3.05		
456	42.50					0.94	4.21
461	43.06	33.20	14.97	-0.34	3.23	0.30	3.91
466	43.61	33.09	9.11	-0.70	2.76	0.91	4.57
471	44.17	34.28	11.42	-0.83	2.74	1.04	4.14
476	44.77	39.85	11.66	-0.71	2.72		
481	45.38	35.45	4.85	-0.66	2.64	0.87	4.31

486	45.99	40.50	3.62	-0.95	2.47	1.94	3.86
491	46.60	37.90	4.61	-0.49	3.03	0.71	3.91
496	47.24	36.10	6.14	-0.93	2.90		
501	47.87	33.09	10.82	-0.83	2.58	0.75	3.73
501	47.87					0.99	3.85
506	48.51	29.52	6.60	-0.80	2.84	0.92	3.80
511	49.15	27.82	11.55	-0.68	3.22	0.46	4.21
516	49.80	34.28	10.25	-0.98	3.09	0.99	4.16
516	49.80					1.23	4.42
521	50.44	34.81	9.90	-0.63	3.05	1.25	4.76
526	51.09	37.46	15.43	-0.98	2.78		
526	51.09					1.44	4.40
535	52.25	38.99	9.97	-0.70	3.17	1.25	4.18
540	52.89	44.49	7.43	-0.63	3.12	0.64	4.18
545	53.53	46.11	9.31	-0.56	2.91	0.99	4.10
550	54.17	45.94	7.19	-0.54	2.91	1.06	3.99
555	54.78	55.50	8.74	-0.55	2.72		
560	55.40	52.90	7.39	-0.39	2.88		
565	56.02	55.36	3.23	-0.45	2.79		
570	56.64	56.13	5.96	-0.41	2.94	1.24	3.94
570	56.64						
575	57.22	57.97	8.27	-0.51	2.87		
580	57.80	56.10	8.71	-0.56	2.71	1.54	4.14
585	58.39	54.56	8.18	-0.40	2.84		
590	58.97	41.86	10.62	-0.68	2.56		
595	59.51	37.16	12.47	-0.70	2.66		
600	60.05	31.83	12.37	-0.80	2.59		
605	60.59	40.93	10.15	-0.71	2.87	1.30	4.10
610	61.12	40.01	11.35	-0.78	3.00	1.26	4.30
615	61.61	37.66	11.66	-0.99	3.05		
615	61.61					0.80	4.15
620	62.10	40.88	7.87	-0.93	3.09		
625	62.59	37.71	8.66	-1.44	2.83	0.95	4.08
630	63.07	47.78	11.97	-1.29	3.00		
635	63.51	43.63	8.62	-1.14	2.94		
640	63.95	41.36	11.33	-1.33	2.72	0.46	3.37
645	64.39	36.52	14.74	-1.01	2.72	0.77	3.92
650	64.82	33.49	8.63	-1.37	2.75	0.86	3.87
655	65.23	32.52	7.46	-0.97	2.81		
660	65.64	34.85	10.63	-0.91	2.94		
665	66.04	28.34	12.43	-1.12	2.68		
670	66.45	28.24	16.37	-1.11	2.69	0.22	4.34
670	66.45					0.25	4.09
675	66.84	29.26	14.13	-1.10	2.77	0.80	4.51
680	67.22	29.57	11.76	-0.85	2.90		
687	67.77	21.87	18.55	-0.63	2.79		
692	68.15	28.42	14.80	-0.61	2.81	0.87	4.17
697	68.53	43.12	11.97	-0.38	2.73		
702	68.90	45.14	10.05	-0.78	2.80	0.57	3.78

702	68.90					0.56	4.36
707	69.28	51.41	8.97	-0.85	2.67	0.75	4.14
712	69.65	52.99	4.54	-0.45	2.37	0.89	4.43
717	70.01	51.80	5.05	-0.51	2.47		
722	70.38	56.26	6.24	-0.73	2.51		
727	70.75	49.07	3.91	-0.38	2.42		
727	70.75					1.38	4.27
732	71.11	49.88	5.62	-0.23	2.53		
737	71.47	48.55	8.74	-0.58	2.50		
742	71.83	59.41	5.95	-0.68	2.45		
747	72.19	59.92	7.73	-0.51	2.47	1.26	3.65
752	72.54	73.68	3.92	-1.13	1.83		
757	72.90	72.32	5.70	-0.35	2.33		
757	72.90					0.62	3.98
762	73.25	69.12	5.61	-0.23	2.53		
767	73.61	69.49	10.75	-0.98	1.68		
772	73.95	60.66	6.75	-0.47	2.03	1.32	4.15
777	74.30	56.22	5.79	-0.10	2.30		
782	74.65	53.71	6.40	-0.25	2.11	1.22	3.55
787	74.99	59.91	7.42	-0.45	2.21		
792	75.31	55.96	9.29	-0.38	2.19		
797	75.63	62.97	4.12	-0.55	2.36		
802	75.94	71.70	3.80	-0.05	2.44		
807	76.26	47.08	9.42	-0.44	2.49		
812	76.57	46.97	12.76	-0.41	2.89		
817	76.87	67.79	2.62	-0.20	2.95		
822	77.18	72.97	6.65	-0.42	3.09		
827	77.48	79.58	5.46	-0.05	3.02		
832	77.79	73.44	3.69	-0.01	2.91		
840	78.27	68.15	5.92	-0.20	3.00		
845	78.57	65.51	4.27	-0.26	3.22		
850	78.87	72.01	5.11	-0.42	3.12		
855	79.17	77.03	3.90	-0.36	2.93		
855	79.17						
860	79.47	76.60	2.69	-0.43	2.86		
865	79.77	78.10	3.93	-0.40	2.94		
870	80.07	77.99	3.42	-0.39	2.69		
875	80.37	79.58	4.01	-0.46	2.65		
880	80.67	78.72	3.96	-0.12	2.72		
885	80.97	75.72	4.03	-0.06	2.78		
890	81.27	75.32	4.17	-0.31	2.71		
895	81.57	75.62	3.91	-0.24	2.79		
900	81.87	74.67	3.15	-0.16	2.78		
905	82.16	71.68	3.69	-0.33	2.66		
910	82.46	70.62	3.70	-0.81	2.29		
915	82.76	69.18	3.26	-0.49	2.48		
920	83.06	67.94	3.79	-0.93	2.05		
925	83.36	65.37	4.98	-0.43	2.49		
930	83.65	63.43	6.64	-0.79	2.48	0.83	3.21

935	83.95	62.50	7.00	-0.54	2.33	1.19	3.22
940	84.25	58.33	8.91	-0.49	2.41		
945	84.55	58.53	11.49	-0.45	2.49		
950	84.85	56.93	8.99	-0.70	2.39		
955	85.14	41.66	14.53	-0.77	2.25		
960	85.44	41.04	15.98	-0.63	2.33		
965	85.74	34.43	15.60	-0.56	2.64		
965	85.74					1.21	3.59
970	86.04	38.75	17.63	-0.50	2.52		
975	86.33	60.49	14.15	-0.54	2.66	0.95	3.72
980	86.63	68.38	10.23	-0.50	2.48		
985	86.93	65.87	12.42	-0.42	2.44		
993	87.41	60.79	13.20	-0.41	2.40	1.41	3.83
998	87.70	52.12	13.74	-0.57	2.23		
1003	88.00	52.65	9.73	-0.66	2.32	0.99	3.69
1008	88.30	47.77	7.28	-0.41	2.45		
1013	88.60	46.65	6.84	-0.33	2.18		
1018	88.89	49.53	7.92	-0.80	2.78	1.55	3.96
1023	89.19	47.79	7.14	-0.98	2.59		
1028	89.49	49.58	5.81	-0.89	2.68		
1033	89.78	51.00	5.57	-0.42	2.58		
1038	90.08	51.74	5.58	-0.76	2.32		
1043	90.38	53.03	3.44	-1.00	2.41		
1048	90.67	56.77	4.75	-0.59	2.64		
1048	90.67						
1053	90.97	57.62	4.51	-1.17	2.46		
1058	91.27	58.46	3.89	-0.99	2.61		
1063	91.56	59.10	2.30	-0.99	2.48		
1068	91.86	61.78	2.27	-0.82	2.53		
1073	92.16	61.60	2.19	-1.18	2.48		
1078	92.45	59.42	2.12	-1.16	2.34		
1083	92.75	60.47	1.78	-1.24	2.31		
1088	93.05	56.43	1.80	-0.96	2.30		
1088	93.05						
1093	93.34	57.84	2.19	-0.96	2.24		
1098	93.64	58.12	3.08	-0.97	2.18		
1103	93.93	83.52	2.34	-0.82	2.01		
1108	94.23	60.68	2.30	-1.12	2.30		
1108	94.23						
1113	94.52	65.01	2.82	-1.08	2.18		
1118	94.82	67.49	2.10	-0.87	2.32		
1123	95.11	67.16	2.14	-1.09	2.14	1.49	3.30
1128	95.41	68.11	1.69	-1.18	2.22		
1133	95.70	65.77	10.62	-0.92	2.36		
1138	96.00	71.66	0.25	-0.84	2.52		
1146	96.47	70.87	1.31	-1.37	1.89		
1151	96.76	71.30	1.40	-1.14	1.95		
1156	97.05	71.38	2.65	-0.99	2.14		
1161	97.34	71.02	2.29	-0.91	2.29		

1166	97.64	70.59	1.29	-1.17	2.15		
1171	97.93	70.47	1.68	-0.99	2.23	0.73	2.42
1176	98.22	70.70	1.17	-0.93	2.20		
1181	98.51	71.12	1.80	-0.79	2.25		
1186	98.80	71.56	2.19	-1.27	2.06		
1191	99.09	68.82	1.91	-0.85	2.14		
1196	99.38	70.40	1.99	-1.04	2.39		
1201	99.67	67.53	2.02	-1.10	2.30		
1206	99.96	63.36	1.95	-0.97	2.45		
1211	100.25	61.59	1.91	-1.02	2.15		
1216	100.53	57.64	7.01	-1.08	2.15		
1221	100.82	60.64	9.65	-1.13	1.94	0.68	3.19
1226	101.10	71.35	3.88	-0.65	2.13		
1231	101.38	75.62	2.25	-0.88	2.23		
1236	101.67	72.61	2.66	-0.95	2.17		
1241	101.95	69.45	2.47	-1.02	2.28		
1246	102.23	66.55	1.79	-0.95	2.05		
1251	102.50	65.66	3.04	-0.93	2.11		
1256	102.78	65.37	3.01	-1.31	2.04	0.90	3.85
1261	103.05	64.80	1.83	-1.02	2.10	1.01	3.66
1266	103.32	67.43	1.88	-0.95	2.05		
1271	103.59	61.32	2.47	-0.94	2.33		
1276	103.86	61.29	2.91	-0.82	1.83		
1281	104.13	62.11	2.40	-1.08	2.08		
1286	104.39	60.08	2.51	-0.89	1.98	1.04	3.56
1291	104.65	62.46	2.80	-0.94	1.96		
1299	105.07	51.31	2.69	-0.86	2.04		
1304	105.33	39.41	10.12	-0.65	2.53		
1309	105.58	60.67	5.47	-0.76	2.38		
1314	105.84	69.88	12.95	-0.47	2.70	0.95	3.96
1314	105.84					1.28	4.07
1319	106.10	74.10	3.07	-0.88	2.27		
1324	106.35	72.60	2.63	-0.80	2.31		
1329	106.60	68.98	5.42	-0.67	2.26		
1334	106.85	67.67	3.18	-1.02	2.10	0.79	3.69
1339	107.10	68.62	3.82	-0.92	1.63	0.75	3.80
1344	107.35	70.24	4.40	-0.83	1.96		
1349	107.59	55.09	3.26	-0.78	2.16		
1354	107.84	52.13	4.97	-0.74	2.08	1.19	3.39
1359	108.08	49.75	3.33	-0.76	2.70		
1359	108.08						
1364	108.33	53.86	3.57	-1.22	2.33	1.06	3.17
1369	108.58	56.33	3.12	-1.12	1.77		
1374	108.82	55.83	3.96	-0.77	1.56		
1379	109.07	59.53	4.46	-0.93	2.02		
1384	109.41	63.80	3.84	-1.21	1.16		
1389	109.80	64.63	2.93	-0.19	2.23		
1394	110.19	63.90	3.48	-0.39	2.32		
1399	110.58	61.75	3.08	-0.15	2.47		

1399	110.58					0.82	3.29
1404	111.12	65.14	3.33	-0.90	1.80		
1409	111.71	68.33	3.77	-1.23	1.53		
1414	112.30	69.19	2.95	-0.83	1.64		
1419	112.90	68.75	3.95	-1.00	1.64		
1424	113.55	68.50	3.24	-0.74	1.24		
1429	114.22	68.97	3.66	-0.66	1.32		
1434	114.90	72.31	2.51	-1.00	1.48		
1439	115.57	72.42	3.51	-0.10	1.50		
1453	117.66	72.73	2.36	-0.08	1.68		
1458	118.42	72.75	4.92	-0.38	1.56		
1463	119.22	74.33	5.35	-1.15	0.85		
1463	119.22					0.87	2.87
1468	120.06	75.48	6.06	-0.74	1.44		
1473	120.89	76.78	6.59	-0.53	1.42		
1478	121.72	77.64	6.90	-1.15	0.85		
1483	122.61	75.06	9.12	-0.74	1.44		
1488	123.53	75.65	11.93	-0.53	1.42		
1488	123.53					0.97	2.76
1493	124.44	75.27	11.94				
1498	125.35	74.32	16.55	-0.97	1.44		
1503	126.33	70.14	19.87	-0.82	1.20	0.75	2.52
1503	126.33					0.87	2.69
1508	127.32	61.95	17.90	-0.70	1.57		
1513	128.31	53.18	10.55	-1.01	1.07		
1518	129.31	42.36	18.37	-1.27	1.19		
1518	129.31					0.55	2.99
1523	130.34	20.96	20.41	-1.13	2.12		
1528	131.39	18.83	19.64	-0.48	2.76	0.73	4.16
1528	131.39					0.59	4.01
1533	132.44	32.79	10.02	-1.57	2.66		
1533	132.44					0.78	4.81
1538	133.48	32.02	13.21	-1.11	3.52		
1538	133.48					0.67	4.48
1543	134.65	38.34	14.75	-1.07	3.47		
1548	135.85	39.57	16.37	-1.07	3.52		
1553	137.04	36.93	13.73	-1.04	3.56	1.07	4.71
1558	138.24	40.63	35.69	-1.11	3.58	0.82	4.54
1563	140.21	35.13	16.94	-1.23	3.46	1.10	4.69
1568	142.30	35.71	12.77	-0.98	3.42		
1568	142.30					0.31	4.45
1573	144.38	34.07	12.99	-1.06	3.23	0.42	4.51
1578	146.46	29.20	18.39	-1.13	3.26	0.30	3.99
1583	149.04	28.65	19.19	-1.10	3.01		
1588	151.65	37.51	16.23	-1.26	2.98		
1593	154.27	33.72	8.10	-1.35	2.52		
1598	156.88	35.99	9.91	-1.24	2.81		
1603	159.42	34.57	6.68	-1.38	2.63		
1606	160.94	37.82	20.50	-0.87	3.49		

1611	163.47	41.02	26.86	-1.05	2.82		
1616	166.00	61.78	19.71	-1.00	2.70		
1621	168.23	53.71	19.52	-1.16	2.61	0.16	4.10
1626	170.27	41.31	11.22	-0.92	2.99	0.92	2.79
1631	172.32	37.26	23.53	-1.44	2.72	0.74	3.37
1636	174.36	34.02	19.98	-1.08	2.87	0.63	3.42
1641	175.68	36.84	27.01	-1.34	2.67	0.74	4.39
1646	176.65	35.24	18.63	-1.19	2.72	0.32	4.03
1651	177.62	25.51	5.27	-1.32	2.52		
1656	178.59	28.01	4.11	-1.45	2.42	0.22	3.63
1661	179.41	25.86	3.81	-1.36	2.49		
1666	180.18	19.93	1.15	-1.48	2.55		
1671	180.94	29.16	13.97	-1.70	2.50		
1676	181.71	34.34	19.94	-1.33	3.17	0.17	3.75
1681	182.47	31.67	27.37	-1.31	2.79	0.53	4.08
1686	183.23	38.08	21.97	-1.21	2.81	0.17	3.96
1691	183.98	40.98	7.02	-1.20	2.37		
1696	184.74	42.60	8.67	-1.08	2.37	0.55	3.75
1701	185.51	43.52	4.66	-0.92	2.43		
1706	186.28	42.02	4.96	-1.06	2.17		
1711	187.06	39.46	6.46	-0.98	1.93		
1716	187.83	38.23	4.80	-0.99	2.19	0.59	3.39
1721	188.62	35.23	7.17	-0.85	2.50		
1726	189.42	34.96	7.87	-0.97	2.56		
1726	189.42					0.87	3.84
1731	190.21	57.23	6.09	-0.80	2.55		
1736	191.01	61.46	3.12	-0.81	2.29		
1736	191.01					0.59	3.67
1741	191.83	62.71	4.49	-0.854	2.067		
1741	191.83					0.86	3.63
1746	192.65	53.72	6.97	-0.716	2.146		
1746	192.65					0.85	3.51
1751	193.47	43.53	3.18	-0.939	2.028		
1760	194.97	58.11	7.50	0.136	1.816		
1765	195.81	65.63	1.51	-0.676	1.986		
1770	196.66	66.84	1.87	-0.619	1.659		
1770	196.66					0.77	3.29
1775	197.51	62.60	2.83	-0.814	1.369		
1780	198.38	60.50	3.13	-0.983	1.653		
1785	199.25	53.09	5.06	-0.986	1.629		
1790	200.13	44.63	7.26	-1.109	1.687	0.43	3.08
1795	201.00	45.73	6.69	-0.894	1.486	0.63	2.85
1800	201.91	34.40	12.84	-0.194	2.034	0.43	3.67
1805	202.83	25.28	10.23	-0.074	2.163	0.15	3.80
1810	203.74	27.43	7.55	-0.053	3.027	0.49	3.88
1815	204.66	36.31	4.08	-0.141	2.369	0.66	4.17
1820	205.59	42.00	4.16	-0.149	1.950	0.56	3.79
1825	206.53	48.68	6.67	-0.60	2.51	0.40	3.77
1830	207.47	49.46	5.02	-0.43	2.41		

1835	208.41	55.11	9.36	-0.24	2.04	0.45	3.55
1840	209.35	53.03	7.65	-0.55	1.86		
1845	210.30	51.79	6.99	-0.78	1.58		
1850	211.24	49.30	5.83	-0.81	1.56		
1855	212.18	54.76	9.58	-0.85	1.81		
1860	213.12	49.99	8.55	-0.96	2.16	0.27	3.28
1865	214.06	48.23	6.64	-0.84	2.14		
1870	215.00	47.83	7.07	-1.05	1.86	0.77	3.07
1875	215.95	34.70	5.69	-1.10	1.91		
1880	216.88	32.70	9.07	-1.23	1.87		
1885	217.82	31.11	12.01	-1.54	1.57	0.21	3.06
1890	218.75	27.27	13.22	-1.17	1.88	0.54	2.84
1895	219.69	20.70	16.28	-1.27	1.87	0.10	2.39
1900	220.62					0.05	3.17
1900	220.62	12.95	10.85	-1.21	2.58		
1905	221.55	28.72	16.62	-1.610	2.115	0.26	3.34
1914	223.23	40.19	11.36	-1.263	2.420	0.22	4.21
1919	224.15	35.81	4.51	-1.128	2.275	0.49	3.88
1924	225.07	31.57	5.76	-1.282	2.319	-0.06	4.20
1929	226.00	39.78	8.34	-0.896	2.600	0.74	4.14
1934	226.92	46.90	7.82	-1.018	2.348	1.00	3.95
1939	227.84	46.17	7.35	-1.051	2.444	0.81	3.77
1944	228.75	45.27	5.02	-0.979	2.206		
1949	229.67	46.36	2.56	-1.165	2.379		
1954	230.59	40.31	4.09	-1.118	2.333	0.81	3.31
1959	231.49	38.22	6.79	-0.799	2.672	0.74	3.24
1964	232.40	41.29	4.62	-0.863	2.607	0.84	3.20
1969	233.31	57.65	3.25	-0.744	2.647		
1974	234.22	60.60	3.95	-0.873	2.412		
1979	235.13	58.92	5.15	-0.892	2.163		
1984	236.03	68.20	5.43	-0.878	1.991		
1989	236.93	72.38	8.58	-0.65	2.16		
1994	237.84	69.12	7.99	-0.78	2.06	0.74	2.80
1999	238.74	70.52	13.63	-0.74	1.92		
2004	239.64	65.51	13.50	-1.36	1.31	0.70	2.89
2009	240.54	54.63	13.91	-0.94	1.45		
2014	241.44	45.18	18.55	-1.26	1.61	0.22	2.93
2019	242.34	24.22	14.02	-0.93	1.53	0.34	3.54
2024	243.24	23.12	13.00	-1.28	2.80	0.13	3.40
2029	244.14	33.26	13.20	-1.35	2.78	0.22	3.78
2034	245.04	27.85	20.55	-1.28	2.84	0.35	3.66
2039	245.94	28.89	12.42	-1.21	3.21		
2044	246.84	27.96	8.03	-1.19	2.96	0.32	3.87
2049	247.75	26.10	4.79	-1.11	3.29		
2054	248.65	23.40	9.55	-1.52	3.37	0.26	4.01
2059	249.57	18.48	12.16	-1.48	2.92		
2068	251.22	25.99	12.25	-0.90	3.30	0.71	4.16
2073	252.13	20.72	12.15	-1.28	3.54	0.69	4.17
2078	253.07	6.86	10.99	-0.97	3.26	0.78	4.01

2083	254.01	11.07	9.62	-0.63	3.62	0.78	4.09
2088	254.95	12.92	7.76	-0.86	3.23	0.69	3.94
2093	255.89	23.15	9.83	-1.10	2.65	0.34	3.86
2098	256.84	38.16	8.77	-1.15	2.46	0.49	3.81
2103	257.80	37.64	6.16	-1.31	2.17		
2108	258.75	34.72	15.55	-1.29	2.38	0.57	3.80
2113	259.70	20.46	22.44	-1.25	3.02	0.27	3.94
2118	260.66	31.08	8.27	-1.32	2.57	0.47	3.75
2123	261.63	31.29	5.96	-1.28	2.72	0.49	3.83
2128	262.59	33.50	14.35	-1.29	2.73	0.40	4.07
2133	263.55	37.27	7.60	-1.46	2.47	0.38	3.86
2138	264.52	38.21	11.81	-1.67	2.50		
2143	265.49	31.17	5.67	-1.52	2.58	0.03	3.82
2148	266.46	26.65	8.02	-1.65	2.48	0.20	3.90
2153	267.43	24.61	16.64	-0.79	2.75		
2158	268.41	38.00	17.01	-1.28	2.57	0.82	3.96
2163	269.39	45.27	9.22	-1.38	2.40	0.52	3.83
2168	270.37	44.17	2.92	-1.17	2.31	0.25	3.57
2173	271.35	45.64	6.28	-0.70	2.30	0.37	3.75
2178	272.34	45.68	8.75	-0.43	2.53		
2183	273.33	62.38	8.08	-0.49	2.76	0.70	3.47
2188	274.32	59.93	3.98	-0.94	2.16		
2193	275.31	60.14	4.17	-0.96	2.30	0.73	3.27
2198	276.30	59.95	3.55	-1.07	2.35		
2203	277.30	57.79	5.51	-0.85	2.35	0.91	3.12
2208	278.30	61.79	4.97	-0.63	2.65	0.98	3.22
2213	279.30	60.65	5.10	-0.65	2.97		
2220	280.71	65.15	3.30	-0.88	2.39		
2225	281.71	64.85	3.13	-0.82	2.42		
2230	282.72	63.37	2.73	-0.86	2.20		
2235	283.73	59.46	5.69	-0.85	2.01	0.65	3.13
2240	284.75	54.72	6.13	-1.02	2.01	0.30	3.04
2245	285.76	48.44	3.30	-0.98	2.15	0.33	3.10
2250	286.78	46.52	6.35	-0.87	2.11	0.29	3.18
2255	287.80	46.08	4.97	-0.80	2.39	0.90	3.26
2260	288.82	44.48	4.95	-1.06	2.12		
2265	289.85	41.49	8.57	-0.98	1.91		
2270	290.87	35.66	19.28	-0.94	2.30	0.61	4.20
2275	291.90	36.43	19.17	-0.72	2.44	0.01	3.99
2280	292.93	37.87	13.63	-0.70	2.66	-0.11	4.07
2285	293.97	40.14	13.94	-0.84	2.66		
2290	295.00	46.68	13.70	-0.85	2.74	0.04	4.19
2295	296.03	53.16	5.77	-0.37	2.26	0.14	4.11
2300	297.07	53.21	6.52	-0.34	2.55	-0.03	3.97
2305	298.10	44.42	6.75	-0.80	2.21		
2310	299.13	47.56	5.88	-0.80	2.09		
2315	300.16	51.65	4.58	-0.74	2.29		
2320	301.20	55.91	5.31	-0.91	2.10		
2325	302.23	57.38	6.01	-0.94	2.14		

2330	303.26	57.94	6.70	-0.63	2.09		
2335	304.29	59.27	6.11	-0.51	2.14		
2340	305.33	61.82	8.06	-0.58	1.94		
2345	306.36	60.18	5.73	-0.61	1.93		
2350	307.39	61.41	7.02	-0.56	1.79	1.17	3.69
2355	308.42	56.25	6.24	-0.34	2.04	0.76	2.82
2360	309.46	56.54	7.72	-0.80	1.84		

Appendix 4: Stable isotope and percent coarse fraction data for core KN166-14 3GGC.

Methodologies for stable isotopes and percent coarse fraction are given in sections 2.3.1 and 3.3.2, respectively. Stable isotope values are reported as ‰ with respect to V-PDB.

Depth (cm)	Age (ka)	% Coarse Fraction	$\delta^{13}\text{C}$ <i>G.bulloides</i>	$\delta^{18}\text{O}$ <i>G.bulloides</i>	$\delta^{13}\text{C}$ <i>N.pachyderma</i> (s)	$\delta^{18}\text{O}$ <i>N.pachyderma</i> (s)	$\delta^{13}\text{C}$ <i>P.wuellerstorfi</i>	$\delta^{18}\text{O}$ <i>P.wuellerstorfi</i>
0	0.00	5.43					0.83	2.85
2	0.26	9.59					0.59	2.75
4	0.53	11.88						
6	0.80	20.89					1.09	2.85
8	1.06	4.66					0.91	2.82
10	1.33	9.23					0.85	2.84
12	1.60	13.49					0.98	2.88
14	1.87	14.56					0.98	2.76
16	2.14	12.42					1.18	2.95
18	2.41	7.35					1.01	2.77
20	2.68	9.38						
22	2.95	10.03					1.11	2.89
24	3.23	10.34					1.13	2.72
26	3.50	7.08					0.94	2.88
28	3.78	7.11					1.09	2.90
30	4.05	13.44					1.15	2.77
32	4.33	5.05						
34	4.60	8.44					0.94	2.80
36	4.88	8.42					1.00	2.81
38	5.16	9.99					1.00	2.82
40	5.44	8.78					1.14	2.78
42	5.72	7.94					0.94	3.02
44	6.00							
46	6.28	3.47						
48	6.57	1.07					1.03	2.73
50	6.85	0.80	-0.97	1.41				
52	7.13	0.41	-0.51	1.20				
54	7.42	0.29	-0.46	1.63				
56	7.71	0.24	-0.95	1.06				
58	7.99	0.39	-0.86	1.29				
60	8.28	0.33	-0.80	1.17				
62	8.57	0.26	-1.05	1.09				
64	8.86	0.06	-0.31	1.44				
66	9.15	0.16	-0.85	1.22				
68	9.44	8.49	-0.54	1.11			1.07	2.82

70	9.73	15.25	-0.74	1.50	0.26	3.78	0.65	2.90
72	10.02	21.33	-0.84	1.78			0.71	2.89
74	10.32	20.51	-0.96	2.00	0.40	3.56	0.65	3.03
76	10.61	23.65	-0.75	2.20			0.60	3.37
78	10.91	25.94	-0.87	2.14			0.73	2.98
80	11.20	24.78	-0.83	2.09	0.25	3.67	0.55	3.20
82	11.50	20.41	-0.97	2.03			0.92	3.00
84	11.80	18.85	-0.93	2.35	0.28	3.83	0.72	3.51
86	12.10	26.87	-0.94	2.38			0.69	3.59
88	12.39	27.49	-0.60	2.57	0.11	3.86	0.35	4.14
90	12.69	24.83	-0.62	2.46			0.75	3.94
92	12.99	21.68	-0.89	2.43	-0.03	4.38	0.34	4.31
94	13.32	22.20	-0.81	2.47			0.42	3.71
96	13.72	27.25	-0.83	2.61	0.20	3.69	0.26	3.68
98	14.15	21.67	-0.59	2.31			0.26	4.02
100	14.58	21.86	-0.85	2.75	-0.15	4.49	1.03	3.77
102	15.00	22.31	-0.80	2.83	0.06	4.35	0.47	4.57
104	15.42	30.38	-0.88	3.19	-0.09	4.45	0.59	4.53
106	15.83	26.49	-0.72	2.26	-0.11	4.53	0.51	4.58
108	16.25	24.30	-0.67	3.21	0.14	4.53	0.32	4.27
110	16.66	24.28	-0.09	3.64	-0.08	4.45	0.40	4.49
112	17.06	22.07	-0.59	3.19	0.08	4.53	0.23	4.42
114	17.47	22.63	-0.42	3.52	0.07	4.55	0.41	4.56
116	17.87	19.42	-0.46	3.38	0.11	4.40	0.51	4.35
118	18.26	15.26	-0.70	3.35	0.06	4.31	0.55	4.51
120	18.66	22.25	-0.76	3.32			0.39	4.36
122	19.05	17.41			0.04	4.37	0.45	4.24
124	19.44	25.72					0.79	4.18
126	19.83	18.60			-0.06	4.40	0.46	4.34
128	20.21	19.96			0.03	4.37	0.57	4.03
130	20.59	14.17	-0.45	3.00	-0.01	4.30	0.65	4.19
132	20.97	17.21					0.85	4.65
134	21.35	18.09			0.25	4.16	0.63	4.40
136	21.72	17.64					1.03	4.27
138	22.10	16.61			0.09	4.18	0.78	4.30
140	22.47	18.17						3.85
142	22.83	16.25			0.20	4.10	0.84	4.09
144	23.20	20.87					1.02	4.11
146	23.56	16.28	-0.24	2.89	0.28	4.03	0.76	4.20
148	23.92	16.04					0.69	4.16
150	24.27	11.86			0.30	4.02	0.65	4.11
152	24.63	7.10					1.18	4.32
154	24.98	4.27			0.06	3.98		
156	25.33	3.73						4.12
158	25.68	8.25	-0.07	3.09	0.17	3.86	0.77	4.21
160	26.02	5.98					1.07	4.30
162	26.37	2.77			0.16	3.83		
164	26.71	6.42					0.96	3.96
166	27.05	1.99			0.35	4.16		4.29

168	27.38	0.78				
170	27.72	1.29	0.28	4.05	0.91	4.36
172	28.05	1.32				
174	28.38	0.15				
176	28.71	0.91				
178	29.03	0.65				
180	29.36	0.18				
182	29.68	0.18				
184	30.00	0.49				

Appendix 5: Average and standard deviation of benthic foraminiferal $\delta^{13}\text{C}$ for all transect sites (ODP site 984, ODP site 983, V29-202, EW9302-JPC8, 11JPC, 3GGC, and BOFS18k) interpolated into 2-kyr bins.

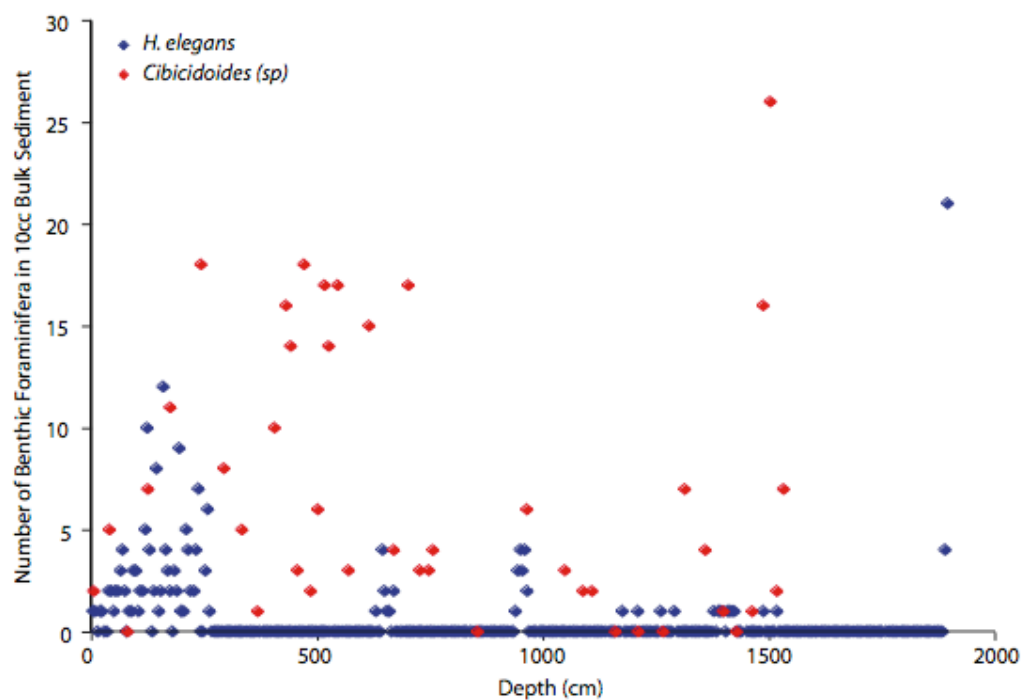
Age (ka)	Average $\delta^{13}\text{C}$	Standard Deviation
1	1.02	0.23
3	1.05	0.18
5	1.02	0.19
7	1.09	0.15
9	0.97	0.15
11	0.84	0.17
13	0.75	0.24
15	0.90	0.37
17	0.87	0.49
19	0.92	0.44
21	0.79	0.26
23	1.00	0.38
25	0.99	0.42
27	0.88	0.34
29	1.28	0.28
31	0.83	0.35
33	0.94	0.33
35	0.74	0.24
37	0.71	0.25
39	0.87	0.28
41	0.86	0.27
43	0.94	0.27
45	1.07	0.20
47	0.94	0.27
49	1.08	0.26
51	1.08	0.27
53	1.15	0.12
55	0.94	0.12
57	0.98	0.31
59	0.87	0.36
61	0.64	0.30
63	0.69	0.28
65	0.75	0.25
67	0.87	0.33
69	0.87	0.25
71	0.92	0.30
73	1.10	0.22
75	1.12	0.21
77	1.18	0.22
79	1.20	0.19
81	1.11	0.20

83	0.97	0.22
85	1.05	0.19
87	1.12	0.16
89	1.19	0.14
91	1.18	0.19
93	1.25	0.17
95	1.14	0.17
97	1.19	0.16
99	1.15	0.21
101	1.03	0.28
103	0.92	0.23
105	0.92	0.21
107	0.96	0.20
109	0.98	0.16
111	0.96	0.24
113	0.81	0.25
115	0.79	0.22
117	0.78	0.16
119	0.82	0.16
121	0.81	0.19
123	0.73	0.16
125	0.67	0.20
127	0.42	0.26
129	0.30	0.28
131	0.83	0.31
133	0.89	0.17
135	0.90	0.20
137	0.76	0.18
139	0.73	0.29
141	0.98	0.28
143	0.93	0.38
145	0.71	0.41
147	0.51	0.19
149	0.45	0.27
151	0.64	0.21
153	0.71	0.20
155	0.72	0.20
157	0.66	0.14
159	0.85	0.13
161	0.73	0.17
163	0.80	0.15
165	0.64	0.08
167	0.78	0.16
169	0.59	0.13
171	0.80	0.09
173	0.86	0.16
175	0.76	0.15
177	0.32	0.00
179	0.44	0.30

181	0.64	0.44
183	0.73	0.25
185	0.62	0.18
187	0.60	0.27
189	0.83	0.06
191	0.76	0.15
193	0.76	0.23
195	0.72	0.00
197	0.75	0.03
199	0.82	0.14
201	0.73	0.25
203	0.88	0.27
205	0.76	0.14
207	0.58	0.27
209	0.45	0.00
211	1.04	0.00
213	0.55	0.39
215	0.84	0.10
217	0.41	0.26
219	0.33	0.28
221	0.22	0.16
223	0.20	0.11
225	0.62	0.36
227	0.78	0.14
229	0.70	0.08
231	0.78	0.25
233	0.81	0.11
235	0.81	0.10
237	0.75	0.15
239	0.33	0.32
241	0.13	0.13
243	0.42	0.39
245	0.41	0.17
247	0.61	0.20
249	0.70	0.33
251	0.75	0.12
253	0.74	0.06
255	0.65	0.21
257	0.49	0.00
259	0.42	0.21
261	0.59	0.20
263	0.51	0.20
265	0.42	0.25
267	0.64	0.30
269	0.50	0.25
271	0.55	0.28
273	0.69	0.32
275	0.60	0.24
277	0.79	0.13

279	0.80	0.16
281	0.71	0.01
283	0.91	0.24
285	0.80	0.36
287	0.75	0.31
289	0.68	0.33
291	0.43	0.28
293	0.34	0.46
295	0.51	0.30
297	0.57	0.39
299	0.75	0.11

Appendix 6: Number of benthic foram tests available for Mg/Ca analysis in ~ 10 cc of bulk sediments from core KN166-14 11JPC.



Appendix 7: Extended site information for core tops used in this *Krithe* Mg/Ca core top calibration are listed by region, including; core name, water depth, bottom water temperature (BWT), and bottom water salinity (BWS). Asterisks designate BWT and BWS data that was collected by shipboard CTD; crosses designate BWT data only was collected by shipboard CTD. Hydrographic parameters of total phosphorous (TP), total silicate (TSil), total alkalinity (TAlk), and Total CO₂ (TCO₂) were used to calculate *in situ* CO₃²⁻ using CO₂sys (Lewis and Wallace, 1998). *In situ* CO₃²⁻ was then used to calculate Δ[CO₃²⁻] (Section 4.3.2). For some sites, a correction was required due to an increase in CO₂ in modern times (e.g., Orr et al., 1995), for those sites, anthropogenic CO₂ (anthro. CO₂) was found from Sabine et al. (2004) for the North Atlantic sites and Jutterstrom et al. (2008) for Norwegian Sea sites, and used to calculate anthropogenic *in situ* CO₃²⁻, and anthropogenic Δ[CO₃²⁻], which are also listed.

Core	Water Depth (m)	BWT (°C)		BWS (psu)	TP (μmol/kg)	TSil (μmol/kg)	TAlk (μmol/kg)	TCO ₂ (μmol/kg)	<i>in situ</i> CO ₃ ²⁻ (μmol/kg)	Anthro. CO ₂ (μmol/kg)	Anthro. CO ₃ ²⁻ (μmol/kg)	ΔCO ₃ ²⁻ (μmol/kg)	Reference #
<u>Cape Hatteras: Cruise KN178</u>													
16MCB	2214	3.4	*	34.94	1.25	18.1	2320	2164	111.7			44.12	1
16MCB	2214	3.4	*	34.94	1.25	18.1	2320	2164	111.7			44.12	1
14MCD	2602	3.0	*	34.93	1.25	20.5	2322	2165	111.6			39.59	1
8MCE	2997	2.5	*	34.91	1.27	24.4	2325	2167	110.8			34.16	1
5MCD	3382	2.2	*	34.88	1.27	26.9	2326	2169	108.4			26.91	1
1MCD	3979	2.2	*	34.88	1.27	28.8	2327	2171	107.1			17.39	1
1MCD	3979	2.2	*	34.88	1.27	28.8	2327	2171	107.1			17.39	1
<u>Gulf of Mexico: Cruise DGOMB</u>													
S36-3	1026	5.1	*	34.94	1.41	16.2	2320	2183	106.4			50.48	2
W4-5	1406	4.3	*	34.97	1.21	14.2	2323	2161	116.9			57.47	2
W4-5	1406	4.3	*	34.97	1.21	14.2	2323	2161	116.9			57.47	2
S38-4	2630	4.3	*	34.99	1.13	22.6	2313	2162	107.5			35.22	2
S38-4	2630	4.3	*	34.99	1.13	22.6	2313	2162	107.5			35.22	2
W5-4	2745	4.3	*	34.99	1.13	22.6	2313	2162	106.2			32.57	2
S39-2	3000	4.3	*	35.00	1.03	24.2	2320	2174	103.3			26.61	2

W6-3	3150	4.4	*	35.00	1.03	24.2	2320	2174	102.5			23.94	2
<u>Sulawesi Margin, Indonesia: Cruise BJ8-03</u>													
40MCF	251	11.5		34.47					110.0			60.60	3
61MCD	292	10.9		34.45					102.5			57.80	3
16MCC	409	8.8		34.47					82.0			31.33	3
<u>New Zealand shelf: Cruise RR05-03</u>													
86MCF	663	4.9	†	34.29	1.74	14.4	2287	2147	110.0			57.23	4
86MCF	663	4.9	†	34.29	1.74	14.4	2287	2147	110.0			57.23	4
82MCG	1623	2.5	†	34.54	2.37	71.2	2339	2245	77.8			16.30	4
22MCB	1682	2.4	†	34.56	2.37	71.2	2339	2245	78.2			16.09	4
22MCC	1682	2.4	†	34.56	2.37	71.2	2339	2245	78.2			16.09	4
22MCC	1682	2.4	†	34.56	2.37	71.2	2339	2245	78.2			16.09	4
92MCG	1818	2.3	†	34.60	2.36	81.2	2351	2255	79.2			15.72	4
102MCA	2055	2.1	†	34.66	2.29	83.8	2353	2253	79.8			13.87	4
102MCA	2055	2.1	†	34.66	2.29	83.8	2353	2253	79.8			13.87	4
118MCF	2252	2.0	†	34.69	2.22	84.8	2353	2249	83.8			15.71	4
118MCF	2252	2.0	†	34.69	2.22	84.8	2353	2249	83.8			15.71	4
118MCF	2252	2.0	†	34.69	2.22	84.8	2353	2249	83.8			15.71	4
26MCF	2418	1.9	†	34.71	2.22	84.8	2353	2249	82.3			15.08	4
26MCF	2418	1.9	†	34.71	2.22	84.8	2353	2249	82.3			15.08	4
106MCF	2472	1.9	†	34.72	2.18	87.9	2355	2248	82.5			14.47	4
<u>Norwegian Sea: Cruise KN177-2</u>													
4MCE	418	0.8	*	34.91	0.89	6.0	2301	2157	107.0	34	126	78.86	5
4MCE	418	0.8	*	34.91	0.89	6.0	2301	2157	107.0	34	126	78.86	5
11MCC	1285	-0.7	*	34.91	0.98	9.5	2302	2164	100.9	24	117	58.89	5
50MCB	1906	-0.8	*	34.91	1.00	11.5	2299	2160	99.5	20	115	47.50	5
50MCB	1906	-0.8	*	34.91	1.00	11.5	2299	2160	99.5	20	115	47.50	5
45MCD	2799	-0.9	*	34.91	1.01	13.2	2306	2169	97.6	19	113	30.43	5
<u>North Atlantic: Cruise KN166-14 and ODP</u>													
15JPC	2300	2.9		34.90	1.07	10.7	2286	2154	84.1	12	94	25.43	6
15JPC	2300	2.9		34.90	1.07	10.7	2286	2154	84.1	12	94	25.43	6
15JPC	2300	2.9		34.90	1.07	10.7	2286	2154	84.1	12	94	25.43	6
11JPC	2707	3.0		34.93	1.12	14.2	2311	2158	112.0			34.86	7
8GGC	2707	3.0		34.93	1.12	14.2	2311	2158	112.0			38.82	7
8GGC	2707	3.0		34.93	1.12	14.2	2311	2158	112.0			38.82	7
12JPC	3078	2.8		34.94	1.12	17.2	2316	2162	107.1			30.05	7
3GGC	3305	2.6		34.92	1.11	17.4	2315	2160	106.8			25.27	8
3GGC	3305	2.6		34.92	1.11	17.4	2315	2160	106.8			25.27	8
607	3427	2.6		34.92	1.09	18.9	2313	2160	105.5			21.77	9
<u>Ceara Rise: ODP cruise</u>													
926	3598	2.5		34.91	1.33	30.5	2339	2174	109.0			23.85	10
928	4010	1.5		34.90	1.33	34.5	2338	2177	108.0			16.45	10
929	4355	1.8		34.89	1.68	65.6	2358	2211	105.0			9.95	10

References for hydrographic information that was not collected by CTD cast are:

- (1) WOCE station A22 S40 from Johnson K., R. Key, F. Millero, C. Sabine, D. Wallace, C. Winn, L. Arlen, K. Erickson, K. Friis, M. Galanter, J. Goen, R. Rotter, C. Thomas, R. Wilke, T. Takahashi, and S. Sutherland. 2003. Carbon Dioxide, Hydrographic, and Chemical Data Obtained During the R/V *Knorr* Cruises in the North Atlantic Ocean on WOCE Sections AR24 (November 2 - December 5, 1996) and A24, A20, and A22 (May 30 - September 3, 1997), A. Kozyr (ed.) ORNL/CDIAC-143, NDP-082. Carbon Dioxide Information Analysis Center, Oak Ridge National Laboratory, U.S. Department of Energy, Oak Ridge, Tennessee.
- (2) WOCE station A05 S97 from Millero, F.J., Fiol, S., Campbell, D.M., Parrilla, G., Allison, L.J. and A. Kozyr. 2000. Carbon Dioxide, Hydrographic, and Chemical Data Obtained During the R/V *Hespérides* Cruise in the Atlantic Ocean (WOCE Section A5, July 14-August 15, 1992). ORNL/CDIAC-125, NDP-074. Carbon Dioxide Information Analysis Center, Oak Ridge National Laboratory, U. S. Department of Energy, Oak Ridge, Tennessee, U.S.A.
- (3) Rosenthal, Y., Lear, C.H., Oppo, D.W., and Linsley, B.K. 2006. Temperature and carbonate ion effects on Mg/Ca and Sr/Ca ratios in benthic foraminifera: aragonitic species *Hoeglundia elegans*. *Paleoceanography*. 21;
- (4) WOCE station P15S S71 from Feely, R., F. Millero, A. Dickson, R. Eanninkhof. 1996. Hydrographic, Chemical and Carbon Data Obtained During the R/V Discoverer cruise in the Pacific Ocean during WOCE Section P14S/P15S (EXPOCODE 31DSCG96_1,2), (05 January - 10 March, 1996). http://cdiac.ornl.gov/oceans/woce_p15s.html. Carbon Dioxide Information Analysis Center, Oak Ridge National Laboratory, US Department of Energy, Oak Ridge, Tennessee.
- (5) TTO station 143 from Brewer, P.G., Takahashi, T., and R.T. Williams. 1986. Transient Tracers in the Oceans (TTO) - Hydrographic data and carbon dioxide systems with revised carbon chemistry data. NDP-004/R1, Carbon Dioxide Information Center, Oak Ridge National Laboratory, Oak Ridge, Tennessee.
- (6) WOCE station A01W S12 from Jones, P. 1994. Total CO₂ and Total Alkalinity Data Obtained During the R/V Hudson in the North Atlantic Ocean during WOCE Section A01W (07 July - 25 August, 1994). http://cdiac.ornl.gov/oceans/woce_a01w.html. Carbon Dioxide Information Analysis Center, Oak Ridge National Laboratory, US Department of Energy, Oak Ridge, Tennessee.
- (7) WOCE station A24 S125 from Johnson K., R. Key, F. Millero, C. Sabine, D. Wallace, C. Winn, L. Arlen, K. Erickson, K. Friis, M. Galanter, J. Goen, R. Rotter, C. Thomas, R. Wilke, T. Takahashi, and S. Sutherland. 2003. Carbon

Dioxide, Hydrographic, and Chemical Data Obtained During the R/V *Knorr* Cruises in the North Atlantic Ocean on WOCE Sections AR24 (November 2 - December 5, 1996) and A24, A20, and A22 (May 30 - September 3, 1997), A. Kozyr (ed.) ORNL/CDIAC-143, NDP-082. Carbon Dioxide Information Analysis Center, Oak Ridge National Laboratory, U.S. Department of Energy, Oak Ridge, Tennessee.

- (8) WOCE station A24 S123 from Johnson K., R. Key, F. Millero, C. Sabine, D. Wallace, C. Winn, L. Arlen, K. Erickson, K. Friis, M. Galanter, J. Goen, R. Rotter, C. Thomas, R. Wilke, T. Takahashi, and S. Sutherland. 2003. Carbon Dioxide, Hydrographic, and Chemical Data Obtained During the R/V *Knorr* Cruises in the North Atlantic Ocean on WOCE Sections AR24 (November 2 - December 5, 1996) and A24, A20, and A22 (May 30 - September 3, 1997), A. Kozyr (ed.) ORNL/CDIAC-143, NDP-082. Carbon Dioxide Information Analysis Center, Oak Ridge National Laboratory, U.S. Department of Energy, Oak Ridge, Tennessee.

- (9) WOCE station A02b 309 from Wallace, D.. 1994. Total CO₂ and Total Alkalinity Data Obtained During the R/V *Meteor* in the North Atlantic Ocean during WOCE Section A02b (11 June - 03 July, 1997). http://cdiac.ornl.gov/oceans/woce_a02b.html/. Carbon Dioxide Information Analysis Center, Oak Ridge National Laboratory, US Department of Energy, Oak Ridge, Tennessee.

- (10) WOCE station A17N 191 from Rios, A., Johnson, K.M., Alvarez-Salgado, X.A., Arlen, L., Billant, A., Bingler, L.S., Branellec, P., Castro, C.G., Chipman, D.W., Roson, G., and D.W.R. Wallace. 2005. Carbon Dioxide, Hydrographic, and Chemical Data Obtained During the R/V *Maurice Ewing* Cruise in the Atlantic Ocean (WOCE Section A17, 4 January21 - March 1994), ed. A. Kozyr. ORNL/CDIAC-148, NDP-084. Carbon Dioxide Information Analysis Center, Oak Ridge National Laboratory, U.S. Department of Energy, Oak Ridge, Tennessee.

Appendix 8: Site information for previously published *Krithe* Mg/Ca data. Region, reference, site location, water depth, and temperature are given for each site.

Hydrographic parameters of total phosphorous (P), total silicate (Sil), total alkalinity (Talk), and Total CO₂ (TCO₂), were used to calculate *in situ* CO₃²⁻ using CO₂sys (Lewis and Wallace, 1998). Then *in situ* CO₃²⁻ was used to calculate Δ[CO₃²⁻]. For Arctic sites, a correction was required due to an increase in CO₂ in modern times (e.g., Orr et al., 1995), anthropogenic CO₂ was found from Jutterstrom and Jeanson (2008), and used to calculate anthropogenic *in situ* CO₃²⁻, and anthropogenic Δ[CO₃²⁻], which are also shown. Mg/Ca values are listed as published, and following a correction of 3.40 mmol/mol due to differences in cleaning (Mg/Ca cor.; Figure 4.6; section 4.4.6).

Site	Water Depth (m)	BWT (°C)	BWS (psu)	TP (μmol/kg)	TSil (μmol/kg)	Talk (μmol/kg)	TCO ₂ (μmol/kg)	[CO ₃ ²⁻] <i>in situ</i> (μmol/kg)	Anthro. CO ₂ (μmol/kg)	Anthro. CO ₃ (μmol/kg)	ΔCO ₃ ²⁻ (μmol/kg)	Mg/Ca (mmol/mol)	Mg/Ca Cor. (mmol/mol)	Reference
<u>Chilean Fjords P93-06 (Dwyer et al., 2002)</u>														
40	112	11.0										16.40	13.00	
40	112	11.0										16.19	12.79	
23	122	8.2										22.05	18.65	
23	122	8.2										14.04	10.64	
23	122	8.2										16.10	12.70	
23	122	8.2										15.85	12.45	
23	122	8.2										14.37	10.97	
23	122	8.2										14.56	11.16	
23	122	8.2										13.34	9.94	
23	122	8.2										13.26	9.86	
23	122	8.2										21.80	18.40	
21	184	8.9										17.85	14.45	
21	184	8.9										18.62	15.22	
18	210	9.1										15.91	12.51	
18	210	9.1										15.45	12.05	
35	330	8.0										14.62	11.22	

08	491	7.8		16.74	13.34
08	491	7.8		19.88	16.48
14	622	4.3		11.50	8.10
14	622	4.3		13.65	10.25
14	622	4.3		15.62	12.22
14	622	4.3		16.02	12.62
27	730	4.0		15.86	12.46
27	730	4.0		12.17	8.77
27	730	4.0		12.89	9.49
27	730	4.0		13.06	9.66
15	1140	2.9		10.75	7.35

Ontong Java Plateau MW91-9 (Dwyer et al., 2002)

BC7	1614	2.8	8.80	10.79	7.39	1
BC7	1614	2.8	8.80	9.81	6.41	1
BC7	1614	2.8	8.80	10.00	6.60	1
BC7	1614	2.8	8.80	9.13	5.73	1
BC7	1614	2.8	8.80	8.80	5.40	1
BC7	1614	2.8	8.80	11.30	7.90	1
BC7	1614	2.8	8.80	11.29	7.89	1
BC7	1614	2.8	8.80	10.63	7.23	1
BC7	1614	2.8	8.80	7.68	4.28	1
BC7	1614	2.8	8.80	8.02	4.62	1
BC7	1614	2.8	8.80	7.68	4.28	1
BC7	1614	2.8	8.80	8.02	4.62	1
BC37	2445	1.9	6.90	8.26	4.86	1
BC37	2445	1.9	6.90	9.65	6.25	1
BC63	3158	1.6	1.00	8.19	4.79	1
BC59	3393	1.5	-3.30	6.90	3.50	1
BC59	3393	1.5	-3.30	7.96	4.56	1
BC59	3393	1.5	-3.30	8.44	5.04	1
BC59	3393	1.5	-3.30	8.11	4.71	1
BC37	2445	1.9	6.90	8.25	4.85	1
BC63	3158	1.6	1.00	6.64	3.24	1

South Coral Sea (Correge & DeDecker, 1997)

23KA	5.9	19.02	15.62
23KB	5.9	16.77	13.37
23KE	5.9	16.59	13.19
23KF	5.9	18.49	15.09
23KG	5.9	17.02	13.62
23KH	5.9	17.38	13.98
29KB	5.0	13.22	9.82
29KC	5.0	15.67	12.27
29KD	5.0	14.70	11.30

29KE	5.0	17.53	14.13
29KF	5.0	15.63	12.23
29KG	5.0	14.71	11.31
29KH	5.0	17.51	14.11
29KI	5.0	17.24	13.84
56KB	4.3	10.90	7.50
56KC	4.3	13.75	10.35
56KD	4.3	16.93	13.53
56KH	4.3	18.35	14.95
34KA	3.0	12.84	9.44
34KB	3.0	11.97	8.57
34KD	3.0	13.41	10.01
34KE	3.0	15.92	12.52
34KF	3.0	12.07	8.67
34KG	3.0	13.29	9.89
34KH	3.0	14.82	11.42
34KI	3.0	14.23	10.83
34KJ	3.0	10.52	7.12
72KA	2.6	10.69	7.29
72KB	2.6	16.31	12.91
72KC	2.6	12.78	9.38
72KD	2.6	10.88	7.48
72KF	2.6	6.66	3.26
72KG	2.6	17.84	14.44
72KH	2.6	9.87	6.47
72KI	2.6	10.65	7.25
72KJ	2.6	11.36	7.96
72KK	2.6	14.21	10.81
12KA	2.3	15.42	12.02
12KB	2.3	12.87	9.47
12KD	2.3	12.74	9.34
12KF	2.3	12.16	8.76
12KH	2.3	9.51	6.11
12KI	2.3	12.31	8.91
12KJ	2.3	8.49	5.09
12KL	2.3	5.05	1.65
12KM	2.3	10.43	7.03
107KA	2.3	7.50	4.10
107KB	2.3	8.74	5.34
107KD	2.3	10.54	7.14
107KE	2.3	7.60	4.20
107KF	2.3	7.01	3.61
107KG	2.3	9.81	6.41

107KH	2.3											10.96	7.56	
107KJ	2.3											9.01	5.61	

North Atlantic CHN82-24 (Cronin et al., 1996)

4PC	3427	2.6										9.84	6.44	
-----	------	-----	--	--	--	--	--	--	--	--	--	------	------	--

Arctic: Almundsen Basin (Cronin et al., 1996)

2193	4337	-1.0	34.94									11.23	7.83	
2175	4411	-0.9	34.94									9.39	5.99	

Arctic: Barents Sea (Cronin et al., 1996)

2143	197	-1.0	34.81									7.75	4.35	
2140	461	1.0	34.92									9.46	6.06	
2140	461	1.0	34.92									10.54	7.14	
2139	752	0.8	34.92									12.74	9.34	

Arctic: Barents Slope (Cronin et al., 1996)

2447	1024	-0.2	34.91									10.60	7.20	
2447	1024	-0.2	34.91									11.17	7.77	
2447	1024	-0.2	34.91									11.19	7.79	
2447	1024	-0.2	34.91									13.07	9.67	
2447	1024	-0.2	34.91									14.27	10.87	
2446	2025	-0.8	34.93									9.82	6.42	
2444	2566	-0.8	34.94									10.62	7.22	
2444	2566	-0.8	34.94									19.97	16.57	
2442	2915	-0.8	34.93									8.70	5.30	
2445	2995	-0.8	34.94									10.03	6.63	
2445	2995	-0.8	34.94									10.09	6.69	
2445	2995	-0.8	34.94									10.48	7.08	
BC02	4004	-0.9	34.94	1.03	13.2	2304	2159	106.8	5	110	19.62	9.12	5.72	2

Arctic: Fram Strait (Cronin et al., 1996)

1904	1182	-1.0	34.92	0.59	5.1	2290	2161	98.0	20	109	51.86	8.43	5.03	3
1904	1182	-1.0	34.92									9.56	6.16	
1704	1195	-0.8	34.92	1.00	4.4	2355	2157	137.1	18	150	92.77	11.07	7.67	4
1704	1195	-0.8	34.92	1.00	4.4	2355	2157	139.3	18	150	92.77	11.76	8.36	4
2215	2019	-1.0	34.92	1.03	11.4	2298	2160	102.6	9	108	42.13	10.09	6.69	5

Arctic: Gakkel Ridge (Cronin et al., 1996)

2206	2993	-0.8	34.39	0.97	10.9	2288	2148	104.1	6	108	30.93	11.42	8.02	6
2163	3047	-1.0	34.39									12.36	8.96	

Arctic: GIN Seas/Fram Strait (Cronin et al., 1996)

1741	2059	-1.2	34.92	0.79	4.2	2297	2146	109.9	9	115	49.09	10.28	6.88	7
1741	2059	-1.2	34.92	0.79	4.2	2297	2146	109.9	9	115	49.09	11.65	8.25	7
23453	2061	-1.0	34.92	0.68	7.1	2297	2158	103.5	9	109	42.60	8.81	5.41	8
23453	2061	-1.0	34.92	0.68	7.1	2297	2158	103.5	9	109	42.60	9.45	6.05	8
23453	2061	-1.0	34.92	0.68	7.1	2297	2158	103.5	9	109	42.60	9.80	6.40	8
23453	2061	-1.0	34.92	0.68	7.1	2297	2158	103.5	9	109	42.60	10.08	6.68	8
23453	2061	-1.0	34.92	0.68	7.1	2297	2158	103.5	9	109	42.60	10.14	6.74	8

23453	2061	-1.0	34.92	0.68	7.1	2297	2158	103.5	9	109	42.60	10.62	7.22	8
23453	2061	-1.0	34.92	0.68	7.1	2297	2158	103.5	9	109	42.60	10.82	7.42	8
23453	2061	-1.0	34.92	0.68	7.1	2297	2158	103.5	9	109	42.60	11.01	7.61	8
23453	2061	-1.0	34.92	0.68	7.1	2297	2158	103.5	9	109	42.60	12.12	8.72	8
23453	2061	-1.0	34.92	0.68	7.1	2297	2158	103.5	9	109	42.60	13.23	9.83	8
23453	2061	-1.0	34.92	0.68	7.1	2297	2158	103.5	9	109	42.60	13.39	9.99	8
1873	2109	-1.0	34.92									9.69	6.29	
1707	2118	-1.0	34.92	0.93	10.4	2307	2158	109.4	8	114	47.38	10.55	7.15	9
1707	2118	-1.0	34.92	0.93	10.4	2307	2158	109.4	8	114	47.38	11.82	8.42	9
23454	2162	-1.0	34.92									9.59	6.19	
23454	2162	-1.0	34.92									9.68	6.28	
23456	2200	-1.1	34.92									8.90	5.50	
23456	2200	-1.1	34.92									9.68	6.28	
23457	2259	-1.0	34.92									9.25	5.85	
23457	2259	-1.0	34.92									9.34	5.94	
23457	2259	-1.0	34.92									9.40	6.00	
23457	2259	-1.0	34.92									9.48	6.08	
23457	2259	-1.0	34.92									9.95	6.55	
23457	2259	-1.0	34.92									10.07	6.67	
23457	2259	-1.0	34.92									10.08	6.68	
23457	2259	-1.0	34.92									10.10	6.70	
23457	2259	-1.0	34.92									10.15	6.75	
23457	2259	-1.0	34.92									10.22	6.82	
23457	2259	-1.0	34.92									10.38	6.98	
23457	2259	-1.0	34.92									10.55	7.15	
23457	2259	-1.0	34.92									10.76	7.36	
23457	2259	-1.0	34.92									10.82	7.42	
23457	2259	-1.0	34.92									11.02	7.62	
23457	2259	-1.0	34.92									11.16	7.76	
23457	2259	-1.0	34.92									11.32	7.92	
23455	2362	-1.1	34.92									9.73	6.33	
23455	2362	-1.1	34.92									10.83	7.43	
1736	3509	-1.1	34.89	0.98	11.6	2301	2155	107.3	5	110	26.98	9.29	5.89	10

Arctic: Greenland Sea (Cronin et al., 1996)

1560	1824	-0.9	34.91	0.66	4.4	2296	2144	110.9	11	117	53.66	10.26	7.49	11
1560	1824	-0.9	34.91	0.66	4.4	2296	2144	110.9	11	117	53.66	13.70	10.93	11

Arctic: Kara Sea (Cronin et al., 1996)

106	265	1.3	34.95	0.84	5.7	2291	2146	106.7	26	122	72.14	10.46	7.06	12
106	265	1.3	34.95	0.84	5.7	2291	2146	106.7	26	122	72.14	11.15	7.75	12
106	265	1.3	34.95	0.84	5.7	2291	2146	106.7	26	122	72.14	12.11	8.71	12

Arctic: Laptev Sea (Cronin et al., 1996)

2461	73	-1.4	33.92	0.50	3.4	2267	2149	92.0	30	109	60.79	6.37	2.97	13
2461	73	-1.4	33.92	0.50	3.4	2267	2149	92.0	30	109	60.79	6.54	3.14	13

2461	73	-1.4	33.92	0.50	3.4	2267	2149	92.0	30	109	60.79	6.66	3.26	13
2461	73	-1.4	33.92	0.50	3.4	2267	2149	92.0	30	109	60.79	7.43	4.03	13
2481	100	-1.2	34.94									6.72	3.32	
2481	100	-1.2	34.35									6.83	3.43	
2481	100	-1.2	34.35									7.57	4.17	
2478	101	-1.1	34.23									6.64	3.24	
2478	101	-1.1	34.23									6.87	3.47	
2478	101	-1.1	34.23									7.66	4.26	
2452	132	-1.0	34.28									9.03	5.63	
2451	144	-1.1	34.32									7.17	3.77	
2451	144	-1.1	34.32									7.29	3.89	
2460	191	1.4	34.85	0.79	5.1	2291	2142	108.9	28	125	76.23	9.13	5.73	14
2484	235	0.2	34.71									9.05	5.65	
2484	235	0.2	34.71									9.45	6.05	
2459	517	0.7	34.87									9.65	6.25	
2476	524	0.5	34.87									9.68	6.28	
2476	524	0.5	34.87									9.92	6.52	
2482	557	0.3	34.83									11.01	7.61	
2482	557	0.3	34.83									13.08	9.68	
2482	557	0.3	34.35									13.31	9.91	
2482	557	0.3	34.83									15.91	12.51	
2483	1216	-0.4	34.88									9.42	6.02	
2464	1760	-0.8	34.92									9.12	5.72	
2464	1760	-0.8	34.92									9.24	5.84	
2464	1760	-0.8	34.92									9.41	6.01	
2464	1760	-0.8	34.92									9.53	6.13	
2464	1760	-0.8	34.92									10.78	7.38	
2468	1991	-0.8	34.94									9.52	6.12	
2468	1991	-0.8	34.93									9.59	6.19	
2468	1991	-0.8	34.94									9.92	6.52	
2468	1991	-0.8	34.93									10.57	7.17	
2468	1991	-0.8	34.93									10.98	7.58	
2468	1991	-0.8	34.93									11.60	8.20	
2468	1991	-0.8	34.93									11.60	8.20	
2469	2332	-0.8	34.94									7.91	4.51	
2469	2332	-0.8	34.94									8.95	5.55	
2469	2332	-0.8	34.94									9.12	5.72	
2469	2332	-0.8	34.94									12.74	9.34	
2459	2420	-0.8	34.93									7.64	4.24	
2456	2520	-0.8	34.93									7.14	3.74	
2456	2520	-0.8	34.93									9.40	6.00	
2456	2520	-0.8	34.93									11.80	8.40	
2472	2620	-0.8	34.94									8.54	5.14	

2472	2620	-0.8	34.94									10.21	6.81
2472	2620	-0.8	34.94									10.45	7.05
2472	2620	-0.8	34.94									10.72	7.32
2471	3048	-0.8	34.94									8.25	4.85
2471	3048	-0.8	34.94									9.69	6.29
2471	3048	-0.8	34.94									9.96	6.56
2471	3048	-0.8	34.94									10.29	6.89
2471	3048	-0.8	34.94									11.30	7.90
2470	3233	-0.8	34.94									8.44	5.04
2470	3233	-0.8	34.94									8.77	5.37
2470	3233	-0.8	34.94									8.78	5.38
2470	3233	-0.8	34.94									8.96	5.56
2455	3429	-0.7	34.94									9.36	5.96
2455	3429	-0.7	34.94									10.39	6.99

Arctic: Lomonosov Ridge (Cronin et al., 1996)

2177	1388	-0.5	34.92	0.93	9.3	2296	2157	103.1	16	112	52.88	11.72	8.32	15
2184	1640	-0.5	34.91	1.01	12.2	2306	2161	107.2	12	114	52.31	17.91	14.51	16
2183	2016	-0.5	34.95	1.01	12.2	2306	2161	107.1	9	112	46.74	12.67	9.27	16

Arctic: Morris Jesup Rise (Cronin et al., 1996)

2200	1074	-0.2	34.89	0.93	8.7	2294	2148	106.9	20	118	61.98	16.41	13.01	17
2202	1083	-0.4	34.89	0.93	8.7	2294	2148	106.9	20	118	61.90	15.12	11.72	17
NP19/14	2500	-0.8	34.92									16.37	12.97	
NP21/3	2793	-0.5	34.93									10.09	6.69	
2204	3899	-0.7	34.94									12.73	9.33	
2204	3899	-0.7	34.94									13.69	10.29	

Arctic: N. Greenland Sea BartLT (Cronin et al., 1996)

35	200	-1.0	34.86									7.21	3.81	
35	200	-1.0	34.86									7.75	4.35	

Arctic: Nansen Basin P191-AR (Cronin et al., 1996)

BC08	1348	-0.6	34.91									10.50	7.10	
------	------	------	-------	--	--	--	--	--	--	--	--	-------	------	--

Arctic: Northwind Ridge P192-AR (Cronin et al., 1996)

B17	402	0.5	34.85	0.87	6.7	2291	2153	102.8	24	116	65.83	9.44	6.04	18
B17	402	0.4	34.85	0.87	6.7	2291	2153	102.8	24	116	65.83	10.51	7.11	18
B17	402	0.5	34.85	0.87	6.7	2291	2153	102.8	24	116	65.83	10.94	7.54	18
B17	402	0.5	34.85	0.87	6.7	2291	2153	102.8	24	116	65.83	11.60	8.20	18
B17	402	0.5	34.85	0.87	6.7	2291	2153	102.8	24	116	65.83	11.77	8.37	18
B17	402	0.5	34.85	0.87	6.7	2291	2153	102.8	24	116	65.83	11.92	8.52	18
B17	402	0.5	34.85	0.87	6.7	2291	2153	102.8	24	116	65.83	12.76	9.36	18
B17	402	0.5	34.85	0.87	6.7	2291	2153	102.8	24	116	65.83	13.03	9.63	18
B16	1388	-0.4	34.90	0.90	7.2	2296	2141	112.2	16	121	62.20	10.08	6.68	18
B16	1388	-0.3	34.90	0.90	7.2	2296	2141	112.2	16	121	62.20	11.30	7.90	18
B16	1388	-0.3	34.90	0.90	7.2	2300	2141	114.9	16	124	64.96	13.08	9.68	18
P1188BC												11.46	8.69	18

Arctic: Norwegian Sea P191-AR (Cronin et al., 1996)

BC10	562	1.8	34.91									10.38	6.98
BC10	562	1.8	34.91									11.04	7.64
BC11	1536	-1.1	34.91									9.15	5.75
BC11	1536	-1.0	34.91									9.16	5.76
BC11	1536	-1.1	34.91									10.54	7.14

Arctic: Yermak Plateau (Cronin et al., 1996)

2214	552	2.0	34.89									11.25	7.85	
2213	897	-0.3	34.90									9.11	5.71	
2212	2485	-0.8	34.92	0.98	11.3	2294	2159	100.8	7	105	34.10	10.17	6.77	19
2212	2485	-0.8	34.92	0.98	11.3	2294	2159	100.8	7	105	34.10	10.80	7.40	19
2212	2485	-0.8	34.92	0.98	11.3	2294	2159	100.8	7	105	34.10	12.06	8.66	19

Little Bahama Bank (Dwyer et al., 1995)

112PC	513	14.5	16.69	0.44	3.2	2373	2124	199.3				147.79	18.10	14.70	20
112PC	513	14.5	36.27	0.44	3.2	2373	2124	170.7				119.18	24.74	21.34	20
112PC	513	14.5	36.27	0.44	3.2	2373	2124	170.7				119.18	21.55	18.15	20
112PC	513	14.3	36.27	0.44	3.2	2373	2124	170.7				119.18	19.69	16.29	20
146PC	542	14.0	36.27	0.44	3.2	2373	2124	170.7				118.94	25.36	21.96	20
146PC	542	14.0	36.27	0.44	3.2	2373	2124	170.7				118.94	23.95	20.55	20
146PC	542	14.0	36.27	0.44	3.2	2373	2124	170.7				118.94	26.76	23.36	20
146PC	542	14.0	36.27	0.44	3.2	2373	2124	170.7				118.94	26.51	23.11	20
146PC	542	14.0	36.27	0.44	3.2	2373	2124	170.7				118.94	23.98	20.58	20
146PC	542	14.1	36.27	0.44	3.2	2373	2124	170.7				118.94	22.92	19.52	20
146PC	542	14.1	36.27	0.44	3.2	2373	2124	170.7				118.94	30.45	27.05	20
	577	13.5	35.80	0.79	6.8	2349	2133	149.8				97.77	22.05	18.65	20
	577	13.5	35.80	0.79	6.8	2349	2133	149.8				97.77	25.51	22.11	20
	577	13.5	35.80	0.79	6.8	2349	2133	149.8				97.77	22.26	18.86	20
4PC	714	10.3	35.25	1.45	15.2	2325	2176	109.0				55.80	17.88	14.48	20
4PC	714	10.0	35.25	1.45	15.2	2325	2176	109.0				55.80	18.22	14.82	20
4PC	714	10.3	35.25	1.45	15.2	2325	2176	109.0				55.80	16.46	13.06	20
4PC	714	10.3	35.25	1.45	15.2	2325	2176	109.0				55.80	17.38	13.98	20
4PC	714	10.3	35.25	1.45	15.2	2325	2176	109.0				55.80	17.45	14.05	20
144PC	833	8.2	35.25	1.45	15.2	2325	2176	109.0				54.78	12.42	9.02	20
36PC	900	7.0	35.25	1.45	15.2	2325	2176	109.0				54.20	15.76	12.36	20
36PC	900	7.0	35.25	1.45	15.2	2325	2176	109.0				54.20	14.25	10.85	20
36PC	900	7.0	35.25	1.45	15.2	2325	2176	109.0				54.20	13.86	10.46	20
36PC	900	7.0	35.25	1.45	15.2	2325	2176	109.0				54.20	18.24	14.84	20
15PC	934	7.4	35.08	1.41	16.2	2325	2183	105.1				50.04	13.37	9.97	20
15PC	934	7.4	35.08	1.41	16.2	2325	2183	105.1				50.04	13.62	10.22	20
15PC	934	7.5	35.08	1.41	16.2	2325	2183	105.1				50.04	12.70	9.30	20
15PC	934	7.5	35.08	1.41	16.2	2325	2183	105.1				50.04	12.63	9.23	20
15PC	934	7.4	35.08	1.41	16.2	2325	2183	105.1				50.04	14.57	11.17	20
15PC	934	7.4	35.08	1.41	16.2	2325	2183	105.1				50.04	15.23	11.83	20

17PC	953	7.0	35.08	1.41	16.2	2325	2183	105.1	49.87	13.80	10.40	20
17PC	953	7.0	35.08	1.41	16.2	2325	2183	105.1	49.87	14.61	11.21	20
17PC	953	7.0	35.08	1.41	16.2	2325	2183	105.1	49.87	8.18	4.78	20
17PC	953	7.0	35.08	1.41	16.2	2325	2183	105.1	49.87	14.68	11.28	20
17PC	953	7.0	35.08	1.41	16.2	2325	2183	105.1	49.87	9.10	5.70	20
141PC	958	6.2	35.08	1.41	16.2	2325	2183	105.1	49.82	9.02	5.62	20
141PC	958	6.2	35.08	1.41	16.2	2325	2183	105.1	49.82	13.75	10.35	20
	965	6.2	35.08	1.41	16.2	2325	2183	105.1	49.76	15.64	12.24	20
154PC	1044	5.3	35.08	1.41	16.2	2312	2183	97.6	41.51	11.25	7.85	20
154PC	1044	5.3	35.08	1.41	16.2	2312	2183	97.6	41.51	15.80	12.40	20
154PC	1044	5.3	35.08	1.41	16.2	2312	2183	97.6	41.51	15.72	12.32	20
100PC	1057	5.1	35.08	1.41	16.2	2312	2183	97.6	41.40	15.05	11.65	20
100PC	1057	5.1	35.08	1.41	16.2	2312	2183	97.6	41.40	13.17	9.77	20
29PC	1149	4.8	35.05	1.41	14.4	2312	2166	107.1	50.06	13.72	10.32	20
29PC	1149	4.8	35.05	1.17	14.4	2312	2166	107.2	50.20	12.66	9.26	20
29PC	1149	4.8	35.05	1.41	14.4	2312	2166	107.1	50.06	20.33	16.93	20
29PC	1149	4.8	35.05	1.41	14.4	2312	2166	107.1	50.06	13.48	10.08	20
23PC	1222	4.5	35.05	1.41	14.4	2312	2166	107.1	49.39	11.98	8.58	20
23PC	1222	4.5	35.05	1.41	14.4	2312	2166	107.1	49.39	13.37	9.97	20
23PC	1222	4.5	35.05	1.41	14.4	2312	2166	107.1	49.39	16.95	13.55	20
23PC	1222	4.5	35.05	1.41	14.4	2312	2166	107.1	49.39	10.58	7.18	20
23PC	1222	4.5	35.05	1.41	14.4	2312	2166	107.1	49.39	17.96	14.56	20
23PC	1222	4.5	35.05	1.41	14.4	2312	2166	107.1	49.39	12.05	8.65	20
23PC	1222	4.5	35.05	1.41	14.4	2312	2166	107.1	49.39	10.61	7.21	20
122PC	1263	4.4	35.05	1.41	14.4	2312	2166	107.1	49.01	12.91	9.51	20
122PC	1263	4.4	35.05	1.41	14.4	2312	2166	107.1	49.01	14.87	11.47	20
120PC	1466	4.1	35.01	1.21	14.2	2323	2161	116.7	56.67	11.25	7.85	20
120PC	1466	4.1	35.01	1.21	14.2	2323	2161	116.7	56.67	11.61	8.21	20
120PC	1466	4.1	35.01	1.21	14.2	2323	2161	116.7	56.67	10.65	7.25	20
21PC	1468	4.1	35.01	1.21	14.2	2323	2161	116.7	56.65	14.47	11.07	20
21PC	1468	4.1	35.01	1.21	14.2	2323	2161	116.7	56.65	10.33	6.93	20
21PC	1468	4.1	35.01	1.21	14.2	2323	2161	116.7	56.65	14.53	11.13	20
9PC	1539	4.1	35.00	1.16	15.0	2315	2162	111.3	50.61	12.72	9.32	20
9PC	1539	4.1	35.00	1.16	15.0	2315	2162	111.3	50.61	14.62	11.22	20
9PC	1539	4.1	35.00	1.16	15.0	2315	2162	111.3	50.61	12.16	8.76	20
19PC	1583	4.1	35.00	1.16	15.0	2315	2162	111.3	50.18	13.61	10.21	20
19PC	1583	4.1	35.00	1.16	15.0	2315	2162	111.3	50.18	10.82	7.42	20
19PC	1583	4.1	35.00	1.16	15.0	2315	2162	111.3	50.18	12.45	9.05	20
19PC	1583	4.1	35.00	1.16	15.0	2315	2162	111.3	50.18	12.86	9.46	20
19PC	1583	4.1	35.00	1.16	15.0	2315	2162	111.3	50.18	12.13	8.73	20
	3645	2.8								10.20	6.80	20
	3645	2.8								8.22	4.82	20
	3808	2.5								7.67	4.27	20

	3837	2.7	10.54	7.14	20
	3837	2.7	11.32	7.92	20
	1029	4.5	9.32	5.92	20
2096	2365	3.0	10.20	6.80	20
2096	2365	3.0	11.02	7.62	20
	2610	2.8	9.08	5.68	20
	2695	2.6	8.01	4.61	20
	2715	2.5	8.93	5.53	20
	3015	3.0	8.01	4.61	20
2165	3310	2.7	8.47	5.07	20
2166	3820	2.5	7.35	3.95	20
2166	3820	2.5	7.49	4.09	20
	3975	2.3	7.56	4.16	20
	3975	2.3	8.45	5.05	20

South Coral Sea ODP 822A (Correge & DeDecker, 1997)

K1A	955	3.5	13.43	10.03	
K1B	955	3.5	12.74	9.34	

South Pacific ELT39 (Cadot & Kaesler, 1977)

2	4720	0.9	8.78	5.38	
13	4785	1.1	8.37	4.97	
13	4785	1.1	8.37	4.97	

Peruvian Margin ELT3 (Cadot & Kaesler, 1977)

50	2725	2.0	5.53	2.13	
50	2725	2.0	4.82	1.42	
		2.2	8.06	4.66	
		2.2	9.69	6.29	
		2.2	8.47	5.07	

Western North Atlantic Atlantis II (Cadot & Kaesler, 1977)

119	2159	3.5	9.39	5.99	
119	2159	3.5	12.04	8.64	

South Pacific ELT39 (Cadot & Kaesler, 1977)

9	950	3.9	11.84	8.44	
---	-----	-----	-------	------	--

Canary Island Margin AII 32 (Cadot & Kaesler, 1977)

142	1710	4.4	10.92	7.52	
142	1710	4.4	7.76	4.36	
142	1710	4.4	8.78	5.38	

South Chilean Margin HE 69 (Cadot & Kaesler, 1977)

57	214	6.1	11.33	7.93	
57	214	6.1	15.23	11.83	
57	214	6.1	16.05	12.65	
57	214	6.1	16.16	12.76	
57	214	6.1	16.57	13.17	

Strait of Magellan/Tasman Plateau/Tasman Sea (Cadot et al., 1972)

CVK-1	7.0	15.90	12.50
CVK-1	4.0	11.70	8.30
CVK-1	2.0	8.20	4.80

References for hydrographic data are:

- (1) Dwyer, G.S., Cronin, T.M., and P.A. Baker. 2002. Trace elements in marine ostracods. *Geophysical monograph*. 131; 205-225.
- (2) CARINA 18SN19940726 S37 from http://cdiac.ornl.gov/oceans/CARINA/Carina_table.html
- (3) CARINA 58AA1961121 S11
- (4) CARINA 58AA19940203 S81
- (5) CARINA 58AA19980308 S58
- (6) CARINA 77DN19910726 S47
- (7) CARINA 58AA19980308 S27
- (8) CARINA 58AA19980308 S42
- (9) CARINA 58JH19930730 S668
- (10) CARINA 58AA19980308 S35
- (11) CARINA 58AA19980308 S47
- (12) CARINA 60AQ19960712 S40
- (13) CARINA 06AQ19960712 S100 from http://cdiac.ornl.gov/oceans/CARINA/Carina_table.html
- (14) CARINA 06AQ19960712 S98
- (15) CARINA 06AQ19960712 S58
- (16) CARINA 18SN19940726 S29
- (17) CARINA 77DN19910726 S43
- (18) CARINA 32H120020718 S33

(19) CARINA 77DN19910726 S54

20) WOCE Station A05 S97 from Millero, F.J., Fiol, S., Campbell, D.M., Parrilla, G., Allison, L.J. and A. Kozyr. 2000. Carbon Dioxide, Hydrographic, and Chemical Data Obtained During the *R/V Hespérides* Cruise in the Atlantic Ocean (WOCE Section A5, July 14-August 15, 1992). ORNL/CDIAC-125, NDP-074. Carbon Dioxide Information Analysis Center, Oak Ridge National Laboratory, U. S. Department of Energy, Oak Ridge, Tennessee, U.S.A. (

Appendix 9: Sample information on species, stage, number of carapaces, staining, visual preservation index (VPI; Dwyer et al., 2002) is listed below. Species abbreviations are *K. morkhovenii* (*mork*), *K. pernoides* (*pern*), *K. aequibilis* (*aeq*), *K. ayressii* (*ayres*), *K. minima* (*min*). Stages of molting are abbreviated as Adult (A) or late stage juvenile (A-1). Carapaces that were stained by Rose Bengal are labeled either ‘y’ for yes or ‘n’ for not stained. Mg/Ca ratios are listed for each sample.

Core	Water Depth (m)	BWT (°C)	Krihe Species	Molt Stage	No. Carapaces	Stain	VPI	Mg/Ca (mmol/mol)
<u>Cape Hatteras: Cruise KN178</u>								
16MCB	2214	3.37	<i>mork</i>	A	1	y	1	8.32
16MCB	2214	3.37	<i>pern</i>	A	2	n	2	8.59
14MCD	2602	3.03	<i>aeq</i>	A	1	n	2	9.19
8MCE	2997	2.51	<i>aeq</i>	A	1	y	1	9.35
5MCD	3382	2.20	<i>pern</i>	A	2	y	2	7.71
1MCD	3979	2.20	<i>mork</i>	A-1	2	n	1	8.61
1MCD	3979	2.20	<i>pern</i>	A	1	n	3	7.74
<u>Ceara Rise: ODP cruise</u>								
926	3598	2.45	<i>mork</i>	A-1	2		1	10.88
928	4010	1.52	<i>mork</i>	A-1	1		1	11.33
929	4355	1.80	<i>pern</i>	A	1		2	5.00
<u>Gulf of Mexico: Cruise DGOMB</u>								
S36-3	1026	5.07	<i>pern</i>	A	1		1	8.73
W4-5	1406	4.33	<i>aeq</i>	A	2		1	8.26
W4-5	1406	4.33	<i>aeq</i>	A	1		1	9.66
S38-4	2630	4.30	<i>mork</i>	A	2		2	8.60
S38-4	2630	4.30	<i>pern</i>	A	1		1	7.96
W5-4	2745	4.31	<i>pern/ aeq</i>	A	2		2	9.39
S39-2	3000	4.33	<i>pern</i>	A	1		1	8.90
W6-3	3150	4.35	<i>mork</i>	A-1	2		3	8.48
<u>Sulawesi Margin, Indonesia: Cruise BJ8-03</u>								
40MCF	251	11.50	<i>ayres</i>	A	1	y	4	16.59
61MCD	292	10.85	<i>ayres</i>	A	1	y	1	15.06
16MCC	409	8.75	<i>mork</i>	A	2	n	2	12.68
<u>New Zealand shelf: Cruise RR05-03</u>								
86MCF	663	4.88	<i>pern</i>	A	2	n	2	5.27
86MCF	663	4.88	<i>pern</i>	A-1	2	y	1	4.26

82MCG	1623	2.45	<i>aeq</i>	A	1	n	1	8.37
22MCB	1682	2.40	<i>pern</i>	A	1	y	2	8.79
22MCC	1682	2.40	<i>aeq</i>	A	1	n	1	7.45
22MCC	1682	2.40	<i>mork</i>	A	2	y	4	7.69
92MCG	1818	2.29	<i>mork</i>	A-1	1	n	1	6.78
102MCA	2055	2.12	<i>pern</i>	A	2	n	2	8.17
102MCA	2055	2.12	<i>pern</i>	A-1	2	n	1	6.22
118MCF	2252	2.04	<i>pern</i>	A	2	n	3	7.41
118MCF	2252	2.04	<i>min</i>	A	2	n	2	7.89
118MCF	2252	2.04	<i>mork</i>	A	2	y	2	7.17
26MCF	2418	1.91	<i>mork</i>	A	2	n	3	6.75
26MCF	2418	1.91	<i>pern</i>	A-1	3	n	2	8.25
106MCF	2472	1.87	<i>pern</i>	A	1	n	3	8.46
<u>North Atlantic: Cruise KN166-14 and ODP</u>								
15JPC	2300	2.91	<i>ayres</i>	A	2		2	10.03
15JPC	2300	2.91	<i>mork</i>	A-1	3		2	8.95
15JPC	2300	2.91	<i>ayres/mork</i>	A	3		2	9.27
11JPC	2707	3.00	<i>ayres</i>	A	2		2	10.36
8GGC	2707	3.00	<i>mork</i>	A	1		3	10.36
8GGC	2707	3.00	<i>mork</i>	A	1		1	8.85
12JPC	3078	2.75	<i>mork</i>	A	1		2	8.90
3GGC	3305	2.56	<i>mork</i>	A	1		3	8.87
3GGC	3305	2.56	<i>pern</i>	A	2		2	9.38
607	3427	2.57	<i>mork</i>	A	1		1	10.07
<u>Norwegian Sea: Cruise KN177-2</u>								
4MCE	418	0.84	<i>ayres</i>	A	2		3	11.65
4MCE	418	0.84	<i>ayres</i>	A	2		1	11.39
11MCC	1285	-0.71	<i>ayres</i>	A	2		3	11.31
50MCB	1906	-0.84	<i>ayres</i>	A	2		1	10.94
50MCB	1906	-0.84	<i>ayres</i>	A	3		2	9.04
45MCD	2799	-0.85	<i>ayres</i>	A	2		3	8.68

Appendix 10: Discussion of possible sources of scatter and error in the *Krithe* Mg/Ca core top calibration.

As with any core top study, some scatter within this calibration may be due to the availability of truly modern core top samples due to bioturbation, low sedimentation rates, or coring issues. The depth transects for Norwegian Sea, Gulf of Mexico, Cape Hatteras, and the New Zealand shelf were cored using box- and multi corers that aim to preserve the sediment-water interface, some of the North Atlantic and Ceara Rise cores were retrieved by piston coring, which has been shown to omit the uppermost sediments (Ross and Riedel, 1967; Skinner and McCave, 2003). Additionally, it is possible that surface sediments were removed prior to coring by down-slope processes, exposing older sediments at the surface, or remobilizing ostracod carapaces that were originally living at shallower depths. For example, late Holocene sediments have been winnowed from the top of northern North Atlantic core KN166-14 15JPC (Neitzke and Wright, 2007); this core top was still included in this calibration since minimal BWT changes are expected at this site since through the Holocene. However, since some of the core tops used in this calibration have not been independently dated, they may not be modern, which could result in small disparities between the *in situ* hydrographic information and the mean Holocene calcification conditions.

Calibration error may also be derived from variability between carapaces due to vital effects (e.g., Dwyer et al., 1995; Corregge and DeDeckker, 1997; Holmes, 2008). Dwyer et al. (1995) identified significant scatter in their single *Krithe* carapace measurements, which corresponded to a temperature error estimate of ± 1.3 °C when

single carapaces were analyzed. The error was reduced by $1/n^{0.5}$ when 'n' carapaces were analyzed (Dwyer et al., 1995). In order to minimize these effects, multiple carapaces were analyzed whenever available.

Studies of foraminifera (Rosenthal et al., 2004; Greaves et al., 2008) and lacustrine ostracods (Holmes, 1992; Jin et al., 2006) have shown that inter-laboratory differences in cleaning and analytical techniques can yield differences in measured Mg/Ca ratios; however, differential cleaning on *Krithe* has not been studied. The cleaning procedure used for this study involves oxidatively- and reductively cleaning the carapaces, which results in the removal of clays, as well as secondary calcite and ferromanganese coatings (Boyle and Keigwin, 1987); all other Mg/Ca *Krithe* measurements were made without oxidatively or reductively cleaning. In foraminifera, samples that were not oxidatively and reductively cleaned were shown to have anomalously high Mg/Ca ratios (Rosenthal et al., 2004; Elderfield et al., 2006). *Krithe* carapaces have ~ 10 times higher concentration of magnesium than benthic foraminifera, and thus the magnesium concentration in secondary calcite may be less apt to affect ostracodal Mg/Ca ratios than foraminiferal Mg/Ca ratios. A rudimentary correction was made by comparing the average Mg/Ca ratios within a temperature range for data generated in other laboratories to the average Mg/Ca ratios within that range generated at RIAL for this study; further inter-laboratory offsets may contribute to error in the paleotemperature equation (Figure 4.8). According to Jin et al. (2006), the maximum difference in Mg/Ca ratios resulting from oxidative and reductive cleaning for lacustrine ostracod is ~ 3.0 mmol/mol, which is roughly equivalent to the correction factor used to compare data from this study with previous studies. This correction factor is rudimentary

and, therefore, I propose that effects of different cleaning methods on *Krithe* should be examined.

Despite the possible errors in this calibration due to post-depositional dissolution, non-modern core tops, vital effects, and differences in cleaning procedure measurements, the global calibration has an error of ($\pm 0.21^{\circ}\text{C}$). Analytical error ($\sim 1\%$) has a small effect on the calibration error, while I propose that an evaluation due to cleaning protocols on *Krithe* may have the largest effect and thus should be systematically examined.

7.0 Curriculum Vitae

Aurora Cassandra Elmore

Colleges Attended and Degrees Earned:

2005-2009	Rutgers University, Ph.D. in Geological Sciences
2003-2005	University of South Carolina, M.S. in Geological Sciences
1999-2003	Boston University, B.A. in Geological Sciences

Positions Held:

2009-	Postdoctoral Research Associate, Institute of Marine and Coastal Sciences, Rutgers Univ.
2007	Geoscientist (May-August), Hess Oil Company, Houston, TX
2006-2008	Teaching Assistant, Dept. of Earth and Planetary Sciences, Rutgers Univ.
2005-2006	Graduate Fellow, Dept. of Earth and Planetary Sciences, Rutgers Univ.
2005-2006	Academic Tutor for Student Athletes, Athletic Department, Rutgers Univ.
2005	Research Assistant, Dept. of Geological Sciences, Univ. South Carolina
2003-2005	Teaching Assistant, Dept. of Geological Sciences, Univ. South Carolina
2001-2003	Laboratory Assistant, Dept. of Earth Sciences, Boston Univ.

Publications

Elmore, A.C., Thunell, R.C., Styles, R., Black, D.E., Murray, R.W., Martinez, N.C., and Y. Astor, 2007. Quantifying the seasonal variations in pluvial and eolian sources of terrigenous material to Cariaco Basin, Venezuela. *Journal of South American Earth Sciences*. doi:10.1016/j.jsames.2008.11.002